Universiteit Leiden
The Netherlands

Dynamic polymer hydrogels as synthetic extracellular matrices for 3D cell culture

Liu, T.

Citation

Liu, T. (2021, October 26). *Dynamic polymer hydrogels as synthetic extracellular matrices for 3D cell culture*. Retrieved from https://hdl.handle.net/1887/3223084

Version:	Publisher's Version
License:	Licence agreement concerning inclusion of doctoral thesis in the Institutional Repository of the University of Leiden
Downloaded from:	https://hdl.handle.net/1887/3223084

Note: To cite this publication please use the final published version (if applicable).

Dynamic polymer hydrogels as synthetic extracellular matrices for 3D cell culture

Proefschrift

ter verkrijging van

de graad van doctor aan de Universiteit Leiden,

op gezag van rector magnificus prof.dr.ir. H. Bijl,

volgens het besluit van het college voor promoties

te verdedigen op maandag 26 Oktober 2021

Klokke 11:15 uur

door

Tingxian Liu

Geboren op 15 November 1990, Xinyang, Henan, China

Promotiecommissie

Promotor: Prof. dr. A. Kros

Copromotor: Dr. R. E. Kieltyka

Overige Leden:

Prof. dr. H.S. Overkleeft (voorzitter), Faculty of Science, LIC

Prof. dr. R.T. Dame (secretaris), Faculty of Science, LIC

Prof. dr. S.E. Le Dévédec, Leiden Academic Centre for Drug Research (LACDR)

Prof. dr. P.C.J.J. Passier, Leiden University Medical Center (LUMC)

Prof. dr. S. Ghosh, Indian Association for the Cultivation of Science (IACS)

Doctoral Thesis, Leiden University, 2021

Cover Design: Tingxian Liu

To my family and friends

致 我的家人和朋友

Table of Content

Chapter 1

Introduction 7

Chapter 2

Squaramide-based supramolecular materials drive HepG2 spheroid differentiation 37

Chapter 3

Co-assembly of integrin-targeting peptides on squaramide supramolecular materials facilitate 3D expansion of hiPSCs 89

Chapter 4

Dynamic, cyclic thiosulfinate-crosslinked hydrogels enable cardiomyocyte natural behaviour in 3D 128

Chapter 5

Engineering macroporous hydrogels using the tetrazine-norbornene click reaction 175

Chapter 6

Summary and perspectives 213

Samenvatting 218

Curriculum Vitae 223

List of Publications 225

Acknowledgement 227

CHAPTER 1

Introduction

1.1 Cell culture models for *in vitro* drug screening

The failure of therapeutics in late-stage clinical trials is largely due to drug safety issues in addition to therapeutic insufficiency. A database of phase II and phase III clinical trials over the past 7 years shows that more than half of all drugs (52%) fail due to insufficient efficacy, and about 24% of drugs fail in phase II due to safety issues including a low therapeutic index.[1] The low drug success rate and high costs during drug discovery pipeline poses an urgent need for researchers to develop new strategies for early and precise prediction of drug therapeutic effect and safety issues.

In vitro cell culture models have become valuable tools to examine drug effectiveness and screening drug toxicity as an intermediate step prior to animal and human clinical trials because of their use of accessible cell sources and scalability. Cells used in these screens are isolated from their native environment and cultured on rigid plastic surfaces in 2D *in vitro*, in a monolayer with limited cell-cell contacts. Though this culture setup is routinely used, cells cultured as a monolayer often exhibit different drug reactivity and sensitivity in comparison to their growth *in vivo*.[2] When cultured on 2D surfaces, some native tissue-derived primary cells (*e.g.* primary hepatocytes) may rapidly lose their functional properties or differentiate.[3] This behavior is unsurprising as cells cultured on 2D surfaces lack the complexity of *in vivo* tissues that provide a three dimensional (3D) structural environment, cell-cell contacts, oxygen and nutrition gradients, as well as multiple cell types. One solution to overcome this challenge is to use multicellular models where the cells are aggregated in compact structures in 3D providing cell-cell contacts, a hypoxic environment, as well as oxygen and nutrient gradients.[4] Spheroids composed of hepatocellular carcinoma cells (HepG2) displayed higher expression (such as CYP2C9, CYP3A4, ALB, UGT1A1) of hepatocyte-related genes when cultured as spheroids in agarose microwells showing increased resistance against antitumor agents in comparison to their culture as a monolayer.[5] Breast cancer cells (MDA-MB-231) assembled into 3D tumor spheroids

within collagen hydrogels were reported to show more robust chemosensitivity during drug treatment in comparison to their culture in 2D.[6] Moreover, Burdick and co-workers recently developed heterogeneous spheroids based on cardiomyocytes and cardiac fibroblasts and demonstrated their use as effective models for engineering scarred cardiac microtissues and their application for therapeutic screening of mRNAs.[7] These examples highlight that moving from 2D to 3D spheroid culture is an efficient means to narrow the gap between *in vitro* and *in vivo* conditions.

1.2 Developing 3D cell culture models *in vitro*

The assembly of cells into 3D structures can involve either scaffold-free or matrix-based (*e.g.* hydrogels) approaches (Figure 1.1). In scaffold-free culture, cell spheroids form 3D structures due to aggregation in a hanging drop, on non-adhesive surfaces or through agitation by continuous stirring. By seeding cells into 96-well ultra-low attachment plates, the Eccles group has developed a 3D spheroid culture protocol for 40 tumor cell lines.[8] The spheroid sizes of different cell lines are maintained in a range of 300-500 µm by optimizing initial cell seeding densities. Within this study, the tightly compacted U-87 MG spheroids show tumor hypoxia transporters and rapid invasion into Matrigel, which indicating cell movement and matrix degradation occur. While 3D spheroids were produced from several cell lines besides U-87 MG, the technique usually involves considerable efforts to optimize culture conditions and special equipment can be required (*i.e.* to agitate the culture). In contrast, matrix-based 3D cell culture involves the use of materials based on hydrogels that can be from natural or synthetic sources to provide a water-rich environment with cues that stimulate cells biophysically or biochemically. More specifically, features of such matrices that have been tuned include cell-adhesiveness through peptide or protein cues, stiffening, micro/macro structure, hydrophobicity and porosity, opening the door to developing *in vitro* cell culture models for a broad range of biological applications.

Besides the increased microenvironmental complexity by moving from 2D to 3D culture, the wide availability of various cell sources provide a platform for researchers to develop increasingly complex *in vitro* cell culture models to answer a broad range of *in vivo* questions in biomedical research. For the liver, a large variety of cell types have been examined to develop models to advance drug toxicity testing, drug discovery and disease modeling. Cell types such as primary human hepatocytes (PHH), hepatoma cell lines (HepG2, HepRG), and hepatocytes derived from stem cells (adult (ASCs), human embryonic (hESCs) and induced pluripotent (iPSCs) iPSC-derived)) each with their various benefits and challenges.[5] More recently, iPSCs are being examined for such applications with great interest because they can provide an inexhaustible source of hepatocytes that can be derived from a patient through reporgramming to provide a personalized view into these areas.[9]

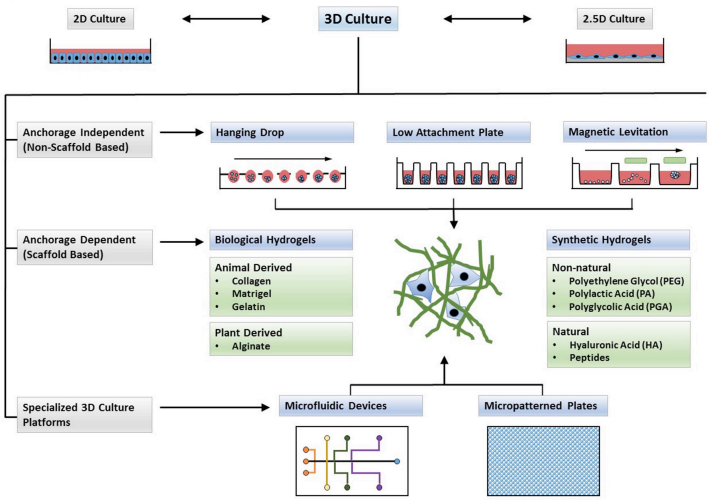

Figure 1.1. Cell culture techniques. In 2D culture, cells are cultured as a monolayer on stiff surfaces, whereas in 2.5D culture cells are plated on a thick layer of ECM-derived materials. Scaffold-free approach (3D self-assembled spheroids culture) or matrix encapsulation (natural ECM-derived materials and synthetic hydrogels) have been applied in 3D. Microfluidic devices and micro-patterned plates can also be involved to provide hybrid and complex microenvironments. Imaged adapted from reference [10].

1.3 Human induced pluripotent stem cell culture

Induced pluripotent stem cells were first reported by Yamanaka in 2006 when his group derived cells that displayed the same morphology and growth as embryonic stem cells (ESCs) by transfecting adult mouse fibroblasts with four reprogramming factors Oct3/4, Sox2, c-Myc and Klf4.[11] Soon after, human induced pluripotent stem cells (hiPSCs) were developed successfully using an optimized retroviral transduction of adult human fibroblasts, paving the way for their application in areas such as tissue engineering, cell transplantation and drug discovery unlocking the potential for a personalized approach.[12] Moreover, this class of cells is attractive for these applications due their capacity for self-renewal, potential to be differentiated to numerous cell types,[13] accessibility,[14,15] available optimized reprogramming protocols,[16–18] lack of ethical controversies in comparison to ESCs and immunocompatibility.[19–23]

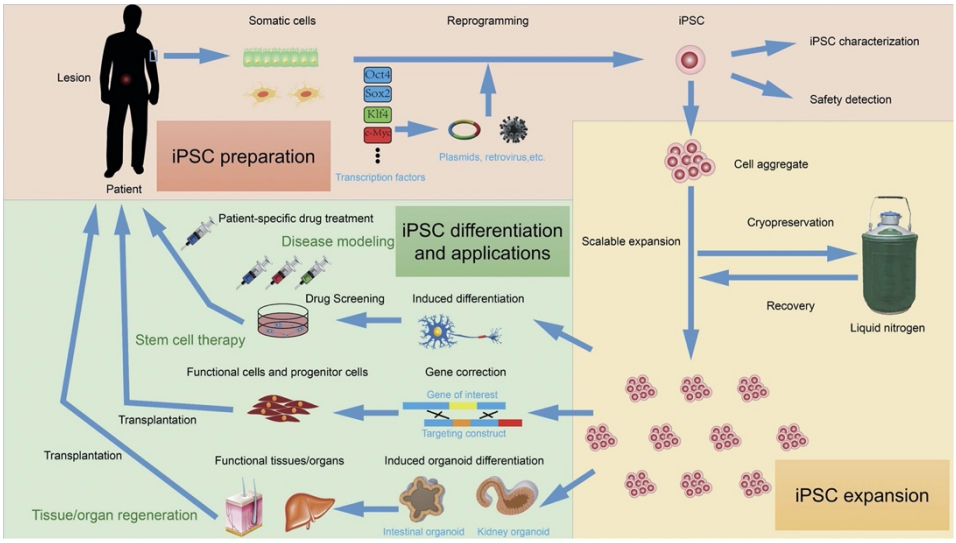

Figure 1.2. iPSCs workflow. Imaged adapted from reference [24].

Initially, 2D culture was the commonly used method to expand hiPSCs in combination with a feeder layer based on mouse embryonic fibroblasts (MEFs). This feeder layer provides growth factors, cell-binding proteins and cell-cell contacts to

support iPSC growth. However, MEF feeder layers can contaminate the stem cell culture with animal pathogens such as retroviruses because of their allogeneic nature. Optimization of a human feeder layer would decrease the immune response and remove its exposure to animal pathogens, however the undefined components and variability in the culture remain challenging.[25] As an alternative to feeder layers surface coatings based on Matrigel™, a commercially available feeder-free tumor derived ECM mixture, or recombinant proteins, such as vitronectin and laminin, have been used. Short peptides have also examined for this purpose because of their synthetically accessible character. Cell-adhesive peptides that target integrin receptors, such as RGD, have been coupled to acrylate polymer surfaces to support cell attachment, proliferation and specific differentiation of stem cells. This 2D culture scaffold is commercially sold as Synthemax™.[26,27] Moreover, Kiessling and co-workers developed a 2D substrate that displays heparin-binding peptides to interact with cell-surface glycosaminoglycans for long-term hES culture (3 months) showing high levels of pluripotency markers and maintenance of normal karyotype.[28] Although platforms for iPSC culture in 2D have advanced significantly, unsolved issues remain such as limited space for growth, diverse physiological functions in different clones, spontaneous differentiation during culture and cumbersome protocols to expand cells into the required cell quantity.

Expansion of iPSCs has been further examined in 3D to provide a more *in vivo*-like environment and space due to the added culture dimension. Matrix-free approaches in 3D have demonstrated that hiPSCs can self-assemble into spheroids, organoids or cell aggregates in liquid medium. Set-ups such as spinner flasks, rotating wall vessels and stirring bioreactors have been used with agitation to allow nutrient and gas exchange. Still challenges remain in optimizing culture conditions, including pH, temperature and dissolved oxygen concentrations, removal of metabolites, waste products and cell agglomeration can occur resulting in lower volumetric yields. Additionally, continuous

shear forces can induce cell death during iPSC culture.[29] As a consequence, gel embedding of these cellular aggregates is a offen used strategy to overcome some of these challenges. The iPSCs can be either encapsulated during the gelation process of polymer solutions, or the cells can be directly mixed with the gel depending on its mechanical properties, namely its capacity for self-recovery. In 2013, Lei *et al.* embedded hiPSCs in a thermoresponsive block co-polymer hydrogel and obtained ∼20-fold expansion of hiPSCs per passage in a 5-day culture. The hiPSCs were proven to maintain a high level of pluripotency and normal karyotype after a 280-day culture with the hydrogel, that is ~10^{72} fold expansion after 60 passages.[28] However, these hydrogels are based on polymers of a high molecular weight where it would be challenging to introduce biological cues for further applications, for example, cell differentiation, highlighting the need for small molecules in a defined manner.

hiPSCs are a potent cell source for developing *in vitro* cell culture models because of their capacity to differentiate into virtually any cell type of the human body. For example, hiPSCs can give rise to cardiomyocytes (CMs), endothelial cells (ECs) or vascular cells using specific differentiation protocols, offering a platform to study and explore heart disease *in vitro* in a personalized manner starting from patient material.[30] By co-assembly of hiPSC-CMs and hiPSC-ECs, Mummery and co-workers have successfully fabricated 3D cardiac microtissues *in vitro*.[31] Moreover, differentiated cells derived from hiPSCs show great potential for cell-based therapeutic applications. For example, hiPSC-derived CMs from healthy donors have been demonstrated to support cardiac reconstruction by enhanced engraftment, cell proliferation and treatment of heart infarct.[32–34] Luo *et al.* developed a 3D approach involving nanofiber hydrogels to enhance hiPSC differentiation to hepatocytes by mimicking their *in vivo* environment. HiPSCs embedded within the hydrogel differentiated into hepatocyte-like cell spheroids and displayed higher levels of albumin secretion, urea production and glycogen synthesis compared to hiPSCs

differentiated in 2D culture.[35] One common prerequisite for these strategies to achieve the 3D culture condition is to incorporate materials, either natural or synthetic, that provide both structural and biological support for cells.

1.4 The Extracellular matrix (ECM) of stem cell niche

In their native environment *in vivo*, cells are surrounded with a hydrated and dynamic network of macromolecules, otherwise known as the extracellular matrix (ECM). The ECM is diverse in composition in between different tissues and areas of the body within with respect to its components, concentrations and structures. The ECM has a high water content being constructed from cell interactive proteins and proteoglycans (PGs). Consequently, ECM-derived proteins, such as collagens, elastins, fibronectins and laminins, have been widely explored for use as stem cell culture substrates.[36] For example, recombinant vitronectin and laminin-511 are used as defined long-term culture substrates for self-renewal and maintenance of hESCs.[37,38]

The extracellular microenvironment is comprised of bioactive cues that can be grouped into three major categories based on their origin: 1) physical signals from insoluble macromolecules (fibrillar proteins, glycoproteins and hydrophilic proteoglycans); 2) biochemical signals from soluble molecules (growth factors, chemokines and cytokines); 3) signals from cell-cell interactions. In general, the biophysical and biochemical signals are communicated from the outside-in through cell surface receptors (*e.g.* integrins) and are subsequently processed through intracellular signaling pathways, enabling cell responses such as coordinated differentiation, proliferation and migration to apoptosis and other specific cell functions (Figure 1.3).

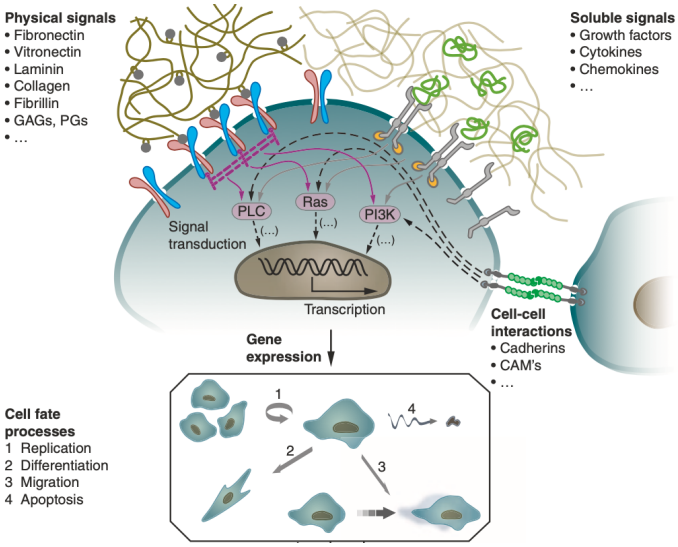

Figure 1.3. Extracellular matrix: fibrous proteins and hydrated proteoglycan form a gel-like network that is composed of soluble signals (*e.g.* growth factors) and physical signals that interact through cell surface receptors (*e.g.* integrins), as well as cell-cell interactions. Image adapted from reference [39].

The microenvironment of a stem cell, also known as the "stem cell niche", consists not only the ECM components, but also supportive stromal cells, vascular tissues as well as secreted soluble factors that initiate cell-cell interaction or signaling cascades. All these factors effect stem cell behavior in concert, and vice versa, they remodel the matrix in response to signals received from their microenvironment. Stem cells can directly interact with ECM proteins through their cell surface integrin receptors, for example, integrin $\alpha v\beta 5$ mediates cell adhesion on vitronectin and integrin $\alpha 6\beta 1$ mediates adhesion to laminin.[40] Some ECM proteins and PGs can act as a reservoir and distribute growth factors, providing them to the stem cell. On the other hand, the degradation of PGs by metalloproteinases releases growth factors that induce the remodeling of ECM microenvironment.[41,42] Moreover, the ECM shows complex dynamics in time and space that dramatically affect stem cell fate, especially during stem cell differentiation, *e.g.* in cardiac differentiation, the stiffness of the ECM

changes significantly from the embryonic (less than 500 Pa) to the adult stage (10 kPa).[43]

Several studies have demonstrated that stem cells cultured in matrices of a similar stiffness to the original tissue promote cell differentiation into the same lineage. For example, stiff substrates with an elasticity of 25-40 kPa supported differentiation of mesenchymal stem cell into bone tissue while soft substrates with an elasticity of 0.1-1 kPa were neurogenic favouring neural lineage specification. Moreover, efficient self-renewal and regeneration of skeletal muscle stem cells was observed when cells were exposed to substrates of an intermediate stiffness (12 kPa).[44–46] Because of the known role of the ECM in these processes, researchers are focusing on materials strategies that can direct and control stem cell fate through manipulation of this interface. Mooney *et al.* demonstrated that osteogenic differentiation of mesenchymal stem cells can be controlled by modulating the stiffness of the 3D microenvironment using substrates from 11 to 30 kPa. Later, by changing the elasticity of a porous hydrogel they obtained significantly improved survival, osteogenesis and bone regeneration of the transplanted stem cells in 3D.[47,48]

1.5 Synthetic covalent hydrogels as ECM mimicking materials

With the growing knowledge in the field of cell biology, researchers are developing a comprehensive chemical picture of the extracellular matrix and functions, such as its capacity to control cell fate. Rebuilding the *in vivo* cell ECM microenvironment in synthetic materials for 3D cell culture would open the door to regulate cell behaviors *in vitro*, such as cell viability, migration, proliferation and differentiation into specific cell lineages for a wide range of biomedical applications. Synthetic polymer hydrogels have been widely applied in this area. Generally, they are insoluble, crosslinked networks that contain a large quantity of water. They show several advantageous properties to mimic the their microenvironment, namely through their water-rich character,

cytocompatibility, structural and mechanical-likeness to the natural ECM.[49] Moreover, the use of specific chemistries within the materials enables precise control over their properties including structural features, mechanical stiffness, cell adhesion, and degradability, that all together play crucial roles in regulating cell morphology, migration and differentiation (Figure 1.4). Pahapale *et al.* fabricated a gelatin hydrogel platform for 3D cell culture, in which the mechanical stiffness can be controlled from soft (400 Pa) to stiff (50 kPa) with hierarchical curvature ranging from 12-120 µm to 1-4 mm (cellular length). The flexibility in tuning various materials properties makes it possible to mimic aspects of native tissues such as stiffness, as well as *in vivo* shapes and forms similarly to those found in intestinal villi, blood vessels and epithelial tissues.[50] Zhang *et al.* were able to modify gene expression profiles of neuronal cells by varying the hydrogel stiffness by increasing the $CaCl_2$ concentration of alginate/Matrigel composite hydrogels, further mimicking the properties of the brain respect to specific regions and different developmental stages.[51]

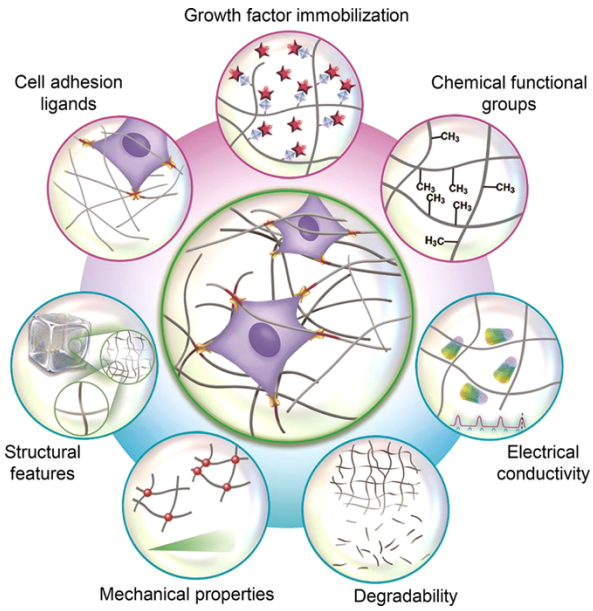

Figure 1.4. Properties of polymer materials used to recapitulate the 3D cell microenvironment. Image adapted from reference [52].

1.5.1 Modulation of mechanical cues

Hydrogels derived from natural polymers (*e.g.* collagen, Matrigel) are biocompatible, biodegradable and generally mechanically soft due to the physical nature of the interactions between their biopolymer chains. Collagen hydrogels can be prepared with shear moduli ranging from 13 to 254 Pa by adjusting the polymer concentration from 1.5 to 6 mg/mL. Though adjustable, their weak mechanical properties restrict their use to applications that require stiffnesses lower than 500 Pa. In contrast, synthetic hydrogels that are chemically defined can be outfitted with controlled cross-linking degrees and specific chemistries. Numerous cytocompatible polymers, such as the widely used poly(ethylene glycol) (PEG), the thermosensitive polymer poly(N-isopropylacrylamide) (PNIPAAm) and their derivatives, have been used as synthetic cell culture substrates. [53] Their amenability to be combined with various cross-linking chemistries, such as *in situ* radical polymerizations, mild schiff base reactions and the fast and efficient click reactions (*e.g* Diels-Alder reaction, thiol-ene addition and azide–alkyne cycloaddition) make them attractive due to their flexibility.[54] Using such cross-linking methods in combination with adjusting the monomer/polymer concentration, control over the crosslink density and thus, mechanical properties of the resultant materials can be achieved. For example, varying the monomer molecular weight, polymer concentration, ultraviolet (UV) light intensity and exposure time resulted in PEG diacrylate (PEGDA) hydrogels that show a wide range of compressive moduli from 0.7 to 233 kPa.[55] Moreover, the mechanical properties of hydrogels can be controlled spatiotemporally to further tune the cell microenvironment on-demand through a UV light-induced crosslinking strategy. Anseth's group designed a two-step crosslinking strategy in PEG hydrogels that contain SPAAC crosslinker that reacts initially without light and can be reacted further on-demand using light. Using this material, encapsulated myoblasts were observed to dynamically respond to the

changes in hydrogel stiffness in two stages by displaying increased circularity and nuclear localization of Yes-associated protein 1 (YAP) (Figure 1.5).[56]

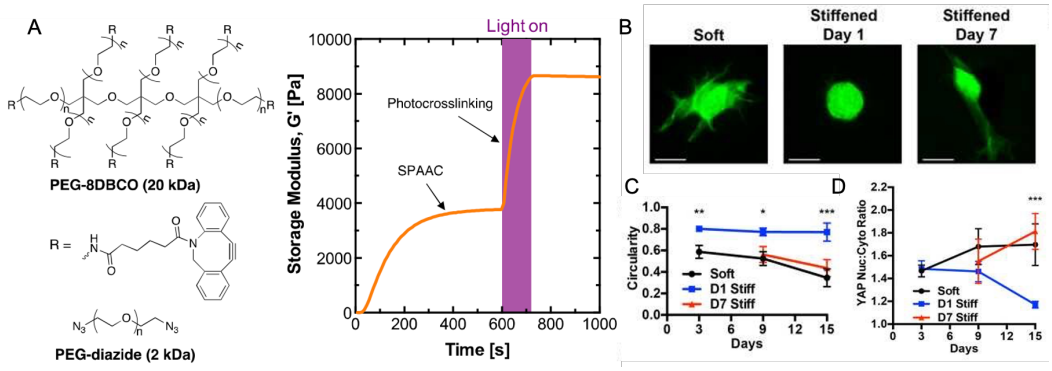

Figure 1.5. A) Primary crosslinking through azide and cyclooctyne (SPAAC) gives an initially soft hydrogel network. UV light-induced crosslinking of unreacted cyclooctyne functionalities improves hydrogel mechanical stiffness in a spatiotemporally controlled manner. B) Morphology of myoblasts cells encapsulated in SPAAC and UV light crosslinked hydrogels over a 15-day culture period. Cells were fluorescently-labelled with CellMask Green. C) Quantitative analysis of cell circularity of myoblasts cells over the 15-day culture, in which lower values indicated more spreading cells. D) Quantification of YAP nuclear over cytoplasmic localization using fluorescence intensity. Image adapted from reference [56].

1.5.2 Use of short peptides

In vivo, biological signals are transmitted via signaling molecules or proteins that are either tethered to the ECM or in solution. Hence, various synthetic peptides that are derived from ECM proteins, also called cell adhesive peptides (CAPs) have been included widely in synthetic polymer materials for cell culture applications. Besides their facile synthesis and stability during chemical processing, short sequence CAPs are the functional sequences of ECM proteins and can induce biological responses in cells. Broadly used peptide sequences include fibronectin-derived RGD, REDV and PHSRN,

YIGSR, IKVAV and PDGSR from laminin and collagen-derived DGEA.[57] Covalent attachment of these peptides into hydrogels has used reactions that involve the thiol, amino or carboxylic groups of the peptides or through their unnatural modification (*e.g.* with azides) that enable bioothogonal reactions. For example, cysteine-terminated peptides (RGD, YIGSR, PHSRN, IKVAV) can be easily coupled onto PEG polymers by the thiol–ene reaction using UV light.[58,59] The copper (I)-catalyzed alkyne azide 1,3-dipolar cycloaddition (CuAAC) click reaction is also frequently used in peptide conjugation because of its remarkable efficiency under mild conditions. The incorporation of the RGD peptide using the CuAAC reaction in a PEG-based hydrogel demonstrated improved cell attachment and enhanced cell proliferation.[60] Thus, using bioactive short peptides in combination with structurally tunable synthetic polymer matrices opens the door for user-defined control over cell growth and tissue formation for wide range application healthcare applications involving 3D cell culture.

1.5.3 Dynamic covalent bonds

Hydrogel materials used in the biomedical field largely consist static or permanent covalent bonds as they can provide a range of mechanical stiffness and stability. However, these irreversible bonds limit possibilities to recapitulate ECM dynamics that play important roles in facilitating various cell behaviors, for example, vascular morphogenesis.[61] Consequently, there is an interest in using networks based on dynamic covalent bonds, where their reversibility enables the material to form, break and reform as necessary to better mimic the ECM, but also for their practical application. Various chemistries have been used to prepare dynamic covalent hydrogels such as boronate,[62,63] disulfide,[64–66] Diels–Alder adducts,[67,68] thioesters,[69,70] Schiff-base,[71,72] or hydrazone bonds.[73–76] Using boronate-based chemistry, Anseth and co-workers designed three boronic acid variants that reacted with nitro-dopamine and formed hydrogels with different stiffnesses and relaxation

times: the strongest bond showed the longest relaxation time indicating slow dynamics and the weakest bond showed the shortest relaxation time meaning faster dynamics. Because of the rapid breaking and reforming of the hydrogel network, they were completely dissolved in the presence of cell culture media, and a second covalent crosslink was necessary to perform cell culture experiments. Human mesenchymal stem cells (hMSC) cultured in the rapidly relaxing matrix showed a more spread cell morphology, larger nuclear volume and localization of YAP/TAZ, meaning that cells engage with the dynamic matrix (Figure 1.6).[62] Similarly, a novel adaptable network was designed based on static thiol-ene photopolymerization and dynamic thiol-thioester exchange reactions. The hMSC encapsulated in these adaptable hydrogels showed reduced circularity in 3D and displayed an increase in proliferation compared to those cultured in purely static networks.[70] Moreover, Lutolf's group demonstrated that a mechanically dynamic PEG hydrogel promoted the growth of intestinal stem cells and their self-organization into organoids.[77] By introducing dynamic covalent chemistries into synthetic hydrogels, the door is open to assemble more complex tissue constructs by further mimicking *in vivo* microenvironment.

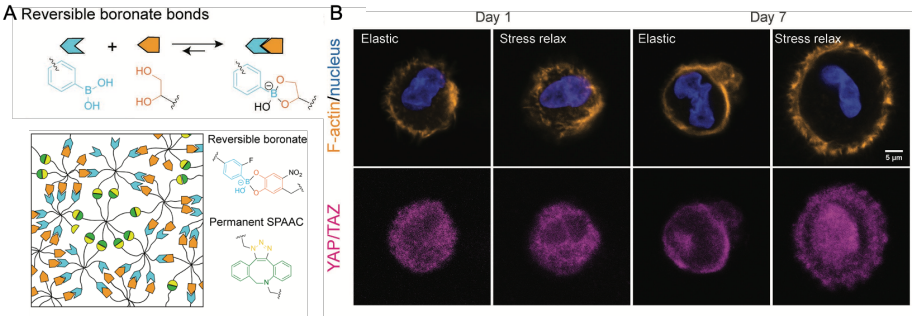

Figure 1.6. A) Two bioorthogonal crosslinking chemistries result in the formation of stress-relaxing hydrogels: dynamic bonds between boronic acids and cis-1,2-diols, and permanent and static SPAAC reactions between an azide and cyclooctyne; B) The hMSCs cultured in stress-relaxing hydrogels demonstrate a transition from YAP/TAZ in the cytosol to its nuclear localization. Image adapted from reference [62].

1.6 Supramolecular polymer materials: a new generation

Although covalent hydrogels have been frequently employed in biomaterials for *in vitro* cell culture, there remains a demand to develop materials that more closely mimic the structure and function of natural tissues with greater control over their properties. In contrast to covalent polymers, supramolecular polymers make use of monomers that are linked together through noncovalent interactions to form materials that have properties such as modularity, tunability, responsiveness and biomimicry due to the inherent dynamic nature of the bonds that hold them together. The non-covalent interactions used in their construction include highly directional hydrogen bonds, π-stacking, hydrophobic forces, ionic and host-guest interactions. In general, supramolecular materials can be prepared through one of the two approaches: 1) one-dimensional supramolecular stacking of monomers to form high aspect ratio

assemblies and 2) molecular recognition induced crosslinking of oligomeric/polymeric precursors (Figure 1.7).[78]

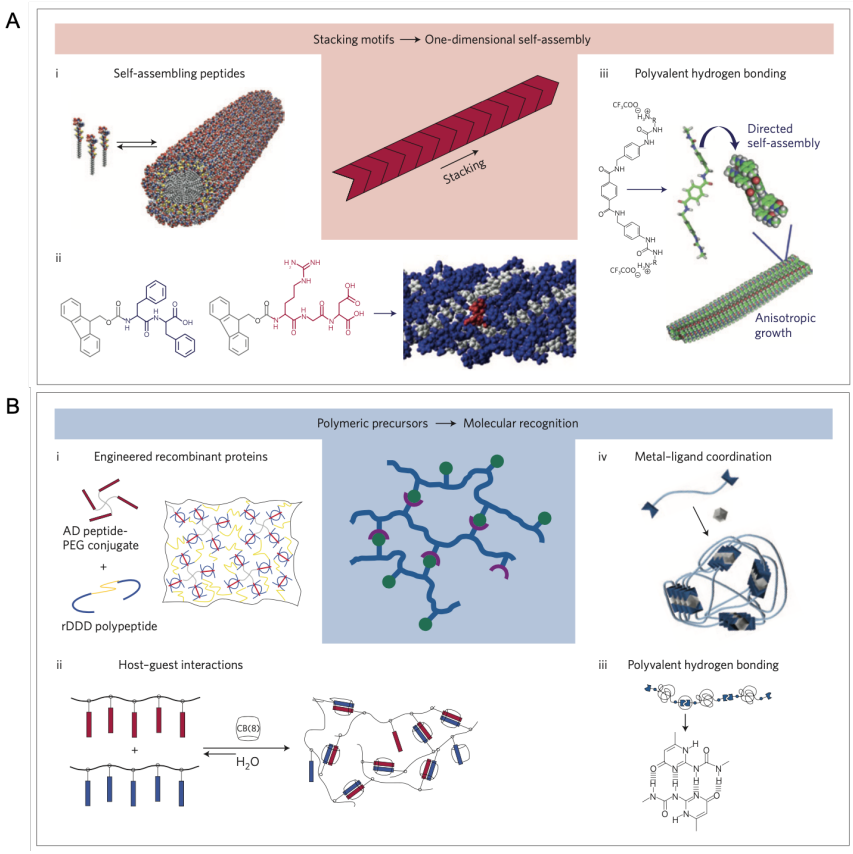

Figure 1.7. Overview and examples of supramolecular building blocks used in the construction of biomaterials. One-dimensional supramolecular stacking of monomers (top) and molecular recognition induced crosslinking of polymeric precursors (bottom). Image adapted from reference[78].

A frequently investigated class of supramolecular materials based on monomer stacking consist of self-assembling peptides. For example, the assembling peptide RADA16, also known as the commercialized product PuraMatrix, uses ionic interactions to facilitate stacking between peptides. Positively charged arginine (R) residue interact electrostatically with aspartic acid (D) and hydrophilic-hydrophobic forces between the alanine units (A), to drive the formation of β-sheets and fibrous self-assemblies with

diameters of 10 nm (Figure 1.7A). The RADA16 peptide-based matrix has shown the potential to support cell attachment and neuronal differentiation, extensive new neuronal projections as well as formation of functional junctions.[79] In an acute injury in a hamster's brain model, this peptide nanofiber scaffold enabled active neural cell migration and formation of abundant junctions, creating an environment for nerve fiber regeneration that reconnects the brain tissues together with sufficient density and function.[80] Moreover, this matrix encouraged the encapsulated stem cells to differentiate into neuronal lineages, which was further transplanted into mouse brains as a treatment demonstrating their use in direct medical application.[81,82] Another outstanding example of peptide-based assembly involves peptide amphiphiles (PAs). PAs consist of hydrophilic amino acids and a long lipophilic tail that induces β-sheet self-assembly and hydrophilic-hydrophobic interactions (Figure 1.7A). Stupp and co-workers have had a long-standing research interest in the self-assembly of PAs and their potential as functional biomaterials for tissue regeneration and cancer therapy. In 2001, the first PA with a peptide sequence of CCCCGGGS(^{PO4})RGD and a C_{16} alkyl tail was reported that yielded high aspect ratio cylindrical nanofibers under physiological conditions through intermolecular packing (Figure 1.8A).[83] Soon after, by changing the amino acid sequences and aliphatic chain length, Stupp and co-workers were able to make nanofibers with various morphologies and surface chemistries demonstrating their versatile composition and potential to fabricate various nanomaterials. Besides the use of pH changes to facilitate their self-assembly, their group also found that self-assembly of the monomers can be driven through their drying on a surface or addition of divalent cations.[84,85] Furthermore, by introducing charged amino acids at the hydrophilic region, researchers have demonstrated that charged self-assemblies can be formed that enable their binding to growth factors,[86] DNA,[87] or glycosaminoglycans,[88] broadening their use in the healthcare area. However, it still remains challenging to improve the efficiency and scale of functional peptide

monomers synthesis, highlighting the need for cheap and synthetically accessible alternatives.[78]

Non-covalent interaction motifs, such as those based on hydrogen bonding groups, can also be scaffolded on amphiphilic monomers. The Meijer group has investigated four-fold hydrogen-bond providing ureidopyrimidinone (UPy) units on several biomedically relevant polymers such as polycaprolactone (PCL),[89] oligo[90] (OEG) and poly(ethylene glycol) (PEG).[91] On amphiphilic scaffolds, UPy-based monomers self-assemble into fibers through hydrophobic, hydrogen bonding and π-π interactions, to form injectable and self-healable supramolecular hydrogel materials for engineering kidney and cardiac tissues (Figure 1.8B).[92,93] Similarly, structures based on benzene-1,3,5-tricarboxamides (BTA) with ethylene glycol modification have been designed to fabricate supramolecular polymers in water through hydrogen bonding, hydrophobic and π-π interactions from the benzene moiety.[94–97] The dynamic properties of the BTA-based supramolecular polymers was demonstrated via Forster resonance energy transfer (FRET),[98] stochastic optical reconstruction microscopy (STORM)[99] and hydrogen/deuterium exchange (HDX) mass spectrometry,[100] respectively. These monomers have shown promise as supramolecular polymer nanoparticles for the intracellular delivery of siRNA and cargo molecules.

More recently, we have validated the use of squaramides to engineer supramolecular biomaterials. Self-assembly of bis-squaramide bolaamphiphiles in water resulted in micrometer-long supramolecular fibers that were visualized by cryogenic transmission electron microscopy (cryo-TEM) and small angle X-ray scattering (SAXS) with a uniform diameter (Figure 1.8C). The hydrogen bonding of the bis-squaramides in a head-to-tail arrangement enhanced the aromatic character of the squaramide ring as evindenced by computational studies, increasing thermodynamic stability of the whole self-assembled structure.[101] By modulating the peripheral PEG and aliphatic chain lengths of the squaramide-based bolaamphiphiles, a morphological

transition from fibres to spheres was observed and a tunable biodistribution behavior *in vivo*.[102] Fibrous structures displayed short blood circulation and rapid capture by venous endothelial cells, whereas spherical aggregates showed significantly longer blood circulation and less accumulation in the caudal vein within the zebrafish embryo model.[103] Furthermore, we reported a novel tripodal tris(2-aminoethyl)amine core (TREN)-based squaramide monomer, in which three squaramide units are embedded within a flexible hydrophobic core (Figure 1.8D). Monomer aggregation was mainly driven by hydrophobic forces and hydrogen bonding of the squaramide moieties, leading to a hydrogel network of entangled micrometer fibrils. These supramolecular hydrogels show self-recovering behavior and are validated to support 3D culture of hiPSCs and their derivatives (Figure 1.8D).[104] While, the lack of bioactive units in this TREN-based hydrogel limit their further applications in this area, such as introducing cell adhesion peptides to engineer cell-matrix interactions for cell culture *in vitro*.

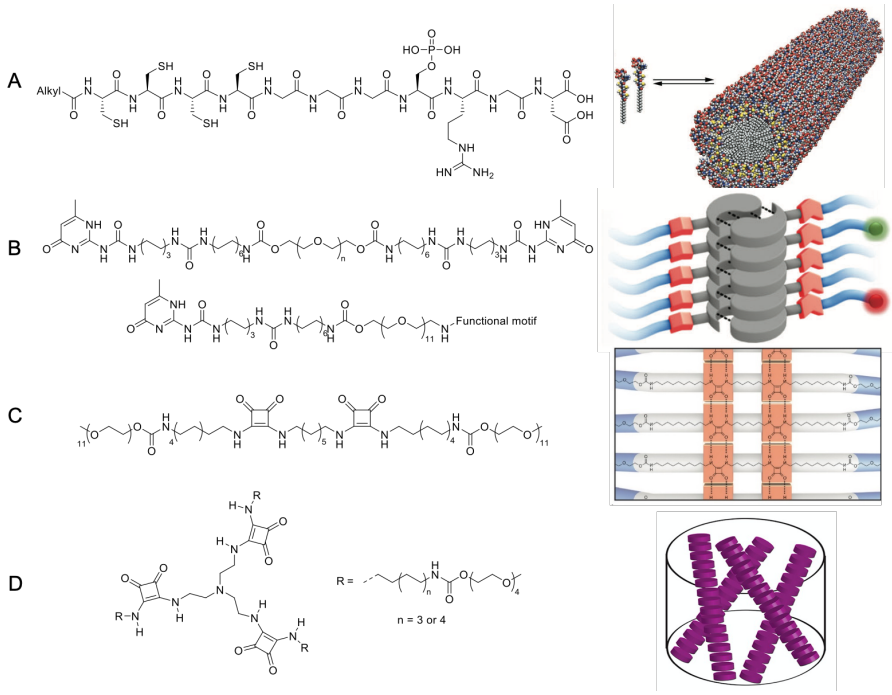

Figure 1.8. A) PAs monomer structure and self-assembly into cylindrical high aspect ratio nanofibers under physiological conditions. Image adapted from reference [83]. B)

Upy-based monomers (with or without functional groups) co-assemble into fibers through directional hydrophobic and hydrogen bonding interactions. Image adapted from reference [105]. C) Squaramide-based bolaamphiphiles chemical structure and intermolecular stacking through directional hydrogen bonding interactions. Image adapted from reference [101]. D) TREN-based squaramide monomer chemical structure and its self-assembly into supramolecular hydrogels. Image adapted from reference [104].

With a better understanding of supramolecular self-assembly principles, researchers are able to design novel functional polymers through a modular co-assembly approach that combines functional monomers together with their native counterparts. The functional groups can be either embedded within the central core of the monomer or tethered on the periphery in a defined manner through chemical synthesis. Stupp and co-workers have incorporated the functional peptide IKVAV that is derived from laminin and known to promote neurite formation, into the PA backbone obtaining a scaffold that rapidly induces neural lineage differentiation from neural progenitor cells.[106] Similarly, VEGF mimicking sequences were incorporated in PA backbone resulting in nanoscale filaments that present VEGF-mimetic peptides with a high density to activate VEGF receptors and promote angiogenesis in endothelial cells displaying enhanced cell proliferation activity, viability, migration and angiogenic response.[107] One of the attractive aspects of the co-assembly approach is its modularity, i.e. it enables the facile formation of functional polymers through the co-assembly of different monomers through mixing and matching. For example, an RGDS-presenting PA co-assembled together with the native PA results in an RGD-functionalized PA scaffold. Bone marrow-derived stem cells and progenitor cells encapsulated within this bioactive scaffold were observed to show enhanced cell attachment, cell proliferation and expression of endothelial-specific markers due to the presentation of this cell adhesive motif.[108] Another notable example of co-assembly is

reported by Albertazzi *et al.*, in which a BTA monomer that is positively charged and fluorescently-labelled co-assembles into functional supramolecular polymers that encapsulate Nile Red and electrostatically bind siRNA showing the facile nature of this approach to fabricate supramolecular nanoparticles with dual delivery function.[109]

Overall, supramolecular polymers show great potential to mimic the native ECM with respect to their reversibility, dynamic character and fibrous structure. Moreover, their modularity in the introduction of bioactive motifs is especially attractive for engineering *in vivo* microenvironment for 3D cell culture and tissue engineering applications, and more broadly, in healthcare.

1.7 Aim and outline

In this thesis, I focus on the preparation of fully synthetic and functional dynamic polymer biomaterials and investigate their application as scaffolds for 3D cell culture *in vitro*, including cancer cell spheroids, hiPSC expansion and differentiation to cardiomyocytes, enhancing maturity of hESCs-derived cardiomyocytes and supporting primary chondrocytes with matrix production.

In **Chapter 2**, I develop a bioactive supramolecular polymer hydrogel through a co-assembly approach. Next to the native squaramide-based monomers, a novel azide-functionalized squaramide-based monomer was prepared to introduce short bioactive peptides. The co-assembly process is characterized by UV-vis spectroscopy, Cryo-TEM, and the hydrogel mechanical properties will be investigated by oscillatory rheology. HepG2 cells are encapsulated within this bioactive hydrogel to understand their potential to support their metabolic maturation.

In **Chapter 3**, I examine the potential for multicomponent supramolecular self-assembly through the introduction of two integrin-targeting peptides for human induced pluripotent stem cell expansion. The co-assembly process is characterized by UV-vis spectroscopy, Cryo-TEM, and the hydrogel mechanical properties will be

investigated by oscillatory rheology. Two hiPSCs cell lines are be encapsulated within these supramolecular hydrogels for 4 days, and in some cases for 3 passages. After expansion, the cell viability, proliferation, pluripotent marker expression, differentiation potential and genetic stability of hiPSCs will be evaluated.

In **Chapter 4**, I introduce a disulfide-based dynamic covalent crosslink in a covalent PEG hydrogel system using a cyclic thiosulfinate. Together with a static covalent crosslink based on thiol Michael addition, we make a dual-crosslinked and dynamic PEG hydrogel. This dynamic PEG hydrogel is investigated with respect to its mechanical and swelling properties, and cytocompatibility. The hESC-derived cardiomyocytes are encapsulated within both static and dynamic PEG hydrogels to evaluate the impact of dynamics on cardiomyocyte behavior.

In **Chapter 5**, I employ an the inverse electron-demand Diels–Alder (iEDDA) reaction to prepare covalent PEG hydrogels using the gas evolution from the bioconjugation reaction to result in pores with diameters on the order of hundred micrometers. The mechanical properties and pore formation are evaluated by oscillatory rheology and confocal microscopy. Primary chondrocytes are cultured within the porous hydrogel, and their viability and subsequently, cell matrix production is investigated.

Chapter 6 summarizes all the synthetic designs and experimental results presented in this thesis. Conclusions and some future prospect are included.

1.7 References

[1] R. K. Harrison, *Nat. Rev. Drug Discov.* **2016**, *15*, 817.

[2] A. L. Howes, R. D. Richardson, D. Finlay, K. Vuori, *PLoS One* **2014**, *9*.

[3] S. Cassim, V. A. Raymond, P. Lapierre, M. Bilodeau, *PLoS One* **2017**, *12*, 1.

[4] S. Sant, P. A. Johnston, *Drug Discov. Today Technol.* **2017**, *23*, 27.

[5] W. Liao, J. Wang, J. Xu, F. You, M. Pan, X. Xu, J. Weng, X. Han, S. Li, Y. Li, K. Liang, Q. Peng, Y. Gao, *J. Tissue Eng.* **2019**, *10*.

[6] D. S. Reynolds, K. M. Tevis, W. A. Blessing, Y. L. Colson, M. H. Zaman, M. W. Grinstaff, *Sci. Rep.* **2017**, *7*, 1.

[7] A. Daly, M. Davidson, J. Burdick, *Nat. Commun.* **2021**, *12*, 753.

[8] M. Vinci, S. Gowan, F. Boxall, L. Patterson, M. Zimmermann, W. Court, C. Lomas, M. Mendiola, D. Hardisson, S. A. Eccles, *BMC Biol.* **2012**, *10*, 29.

[9] Z. Hannoun, C. Steichen, N. Dianat, A. Weber, A. Dubart-Kupperschmitt, *J. Hepatol.* **2016**, *65*, 182.

[10] S. A. Langhans, *Front. Pharmacol.* **2018**, *9*, 1.

[11] K. Takahashi, S. Yamanaka, *Cell* **2006**, *126*, 663.

[12] K. Takahashi, K. Tanabe, M. Ohnuki, M. Narita, T. Ichisaka, K. Tomoda, S. Yamanaka, *Cell* **2007**, *131*, 861.

[13] J. Zhang, G. F. Wilson, A. G. Soerens, C. H. Koonce, J. Yu, S. P. Palecek, J. A. Thomson, T. J. Kamp, *Circ. Res.* **2009**, *104*, 30.

[14] S. Conrad, M. Renninger, J. Hennenlotter, T. Wiesner, L. Just, M. Bonin, W. Aicher, H. J. Bühring, U. Mattheus, A. Mack, H. J. Wagner, S. Minger, M. Matzkies, M. Reppel, J. Hescheler, K. D. Sievert, A. Stenzl, T. Skutella, *Nature* **2008**, *456*, 344.

[15] T. Aasen, A. Raya, M. J. Barrero, E. Garreta, A. Consiglio, F. Gonzalez, R. Vassena, J. Bilić, V. Pekarik, G. Tiscornia, M. Edel, S. Boué, J. C. I. Belmonte, *Nat. Biotechnol.* **2008**, *26*, 1276.

[16] K. Okita, Y. Matsumura, Y. Sato, A. Okada, A. Morizane, S. Okamoto, H. Hong, M. Nakagawa, K. Tanabe, K. I. Tezuka, T. Shibata, T. Kunisada, M. Takahashi, J. Takahashi, H. Saji, S. Yamanaka, *Nat. Methods* **2011**, *8*, 409.

[17] K. Kaji, K. Norrby, A. Paca, M. Mileikovsky, P. Mohseni, K. Woltjen, *Nature* **2009**, *458*, 771.

[18] D. Huangfu, K. Osafune, R. Maehr, W. Guo, A. Eijkelenboom, S. Chen, W. Muhlestein, D. A. Melton, *Nat. Biotechnol.* **2008**, *26*, 1269.

[19] A. Wang, Z. Tang, I. H. Park, Y. Zhu, S. Patel, G. Q. Daley, S. Li, *Biomaterials* **2011**, *32*, 5023.

[20] F. Bastami, P. Nazeman, H. Moslemi, M. Rezai Rad, K. Sharifi, A. Khojasteh, *Cell Prolif.* **2017**, *50*.

[21] J. Jang, J. E. Yoo, J. A. Lee, D. R. Lee, J. Y. Kim, Y. J. Huh, D. S. Kim, C. Y. Park, D. Y. Hwang, H. S. Kim, H. C. Kang, D. W. Kim, *Exp. Mol. Med.* **2012**, *44*, 202.

[22] Y. S. Chun, P. Chaudhari, Y. Y. Jang, *Int. J. Biol. Sci.* **2010**, *6*, 796.

[23] A. S. T. Smith, J. Macadangdang, W. Leung, M. A. Laflamme, D. H. Kim, *Biotechnol. Adv.* **2017**, *35*, 77.

[24] Y. Li, L. Li, Z. N. Chen, G. Gao, R. Yao, W. Sun, *Biofabrication* **2017**, *9*.

[25] M. Richards, C. Y. Fong, W. K. Chan, P. C. Wong, A. Bongso, *Nat. Biotechnol.* **2002**, *20*, 933.

[26] S. Jin, H. Yao, J. L. Weber, Z. K. Melkoumian, K. Ye, *PLoS One* **2012**, *7*.

[27] Z. Melkoumian, J. L. Weber, D. M. Weber, A. G. Fadeev, Y. Zhou, P. Dolley-Sonneville, J. Yang, L. Qiu, C. A. Priest, C. Shogbon, A. W. Martin, J. Nelson, P. West, J. P. Beltzer, S. Pal, R. Brandenberger, *Nat. Biotechnol.* **2010**, *28*, 606.

[28] J. R. Klim, L. Li, P. J. Wrighton, M. S. Piekarczyk, L. L. Kiessling, *Nat. Methods* **2010**, *7*, 989.

[29] C. McKee, G. R. Chaudhry, *Colloids Surfaces B Biointerfaces* **2017**, *159*, 62.

[30] R. Passier, V. Orlova, C. Mummery, *Cell Stem Cell* **2016**, *18*, 309.

[31] E. Giacomelli, M. Bellin, V. V. Orlova, C. L. Mummery, *Curr. Protoc. Hum. Genet.* **2017**, *95*, 21.9.1.

[32] D. T. Paik, M. Chandy, J. C. Wu, *Pharmacol. Rev.* **2020**, *72*, 320.

[33] S. Funakoshi, K. Miki, T. Takaki, C. Okubo, T. Hatani, K. Chonabayashi, M. Nishikawa, I. Takei, A. Oishi, M. Narita, M. Hoshijima, T. Kimura, S. Yamanaka, Y. Yoshida, *Sci. Rep.* **2016**, *6*, 1.

[34] X. Guan, W. Xu, H. Zhang, Q. Wang, J. Yu, R. Zhang, Y. Chen, Y. Xia, J. Wang, D. Wang, *Stem Cell Res. Ther.* **2020**, *11*, 1.

[35] Y. Luo, C. Lou, S. Zhang, Z. Zhu, Q. Xing, P. Wang, T. Liu, H. Liu, C. Li, W. Shi, Z. Du, Y. Gao, *Cytotherapy* **2018**, *20*, 95.

[36] C. Frantz, K. M. Stewart, V. M. Weaver, *J. Cell Sci.* **2010**, *123*, 4195.

[37] S. R. Braam, L. Zeinstra, S. Litjens, D. Ward-van Oostwaard, S. van den Brink, L.

van Laake, F. Lebrin, P. Kats, R. Hochstenbach, R. Passier, A. Sonnenberg, C. L. Mummery, *Stem Cells* **2008**, *26*, 2257.

[38] S. Rodin, A. Domogatskaya, S. Ström, E. M. Hansson, K. R. Chien, J. Inzunza, O. Hovatta, K. Tryggvason, *Nat. Biotechnol.* **2010**, *28*, 611.

[39] M. P. Lutolf, J. A. Hubbell, *Nat. Biotechnol.* **2005**, *23*, 47.

[40] S. R. Braam, L. Zeinstra, S. Litjens, D. Ward-van Oostwaard, S. van den Brink, L. van Laake, F. Lebrin, P. Kats, R. Hochstenbach, R. Passier, A. Sonnenberg, C. L. Mummery, *Stem Cells* **2008**, *26*, 2257.

[41] C. Bonnans, J. Chou, Z. Werb, *Nat. Rev. Mol. Cell Biol.* **2014**, *15*, 786.

[42] F. Gattazzo, A. Urciuolo, P. Bonaldo, *Biochim. Biophys. Acta - Gen. Subj.* **2014**, *1840*, 2506.

[43] J. L. Young, A. J. Engler, *Biomaterials* **2011**, *32*, 1002.

[44] A. J. Engler, S. Sen, H. L. Sweeney, D. E. Discher, *Cell* **2006**, *126*, 677.

[45] P. M. Gilbert, K. L. Havenstrite, K. E. G. Magnusson, A. Sacco, N. A. Leonardi, P. Kraft, N. K. Nguyen, S. Thrun, M. P. Lutolf, H. M. Blau, *Science (80).* **2010**, *329*, 1078.

[46] P. C. Georges, W. J. Miller, D. F. Meaney, E. S. Sawyer, P. A. Janmey, *Biophys. J.* **2006**, *90*, 3012.

[47] N. Huebsch, P. R. Arany, A. S. Mao, D. Shvartsman, O. A. Ali, S. A. Bencherif, J. Rivera-Feliciano, D. J. Mooney, *Nat. Mater.* **2010**, *9*, 518.

[48] N. Huebsch, E. Lippens, K. Lee, M. Mehta, S. T. Koshy, M. C. Darnell, R. M. Desai, C. M. Madl, M. Xu, X. Zhao, O. Chaudhuri, C. Verbeke, W. S. Kim, K. Alim, A. Mammoto, D. E. Ingber, G. N. Duda, D. J. Mooney, *Nat. Mater.* **2015**, *14*, 1269.

[49] F. Edalat, I. Sheu, S. Manoucheri, A. Khademhosseini, *Curr. Opin. Biotechnol.* **2012**, *23*, 820.

[50] G. J. Pahapale, S. Gao, L. H. Romer, D. H. Gracias, *ACS Appl. Bio Mater.* **2019**, *2*, 6004.

[51] H. Tekin, S. Simmons, B. Cummings, L. Gao, X. Adiconis, C. C. Hession, A. Ghoshal, D. Dionne, S. R. Choudhury, V. Yesilyurt, N. E. Sanjana, X. Shi, C. Lu, M. Heidenreich, J. Q. Pan, J. Z. Levin, F. Zhang, *Nat. Biomed. Eng.* **2018**, *2*, 540.

[52] G. Huang, F. Li, X. Zhao, Y. Ma, Y. Li, M. Lin, G. Jin, T. J. Lu, G. M. Genin, F. Xu, *Chem. Rev.* **2017**, *117*, 12764.

[53] E. S. Place, J. H. George, C. K. Williams, M. M. Stevens, *Chem. Soc. Rev.* **2009**, *38*, 1139.

[54] P. M. Kharkar, K. L. Kiick, A. M. Kloxin, *Chem. Soc. Rev.* **2013**, *42*, 7335.

[55] M. Parlato, S. Reichert, N. Barney, W. L. Murphy, *Macromol. Biosci.* **2014**, *14*, 687.

[56] T. E. Brown, J. S. Silver, B. T. Worrell, I. A. Marozas, F. M. Yavitt, K. A. Günay, C. N. Bowman, K. S. Anseth, *J. Am. Chem. Soc.* **2018**, *140*, 11585.

[57] J. Zhu, *Biomaterials* **2010**, *31*, 4639.

[58] K. A. Kyburz, K. S. Anseth, *Acta Biomater.* **2013**, *9*, 6381.

[59] E. M. Ovadia, D. W. Colby, A. M. Kloxin, *Biomater. Sci.* **2018**, *6*, 1358.

[60] S. Q. Liu, P. L. Rachel Ee, C. Y. Ke, J. L. Hedrick, Y. Y. Yang, *Biomaterials* **2009**, *30*, 1453.

[61] Z. Wei, R. Schnellmann, H. C. Pruitt, S. Gerecht, *Cell Stem Cell* **2020**, *27*, 798.

[62] S. Tang, H. Ma, H. C. Tu, H. R. Wang, P. C. Lin, K. S. Anseth, *Adv. Sci.* **2018**, *5*, 1.

[63] Y. Chen, D. Diaz-Dussan, D. Wu, W. Wang, Y. Y. Peng, A. B. Asha, D. G. Hall, K. Ishihara, R. Narain, *ACS Macro Lett.* **2018**, *7*, 904.

[64] S. Y. Choh, D. Cross, C. Wang, *Biomacromolecules* **2011**, *12*, 1126.

[65] F. Yang, J. Wang, L. Cao, R. Chen, L. Tang, C. Liu, *J. Mater. Chem. B* **2014**, *2*, 295.

[66] G. A. Barcan, X. Zhang, R. M. Waymouth, *J. Am. Chem. Soc.* **2015**, *137*, 5650.

[67] C. M. Madl, S. C. Heilshorn, *Chem. Mater.* **2019**, *31*, 8035.

[68] S. Mukherjee, M. R. Hill, B. S. Sumerlin, *Soft Matter* **2015**, *11*, 6152.

[69] M. D. Konieczynska, J. C. Villa-Camacho, C. Ghobril, M. Perez-Viloria, K. M. Tevis, W. A. Blessing, A. Nazarian, E. K. Rodriguez, M. W. Grinstaff, *Angew. Chemie* **2016**, *128*, 10138.

[70] T. E. Brown, B. J. Carberry, B. T. Worrell, O. Y. Dudaryeva, M. K. McBride, C. N. Bowman, K. S. Anseth, *Biomaterials* **2018**, *178*, 496.

[71] Z. Wei, D. M. Lewis, Y. Xu, S. Gerecht, *Adv. Healthc. Mater.* **2017**, *6*, 1.

[72] Z. Wei, S. Gerecht, *Biomaterials* **2018**, *185*, 86.

[73] D. D. McKinnon, D. W. Domaille, J. N. Cha, K. S. Anseth, *Adv. Mater.* **2014**, *26*, 865.

[74] P. K. Sharma, S. Taneja, Y. Singh, *ACS Appl. Mater. Interfaces* **2018**, *10*, 30936.

[75] Z. Li, F. Zhou, Z. Li, S. Lin, L. Chen, L. Liu, Y. Chen, *ACS Appl. Mater. Interfaces* **2018**, *10*, 25194.

[76] L. L. Wang, C. B. Highley, Y. C. Yeh, J. H. Galarraga, S. Uman, J. A. Burdick, *J. Biomed. Mater. Res. Part A* **2018**, *106*, 865.

[77] N. Gjorevski, N. Sachs, A. Manfrin, S. Giger, M. E. Bragina, P. Ordóñez-Morán, H. Clevers, M. P. Lutolf, *Nature* **2016**, *539*, 560.

[78] M. J. Webber, E. A. Appel, E. W. Meijer, R. Langer, *Nat. Mater.* **2015**, *15*, 13.

[79] R. G. Ellis-Behnke, Y. X. Liang, S. W. You, D. K. C. Tay, S. Zhang, K. F. So, G. E. Schneider, *Proc. Natl. Acad. Sci. U. S. A.* **2006**, *103*, 5054.

[80] S. Zhang, *Second Smith Nephew Int. Symp. - Tissue Eng. 2000 Adv. Tissue Eng. Biomater. Cell Signal.* **2000**, 12.

[81] N. L. Francis, N. K. Bennett, A. Halikere, Z. P. Pang, P. V. Moghe, *ACS Biomater. Sci. Eng.* **2016**, *2*, 1030.

[82] W. Shi, C. J. Huang, X. D. Xu, G. H. Jin, R. Q. Huang, J. F. Huang, Y. N. Chen, S. Q. Ju, Y. Wang, Y. W. Shi, J. B. Qin, Y. Q. Zhang, Q. Q. Liu, X. B. Wang, X. H. Zhang, J. Chen, *Acta Biomater.* **2016**, *45*, 247.

[83] T. J. Mitchison, J. C. Biol, J. F. Kelleher, S. J. Atkinson, T. D. Pollard, J. C. Biol, J. D. Hartgerink, E. Beniash, S. I. Stupp, **2001**, *294*, 1684.

[84] J. D. Hartgerink, E. Beniash, S. I. Stupp, *Proc. Natl. Acad. Sci. U. S. A.* **2002**, *99*, 5133.

[85] H. Cui, T. Muraoka, A. G. Cheetham, S. I. Stupp, *Nano Lett.* **2009**, *9*, 945.

[86] R. N. Shah, N. A. Shah, M. M. D. R. Lim, C. Hsieh, G. Nuber, S. I. Stupp, *Proc. Natl. Acad. Sci. U. S. A.* **2010**, *107*, 3293.

[87] R. S. Tu, R. Marullo, R. Pynn, R. Bitton, H. Bianco-Peled, M. V. Tirrell, *Soft Matter* **2010**, *6*, 1035.

[88] K. Rajangam, H. A. Behanna, M. J. Hui, X. Han, J. F. Hulvat, J. W. Lomasney, S. I.

Stupp, *Nano Lett.* **2006**, *6*, 2086.

[89] P. Y. W. Dankers, E. N. M. van Leeuwen, G. M. L. van Gemert, A. J. H. Spiering, M. C. Harmsen, L. A. Brouwer, H. M. Janssen, A. W. Bosman, M. J. A. van Luyn, E. W. Meijer, *Biomaterials* **2006**, *27*, 5490.

[90] R. E. Kieltyka, M. M. C. Bastings, G. C. van Almen, P. Besenius, E. W. L. Kemps, P. Y. W. Dankers, *Chem. Commun.* **2012**, *48*, 1452.

[91] P. Y. W. Dankers, T. M. Hermans, T. W. Baughman, Y. Kamikawa, R. E. Kieltyka, M. M. C. Bastings, H. M. Janssen, N. A. J. M. Sommerdijk, A. Larsen, M. J. A. Van Luyn, A. W. Bosman, E. R. Popa, G. Fytas, E. W. Meijer, *Adv. Mater.* **2012**, *24*, 2703.

[92] P. Y. W. Dankers, M. J. A. Van Luyn, A. Huizinga-Van Der Vlag, A. H. Petersen, J. A. Koerts, A. W. Bosman, E. R. Popa, *Eur. Polym. J.* **2015**, *72*, 484.

[93] M. M. C. Bastings, S. Koudstaal, R. E. Kieltyka, Y. Nakano, A. C. H. Pape, D. A. M. Feyen, F. J. van Slochteren, P. A. Doevendans, J. P. G. Sluijter, E. W. Meijer, S. A. J. Chamuleau, P. Y. W. Dankers, *Adv. Healthc. Mater.* **2014**, *3*, 70.

[94] P. J. M. Stals, M. M. J. Smulders, R. Martín-Rapún, A. R. A. Palmans, E. W. Meijer, *Chem. - A Eur. J.* **2009**, *15*, 2071.

[95] M. M. J. Smulders, I. A. W. Filot, J. M. A. Leenders, P. Van Der Schoot, A. R. A. Palmans, A. P. H. J. Schenning, E. W. Meijer, *J. Am. Chem. Soc.* **2010**, *132*, 611.

[96] S. Cantekin, T. F. A. de Greef, A. R. A. Palmans, *Chem. Soc. Rev.* **2012**, *41*, 6125.

[97] F. Paquin, J. Rivnay, A. Salleo, N. Stingelin, C. Silva, *J. Mater. Chem. C* **2015**, *3*, 10715.

[98] L. Albertazzi, F. J. Martinez-Veracoechea, C. M. A. Leenders, I. K. Voets, D. Frenkel, E. W. Meijer, *Proc. Natl. Acad. Sci. U. S. A.* **2013**, *110*, 12203.

[99] L. Albertazzi, D. Van Der Zwaag, C. M. A. Leenders, R. Fitzner, R. W. Van Der Hofstad, E. W. Meijer, *Science (80).* **2014**, *344*, 491.

[100] X. Lou, R. P. M. Lafleur, C. M. A. Leenders, S. M. C. Schoenmakers, N. M. Matsumoto, M. B. Baker, J. L. J. Van Dongen, A. R. A. Palmans, E. W. Meijer, *Nat. Commun.* **2017**, *8*, 1.

[101] V. Saez Talens, P. Englebienne, T. T. Trinh, W. E. M. Noteborn, I. K. Voets, R. E. Kieltyka, *Angew. Chemie* **2015**, *127*, 10648.

[102] V. Saez Talens, D. M. M. Makurat, T. Liu, W. Dai, C. Guibert, W. E. M. Noteborn, I. K. Voets, R. E. Kieltyka, *Polym. Chem.* **2019**, *10*, 3146.

[103] V. Saez Talens, G. Arias-Alpizar, D. M. M. Makurat, J. Davis, J. Bussmann, A. Kros, R. E. Kieltyka, *Biomacromolecules* **2020**, *21*, 1060.

[104] C. Tong, T. Liu, V. Saez Talens, W. E. M. Noteborn, T. H. Sharp, M. M. R. M. Hendrix, I. K. Voets, C. L. Mummery, V. V. Orlova, R. E. Kieltyka, *Biomacromolecules* **2018**, *19*, 1091.

[105] S. I. S. Hendrikse, S. P. W. Wijnands, R. P. M. Lafleur, M. J. Pouderoijen, H. M. Janssen, P. Y. W. Dankers, E. W. Meijer, *Chem. Commun.* **2017**, *53*, 2279.

[106] G. A. Silva, C. Czeisler, K. L. Niece, E. Beniash, D. A. Harrington, J. A. Kessler, S. I. Stupp, *Science (80).* **2004**, *303*, 1352.

[107] M. J. Webber, J. Tongers, C. J. Newcomb, K. T. Marquardt, J. Bauersachs, D. W. Losordo, S. I. Stupp, *Proc. Natl. Acad. Sci. U. S. A.* **2012**, *109*, 9220.

[108] M. J. Webber, J. Tongers, M. A. Renault, J. G. Roncalli, D. W. Losordo, S. I. Stupp, *Acta Biomater.* **2010**, *6*, 3.

[109] M. H. Bakker, C. C. Lee, E. W. Meijer, P. Y. W. Dankers, L. Albertazzi, *ACS Nano* **2016**, *10*, 1845.

CHAPTER 2

Squaramide-based supramolecular materials drive HepG2 spheroid differentiation

This chapter was published as an original reseach paper: Tingxian Liu, Linda van den Berk, Joeri A.J. Wondergrem, Ciqing Tong, Markus C. Kwakernaak, Bas ter Braak, Doris Heinrich, Bob van de Water, Roxanne E. Kieltyka*, *Adv. Healthcare. Mater.* **2021**, *10*, 2001903. https://doi.org/10.1002/adhm.202001903

2.1 Abstract

A major challenge in the use of HepG2 cell culture models for drug toxicity screening is their lack of maturity in 2D culture. 3D culture in Matrigel promotes the formation of spheroids that express liver-relevant markers, yet they still lack various primary hepatocyte functions. Therefore, alternative matrices where chemical composition and materials properties are controlled to steer maturation of HepG2 spheroids remain desired. Herein, a modular approach was taken based on a fully synthetic and minimalistic supramolecular matrix based on squaramide synthons outfitted with a cell-adhesive peptide, RGD for 3D HepG2 spheroid culture. Co-assemblies of RGD-functionalized squaramide-based and native monomers resulted in soft and self-recovering supramolecular hydrogels with a tunable RGD concentration. HepG2 spheroids were self-assembled and grown (~150 µm) within the supramolecular hydrogels with high cell viability and maturation over a 21-day culture. Importantly, significantly higher mRNA and protein expression levels of phase I and II metabolic enzymes, drug transporters and liver markers were found for the squaramide hydrogels in comparison to Matrigel. Overall, the fully synthetic squaramide hydrogels were proven to be synthetically accessible and effective for HepG2 differentiation showcasing the potential of this supramolecular matrix to rival and replace naturally-derived materials classically used in high-throughput toxicity screening.

2.2 Introduction

The liver is a critical organ of the human body that performs the biotransformation of drugs and other xenobiotics. Chemical transformations, such as oxidation, reduction, hydrolysis or other organic reactions, of these foreign agents give rise to active or inactive metabolites that can even be hepatotoxic.[1] Toxic insults to the liver from drug metabolites can eventually result in acute or chronic failure, otherwise known as drug-induced liver injury (DILI). DILI can occur from nearly every class of medication, and when encountered often results in abandonment of the therapy.[2] Thus, a major challenge in the drug discovery pipeline is to more accurately predict DILI early on, as hepatotoxic responses observed in animal models do not fully recapitulate those observed in humans resulting in drug candidates that fail in late stage clinical trials or even after approval in the clinic.[3]

Primary human hepatocytes (PHH) are the current gold standard for *in vitro* modeling of liver metabolism and toxicity as they represent 70% of total liver cell population. However, these cells are challenged by their limited availability and high donor variability, rapid loss of metabolic activity once harvested for *ex vivo* culture and costly derivation.[4,5] As an alternative cell source to model liver hepatic processes *in vitro*, human liver carcinoma cells (HepG2) are used due their wide availability, immortality, facile handling and stable phenotype in culture. However, these cells often show low expression levels of metabolic enzymes, namely cytochrome P450s that are relevant for xenobiotic metabolism, which has been correlated with the 2D culture methods used to expand them.[6] Three-dimensional (3D) culture methods have been used to improve the metabolic characteristics of HepG2 cells mainly using Matrigel, a biological matrix derived from murine tumor tissues, consisting of laminin, collagen IV, and entactin.[7] When encapsulated in Matrigel, HepG2 cells self-organize into

spheroidal structures and differentiate resulting in increased levels of various metabolic markers and can be dosed repeatedly with increased sensitivity to various hepatotoxic agents in comparison to HepG2 cells cultured in 2D.[8,9] However, Matrigel is costly, lacks definition with lot-to-lot variability,[7] its murine origin is problematic for some applications and chemical modification or decoupling of cues is difficult, leading to the exploration of synthetic polymers for use in 3D hepatocyte culture.

Matrices held together by covalent and non-covalent interactions have demonstrated the capacity to form spheroids from liver-derived cells in 3D, including a handful of recent reports examining the effect of cell interactive moieties to facilitate their differentiation and culture with varying degrees of success.[10–19] More recent studies have examined the capacity of the short integrin-binding peptide RGD to guide this process highlighting the importance of peptides derived from extracellular matrix proteins in synthetic materials. While a fully synthetic and covalent PEG hydrogel functionalized with RGD supported the growth of liver organoids, the addition of laminin-entactin complex was necessary for a non-covalent hydrogel based on a polyisocyanopeptide polymer to stimulate cell proliferative pathways demonstrating the importance of peptide concentration.[17,18] We thus became interested in examining a supramolecular polymer matrix based on stacked monomers for HepG2 cell culture to improve their growth and differentiation in 3D. However, such supramolecular systems that have the short peptides derived from matrix proteins is yet to be explored for the preparation of HepG2 spheroids, but can more broadly provide a powerful synthetic polymer platform for 3D cell culture where the peptide concentration can be tuned easily and facile cell seeding and release can be achieved.

In order to construct supramolecular polymer materials, monomers that contain highly directional, specific and reversible non-covalent interactions are needed.[20–24] In particular, squaramide synthons because of their ditopic presentation of hydrogen bond donors and acceptors on a minimal scaffold in combination with their synthetic

accessibilty are of interest for this aim.[25–32] We recently demonstrated their application in a tripodal hydrogelator for the culture of human induced pluripotent stem cells (hiPSCs), using the soft and self-recovering nature of the supramolecular matrix that supports cell self-assembly into spheroids driven by cell-cell contacts.[31] However, cell proliferation within these materials was found to be limited, pointing out the need to further modify this synthetic matrix with bioactive peptides to enable cell-matrix interaction. One short peptide that has been implemented in materials to provide such interactions is the RGD peptide, a short sequence derived from the FN-III repeat in the 10th domain of fibronectin, that binds the α5β1 and αVβ3 integrins on the cell surface. We therefore sought to introduce this cell-adhesive peptide within squaramide-based supramolecular materials through co-assembly of functional monomers as a facile means to tune peptide concentration for applications in 3D HepG2 culture and differentiation.

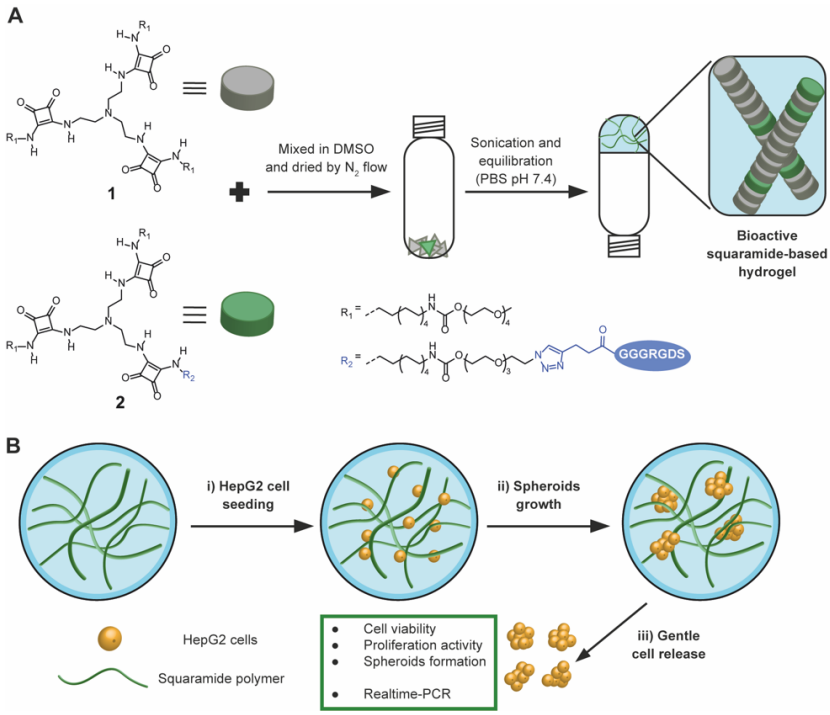

Scheme 2.1. A) Preparation of bioactive squaramide-based supramolecular hydrogels: RGD-functionalized squaramide monomers (**2**) were mixed with the native tripodal monomer (**1**) in DMSO. The dried solid was rehydrated in phosphate buffered saline (PBS, pH 7.4) by sonication, followed by being left to equilibrate overnight to obtain the co-assembled bioactive hydrogels. B) HepG2 spheroids cultured in bioactive squaramide-based supramolecular hydrogel for 21 days: i) HepG2 cells were mixed and encapsulated within the hydrogel by pipetting using its self-recovery property; ii) HepG2 cells self-assemble into spheroids, proliferate and differentiate within the hydrogel; iii) HepG2 spheroids were released by dilution and used for further analysis including cell proliferation and gene expression.

2.3 Results and Discussion

Design, synthesis and co-assembly of RGD-modified squaramide monomers to form bioactive supramolecular materials. Earlier, we designed a tripodal squaramide-based monomer (**1**) where three squaramides were embedded within a hydrophobic core consisting of tris(2-aminoethylamine) (TREN), aliphatic and a peripheral hydrophilic domain with oligo(ethylene glycol) chains. In this study, we further sought to incorporate the RGD peptide into these squaramide monomers (molecule **2**) to aid in cell proliferation, but also to provide a cell adhesive contact for cells (Scheme 2.1)**.** However, the lack of reactive handle, namely the terminal methyl group on the oligo(ethylene glycol) chains of the monomer preclude it from further functionalization with any cargo, such as fluorescent dyes, crosslinkers, peptides or proteins. Therefore, a desymmetrized tripodal squaramide-based monomer where one of the three arms was end-functionalized with an azide (molecule **3**) was designed and synthesized starting from a monotrityl-protected TREN core. The azide functionality was first introduced onto tetraethylene glycol by tosylation (Scheme S2.1).[33] The tetraethylene glycol monomethyl ether and monoazide tetraethylene glycol were then independently activated using 1,1-carbonyldiimidazole and further reacted with monotrityl-protected C10 diamine in presence of N,N-Diisopropylethylamine (DIPEA) resulting in yields of 63% (methyl-terminated) and 74% (azide-terminated), respectively. The trityl protecting group was deprotected by TFA under an inert atmosphere, followed by its subsequent reaction with dibutyl squarate to provide the methyl-terminated and azide-terminated squaramide amphiphiles in yields of 87% and 47%, respectively (Scheme S2.2). Subsequently, the methyl-terminated squaramide amphiphile was reacted onto the desymmetrized TREN core resulting in a yield of 54%. Lastly, the trityl group on TREN core was deprotected using TFA and further coupled to the azide-terminated squaramide amphiphile giving the final compound **3** in a 56% yield (Scheme S2.3). The

RGD peptides (GGGRGDS, **PEP1**) were then synthesized by solid-phase peptide synthesis with the introduction of 4-pentyonic acid at the N-terminus to provide a reactive handle for bioconjugation. In a final step, the alkyne-ended RGD peptides (**PEP2**) were coupled to molecule **3** by copper(I)-catalyzed azide-alkyne cycloaddition (CuAAc) obtaining the peptide-functionalized squaramide monomers **2** (Scheme S2.4). Monomers **1** and **2** were purified by high performance liquid chromatography (HPLC) prior to self-assembly and gel preparation. Detailed synthetic information can be found in the Supporting Information.

For subsequent 3D cell culture studies, a supramolecular co-assembly protocol was developed to mix both native monomer **1** and RGD-functionalized squaramide monomer **2** (Scheme 2.1A and Figure S2.1). DMSO stock solutions of monomers **1** and **2** were first prepared at concentrations of 25 mM and 5 mM, respectively, followed by mixing in a controlled and tunable manner based on concentration and volume calculations. The DMSO mixture was then exposed to nitrogen flow overnight to obtain a dried film. Afterwards, hydrogel preparation was performed by rehydration in PBS, vortexing, and sonication in an ice-water bath (4˚C, ~ 30 min). Lastly, the obtained transparent solution was incubated at 37˚C for 30 min and equilibrated overnight prior to further use for subsequent experiments.

UV-Vis spectroscopy measurements were performed to understand the effect of the mixing protocol on the functional squaramide-based supramolecular monomers and mixtures at the molecular level. UV-Vis spectra of both monomer **1** and **2** in DMSO showed a single band at 293 nm that consistent with depolymerization of the squaramide monomers (Figure S2.1).[29] After rehydration of the films in PBS, samples containing 2, 5, 10 and 15 mol% of monomer **2** (SQ-2RGD, SQ-5RGD, SQ-10RGD and SQ-15RGD) displayed two absorption bands at 262 nm and 322 nm corresponding to the HOMO−LUMO+1 and HOMO−LUMO transitions of squaramide, respectively (Figure S2.5).[29][31] These bands are identical to the supramolecularly polymerized monomer **1**

on its own suggesting that the mixing of monomer **2** up to 15 mol% does not modify its aggregation at the molecular level. However, further increasing the amount of monomer **2** up to 40 mol%, the HOMO−LUMO+1 and HOMO−LUMO transitions were recorded at 267 nm and 319 nm, pointing to a slightly lower degree of aggregation compared to the native monomer **1**. Together these results suggest DMSO depolymerizes the squaramide monomers, including those with the RGD peptide functionality, and repolymerization is achieved when prepared as co-assemblies in buffered solutions.

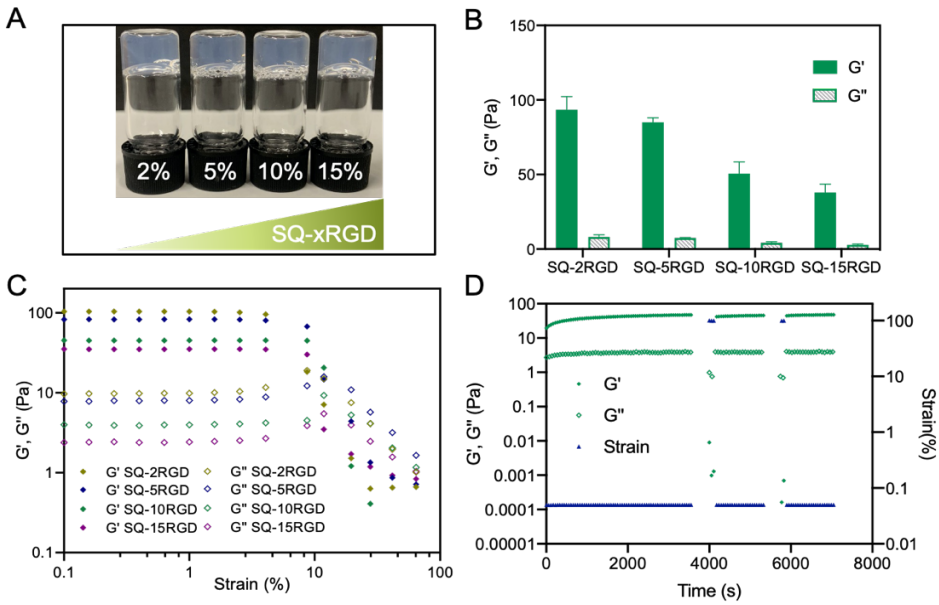

Figure 2.1. A) Gel inversion test of RGD-functionalized squaramide hydrogels (3.1 mM) prepared in PBS (pH 7.4) SQ-xRGD: hydrogels containing x mol% of the monomer **2**. Oscillatory rheology measurements: B) Averaged (N = 3) storage (G') and loss (G'') moduli of hydrogels (3.1 mM, PBS) collected at 37 ± 0.2˚C by a time-sweep measurement with a fixed frequency of 1 Hz and strain of 0.05%. C) Amplitude sweep of RGD-functionalized squaramide hydrogels at 37 ± 0.2˚C with a frequency of 1 Hz and strain from 0.1% to 100%. D) Step-strain measurements of hydrogel SQ-10RGD (3.1 mM) at 37 ± 0.2˚C with a frequency of 1 Hz. Frequency-sweep measurements (from

0.01 to 2 Hz, γ = 0.05%) were performed between application of low (0.05%) and high strain (100%) (Data was not show in this graph).

Physicochemical properties of bioactive squaramide-based supramolecular materials. RGD-functionalized squaramide hydrogels were prepared with various mol% of monomer **2** and their capacity to gelate water was first approximated by a gel inversion test. The total squaramide monomer concentration was maintained at 3.1 mM and the effect of increasing the amount of monomer **2** on co-assembly was examined (0.06 - 0.45 mM RGD peptides) (Figure 2.1A). Non-flowing hydrogel materials were observed up to 15 mol% **2**. The mechanical properties of RGD-functionalized squaramide hydrogels were further assessed quantitatively by performing oscillatory rheology. From the time sweep measurements, hydrogel formation was confirmed with storage moduli (G') being greater loss moduli (G'') for the various samples. Mechanically soft hydrogels were formed for all compositions with a G' lower than 100 Pa; a decreasing trend was observed with the increase of monomer **2** (Figure 2.1B). An amplitude sweep experiment in a range of strain from 0.1% to 100% was used to determine the linear viscoelastic (LVE) region of the various materials. In the case of hydrogels SQ-2RGD and SQ-5RGD, G' and G'' remained constant until 4% strain, whereas for hydrogels SQ-10RGD and SQ-15RGD the exit from the linear regime was observed at 6% strain (Figure 2.1C). Moreover, frequency sweep measurements showed rheological profiles consistent with viscoelastic materials in a frequency range from 0.01 Hz to 2 Hz for all hydrogels up to 15 mol% monomer **2** with G' was greater than G'' by an order of magnitude (Figure S2.2). Lastly, step-strain measurements were executed to evaluate the effect of the added monomer **2** on the self-recovery properties of the supramolecular hydrogels. With the addition of monomer **2** up to 15 mol%, the RGD-functionalized squaramide hydrogels showed similar self-recovery behavior to the previously reported native hydrogel SQ, namely the decrease and inversion of both moduli (G' and G") in response to large amplitude strain, and recovery of the material

to its initial state after its removal over two cycles (Figure 2.1D and S2.3).[31] To better understand the effect of increasing peptide monomer concentration, a sample with a greater mol percentage of monomer **2** (SQ-40RGD) was examined. While G' > G" in time sweep measurements, G' and G" were found to decrease (G' = 1.26 Pa, G" = 0.27 Pa) significantly (Figure S2.4) demonstrating a negative effect of the peptide monomer on gelation properties.

Further insight into the origin of the measured rheological properties was provided by cryogenic transmission electron microscopy (cryo-TEM). As shown in Figure S2.5, flexible, micron-length nanofibers were observed for SQ-10RGD hydrogels (3.1 mM, PBS) indistinguishable from the SQ hydrogels with a slightly smaller width of 4.8 ± 0.4 nm. Because of the difference in gel rheological properties with increasing peptide concentration, we further examined the effect of increasing monomers **2** on the nanoscale structure of the squaramide-based supramolecular polymer fibres. Similarly, entangled fibers were observed in SQ-40RGD solution, with comparable fibre width of 4.6 ± 0.6 nm, indicating that the co-assembly of monomer **2** was comparable at the nanoscale level (Figure S2.6).

Encapsulated NIH3T3-mCherry-LifeAct cells recognize RGD peptides in the supramolecular network and migrate. RGD peptides bind cell-surface integrins and through these receptors they stimulate actin polymerization upon cell attachment, facilitating cell spreading and contractile movements.[34,35] Therefore, before applying the co-assembled supramolecular polymers for 3D cell culture, we first investigated whether cells can recognize and respond to the RGD peptides presented by the squaramide-based polymers. Consequently, NIH3T3-LifeAct-mCherry cells transduced to express m-Cherry-labelled actin were encapsulated and cultured in squaramide-based hydrogels. Branched, large protrusions (pseudopods) tipped with actin rich filopodia outside of the cell body were observed in the SQ-10RGD and SQ-15RGD hydrogels, as previously reported in ECM-derived collagen hydrogels (Video S2.1 and

S2.2). [36,37] Additional to protrusion formation, cell migration was also observed indicating extensive cell-hydrogel interactions in 3D. In contrast, cells in native SQ hydrogels displayed a highly rounded morphology, with minimal spreading and were rarely observed to migrate (Video S2.3). This indicates that the inclusion of RGD peptides is essential for cell spreading and migration in the squaramide-based supramolecular hydrogel. To further quantify cell spreading efficiency as a function of RGD concentration, cells were cultured in squaramide-based hydrogels for 24h and then subsequently imaged (2.5 µm stepped z-stacks). Using image analysis, all cells in each imaged volume slice were recognized and a local two-dimensional z-projection was made around each cell to individually analyze and extract appropriate cell edges. The cell edges were used to calculate morphological parameters such as cell area, perimeter, circularity, summated skeleton branch length, min- and max Feret diameter and aspect ratio. Cells tended to spread significantly more in RGD-functionalized squaramide hydrogels, as shown in Figure 2.2A and S2.8, and quantitatively displayed larger cell areas and longer perimeters in comparison to those in SQ ($P<0.001$, Figure 2.2B and S2.8). Consistently, cell circularity was much lower in RGD-functionalized hydrogels, calculated to be 0.726, 0.619 and 0.694 for cells in SQ-5RGD, SQ-10RGD and SQ-15RGD, respectively, in comparison to that in SQ (0.903). To gather further information of cell protrusion formation, the cell shapes were skeletonized, the Feret diameters were measured and aspect ratios were calculated. Significantly larger Feret diameters were observed for cells cultured in RGD-functionalized hydrogel in comparison to that in SQ ($P<0.001$), supporting cell elongation within the RGD-presenting materials. Among them, the lowest aspect ratio was calculated from cells cultured in SQ-10RGD, as shown in Figure 2.2B. Moreover, the summated skeleton branch lengths for each cell, used as an indicator of protrusion length, was found to be 22.4 ± 3.3 µm in SQ-10RGD, a 4-fold increase over that in SQ (5.2 ± 1.2 µm) (Figure 2.2B and Table S2.1). Taken together, the cells displayed a more spread and branched morphology with highly dynamic actin polymerization along the cell membrane,

especially at the end of branched protrusions as a consequence of interaction with RGD peptides in the bioactive squaramide-based hydrogels as previously reported in literature powering cell migration within the hydrogels.[34]

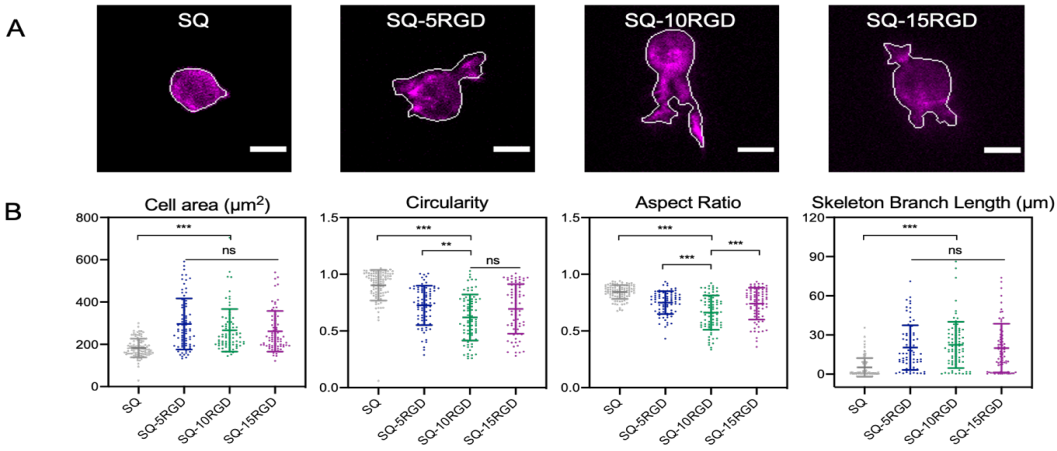

Figure 2.2. A) Representative images of NIH3T3-LifeAct-mCherry cells cultured within squaramide-based hydrogels after 24h, scale bar: 10 µm; B) Quantitative analysis of mean projected cell area, perimeter, circularity and skeleton branch length from NIH3T3-mCherry-LifeAct cells cultured for 24h within squaramide-based hydrogel. For each data set, 74-100 cells were analyzed. The mean and standard deviation are marked within the graphs. (*P< 0.05, **P< 0.01, ***P< 0.001 one-way Anova)

Impact of the RGD-functionalized squaramide hydrogels on HepG2 spheroids formation and growth. The aggregation of HepG2 cells into spheroidal structures that resemble their presentation *in vivo* provide a versatile tool to investigate hepatic metabolism, stemness, cancer and chemical safety assessment.[38–40] Because bioactive squaramide-based hydrogels containing an RGD-ligand support active cell migration and proliferation, we became interested if these materials would further enable the self-assembly of HepG2 cells into spheroids and facilitate their differentiation. A recent study demonstrated that low concentrations of RGD peptide (~0.2 mM) may be not sufficient for human liver organoid proliferation,[17] thus bioactive squaramide-based hydrogels were examined at 0.3 and 0.45 mM RGD with hydrogels lacking the RGD

monomer **2** and Matrigel being used as controls. As expected, HepG2 cells grew within SQ-10RGD hydrogel by starting from single cells (1 x 10^5 cells/mL) on day 3 to small aggregates on day 7, and finally, rounded spheroids on day 14 that continued to increase slightly in size until day 21 (Figure 2.3A). HepG2 cells grew similarly in SQ and SQ-15RGD hydrogels forming compact spheroids on day 14. As a control, spheroids cultured in Matrigel, the current gold standard cell culture matrix, displayed a slightly less compacted morphology throughout the culture period. Spheroid diameter was measured to quantitatively compare the performance of the supramolecular matrix against Matrigel in generating these morphological structures. Increase in the spheroidal diameter over the 21-day culture period was confirmed by plotting the measured size distributions in Figure 2.3B. Cellular aggregates of 58 ± 18, 69 ± 17 and 64 ± 17 µm were obtained on day 7 in SQ, SQ-10RGD and SQ-15RGD hydrogels, and grew into spheroids with diameters of 116 ± 40 µm, 112 ± 32 µm, and 129 ± 49 µm on day 14, respectively. From day 14 to day 21, spheroids in SQ and SQ-10RGD hydrogels were comparable in diameter, 127 ± 30 µm and 119 ± 30 µm, respectively. Conversely, HepG2 cells cultured in Matrigel formed spheroids with average diameter of 102 ± 31 µm on day 7 and increased in size to 128 ± 40 µm on day 14 and 122 ± 22 µm on day 21, respectively. From all hydrogel conditions tested, the HepG2 spheroids in SQ-15RGD hydrogel displayed highest diameters at 163 ± 66 µm on day 21, yet remained below 200 µm providing sufficient oxygen diffusion throughout the spheroid.[41,42] This increase in spheroid diameter in the squaramide-based hydrogels suggests proliferation of HepG2 cells during the culture period.

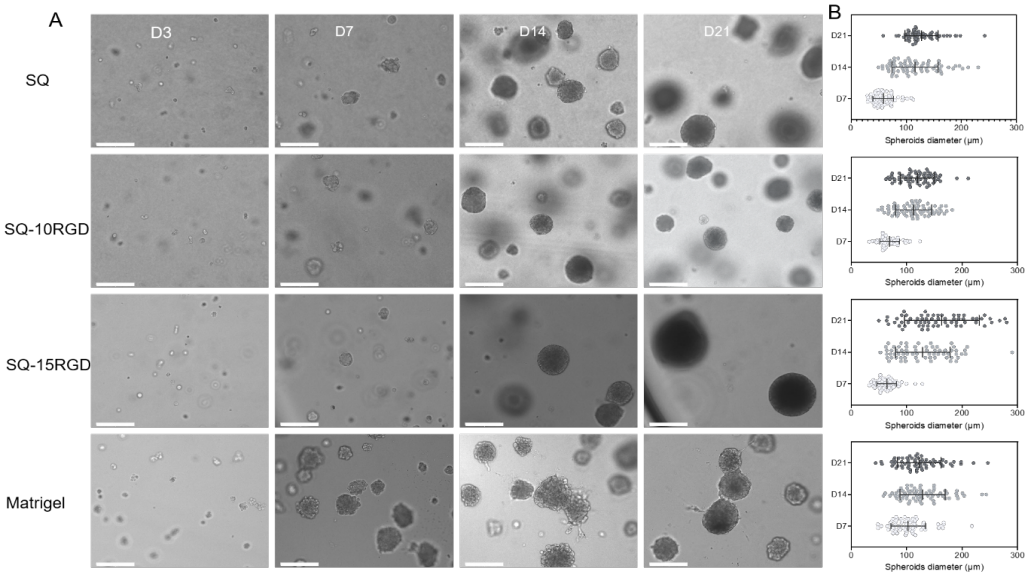

Figure 2.3. 3D HepG2 cell culture in squaramide-based hydrogels over a 21-day period. A) Bright field images taken on day 3 (D3), 7 (D7), 14 (D14) and 21 (D21). Scale bar: 200 µm. B) Size distribution of HepG2 spheroids during the 21-day culture period in squaramide-based hydrogels and Matrigel (LOT5215008). For each group, 66 spheroids were measured in Fiji by manually drawing a straight line horizontally (angle < 3°). The means and standard deviations are marked inside the graphs.

Proliferation of the HepG2 spheroids cultured in the bioactive squaramide-based hydrogels were further assessed by their imaging with 5-ethynyl-2'-deoxyuridine (EdU). In order to facilitate their staining, the HepG2 spheroids were released from the hydrogels by dilution of the supramolecular matrix at pre-determined time points, imaged and analyzed quantitatively for EdU positive cells. Proliferative cells were observed to be randomly distributed throughout the HepG2 spheroids suggesting that sufficient nutrient diffusion through squaramide-based hydrogels and the spheroids occurs during culture (Figure 2.4B). In the SQ hydrogel lacking RGD peptides, HepG2 cells displayed comparable proliferative activity based on the EdU-positive percentage over the culture period, namely 18 ± 16.2% on day 7, 8 ± 6.4% on day 14 and 10 ± 6.2% on day 21, respectively. In the RGD-functionalized squaramide-based hydrogel, HepG2

cells were found to proliferate actively at the beginning of the culture period with the measured percentage of EdU-positive cells on day 7 being 25 ± 9.9% and 45 ± 8.4% in SQ-10RGD and SQ-15RGD hydrogels, respectively. Notably, HepG2 cells cultured in Matrigel displayed an EdU-positive percentage of 41 ± 12.8% on day 7 that declined to 7 ± 5.0% on day 14 and eventually ended at 6 ± 5.2%. As the culture progressed from day 7 to 14 in both Matrigel and squaramide hydrogels, a dramatic decrease in the percentage of EdU-positive cells was measured pointing to decreased proliferation and suggestive of their differentiation. SQ-15RGD showed the highest proliferation of the HepG2 cells in comparison to Matrigel, SQ and SQ-10RGD hydrogels on day 14, and is consistent with the significantly larger measured diameter of the spheroids. In the case of SQ-10RGD and SQ-15RGD slightly increased proliferation of 13 ± 9.2% and 14 ± 2.8%, respectively, was recorded at the end of culture and is slightly greater than for the SQ monomer (10 ± 6.2%) (Figure 2.4C and S2.10). Besides the early active cell proliferation, HepG2 spheroids cultured within squaramide-based hydrogels were largely calcein AM positive with few dead cells confirming high cell viability and the absence of a necrotic core during the culture (Figure 2.4A and S2.9). Collectively, RGD-functionalized squaramide hydrogels support the formation of HepG2 spheroids with a size greater than 150 µm initially showing active cell proliferation that decreases towards the end of the 21-day culture period. The initial increased cell proliferation could further affect HepG2 cell differentiation resulting in the induction of metabolic enzymes and expression of hepatic markers.

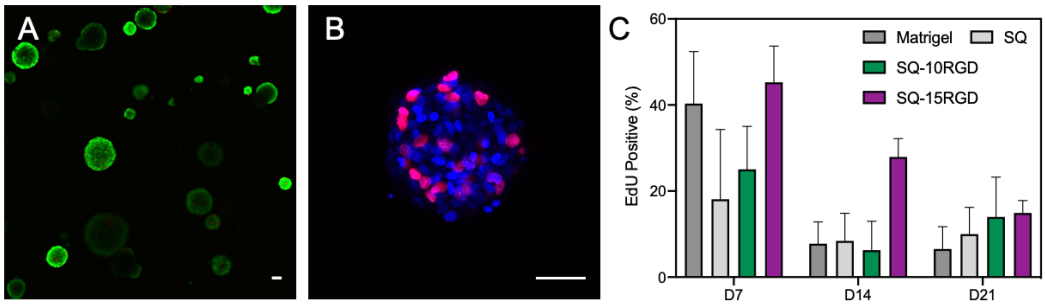

Figure 2.4. A) Cell viability assay of HepG2 spheroids cultured in SQ-10RGD hydrogel for 21 days stained by a LIVE/DEAD assay with calcein AM (viable cells, *green*) and propidium iodide (PI) (dead cells, *red*). B) EdU staining of released HepG2 spheroids cultured in SQ-10RGD hydrogels. Proliferating cells were labelled with EdU-Alexa fluor 594 (*red*) and cell nuclei were stained with Hoechst 33342 (*blue*). Scale bar: 50 µm. C) Quantification of EdU percentage in HepG2 spheroids cultured within Matrigel, SQ, SQ-10RGD and SQ-15RGD hydrogels. N=3.

Improved metabolic enzyme and hepatic marker expression of HepG2 spheroids after culture in RGD-functionalized squaramide hydrogels. HepG2 cells showed spheroid formation in SQ, SQ-10RGD and SQ-15RGD hydrogels with high cell viability and increased proliferation in the bioactive gels early on in the culture. However, it was previously demonstrated that the formation of these *in vivo* mimicking structures in 3D in peptide nanofiber hydrogel-based does not necessarily result in the distinct expression of metabolizing enzymes by RT-PCR. [11] Consequently, to assess the bioactive squaramide-based materials on the maturation of HepG2 spheroids, RT-PCR experiments were performed to evaluate the expression of a panel of metabolic enzymes and hepatic markers. As hypothesized, the HepG2 spheroids showed higher expression of various phase I and II metabolic enzymes and drug transporters in the 3D cultures performed in comparison to 2D (Figure 2.5A). mRNA expression of CYP1A2 measured from cells cultured in 3D in the Matrigel matrix control was over 40-fold in

comparison to the 2D condition. Similarly, both CYP2C19 and CYP3A4 showed an over 10-fold enhancement in 3D in comparison to 2D culture and CYP2C9 and CYP2D6 expression was increased 3- and 4.5-fold, respectively. Additionally, mRNA levels of the phase II xenobiotic-metabolizing enzymes UGT1A1 increased by over 45-fold and expression of hepatic markers HNF4a and NCTP were also found to increase over two times during hydrogel-based culture. The overall higher gene expression of metabolic enzymes and hepatic markers are consistent with previous reports that the formation of compact spheroids in 3D are beneficial for hepatocyte maturation.[8,12] When compared against the HepG2 spheroids cultured in Matrigel, cells cultured in the bioactive squaramide-based hydrogel SQ-10RGD in 3D displayed significantly higher mRNA expression in case of CYP2D6 (4.7-fold), CYP2C19 (4.2-fold), CYP2C9 (3.6-fold), and NCTP (4.9-fold) and comparable level in CYP1A2 (1.8-fold), UGT1A1 (1.4-fold), CYP3A5 (1.5-fold), and HNF4a (1.5-fold). These results strongly suggest that the fully synthetic bioactive squaramide-based hydrogel can function well as an alternative matrix of Matrigel for HepG2 culture. More importantly, in comparison to the control SQ hydrogel, cells were cultured within SQ-10RGD hydrogel displayed significant improved mRNA expression of NCTP (**$P<0.01$) and advantageous expression of CYP2D6, CYP2C19, CYP1A2, HNF4a and UGT1A1, confirming the importance of incorporating bioactive peptides to further stimulate differentiation. The overall enhancement in gene expression in HepG2 spheroids by introducing RGD peptides is less obvious than that of transferring cells from 2D to 3D culture, implying cell-cell contact plays a critical role in their differentiation rather than cell-matrix interactions, at least under the tested cell seeding condition.[43,44] However, matrix proteins have been earlier demonstrated to play an important role in the assembly of HepG2 spheroids and this can also explain the subtle increases between the RGD and native conditions.[45]

To further probe the differentiation of spheroids in 3D in squaramide-based hydrogels, immunostaining of albumin and bile canaliculi-like structures through MRP2 was performed (Figure 2.5B and S2.12).[8,9] Albumin expression was present in both Matrigel and squaramide-based hydrogels culture systems. In contrast, MRP2 expression was localized in actin-rich regions suggesting bileduct formation, with a more intense staining in hepG2 spheroids that were cultured in SQ and SQ-10RGD hydrogels in comparison to those in Matrigel. Conversely, MRP2 staining was hardly observed in spheroids from the SQ-15RGD hydrogel that had the largest aggregates. Moreover, β-catenin expression at the borders of the hepG2 spheroids indicate that independent of the gel used the cells establish basal-lateral polarity.

To summarize, the quantified mRNA expression of metabolic enzymes and hepatic makers from HepG2 cells cultured in squaramide-based hydrogels confirms our hypothesis that our bioactive and chemical-defined synthetic matrix can be an alternative to Matrigel to support their 3D cell culture, and importantly, incorporation of cell adhesion motifs (RGD) enhanced cell proliferation and thus improve cell hepatic makers expression in 3D. Still, as observed from real-time PCR analysis in Figure 2.5A, some variation between biological replicates was observed in the gene expression, which was comparable to that of Matrigel from different lots (Figure S2.11), especially with respect to CYP1A2 and UGT1A1 expression. Likely these variations are due to the non-uniform size of the formed spheroids in 3D within the materials that influence the metabolic activity of the HepG2 cells and further refinement of the overall synthetic matrix composition and/or culture protocol will require methods to control spheroid size prior to cell culture within the materials.[46,47] Gratifyingly, this fully synthetic supramolecular squaramide-based matrix can support HepG2 early proliferation and differentiation with the expression of several key metabolic enzymes and hepatic markers to a greater extent than Matrigel.

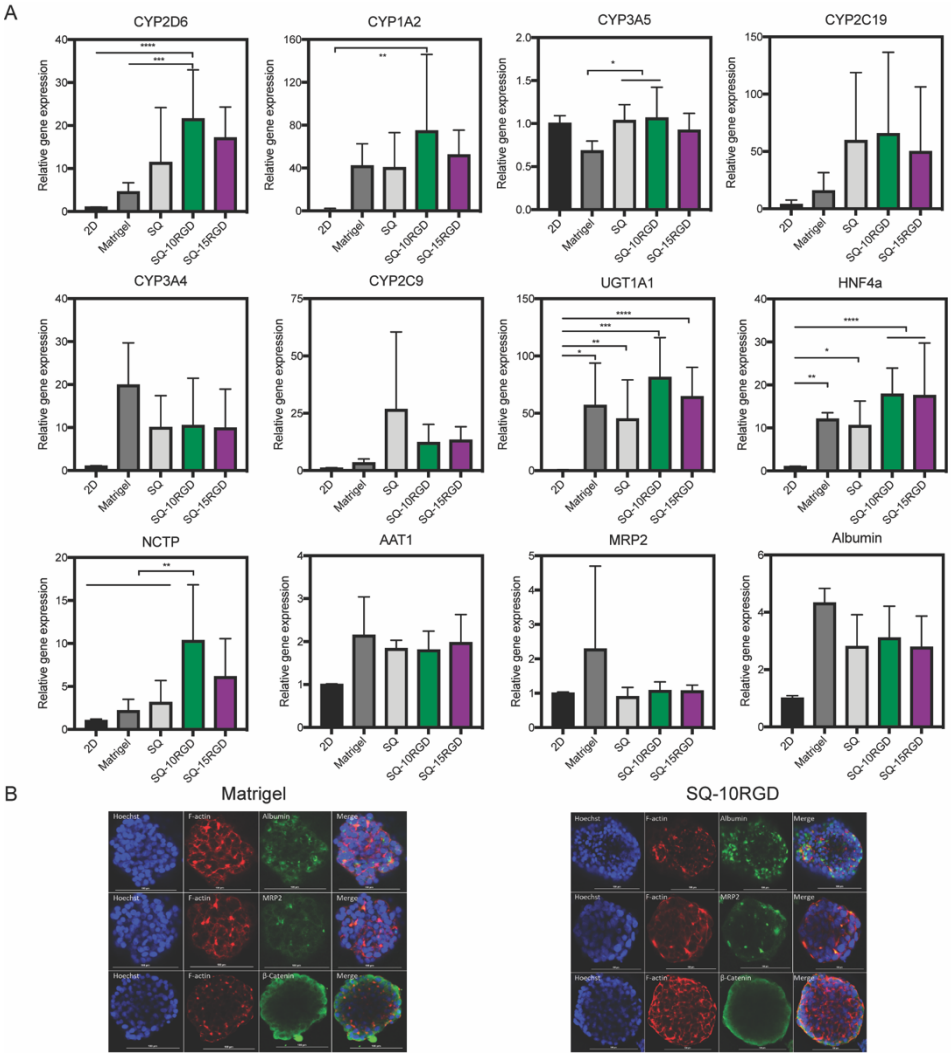

Figure 2.5. A) Real-time PCR analysis of metabolic enzymes and liver-specific markers in 2D and 3D culture. Fold change gene expression levels of spheroids after a 21-day 3D culture compared to 3-day 2D cultured HepG2 cells. Data are collected from three biological replicates (*P< 0.05, **P< 0.01, ***P< 0.001, ****P< 0.0001 one-way Anova). B) Immunofluorescence staining of the liver markers albumin (upper row), MRP2 (middle row) and β-catenin (lower row) in green, and counter-stained with F-actin rhodamine phalloidin (*red*) and the nuclear stain Hoechst33342 (*blue*). Merged channels consist of all three stainings. Scale bar: 100 µm.

2.4 Conclusions

A fully synthetic and bioactive squaramide-based supramolecular hydrogel material bearing RGD peptides was prepared for 3D cell culture. The co-assembly approach of the synthesized monomers **1** and **2** to prepare the hydrogel materials enables tuning of the peptide concentration within the materials. The RGD-functionalized squaramide-based hydrogels were demonstrated to be optically clear, mechanically soft and self-recovering. Encapsulated cells recognize the RGD peptides (0.15-0.45 mM) embedded within the network by spreading, initiating actin polymerization and inducing cell migration in 3D. These RGD-functionalized squaramide hydrogels support the growth of HepG2 cells into compact spheroids with high cell viability, active proliferation and differentiation, resulting in significantly higher gene expression of metabolic enzymes and hepatic markers as well as the formation of liver structures and basal-lateral polarization. This chemically well-defined monomers enable a facile preparation protocol through their co-assembly, cytocompatibility and capacity to trigger differentiation on par with natural materials challenging Matrigel, the current gold standard for liver spheroid culture, but can be more broadly applied in other areas of tissue culture where cell-matrix interactions are necessary to facilitate various aspects of cell behaviour. Moreover, their self-recovering properties enable gentle spheroid release which can be used for downstream analysis. Finally, the terminal azide on squaramide monomer **3** leaves the door open to further chemically modification and crosslinks for future biomaterials designs, e.g. tuning the stiffness of supramolecular network in a straightforward manner to provide a closer *in vivo* mimicking microenvironment for cells.

2.5 References

[1] O. A. Almazroo, M. K. Miah, R. Venkataramanan, *Clin. Liver Dis.* **2017**, *21*, 1.

[2] R. J. Andrade, G. P. Aithal, E. S. Björnsson, N. Kaplowitz, G. A. Kullak-Ublick, D.

Larrey, T. H. Karlsen, *J. Hepatol.* **2019**, *70*, 1222.

[3] G. A. Kullak-Ublick, R. J. Andrade, M. Merz, P. End, A. Benesic, A. L. Gerbes, G. P. Aithal, *Gut.* **2017**, *66*, 1154.

[4] J. A. Heslop, C. Rowe, J. Walsh, R. Sison-Young, R. Jenkins, L. Kamalian, R. Kia, D. Hay, R. P. Jones, H. Z. Malik, S. Fenwick, A. E. Chadwick, J. Mills, N. R. Kitteringham, C. E. P. Goldring, B. Kevin Park, *Arch. Toxicol.* **2017**, *91*, 439.

[5] C. Rowe, D. T. Gerrard, R. Jenkins, A. Berry, K. Durkin, L. Sundstrom, C. E. Goldring, B. K. Park, N. R. Kitteringham, K. P. Hanley, N. A. Hanley, *Hepatology* **2013**, *58*, 799.

[6] H. H. J. Gerets, K. Tilmant, B. Gerin, H. Chanteux, B. O. Depelchin, S. Dhalluin, F. A. Atienzar, *Cell Biol. Toxicol.* **2012**, *28*, 69.

[7] C. S. Hughes, L. M. Postovit, G. A. Lajoie, *Proteomics.* **2010**, *10*, 1886.

[8] S. C. Ramaiahgari, M. W. Den Braver, B. Herpers, V. Terpstra, J. N. M. Commandeur, B. Van De Water, L. S. Price, *Arch. Toxicol.* **2014**, *88*, 1083.

[9] S. Hiemstra, S. C. Ramaiahgari, S. Wink, G. Callegaro, M. Coonen, J. Meerman, D. Jennen, K. van den Nieuwendijk, A. Dankers, J. Snoeys, H. de Bont, L. Price, B. van de Water, *Arch. Toxicol.* **2019**, *93*, 2895.

[10] K. R. Stevens, J. S. Miller, B. L. Blakely, C. S. Chen, S. N. Bhatia, *J. Biomed. Mater. Res. -Part A* **2015**, *103*, 3331.

[11] M. M. Malinen, H. Palokangas, M. Yliperttula, A. Urtti, *Tissue Eng. - Part A* **2012**, *18*, 2418.

[12] H. Jeon, K. Kang, S. A. Park, W. D. Kim, S. S. Paik, S. H. Lee, J. Jeong, D. Choi, *Gut Liver* **2017**, *11*, 121.

[13] N. S. Bhise, V. Manoharan, S. Massa, A. Tamayol, M. Ghaderi, M. Miscuglio, Q. Lang, Y. S. Zhang, S. R. Shin, G. Calzone, N. Annabi, T. D. Shupe, C. E. Bishop, A. Atala, M. R. Dokmeci, A. Khademhosseini, *Biofabrication* **2016**, *8*, 014101.

[14] J. Christoffersson, C. Aronsson, M. Jury, R. Selegård, D. Aili, C. F. Mandenius, *Biofabrication* **2019**, *11*, 015013.

[15] M. Krüger, L. A. Oosterhoff, M. E. van Wolferen, S. A. Schiele, A. Walther, N. Geijsen, L. De Laporte, L. J. W. van der Laan, L. M. Kock, B. Spee, *Adv. Healthc. Mater.* **2020**, *9*, 1901658.

[16] B. J. Klotz, L. A. Oosterhoff, L. Utomo, K. S. Lim, Q. Vallmajo-Martin, H. Clevers, T. B. F. Woodfield, A. J. W. P. Rosenberg, J. Malda, M. Ehrbar, B. Spee, D. Gawlitta, *Adv. Healthc. Mater.* **2019**, *8*, 1900979.

[17] S. Ye, J. W. B. Boeter, M. Mihajlovic, F. G. van Steenbeek, M. E. van Wolferen, L. A. Oosterhoff, A. Marsee, M. Caiazzo, L. J. W. van der Laan, L. C. Penning, T. Vermonden, B. Spee, K. Schneeberger, *Adv. Funct. Mater.* **2020**, *2000893.*

[18] G. Sorrentino, S. Rezakhani, E. Yildiz, S. Nuciforo, M. H. Heim, M. P. Lutolf, K. Schoonjans, *Nat. Commun.* **2020**, *11*, 1.

[19] M. Kumar, B. Toprakhisar, M. Van Haele, A. Antoranz, R. Boon, bioRxiv **2020**. 280883.

[20] M. J. Webber, E. A. Appel, E. W. Meijer, R. Langer, *Nat. Mater.* **2015**, *15*, 13.

[21] C. L. Maikawa, A. A. A. Smith, L. Zou, G. A. Roth, E. C. Gale, L. M. Stapleton, S. W. Baker, J. L. Mann, A. C. Yu, S. Correa, A. K. Grosskopf, C. S. Liong, C. M. Meis, D. Chan, M. Troxell, D. M. Maahs, B. A. Buckingham, M. J. Webber, E. A. Appel, *Nat. Biomed. Eng.* **2020**, *4*, 507.

[22] D. Straßburger, N. Stergiou, M. Urschbach, H. Yurugi, D. Spitzer, D. Schollmeyer, E. Schmitt, P. Besenius, *ChemBioChem.* **2018**, *19*, 912.

[23] S. Spaans, P. P. K. H. Fransen, M. J. G. Schotman, R. Van Der Wulp, R. P. M. Lafleur, S. G. J. M. Kluijtmans, P. Y. W. Dankers, *Biomacromolecules.* **2019**, *20*, 2360.

[24] Y. Wang, K. M. Dillon, Z. Li, E. W. Winckler, J. B. Matson, *Angew. Chemie.* **2020**, 16841.

[25] J. Ramos, S. Arufe, H. Martin, D. Rooney, R. B. P. Elmes, A. Erxleben, R. Moreira, T. Velasco-Torrijos, *Soft Matter.* **2020**, *16*, 7916.

[26] L. A. Marchetti, L. K. Kumawat, N. Mao, J. C. Stephens, R. B. P. Elmes, *Chem.* **2019**, *5*, 1398.

[27] C. López, M. Ximenis, F. Orvay, C. Rotger, A. Costa, *Chem. - A Eur. J.* **2017**, *23*, 7590.

[28] E. Castellanos, B. Soberats, S. Bujosa, C. Rotger, R. De Rica, A. Costa, *Biomacromolecules.* **2020**, *21*, 966.

[29] V. Saez Talens, P. Englebienne, T. T. Trinh, W. E. M. Noteborn, I. K. Voets, R. E.

Kieltyka, *Angew. Chemie.* **2015**, *127*, 10648.

[30] V. Saez Talens, D. M. M. Makurat, T. Liu, W. Dai, C. Guibert, W. E. M. Noteborn, I. K. Voets, R. E. Kieltyka, *Polym. Chem.* **2019**, *10*, 3146.

[31] C. Tong, T. Liu, V. Saez Talens, W. E. M. Noteborn, T. H. Sharp, M. M. R. M. Hendrix, I. K. Voets, C. L. Mummery, V. V. Orlova, R. E. Kieltyka, *Biomacromolecules.* **2018**, *19*, 1091.

[32] V. Saez Talens, G. Arias-Alpizar, D. M. M. Makurat, J. Davis, J. Bussmann, A. Kros, R. E. Kieltyka, *Biomacromolecules.* **2020**, *21*, 1060.

[33] K. D. Park, R. Liu, H. Kohn, *Chem. Biol.* **2009**, *16*, 763.

[34] C. H. Yu, J. B. K. Law, M. Suryana, H. Y. Low, M. P. Sheetz, *Proc. Natl. Acad. Sci. U. S. A.* **2011**, *108*, 20585.

[35] P. T. Caswell, T. Zech, *Trends Cell Biol.* **2018**, *28*, 823.

[36] K. M. Hakkinen, J. S. Harunaga, A. D. Doyle, K. M. Yamada, *Tissue Eng. - Part A* **2011**, *17*, 713.

[37] H. Liu, M. Wu, Y. Jia, L. Niu, G. Huang, F. Xu, *NPG Asia Mater.* **2020**, *12*, 45.

[38] F. van Zijl, W. Mikulits, *World J. Hepatol.* **2010**, *2*, 1.

[39] S. E. Kim, S. Y. An, D. H. Woo, J. Han, J. H. Kim, Y. J. Jang, J. S. Son, H. Yang, Y. P. Cheon, J. H. Kim, *Stem Cells Dev.* **2013**, *22*, 1818.

[40] D. S. Reynolds, K. M. Tevis, W. A. Blessing, Y. L. Colson, M. H. Zaman, M. W. Grinstaff, *Sci. Rep.* **2017**, *7*, 1.

[41] A. Asthana, W. S. Kisaalita, *Drug Discov. Today* **2012**, *17*, 810.

[42] X. Cui, Y. Hartanto, H. Zhang, *J. R. Soc. Interface* **2017**, *14*, 20160877.

[43] T. A. Brieva, P. V. Moghe, *Biotechnol. Bioeng.* **2004**, *85*, 283.

[44] R. Z. Lin, L. F. Chou, C. C. M. Chien, H. Y. Chang, *Cell Tissue Res.* **2006**, *324*, 411.

[45] R. Akasov, D. Zaytseva-Zotova, S. Burov, M. Leko, M. Dontenwill, M. Chiper, T. Vandamme, E. Markvicheva, *Int. J. Pharm.* **2016**, *506*, 148.

[46] Y. Miyamoto, M. Ikeuchi, H. Noguchi, T. Yagi, S. Hayashi, *Cell Med.* **2015**, *8*, 47.

[47] T. Nishikawa, Y. Tanaka, M. Nishikawa, Y. Ogino, K. Kusamori, N. Mizuno, Y. Mizukami, K. Shimizu, S. Konishi, Y. Takahashi, Y. Takakura, *Biol. Pharm. Bull.*

2017, *40*, 334.

2.6 Supporting Information

2.6.1 Materials

All chemicals used in the synthesis of monomers **1** and **2** were purchased from Sigma Aldrich and used without further purification. Fmoc-protected amino acids for peptide synthesis were obtained from Novabiochem. Dulbecco's modified eagle cell culture medium (DMEM), DMEM/F12, fetal calf serum, penicillin, streptomycin, GlutaMAX, pyruvate and trypsin were received from Thermo Fisher Scientific. Angiogenesis slides (15-well) were obtained from Ibidi. Dulbecco's Phosphate Buffered Saline (DPBS), calcein AM (AM = acetoxymethyl), and propidium iodide (PI) were acquired from Sigma-Aldrich. The Click-iT EdU Imaging kit was purchased from Invitrogen. Total RNA Isolation (TRI) Reagent was from Sigma-Aldrich. RevertAid H Minus First Strand cDNA Synthesis Kit and PowerUp™ SYBR™ Green Master Mix were obtained from Thermo Fisher Scientific.

2.6.2 Instruments

All synthetic intermediates were characterized by ^{1}H-NMR and ^{13}C-NMR collected on a Bruker DMX-400 operating at 400 MHz and 100 MHz at 298 K, respectively. LC-MS analysis was performed on a TSQ Quantum Access MAX system equipped with a Gemini 3 µm C18 110 Å 50×4.60 mm column (UV detection at 214 nm and 254 nm, mass detection range: 160 to 3000 (Da)). The mobile phase consisted of a gradient of 10-90% of H_2O-CH_3CN with 0.1% trifluoroacetic acid (TFA) over 13.5 minutes. HPLC purification of the monomers was executed on setup equipped with C18 column. A gradient from 10%-90% CH_3CN (0.1% TFA) in H_2O (0.1% TFA) over 15 min at a flow rate of 12 mL/min was used. Matrix-assisted laser desorption ionization-time-of-flight mass spectra (MALDI-TOF-MS) were collected on a Bruker Microflex LRF mass spectrometer on a ground steel target plate. A linear positive-ion mode with an α-cyano-4-

hydroxycinnamic acid matrix (5 mg/ml in CH_3CN/ H_2O 1:1 v/v) was used. High resolution mass spectra (HR-MS) were collected on a Thermo Fisher LTQ Orbitrap mass spectrometer equipped with an electrospray ion source in positive mode (resolution R = 60000). The spectra were collected by direct injection of samples (2 µM in H_2O-CH_3CN 50/50 v/v) and recorded with a mass range of 150-2000 and dioctylpthalate (m/z = 391.28428) as a "lock mass". Oscillatory rheology experiments were executed on a Discovery HR-2 hybrid rheometer using a cone-plate geometry (40 mm, 1.995°) at 37 ± 0.2 °C with a peltier-based temperature controller and solvent trap. Cryo-TEM images were acquired on a Tecnai F12 (FEI Company, The Netherlands) equipped with a field emission gun operating at 120 keV using a Gatan UltraScan charge-couple device (CCD) camera (Gatan company, Germany) with a defocus between −6 and −9 µm. UV absorption spectra were recorded on a Cary 300 Bio UV-V~~v~~is spectrometer, scanning from 200 nm to 400 nm with 1 nm intervals with a scan rate of 120 nm/min. Bright field images were taken on an EVOS FL AUTO2 equipped with temperature and a CO_2 gas controller. Confocal fluorescent images were acquired on Leica TCS SP8 confocal laser scanning microscope equipped with a 10× air objective and a 40× oil immersion objective. Images were processed using the Fiji Image J software. Real-time polymerase chain reaction (RT-PCR) measurements were performed on a QuantStudio™ 6 and 7 Flex Real-Time PCR (Applied Biosystems®).

2.6.3 Synthetic procedures

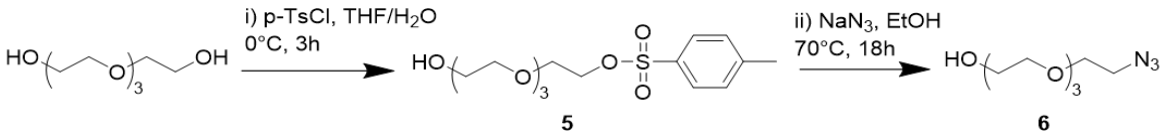

Scheme S2.1. Synthesis route for compound **6**.[1]

Compound 5. An aqueous NaOH (1.53 g, 38.25 mmol) solution (10 mL) was added to a solution of tetraethylene glycol (45.00 g, 231.68 mmol) dissolved in tetrahydrofuran

(THF) (10 mL) at 0°C. *p*-Toluenesulfonyl chloride (4.31 g, 22.61 mmol) dissolved in THF (30 mL) was added dropwise to the reaction mixture over 1h. After stirring at 0 °C for 2h, the reaction mixture was poured onto ice water (150 mL) and extracted 3x with DCM (200 mL). The combined organic layers were then washed with water (2 x 100 mL), dried with $MgSO_4$, and concentrated on a rotary evaporator. The crude was purified by column chromatography (petroleum ether (PE) /ethyl acetate (EtOAc) 60/40-0/100 v/v). The product was concentrated by rotary evaporation and dried in vacuum oven overnight to obtain a light yellow oil. Yield: 58%, 4.55 g. ^{1}H-NMR ($CDCl_3$, 400 MHz): 7.81-7.77 (d, 2H), 7.36-7.34 (d, 2H), 4.18-4.14 (m, 2H), 3.71-3.59 (m, 14H), 2.86 (s, 1H), 2.45 (s, 3H). ^{13}C-NMR ($CDCl_3$, 100 MHz): 144.88, 132.94, 129.87, 127.96, 72.51, 70.69, 70.63, 70.44, 70.30, 69.33, 68.66, 61.65, 21.65.

Compound 6. The obtained compound **5** (5.85 g, 16.80 mmol) was dissolved in ethanol (120 mL) and NaN_3 (2.79 g, 42.92 mmol) was added while stirring. The reaction mixture was then refluxed at 70 °C for 18h and water (100 mL) was added prior to concentrating the reaction mixture on a rotary evaporator. The concentrated solution was extracted with EtOAc (3 × 100 mL). The combined organic phases were dried over Na_2SO_4 and evaporated in vacuum to obtain compound **6** as a yellow oil. Yield: 77%, 2.83 g. ^{1}H-NMR ($CDCl_3$, 400 MHz): 3.71-3.58 (m, 14H), 3.40-3.36 (m, 2H), 3.13 (br s, 1H). ^{13}C-NMR ($CDCl_3$, 100 MHz): 72.47, 70.57, 70.54, 70.47, 70.21, 69.95, 61.51, 50.57.

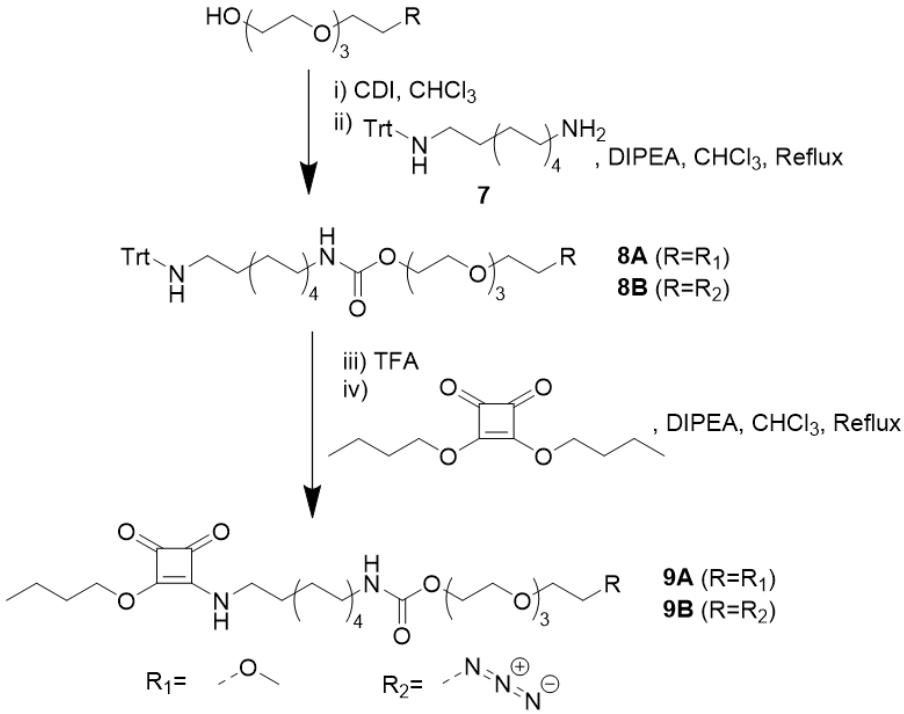

Scheme S2.2. Synthetic route for compound **9A** and **9B**.

Compound 7.[2] Triphenylmethyl chloride (2.73 g, 9.82 mmol) was dissolved in dichloromethane (DCM) (100 mL), added dropwise over 2h into a cooled (0°C), stirred solution of 1,10-diaminodecane (6.66 g, 38.65 mmol) in DCM (150 mL) and left to stir overnight at room temperature. Subsequently, the reaction mixture was concentrated by rotary evaporation and EtOAc (200 mL) was added before extracting with water (3 x 100 mL). The organic layer was collected, dried with anhydrous Na_2SO_4 and concentrated on a rotary evaporator. The crude was then purified by column chromatography (PE/EtOAC/methanol (MeOH) 50/50/0-50/50/20 v/v/v) and concentrated by rotary evaporation and dried in vacuum oven overnight to obtain a yellow oil. Yield: 79%, 3.20 g. ^{1}H-NMR ($CDCl_3$, 400 MHz): 7.51-7.48 (d, 6H), 7.26-7.22 (t, 6H), 7.19-7.12 (t, 3H), 2.70-2.64 (t, 2H), 2.16-2.10 (t, 2H), 1.51-1.44 (m, 4H), 1.33-1.02 (m, 12H). ^{13}C-NMR ($CDCl_3$, 100 MHz): 146.37, 128.65, 127.71, 126.12, 70.86, 43.56, 41.94, 33.19, 30.90, 29.64, 29.60, 29.58, 29.48, 27.37, 26.89. HR-MS: $[M+H]^+$: calcd: 415.3108, found: 415.3103.

Compound 8A. Tetraethyleneglycol monomethyl ether (0.90 g, 4.32 mmol) was activated with 1,1'-carbonyldiimidazole (CDI) (0.78 g, 4.81 mmol) for 1h at room temperature. Subsequently, compound **7** (2.19 g, 5.28 mmol), N,N-Diisopropylethylamine (DIPEA) (2.30 mL, 13.20 mmol) and chloroform ($CHCl_3$) (15 mL) were added to the reaction mixture and refluxed overnight. Then, DCM (30 mL) was added and the solution was extracted with water (30 mL). The aqueous layer was extracted twice with DCM (30 mL). The organic fractions were combined and dried with Na_2SO_4, filtered and the solvent was removed on a rotary evaporator before purification by column chromatography (PE/EtOAc 100/0-0/100 v/v). The product was concentrated by rotary evaporation and dried in vacuum to obtain an oil. Yield: 63%, 1.77 g. ^{1}H-NMR ($CDCl_3$, 400 MHz): 7.44-7.41 (d, 6H), 7.21-7.15 (t, 6H), 7.11-7.05 (t, 3H), 5.12 (br s, 1H), 4.15-4.12 (m, 2H), 3.61-3.55 (m, 12H), 3.48-3.45 (m, 2H), 3.29 (s, 3H), 3.10-3.03 (m, 2H), 2.08-2.04 (t, 2H), 1.41-1.37 (m, 4H), 1.25-1.14 (12H, m). ^{13}C-NMR ($CDCl_3$, 100 MHz): 156.23, 146.12, 128.3, 127.46, 125.87, 71.68, 70.60, 70.34, 70.31, 70.24, 69.40, 68.64, 66.78, 63.46, 60.03, 54.41, 43.30, 40.75, 30.61, 29.72, 29.35, 29.28, 29.05, 27.10, 26.51. MALDI-TOF-MS: m/z calcd: 648.41; found: 671.74 $[M+Na]^+$.

Compound 8B. Compound **6** (0.78 g, 3.55 mmol) was activated with CDI (0.64 g, 3.95 mmol) for 1h at room temperature. Subsequently, compound **7** (1.61 g, 3.88 mmol), DIPEA (2.00 mL, 5.74 mmol) and $CHCl_3$ (15 mL) were added to the reaction mixture and refluxed overnight. Then, DCM (30 mL) was added and the solution was extracted with water (30 mL). The aqueous layer was extracted twice with DCM (30 mL). The organic fractions were combined and dried with Na_2SO_4, filtered and the solvent was removed in rotary evaporator before purification by column chromatography (PE/EtOAc 100/0-0/100 v/v). The product was concentrated by rotary evaporation and dried in vacuum to obtain an oil. Yield: 74 %, 1.74 g. ^{1}H-NMR ($CDCl_3$, 400 MHz): 7.52-7.48 (d, 6H), 7.31-7.25 (t, 6H), 7.21-7.17 (t, 3H), 4.87-4.83 (br s, 1H), 4.32-4.20 (t, 2H), 3.72-3.68 (m, 12H), 3.41-3.38 (m, 2H), 3.20-3.13 (m, 2H), 2.15-2.11 (t, 2H), 1.51-1.44 (m, 4H), 1.35-1.26 (m,

12H). ^{13}C-NMR ($CDCl_3$, 100 MHz): 146.46, 128.76, 127.82, 126.23, 70.97, 70.81, 70.78, 70.76, 70.63, 70.16, 69.80, 69.06, 66.93, 63.91, 50.78, 43.67, 41.15, 30.97, 30.05, 29.71, 29.62, 29.38, 27.45, 26.85. MALDI-TOF-MS: m/z calcd: 659.40; found: 659.12 $[M+H]^+$.

Compound 9A. Compound **8A** (1.68 g, 2.58 mmol) was dissolved in TFA (1 mL) stirred at room temperature for ~ 20 min. When the reaction was complete (as determined by TLC), the TFA was removed by a gentle stream of air and the solid was redissolved in $CHCl_3$ (15 mL). Subsequently, 3,4-dibutoxy-3-cyclobutene-1,2-dione (0.68 mL, 3.13 mmol) and DIPEA (6.00 mL, 34.44 mmol) were added to the reaction mixture and refluxed overnight. Then, DCM (30 mL) was added and the solution was extracted with water (30 mL). The aqueous layer was extracted with DCM (2 x 30 mL). The organic fractions were combined and dried with Na_2SO_4, filtered and the solvent was removed in rotary evaporator prior to purification by column chromatography (PE/EtOAc 100/0-0/100 v/v). The product was then concentrated by rotary evaporation and dried in vacuum to obtain an oil. Yield: 87%, 1.26 g. ^{1}H-NMR ($CDCl_3$, 400 MHz): 7.14 (s, 1H), 4.96 (s, 1H), 4.71-4.62 (m, 2H), 4.16-4.13 (t, 2H), 3.63-3.56 (m, 12H), 3.52-3.48 (m, 2H), 3.40-3.32 (m, 5H), 3.12-3.05 (m, 2H), 1.78-1.68 (m, 2H), 1.58-1.51 (m, 2H), 1.44-1.41 (m, 4H), 1.26-1.18 (m, 12H), 0.94-0.89 (t, 3H). ^{13}C-NMR ($CDCl_3$, 100 MHz): 189.75, 182.75, 177.46, 172.51, 156.54, 73.41, 71.96, 70.62, 70.57, 70.55, 70.53, 69.69, 63.85, 60.46, 44.93, 41.06, 32.08, 30.69, 29.96, 29.73, 29.42, 29.23, 29.13, 26.73, 26.40, 18.71, 13.73. MALDI-TOF-MS: m/z calcd: 558.35; found: 580.86 $[M+Na]^+$.

Compound 9B. Compound **8B** (1.74 g, 2.64 mmol) was dissolved in TFA (1 mL) stirred at room temperature for ~ 20 min . When the reaction was complete (as determined by TLC), the TFA was removed by a gentle stream of air and the product was redissolved in $CHCl_3$ (15 mL). Subsequently, 3,4-dibutoxy-3-cyclobutene-1,2-dione (0.68 mL, 3.13 mmol) and DIPEA (5.00 mL, 28.70 mmol) were added to the reaction mixture and refluxed overnight. Then, DCM (30 mL) was added and the solution was extracted with water (30 mL). The aqueous layer was extracted twice with DCM (30 mL). The organic

fractions were combined and dried with Na_2SO_4, filtered and the solvent was removed in a rotary evaporator prior to purification by column chromatography (PE/EtOAc 100/0-0/100 v/v). The product was concentrated by rotary evaporation and dried in vacuum to obtain an oil. Yield: 47%, 0.71 g. ^{1}H-NMR ($CDCl_3$, 400 MHz): 7.00-6.95 (m, 1H), 4.87-4.84 (m, 1H), 4.72-4.64 (m, 2H), 4.20-4.16 (t, 2H), 3.70-3.62 (m, 12H), 3.41-3.34 (m, 4H), 3.14-3.09 (m, 2H), 1.79-1.71 (m, 2H), 1.61-1.56 (m, 2H), 1.46-1.37 (m, 4H), 1.31-1.24 (m, 12H), 0.95-0.92 (t, 3H). ^{13}C-NMR ($CDCl_3$, 100 MHz): 189.79, 182.83, 177.62, 172.99, 172.51, 156.54, 73.49, 70.79, 70.75, 70.72, 70.61, 70.15, 69.76, 68.97, 67.15, 63.93, 50.78, 44.99, 41.11, 32.11, 31.13, 30.73, 29.99, 29.45, 29.26, 29.16, 26.76, 26.43, 18.75, 13.78. MALDI-TOF-MS: m/z calcd: 569.34; found: 591.40 $[M+Na]^+$.

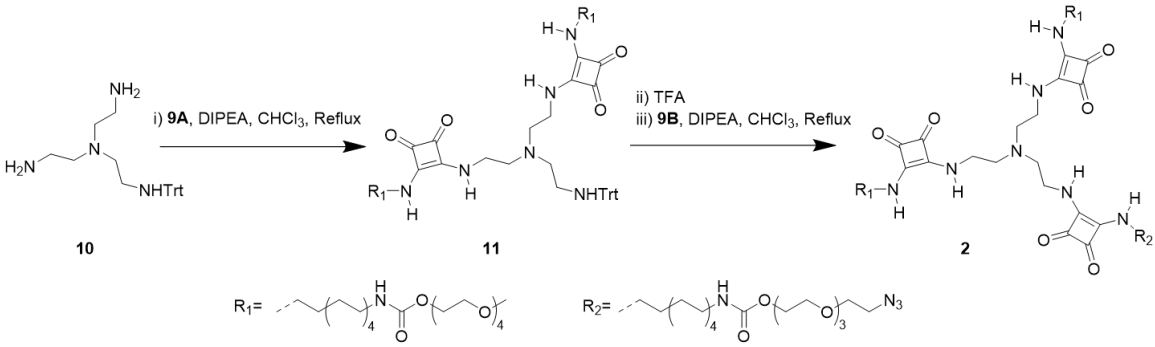

Scheme S2.3. Synthetic route for compound **3**.

Compound 10. Tris(2-aminoethyl)amine (2.99 g, 20.47 mmol) was dissolved in dry DCM (100 mL) and triphenylchloromethane (1.02 g, 3.66 mmol) in dry DCM (100 mL) was added dropwise at room temperature. The mixture was stirred overnight and then washed with 10 wt% NaOH solution (100 mL) and brine (100 mL). The organic phase was dried over Na_2SO_4 and concentrated in rotary evaporator. The crude was purified by column chromatography (DCM/MeOH/NH_4OH 100/0/0-85/15/0.1 v/v/v). The product was concentrated by rotary evaporation and dried in vacuum to give compound **10** as a yellowish oil. Yield: 62%, 0.88 g. ^{1}H-NMR ($CDCl_3$, 400 MHz): 7.51-7.48 (d, 6H), 7.31-7.26 (t, 6H), 7.21-7.16 (t, 3H), 2.69-2.65 (t, 4H), 2.62-2.58 (t, 2H), 2.36-2.32

(t, 4H), 2.26-2.22 (t, 2H). ^{13}C-NMR ($CDCl_3$, 100 MHz): 146.26, 128.68, 127.91, 126.36, 70.77, 57.51, 55.06. 41.04, 39.83. HR-MS: $[M+H]^+$: calcd: 389.2700, found: 389.2696.

Compound 11. Compound **9A** (0.52 g, 0.93 mmol) was dissolved in $CHCl_3$ (10 mL) in a round bottom flask. Compound **10** (0.16 g, 0.41 mmol) and DIPEA (0.50 mL, 2.87 mmol) were added before refluxing the reaction mixture overnight. The crude was concentrated and purified by column chromatography (EtOAc/MeOH 100/0-100/20 v/v). The product was concentrated by rotary evaporation and dried in a vacuum oven to obtain an oil. Yield: 54%, 0.30 g. ^{1}H-NMR ($CDCl_3$, 400 MHz): 8.23 (br s, 2H), 8.05 (br s, 2H), 7.41-7.38 (d, 6H), 7.22-7.17 (t, 6H), 7.13-7.08 (t, 3H), 5.08 (br s, 2H), 4.20-4.17 (t, 4H), 3.66-3.51 (m, 32H), 3.35 (s, 6H), 3.17-3.07 (m, 4H), 2.60-2.55 (m, 8H), 1.61-1.54 (m, 4H), 1.46-1.39 (8H, m), 1.27-1.22 (m, 24H). ^{13}C-NMR ($CDCl_3$, 100 MHz): 182.73, 181.77, 168.95, 167.16, 156.66, 128.75, 127.91, 126.36, 71.96, 70.57, 70.54, 70.50, 69.88, 63.86, 55.87, 54.42, 44.80, 42.67, 41.21, 31.15, 30.07, 29.83, 29.64, 29.61, 29.41, 29.39, 26.91, 26.68. MALDI-TOF-MS: m/z calcd: 1356.82; found: 1379.95 $[M+Na]^+$.

Compound 3. Compound **11** (0.15 g, 0.11 mmol) was dissolved in TFA (1 mL) and stirred at room temperature for ~ 20 min. When the reaction was complete (as determined by TLC), the TFA removed by a gentle stream of air and the solid was redissolved in $CHCl_3$ (15 mL). Subsequently, compound **9B** (0.08 g, 0.14 mmol) and DIPEA (3.00 mL, 17.22 mmol) were added to the reaction mixture and refluxed overnight. The crude was concentrated and purified by column chromatography (EtOAc/DCM/MeOH 100/0/0-0/100/0-0/100/10 v/v/v). The product was concentrated by rotary evaporation and dried in vacuum oven to obtain a sticky solid. Yield: 56%, 0.10 g. ^{1}H-NMR ($CDCl_3$, 400 MHz): 7.90-7.80 (m, 6H), 5.12-5.00 (m, 3H), 4.20-4.18 (t, 6H), 3.71-3.53 (m, 52H), 3.39-3.36 (m, 6H), 3.14-3.09 (q, 6H), 2.78 (br s, 6H), 1.61-1.24 (m, 50H). ^{13}C-NMR ($CDCl_3$, 100 MHz): 182.92, 169.48, 167.09, 156.69, 72.03, 70.86, 70.82, 70.80, 70.66, 70.62, 70.59, 70.22, 69.90, 69.86, 63.94, 59.21, 50.78, 44.99, 41.24,

31.27, 30.14, 29.72, 29.50, 26.98, 26.74. LC-MS: t = 6.84 min, m/z: 1610.52. MALDI-TOF-MS: m/z calcd: 1609.98; found: 1631.48 $[M+Na]^+$.

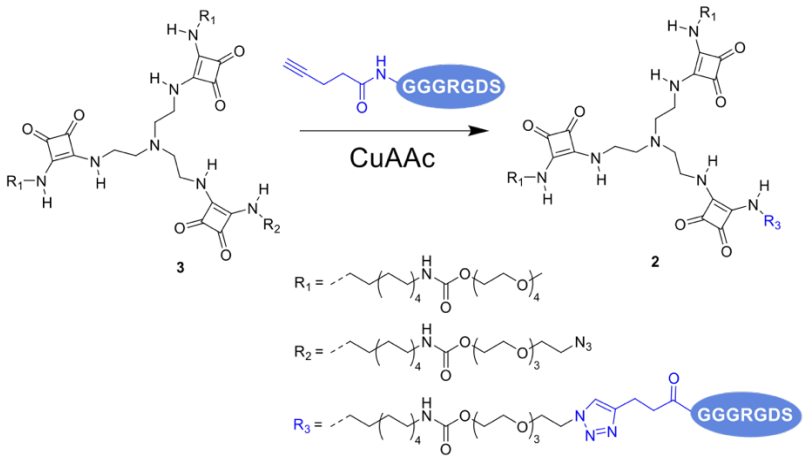

Scheme S2.4. Synthesis of compound **2**.

Peptide synthesis. RGD Peptides (GGGRGDS, **PEP1**) were synthesized on an automatic CEM peptide synthesizer on a 100 µmol scale. Fmoc-Rink amide AM resin with a loading capacity of 0.74 mmol/g was used. Amino acid coupling was performed with 4 eq. of the amino acid, 4 eq. of the activator HCTU and 8 eq. of DIPEA. Fmoc-deprotection was executed using pyridine: dimethylformamide (DMF) (2:8 v/v). The peptides were cleaved in a TFA solution with 2.5% H_2O and 2.5% Triisopropylsilane (TIPS) for 2h, precipitated in cold diethyl ether, dried and dissolved in water prior to injection into LCMS. **PEP1**: LC-MS: t =0.69 min, m/z calcd: 604.26, found: 604.47$[M+H]^+$.

Coupling of the alkyne functionality. Coupling of the alkyne was manually performed on the solid phase. Briefly, the obtained resins (100 µmol) from the peptide synthesizer were suspended in DMF (2 mL) for 15 min. 4-Pentynoic acid (53.3 mg, 0.54 mmol) was coupled to the N-terminus of the peptide by incubation with HCTU (206.8 mg, 0.50 mmol) and DIPEA (175 µL, 1.00 mmol) in DMF (4 mL) at room temperature for 1h. Afterwards, the alkyne-functionalized peptides were cleaved from the resin using a TFA solution with 2.5% H_2O and 2.5% TIPS for 2h and precipitated in cold diethyl ether,

dissolved in water, and lyophilized to obtain a pale-yellow solid. The alkyne-functionalized RGD peptides were presented as **PEP2**. The products were confirmed by LC-MS. **PEP2**: LC-MS: t =0.69 min, m/z calcd:684.28; found: 684.40 $[M+H]^+$.

Compound 2. Sodium L-ascorbate (38.0 mg, 191.9 µmol) and copper (II) sulfate pentahydrate (6.4 mg, 25.6 µmol) were first dissolved separately in water (100 µL) and then, mixed using a vortex for 30s resulting in a bright yellow solution. Afterwards, tris(3-hydroxypropyltriazolylmethyl) amine (THPTA, 5.5 mg, 12.6 µmol) dissolved in ethanol (200 µL) and compound **2** (51.6 mg, 32.0 µmol) dissolved in DMF (1.2 mL) were added to the mixture. Lastly, **PEP2** (43.8 mg, 64.0 µmol) dissolved in DMF:H_2O (400 µL, v/v 1:1) was added and the reaction mixture was stirred at room temperature for 2h. The crude was first dialyzed against water (Mw 500-1000 Da) for 48 h and purified by HPLC. The product was concentrated by evaporation and lyophilized overnight to obtain a white solid. Yield: 35%, 34.9 mg. LC-MS: t = 5.86 min, m/z calcd: 2295.27; found: 1148.27 [M+1] /2.

2.6.4 Two-component squaramide-based supramolecular hydrogel preparation method

Compound **1** was synthesized and prepared as a hydrogel as previously reported. [3] However, to prepare the two-component hydrogels with peptide-labelled monomers, a three-step protocol was used. First, stock solutions of compound **1** (25 mM in DMSO) and compound **2** (5 mM in DMSO) were made separately, and then pipetted with the appropriate ratios into a new vial and vortexed to obtain a transparent mixture. The mixed solutions in DMSO were left overnight under a gentle flow of nitrogen to yield a dry film. The films were suspended in PBS (pH 7.4) at a final monomer concentration at 3.44 mM in a sterilized flow cabinet, followed by 30 s vortex and sonication in ice-water bath until transparent solutions were obtained (~30 min). Lastly, the transparent

solutions were incubated at 37°C for 30 min and left on the bench overnight at room temperature prior to further testing.

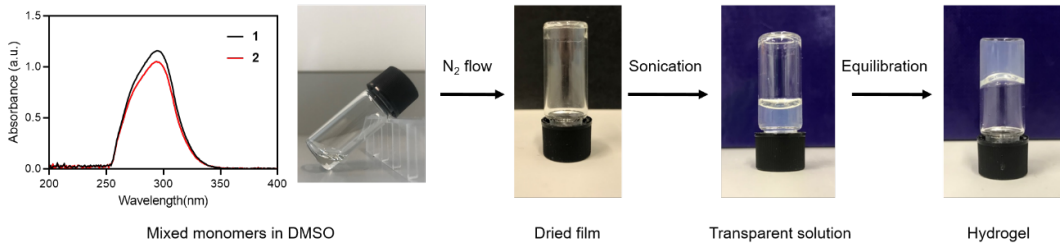

Figure S2.1. Workflow for the preparation of RGD-functionalized squaramide hydrogels. 1) UV spectra show that the squaramide monomers are depolymerized in DMSO due to a broad band centered around 293 nm. 2) Preparation of a mixture of monomer **1** and **2** starting from their respective DMSO stock solutions. 3) Representative image of a film obtained after applying a gentle flow of nitrogen gas overnight. 4) Dried films in PBS (pH 7.4) were sonicated for ~30 min in an ice-water bath (4 °C) until transparent solutions were obtained. 5) Transparent hydrogels are formed after incubation of the vial at 37°C for 30 min and being left to stand at room temperature overnight.

2.6.5 Oscillatory rheology

The mechanical properties of the squaramide-based hydrogels were measured on a Discovery HR-2 hybrid rheometer using cone-plate geometry (40 mm, 1.995°) at 37 ± 0.2 °C with a Peltier-based temperature controller and a solvent trap. Hydrogels with various molar percentages of monomer **2** (SQ-2RGD, SQ-5RGD, SQ-10RGD, SQ-15RGD) were prepared according to the protocol above to result in a total final monomer concentration of 3.1 mM. The hydrogels (600 µL) were left to stand overnight and then pipetted onto the lower plate and the geometry was lowered to a gap distance of 54 µm. Time sweep measurements were executed at a frequency of 1.0 Hz and strain of 0.05% and frequency sweeps were conducted from 0.01−2 Hz with 0.05% strain. Subsequently, a step-strain measurement was performed after a plateau in the storage

modulus was reached in the time sweep. Then, 100% strain was applied to the squaramide-based hydrogels for 120 s. The hydrogels were left to recover for 20 min while measuring at 0.05% strain (f = 1.0 Hz), during which the storage modulus returned to the original plateau. The measurement was repeated for two cycles. Lastly, an amplitude sweep was performed within the strain range from 0.01% to 100% to determine the linear viscoelastic regime (f = 1.0 Hz).

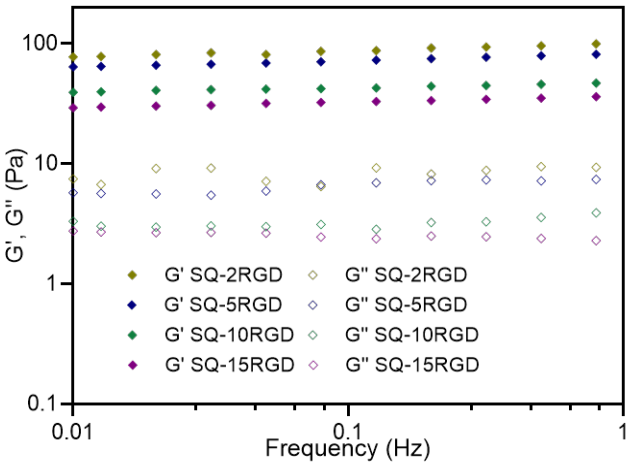

Figure S2.2. Frequency sweep measurements of RGD-functionalized squaramide hydrogels in PBS (pH 7.4) at 37 ± 0.2 °C. Frequency sweep data was collected in a range of 0.01 Hz to 2 Hz with strain of 0.05%. (N = 3)

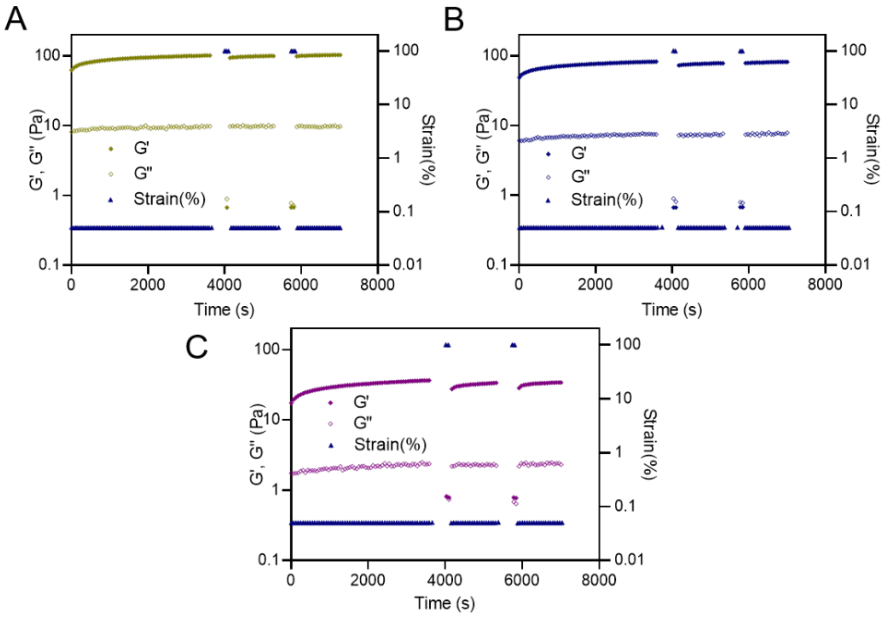

Figure S2.3. Step-strain measurement of RGD-functionalized squaramide hydrogels in PBS (pH 7.4) at 37 ± 0.2 °C. The data were collected at a frequency of 1 Hz. The absence of data between the application of low and high strain is due to the acquisition of a frequency sweep (from 0.01 to 2 Hz, γ= 0.05%) in between these steps. (N = 3)

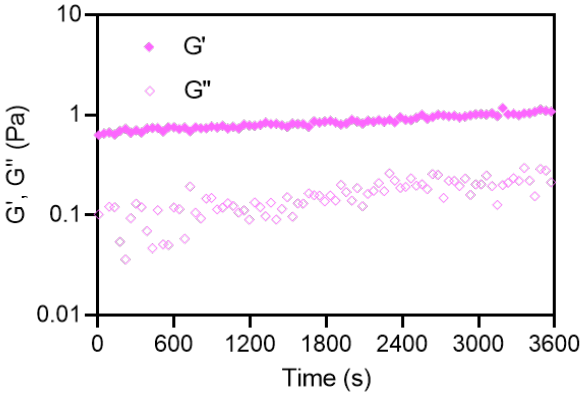

Figure S2.4. Time sweep measurement of SQ-40RGD solution at 37 ± 0.2 °C. Time sweep measurements with strain at 0.05% and frequency of 1 Hz.

2.6.6 Cryo-TEM

Cryo-TEM images of the vitrified samples were acquired with a Tecnai F12 (FEI Company, The Netherlands) equipped with a field emission gun operating at 120 keV using a Gatan UltraScan charge-couple device (CCD) camera (Gatan company, Germany) with a defocus between −6 and −9 µm. Cryo-TEM samples were prepared by applying 3 µL of a SQ-10RGD, hydrogel (3.1 mM) and a SQ-40RGD solution (3.1 mM) to a freshly glow-discharged 300 mesh copper grid with a lacey-carbon support film (Supplier-Electron Microscopy Sciences, Pennsylvania, USA). Excess liquid was blotted away for 2 s (95% humidity, 21 °C, Whatman No. 4 filter paper) and plunge-frozen in liquid ethane at −196 °C using a Leica EM GP (Leica Microsystems, Wetzlar, Germany). The samples were stored in liquid nitrogen before imaging.

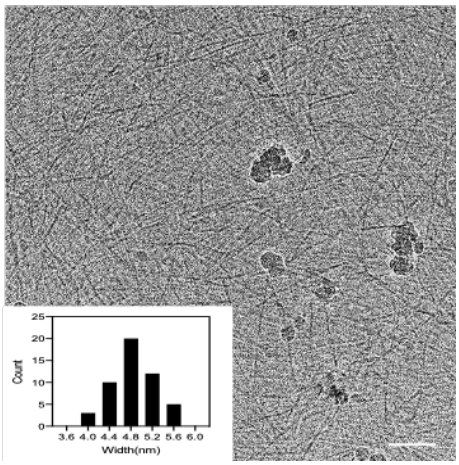

Figure S2.5. Cryo-TEM image of SQ-10RGD hydrogel (3.1 mM, PBS, pH 7.4) as prepared by the gelation protocol. Scale bar: 100 nm. Insert image: histograms of fibre width distribution collected from a sample size N = 50.

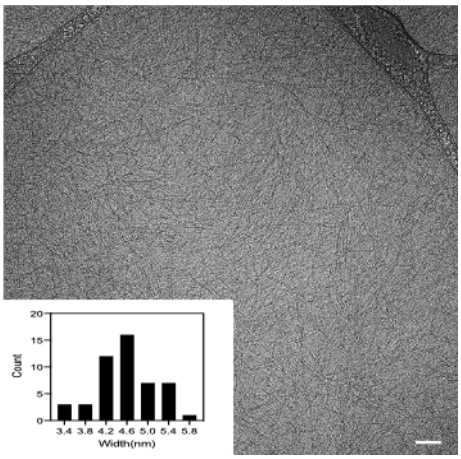

Figure S2.6. Cryo-TEM image of SQ-40RGD solution (B) (3.1 mM, PBS, pH 7.4) as prepared by the gelation protocol above. Scale bar: 100 nm. Insert image: histograms of fibre width distribution collected from a sample size N = 50.

2.6.7 UV–Vis Spectroscopy

UV-Vis spectra were recorded on a Cary 300 UV-Vis spectrophotometer using a quartz cuvette with a path length of 1 cm. The dry film of monomers mixture was prepared according to gelation protocol above. Then, the films were suspended in PBS (pH 7.4) at a final monomer concentration of 1.0 mM, followed by vortexing for 30 s and sonication (~20 min) in ice-water bath to obtain transparent solutions. The solutions were left to stand overnight and diluted into 30 µM with PBS (pH 7.4) prior to measurement.

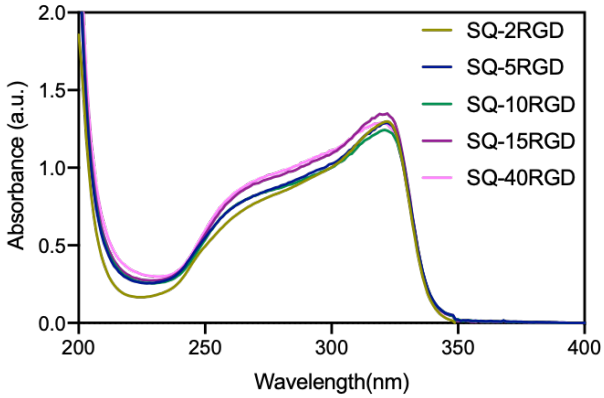

Figure S2.7. UV-Vis spectra of squaramide-based supramolecular polymer solutions (30 µM) containing 2-40 mol% **3** in PBS (pH7.4).

2.6.8 NIH 3T3-LifeAct- mCherry cell migration and spreading in 3D

NIH 3T3 fibroblasts with mCherry-LifeAct were cultured in high glucose DMEM supplemented with 10% newborn calf serum (NCS), 1% Glutamax, and 0.2% penicillin-streptomycin in a 37 °C incubator with 5% CO_2. The cells were kindly provided by T. Schmidt (LION, Leiden University) and previously transduced with LifeAct-mCherry through lentiviral infection. [4] In culture, cells were selected for expression of LifeAct-mCherry with 2 µg/ml puromycin. The culture was maintained with a confluency below 70%. Prior to seeding into hydrogel, NIH3T3-LifeAct-mCherry cells cultured in T-75 flask were dissociated and re-suspended in DMEM medium with a final cell concentration at 2.5×10^7 cells/mL. The cell suspension (50 µL) and the prepared hydrogel (450 µL) were mixed by gentle pipetting and transferred to the µ-Slide 8 well (200 µL/well). After gelation at 37 °C for 15 min, the hydrogels were mounted with fresh medium for cell culture. Five positions per well were chosen and time-lapse confocal imaging was performed over 20 hours. Images were captured every 5 minutes under a 40x air objective (Nikon) on a Nikon Eclipse Ti microscope equipped with a confocal spinning disk unit operated at 10,000 rpm (Yokogawa). Images were captured using an exposure time of 300 ms by an Andor iXon Ultra 897 High Speed EM-CCD camera (Andor

Technology). During imaging, cells were kept at 37 °C and 5% CO_2 in a humidity-controlled incubator (Tokai hit). To quantify cell-gel interaction by cell spreading efficiency, cells were cultured under various conditions (SQ, SQ-5RGD, SQ-10RGD, SQ-15RGD) for 24-hours and then imaged. Cell-laden hydrogels were prepared as described above, but with a final cell density at 1×10^6 cell/mL to ensure single cell resolution during edge-detection. After preparation, the cell-gel mixture was pipetted into custom-made mini-well inserts, 20 mm x 30 mm (~20 µL/well), placed in larger 4-well µ-Slides (Ibidi). The well inserts were fabricated as previously described. [5] After gelation, at 37 °C for 15 min, each mini-well was submersed in 1 mL high glucose DMEM medium. After 24-hours, a volume-slice (1.2 mm x 1.2 mm x 0.15 mm, 2.5 µm z-stacks) of each gel was imaged under the same objective, starting at a height of least 50 µm into the gel (above the bottom of the slide). The mCherry fluorescent protein was excited using a 0.2W 561 nm solid-state diode laser (Coherent) supported in an Agilent MLC4 unit (Agilent Technologies), at reduced intensity and controlled by an Acousto-Optic Tunable Filter. Images were captured using an exposure time of 500 ms by an Andor iXon Ultra 897 High Speed EM-CCD camera (Andor Technology). An in-house Matlab (Mathworks) code was used to quantify cell spreading, which allows automated adaption of edge-detection settings for every individual cell recognized. Before edge detection, all images were flattened using FIJI plugin BaSiC [6] and then imported into Matlab. The cell-edge is defined as the perimeter of pixels at the boundary of the cell area in the binary mask. Using the binary mask, the cell area, perimeter, summated skeleton branch length and Feret-diameters were calculated using the scale (0.3449 µm/pix). The skeleton of each cell was found by reducing the area to a line using their corresponding binary image (*bwskel* algorithm, MATLAB 2019a). Circularity and Aspect Ratio were calculated based on following equations.

$$\boxed{Circularity = (4 * pi * Area)/(Perimeter\text{^}2)}$$

equation 1

$$\boxed{Aspect\ Ratio = Min\ Feret\ Diameter / Max\ Feret\ Diameter}$$

equation 2

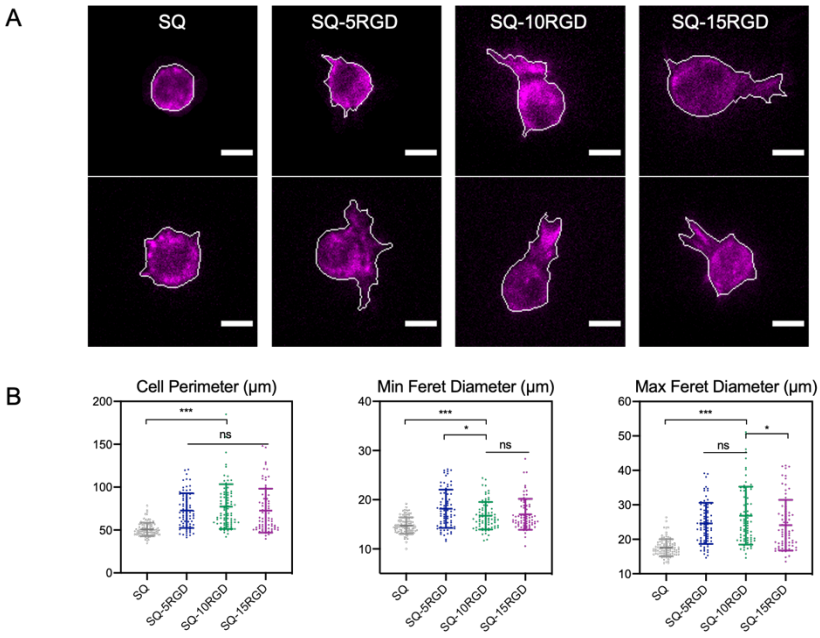

Figure S2.8. A) Representative images of NIH3T3-LifeAct-mCherry cultured within squaramide-based hydrogels, scale bar: 10 µm; B) Quantitative analysis of cell perimeter, minimum and maximum Feret diameter of NIH3T3-LifeAct-mCherry cells cultured for 24h within squaramide-based hydrogel in 3D. The means and standard deviations are marked inside the graphs.

Table S2.1. Summary of quantitative analyses (mean ± 95% confidence intervals)

	SQ	SQ-5RGD	SQ-10RGD	SQ-15RGD
Number of cells	100	76	78	74
Area (μm^2)	183.0±7.3	296.3±23.1	266.5±19.0	261.6±18.6
Perimeter (µm)	50.8±1.3	72.7±3.9	77.3±4.9	72.6±5.0
Circularity	0.903±0.022	0.726±0.030	0.619±0.038	0.694±0.042
Skeleton branch length (µm)	5.2±1.2	20.3±3.3	22.4±3.3	20.00±3.6
Min Feret diameter (µm)	14.7±0.2	18.2±0.8	16.7±0.5	17.0±0.6
Max Feret diameter (µm)	17.6±0.4	24.6±1.1	26.9±1.59	24.1±1.4
Aspect ratio	0.844±0.01	0.750±0.02	0.662±0.028	0.741±0.026

2.6.9 HepG2 cell encapsulation and culture in 3D

HepG2 cells cultured in a T-75 flask were first trypsinized, counted and re-suspended in DMEM/F12 supplemented with 10% (v/v) fetal bovine serum (FBS), 25 U/mL penicillin

and 25 µg streptomycin and diluted to a final cell concentration of 1×10^6 cells/mL. The cell suspension (20 µL) and the pre-prepared squaramide-based hydrogel (180 µL) according to the gelation protocol were mixed through by gentle pipetting and then, the cell-gel suspension–was ~~were~~ transferred to an angiogenesis slide (12 µL/well). After being left to stand at 37 °C for 15 min, the hydrogels were mounted with an additional amount of medium (48 µL) for cell culture. For Growth Factor Reduced Matrigel (Corning) encapsulation, Matrigel was diluted to 5 mg/mL and cells were cultured as previously described.[7] The medium was refreshed twice per week during the three-week culture period in the same volume.

2.6.10 Spheroids diameter determination

HepG2 spheroids were imaged using the EVOS FL AUTO2 equipped with a temperature and CO_2 gas controller at pre-defined time points. Z-stack images were acquired under a 10× objective and an environment of 37°C and 5% CO_2 was maintained during the measurement. The spheroid diameter was measured in Fiji by drawing a straight line horizontally (angle < 3°) with the corresponding scale. Sixty-six spheroids were counted for each group.

2.6.11 LIVE/DEAD staining

At pre-determined time points, the medium on top of the hydrogel was removed by pipetting, rinsed twice with PBS (pH 7.4, 45 µL) and incubated with a prepared staining solution (48 µL) (calcein AM (2 µM) and propidium iodide (1.5 µM)) at 37 °C for 30 min. The staining solution was removed and the hydrogel was rinsed again with PBS two times (48 µL). The stained cell-laden hydrogel was imaged with Leica TCS SP8 confocal laser scanning microscope equipped with a 10× air objective. Fluorescent images were acquired at a resolution of 1024 × 1024 pixels using an excitation wavelength of 488

nm and an emission filter of 500−545 nm for calcein AM and an excitation wavelength of 532 nm and an emission filter of 594−686 nm for propidium iodide.

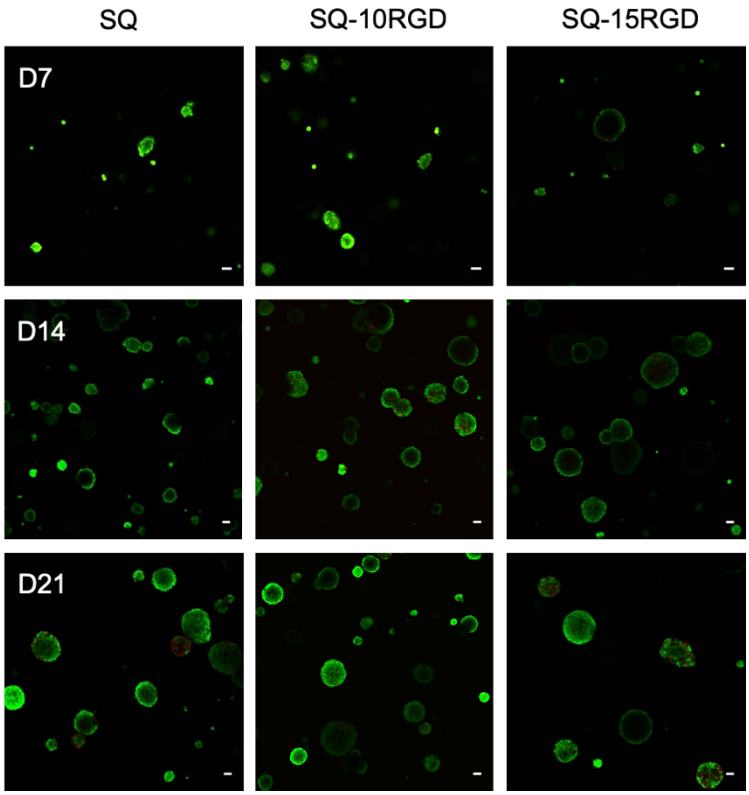

Figure S2.9. Cell viability assay of HepG2 spheroids over the a 21-day culture period. LIVE/DEAD staining with calcein AM (viable cells, *green*) and propidium iodide (PI) (dead cells, *red*). Scale bar: 50 µm.

2.6.12 EdU staining

At pre-determined time points, cell-laden hydrogels were first diluted with cold medium (4 °C) (100x volume), pipetted and spun down to collect the HepG2 spheroids. Proliferating cells were labelled according to the protocol described in the Click-iT EdU Alexa Fluor 594 Imaging Kit. Briefly, the released HepG2 spheroids were first treated with the EdU solution (10 µM) at 37°C for 4h. Afterwards, the cells were fixed with 5% (w/v) PFA solution for 15 min at room temperature, followed by a 20-min penetration

by 0.5% (w/v) Triton X-100 at room temperature. After washing with BSA solution (3%), the cells were incubated with the Click-iT® reaction cocktail for 30 min, followed by another wash and hoechst 33342 (5 µg/mL) incubation for 30 min to stain cell nuclei. The stained cell sample was transferred into another chamber slide that is protected from light and imaged on Leica TCS SP8 confocal laser scanning microscope equipped with a 40× oil immersion objective. Fluorescent Z-stack images were acquired at a resolution of 1024 × 1024 pixels with a step size at 1 µm. The Z-stack images from 3D HepG2 spheroids were projected into 2D by Fiji. Corrected total cell fluorescence (CTCF) for both channels were measured by Fiji and EdU positive ratios were calculated based on according to following equation:

$$CTCF = Integrated\ Density - (area\ of\ selected\ cell\ \times Mean\ fluorescence\ of\ background\ reading)$$

equation 3

$$EdU\ positive\ ratios = CTCF_{EdU}/CTCF_{Hoechst} \times 100\%$$

equation 4

In each measurement, three random areas around the cell were measured as background. Three spheroids were measured for all the groups.

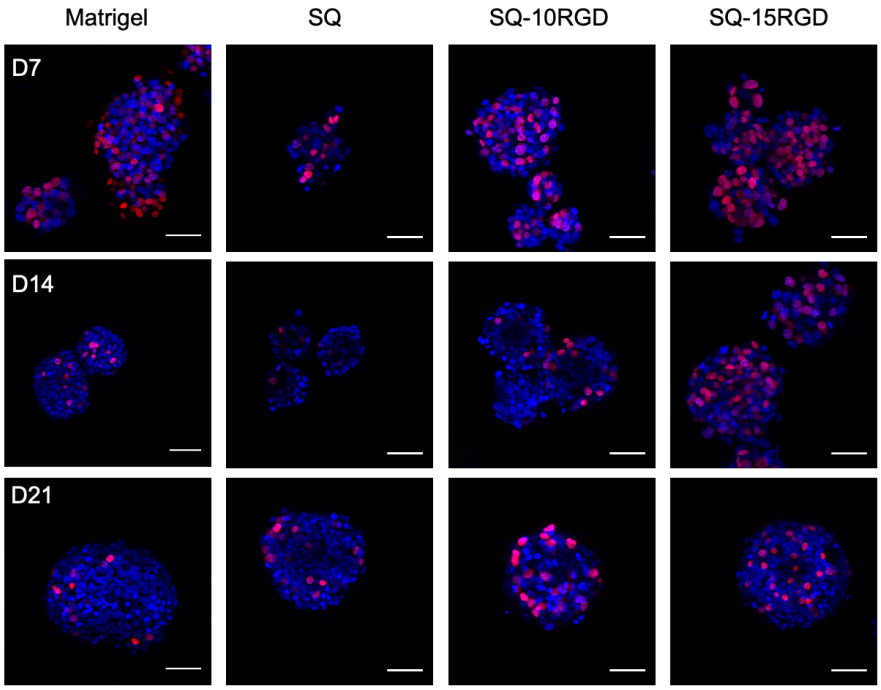

Figure S2.10. Representative images of EdU staining in HepG2 spheroids released during culture in Matrigel and squaramide-based hydrogels. Proliferating cells were labelled with EdU-Alexa fluor 594 (*red*) and cell nuclei were stained with Hoechst 33342 (*blue*). Scale bar: 50 µm.

2.6.13 RT-PCR

The cell-laden hydrogels were cultured at 37°C as previously described. On day 21, the total RNA was extracted using the TRI Reagent. RNA yield and purity were determined using the NANODROP spectrophotometer. 800 ng RNA was used to generate cDNA construct using the RevertAid H Minus First Strand cDNA Synthesis Kit. For RT-qPCR, 5x diluted cDNA was mixed with 1 µM forward and reverse primers (Table S2) and X10 POWRUP SYBR MASTER MIX. Parameters used for RT-qPCR were: 50 ºC for 2 minutes, 95 ºC for 10 minutes, followed by 40 cycles at 95 ºC for 15 seconds and 60 ºC for 1 minute, 95 ºC for 15 seconds, 60 ºC for 1 minute, and finally 95 ºC for 15 seconds and run on a QuantStudio™ 6 Flex Real-Time PCR System (Applied Biosystems®). Samples

were measured in triplicate and mRNA expression was quantified using the delta-delta Ct (2–ΔΔCt) method. GAPDH was used as housekeeping gene.

Table S2.2. Primer sequences

Gene	Forward 5’- 3’	Reverse 5’ -3’
CYP3A4	TTCCTCCCTGAAAGATTCAGC	GTTGAAGAAGTCCTCCTAAGCT
CYP1A2	CTTTGACAAGAACAGTGTCCG	AGTGTCCAGCTCCTTCTGGAT
CYP3A5	CTCTCTGTTTCCAAAAGATACC	TGAAGATTATTGACTGGGCTG
CYP2D6	CCTACGCTTCCAAAAGGCTTT	AGAGAACAGGTCAGCCACCACT
CYP2C9	GAACACCAAGAATCGATGGACA	TCAGCAGGAGAAGGAGAGCATA
CYP2C19	CAACAACCCTCGGGACTTTA	GTCTCTGTCCCAGCTCCAAG
AAT1	ACTGGGGTGACCTTGGTTAAT	GACGGCATTGTCGATTCACTG
UGT1A1	CAGCAGAGGGGACATGAAAT	ACGCTGCAGGAAAGAATCAT
HNF4a	ACTACGGTGCCTCGAGCTGT	GGCACTGGTTCCTCTTGTCT
MRP2	GGCAGTGAAGAAGAAGACGATGA	ATTGGACCTAGAACTGCGGCT
NCTP	ATCGTCCTCAAATCCAAACG	CCACATTGATGGCAGAGAGA
Albumin	ATGCTGAGGCAAAGGATGTC	AGCAGCAGCACGACAGAGTA
GAPDH	CTGGTAAAGTGGATATTGTTGCCAT	TGGAATCATATTGGAACATGTAAACC

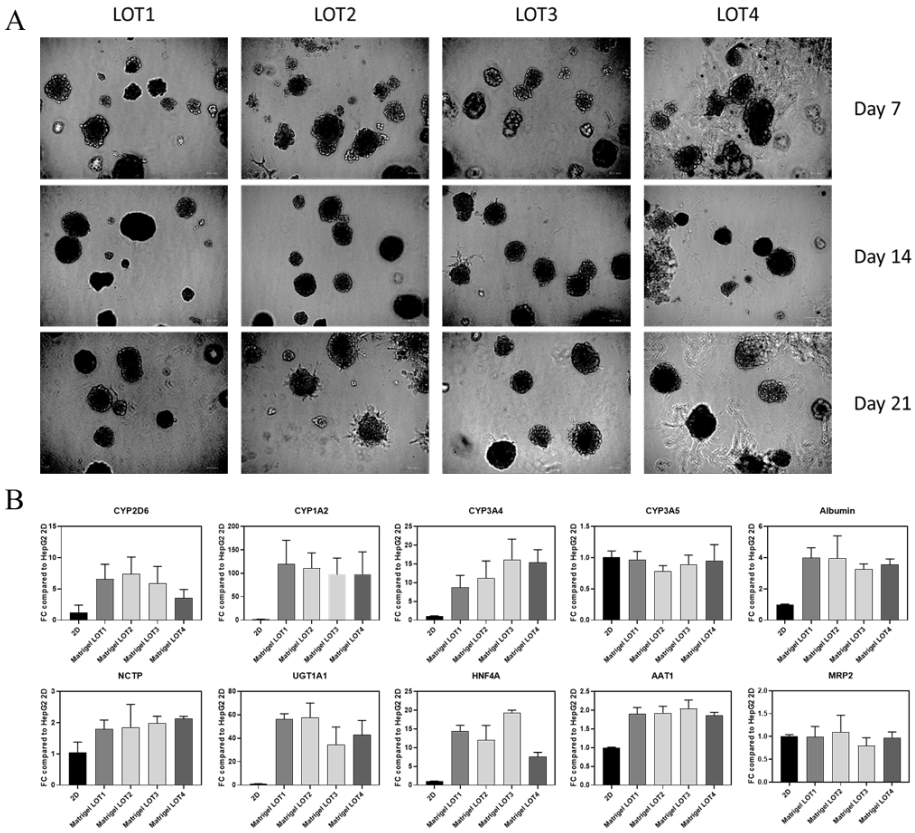

Figure S2.11. A) 3D HepG2 cell culture in four different LOTs of Matrigel (LOT5215008, LOT2326787, LOT5061003 and LOT2104930): A) Bright field images taken on day 7, 14 and 21. B) Fold change hepatic gene expression levels of HepG2 spheroids after a 21-day culture in Matrigel in comparison to 2D on tissue culture plates. (N = 3)

2.6.14 Immunofluorescence Analysis

Cells were cultured at 37°C as previously described. On day 21, the spheroids were fixed with 4% PFA for 30 minutes. Subsequently, the samples were blocked and permeabilized in 0.2% Triton X-100, 0.5% BSA in 1X PBS (TBP) for 1 hour. Spheroids were stained with the primary antibodies against albumin (1:1000, Bethyl laboratories, A80-229F), MRP2 (1:50, Abcam, M2III6) and β-catenin (1:50, Invitrogen, 71-7200) in TBP overnight at 4°C. After washing the samples three times in 1X PBS, spheroids were

counter-stained with secondary antibodies (1:1000, Molecular probes, A11001, A11008), Hoechst 33342 (2µg/mL, Sigma) and Rhodamine Phalloidin (1:10.000, Sigma, P1951) in TBP for 1 hour at room temperature and finally washed three times with 1X PBS. Images were acquired with a Nikon TiE2000 confocal microscope with a 20X objective and 2X zoom.

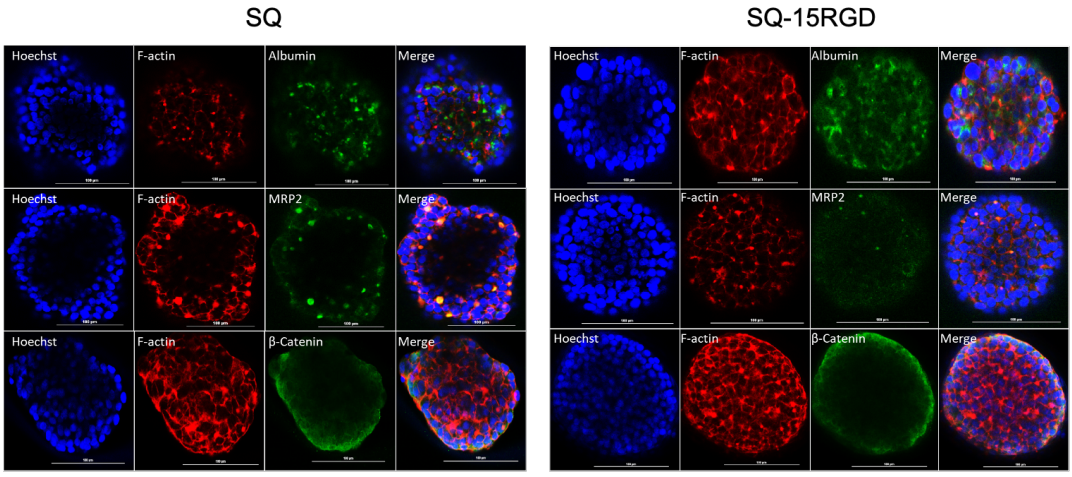

Figure S2.12. Immunofluorescence staining of the liver markers albumin (upper row), MRP2 (middle row) and β-catenin (lower row) in green counter-stained with F-actin rhodamine phalloidin (*red*) and the nuclear staining Hoechst33342 (*blue*). Merged channels consist of all three stains. Scale bar: 100 µm

2.6.15 References

[1] K. D. Park, R. Liu, H. Kohn, *Chem. Biol.* **2009**, *16*, 763.

[2] A. M. Albrecht-Gary, S. Blanc, F. Biaso, F. Thomas, P. Baret, G. Gellon, J. L. Pierre, G. Serratrice, *Eur. J. Inorg. Chem.* **2003**, 2596.

[3] C. Tong, T. Liu, V. Saez Talens, W. E. M. Noteborn, T. H. Sharp, M. M. R. M. Hendrix, I. K. Voets, C. L. Mummery, V. V. Orlova, R. E. Kieltyka, *Biomacromolecules.* **2018**, *19*, 1091.

[4] H. van Hoorn, Cellular Forces : Adhering, Shaping, Sensing and Dividing, Dr.Thesis, Leiden University, **2014**.

[5] C. Tong, J. A. J. Wondergem, D. Heinrich, R. E. Kieltyka, *ACS Macro Lett.* **2020**, *9*, 882.

[6] T. Peng, K. Thorn, T. Schroeder, L. Wang, F. J. Theis, C. Marr, N. Navab, *Nat. Commun.* **2017**, *8*, 1.

[7] S. C. Ramaiahgari, M. W. Den Braver, B. Herpers, V. Terpstra, J. N. M. Commandeur, B. Van De Water, L. S. Price, *Arch. Toxicol.* **2014**, *88*, 1083.

CHAPTER 3

Co-assembly of integrin-targeting peptides on squaramide supramolecular materials facilitate 3D expansion of human induced pluripotent stem cells

This chaper was prepared as an original research paper: Tingxian Liu, Merel Janssen, Lucie Delfos, Roxanne E. Kieltyka*

3.1 Abstract

Human induced pluripotent stem cells (hiPSCs) have recently advanced drug screening, disease modeling, and tissue engineering research because of their capacity to be differentiated into numerous cell types. To meet the large cell number required for these applications efficient and scalable cell expansion is a prerequisite. Herein, we develop a synthetically supramolecular hydrogels as a 3D bio-matrix for hiPSCs expansion, bearing two integrin-targeting peptides to provide cell-matrix interactions. The squaramide-based monomers co-assemble to form supramolecular polymers with a fibrous structure and eventually form a self-healable hydrogel with soft mechanical properties, as evidenced by spectroscopy and rheological measurements. A six-fold expansion was achieved over a four-day culture period in the absence of ROCK inhibitor. The hiPSCs embedded in this matrix displayed high cell viability, cell proliferation, maintenance of pluripotency and differentiation capacity after release. Starting from a single cell suspension, peptide-containing supramolecular hydrogel facilitated cells expansion by 4.8-fold of that without peptides in the condition of single cell seeding. Overall, this integrin-targeting supramolecular hydrogels was proven to be synthetically accessible, cytocompatible, and efficient as a bio-matrix for hiPSCs expansion, demonstrating its applicability for the expansion of hiPSCs.

3.2 Introduction

Human induced pluripotent stem cells (hiPSCs) are rapidly growing in use in the biomedical field because they can be differentiated into any cell type of the body. They can be used to develop various *in vitro* cell culture models for drug discovery research, and the lack the ethical controversies of human embryonic stem cells (hESCs) making them readily accessible.[1–4] A key issue for their application in these areas is that large cell numbers are required, yet their expansion remains challenging.[5–7] Current matrices to expand hiPSCs on two-dimensional (2D) surfaces involve animal-derived (*e.g.* Matrigel) and extracellular matrix (ECM) proteins under static conditions. Besides the limited scale up capacity, these biological matrices can be problematic for their immunogenicity and batch-to-batch variations due to the natural substrates used. An improved method involves the use of suspension culture in a matrix-free manner to overcome the limited scale up of capacity. The cells are cultured as aggregates and subject to shear forces and distribution of gas and nutrients through stirring, wave spinning, rotation or microfluidics throughout the culture vessel providing a new dimension to the culture, but also may compromise their viability and/or genetic stability.[8] Hence, synthetic matrices have been applied in dynamic suspension culture, and are referred to as microcarriers that support cell adhesion and show the potential to protect cells from shear induced effects. Though they can positively impact dynamic culture, preparation of microcarrier can be labour-intensive based on the selected polymer and its subsequent removal from the cells can be time-consuming.[9,10] Hence, developing defined, cytocompatible and accessible matrices that support easy processing, scalable and efficient 3D cell culture is appealing to produce hiPSCs for clinical and fundamental research.

Synthetic hydrogels have been exploited in the field of 3D cell culture to provide a chemically-defined environment with structural support. Controlled mechanical

stiffness, incorporation of functional cargos (*e.g.* proteins, peptides, growth factors), degradability and variable topographies can be introduced into the materials to mimic the natural extracellular matrix.[11–13] Synthetic polymer hydrogels based on thermoreversible and covalent polymers, such as poly(N-isopropylacrylamide)-co-poly(ethylene glycol) (PNIPAAm-PEG), and hyaluronic acid-PNIPAAm were previously used by Schaffer and co-workers highlighting their applicability for induced pluripotent stem cell culture.[14–16] However, these hydrogels are based on high molecular weight polymers that can be challenging for the introduction of bioactive cues that are necessary for applications such as cell differentiation, highlighting the need for alternative synthetic polymer hydrogel strategies. Filamentous supramolecular polymers, in which well-defined small molecular monomers self-assemble through non-covalent interactions, can provide a viable alternative to overcome this challenge through their straightforward combination with short peptides to form bioactive 3D cell culture materials that are dynamic and responsive.[17–20]

In native ECM, the filamentous ECM proteins, *i.e.* collagens, elastins, fibronectins and laminins support and interact with cell surface receptors, *e.g.* integrins, engaging in bidirectional signalling to drive numerous cellular processes.[21,22] Therefore, there is an interest in using short peptides in biomaterials to provide a cell relevant environment in a facile manner, both chemically and synthetically. A short peptide routinely used to guide cell adhesion and proliferation in biomaterials is RGD. This peptide originates from the 9th-10th domain of fibronectin and targets various integrin receptors.[23,24] Another short peptide that can target integrin receptors, namely $\alpha v\beta 5$ that binds vitronectin, a common substrate used in iPSC culture, is KKQRFRHRNRKG (AB). This peptide has been employed to support stem cell adhesion, proliferation, maintenance of pluripotency and differentiation.[25–31] Moreover, 2D substrates covalently functionalized with these two short peptides supported stem cell culture without the use of ROCK inhibitor.[27] However, cells interact with their microenvironment in 3D

and in a dynamic manner, and how these two short peptides can affect stem cell behaviour in 3D in a dynamic material has not been explored.[32,33] We therefore examine the combination of these peptides within a supramolecular material and investigate their potential for 3D iPSC expansion.

We previously reported the formation of a filamentous supramolecular hydrogel that can be used for hiPSCs culture using amphiphilic monomers that rely on directional hydrogen-bonding between squaramide units and hydrophobic interactions.[34–37] However, these materials lacked possibilities to introduce bioactivity or change their mechanical properties. In order to introduce bioactive cues into these materials, we designed an azide-terminated squaramide-based monomer for further click reaction with peptides (Chapter 2). Using a supramolecular co-assembly approach, RGD-functionalized squaramide-based supramolecular hydrogels that support HepG2 spheroids assembly, proliferation and differentiation were obtained. To examine and compare the effect of integrin targeting peptides, RGD and KKQRFRHRNRKG (AB) on hiPSCs culture in 3D, we synthesized two peptide-functionalized monomers, **SQ-RGD** and **SQ-AB**. Supramolecular co-assembly of these two peptide-functionalized monomers with native monomer **SQ** result in hydrogels with tunable bioactive character for stem cell culture. We examine their material properties and potential to effect hiPSC viability, proliferation and expansion to better understand the materials features needed to facilitate hiPSCs growth (Scheme 3.1).

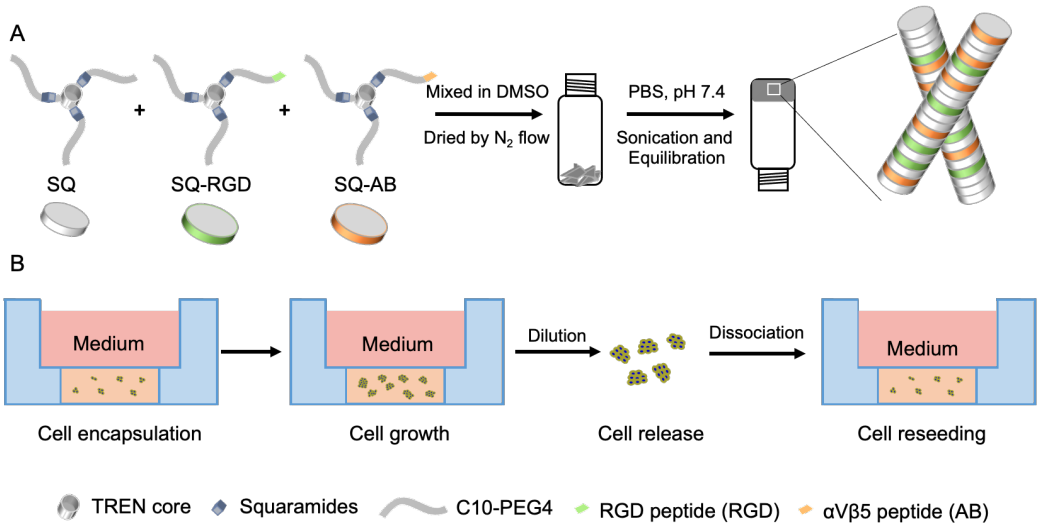

Scheme 3.1. Integrin-targeting squaramide-based supramolecular hydrogels for hiPSC expansion. A) Preparation of multicomponent squaramide-based hydrogels through supramolecular co-assembly of monomers **SQ**, **SQ-RGD** and **SQ-AB**. B) hiPSCs cultured within multicomponent squaramide-based hydrogels: cells were encapsulated by gently mixing cells and hydrogels using a pipet; cells aggregate and grow during the culture; expanded hiPSCs were released from hydrogel by dilution and dissociated for the next round of seeding and culture.

3.3 Results and Discussion

Design and synthesis of integrin-targeting monomers and their co-assembly into squaramide-based supramolecular hydrogels. The native tripodal squaramide-based monomer (**SQ**) was synthesized as previously published and purified by High Performance Liquid Chromatography (HPLC) prior to hydrogel preparation.[37] An azide-terminated tripodal squaramide-based monomer (**SQ-N$_3$**) was synthesized and purified by silica column chromatography using the protocol described in Chapter 2. RGD and AB (KKQRFRHRNRKG) peptides were prepared by solid-phase peptide synthesis and

were made alkyne-terminated through the use of 4-pentyonic acid in a final coupling step at the N-terminus. Similarly to Chapter 2, peptide coupling on **SQ-N$_3$** monomers by copper(I)-catalyzed alkyne-azide cycloaddition (CuAAc) was performed and purified by HPLC to obtain the peptide-labelled squaramide monomers **SQ-RGD** and **SQ-AB**. The synthetic details are included in the supporting information.

Co-assembled integrin-targeting squaramide-based hydrogels were prepared similarly as described in Chapter 2. Briefly, DMSO stock solutions of **SQ**, **SQ-RGD** and **SQ-AB** monomers were prepared at concentrations of 25 mM, 5 mM and 5 mM, respectively. The monomer solutions, **SQ** with **SQ-RGD** and/or **SQ-AB**, were mixed at various ratios, vortexed and then dried overnight under nitrogen flow to obtain a white film. The dried solid was rehydrated in PBS (pH 7.4), vortexed, and subsequently sonicated in an ice bath (4°C). The obtained transparent solution was incubated at 37°C for 30 min and equilibrated overnight at room temperature prior to further study. UV-Vis spectroscopy measurements were then performed to understand the effect of the mixing protocol on the squaramide-based supramolecular polymer at the molecular level. In DMSO, **SQ-AB** monomers showed a single band at 293 nm that is consistent with depolymerization of the squaramide monomers (Figure S3.2). The sample with 10 mol% of SQ-RGD (SQ-10RGD) displayed two absorption bands at 262 nm and 322 nm upon aggregation that correspond to the HOMO−LUMO and HOMO−LUMO+1 transitions, respectively. These bands are identical to self-assembly of the native **SQ** monomers on its own suggesting that the mixing of the **SQ-RGD** does not alter their assembly at the molecular level (Figure 3.1D). In the samples with 10 mol% of SQ-AB (SQ-10AB) and 10 mol% of both **SQ-RGD** and **SQ-AB** (SQ-10COM), the two HOMO−LUMO and HOMO−LUMO+1 transitions were less red and blue-shifted at 267 nm and 319 nm, and are thus indicative of a lower degree of aggregation compared to that of native **SQ** monomers. Collectively, these results suggest a depolymerization of all monomers in DMSO and their likely co-assembly in buffered solutions.

Physicochemical properties of squaramide-based supramolecular hydrogels. Squaramide-based hydrogels co-assembled with **SQ-RGD** and **SQ-AB** at various monomer ratios were first evaluated for their capacity to gelate by the gel-inversion method. The total squaramide-based monomer concentration was maintained at 3.1 mM, in which increasing peptide-functionalized monomers were added from 5-20 mol% (Figure S3.1). Gel phase materials were observed on increasing the **SQ-RGD** monomer concentration within this range. Similarly, when **SQ-AB** monomers were added, non-flowing hydrogels were obtained up to 10 mol%, whereas samples with higher than 15 mol% of **SQ-AB** lacked the capacity to form immobile gels. This weakening of the supramolecular hydrogels may be due to the increased charge and length of the AB peptide relative to RGD peptide resulting in its higher aqueous solubility and decreased aggregation observed in UV-Vis spectroscopy. Hence, the **SQ-AB** monomer was kept less than 15 mol% in the preparation of the integrin-targeting peptide hydrogels. The optimal ratio between RGD and AB peptides for 2D pluripotent stem cell culture was previously demonstrated by Kiessling et al. to be 3:7 resulting in long term maintenance of pluripotency even in the absence of ROCK inhibitor. [27] On this basis, **SQ-RGD** and **SQ-AB** were mixed in a molar ratio of 3:7 for integrin-targeting squaramide hydrogel (SQ-xCOM). The combination of **SQ-RGD** and **SQ-AB** peptides at a 15 mol% concentration (SQ-15COM) resulted in non-flowing hydrogels.

Oscillatory rheology measurements further confirmed the trends observed in gel inversion tests and provided a means to quantify the effect of the integrin-targeting peptides on hydrogel properties. Time sweep measurements showed comparable profiles and storage moduli at plateau for the native squaramide hydrogel (SQ, G'= 60.8 ± 4.5 Pa) and 10 mol% RGD-containing squaramide hydrogel (SQ-10RGD, G'= 46.7 ± 5.9 Pa). On the other hand, lower storage moduli were recorded in comparison to the SQ for 10 mol% AB-containing squaramide hydrogel (SQ-10AB, G'= 24.7 ± 1.1 Pa), and 10 mol% integrin-targeting squaramide hydrogel (SQ-10COM, G'= 28.3 ± 0.8 Pa) (Figure

3.1A). During an amplitude sweep, the storage modulus (G') and loss modulus (G") of SQ-10RGD remained constant until a strain of 5% was applied. In the case of SQ-10AB and SQ-10COM, both moduli (G' and G") remained constant before the application of 15% strain. For all three hydrogels, G' was an order of magnitude higher than G'' from 0.01 Hz to 2 Hz in frequency sweep measurement confirming the formation of viscoelastic hydrogels (Figure S3.4, S3.5 and S3.6). Lastly, step-strain measurements were performed to evaluate the effect of the added peptides on the self-recovery of these hydrogels (Figure 3.1B). The peptide-containing squaramide hydrogels showed similar behavior, compared with SQ, namely the decrease and inversion of both moduli (G' and G") in response to large amplitude strain, and recovery of the material to its initial state after its removal over two cycles. To explore the limit of co-assembly, hydrogels with higher ratio of AB peptide were prepared and their rheological properties were tested. Similar to 40mol% of **SQ-RGD** in Chapter 2, G' was slightly higher than G'' for the sample that contains 20mol% of **SQ-AB** (G'= 2.53 Pa, G''= 0.47 Pa), indicative of the formation of a weak gel (Figure S3.7).

Cryogenic transmission electron microscopy (cryo-TEM) was performed to provide insight into the self-assembly of the SQ-10COM (Figure 3.1C). Cryo-TEM images of the SQ-10COM (3.1 mM, PBS) showed a nanofibrous structure indistinguishable from the SQ confirming that hydrogel formation is driven by fiber entanglement. The fibers from SQ-10COM displayed a width of 6.2 ± 0.7 nm, which is slightly larger than that of the SQ. This larger fiber width likely results from weaker hydrophilic-hydrophobic interactions after introducing the larger AB peptide, which is on par with gel-inversion and rheological measurements.

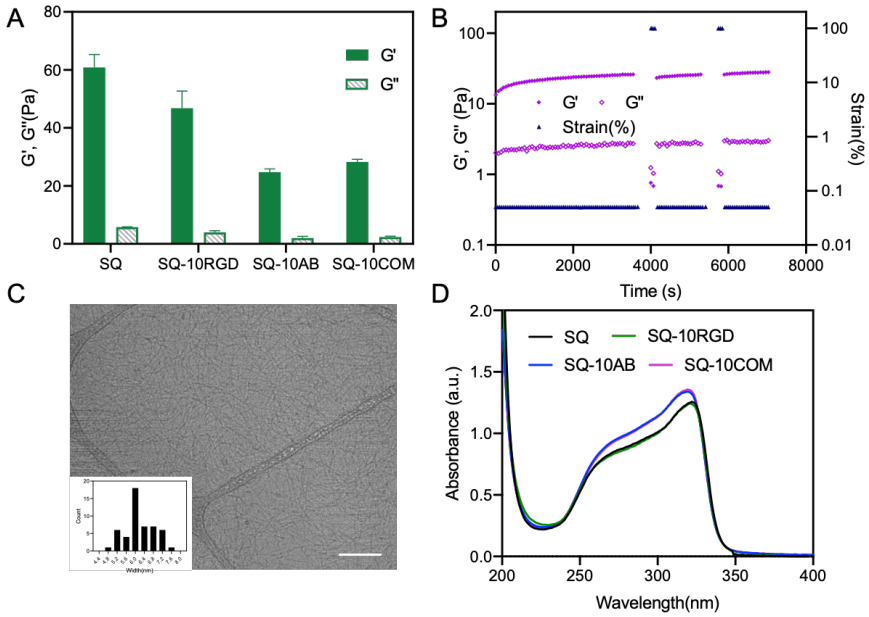

Figure 3.1. A) Averaged storage (G') and loss (G'') moduli of hydrogels (3.1 mM, PBS) collected at 37˚C by time-sweep measurement with a fixed frequency of 1 Hz and strain of 0.05% until a plateau in the storage moduli was obtained. (N = 3) B) Step-strain measurements of SQ-10COM (3.1 mM) at 37˚C with a frequency of 1 Hz; Frequency sweep (from 0.01 to 2 Hz with strain at 0.05%) was performed prior to application of high strain (100%). C) Cryo-TEM image of SQ-10COM (3.1 mM, pH 7.4 PBS) showing engtangled nanoscale fibres. Insert: Histograms of of the fiber width distribution for a sample size of n = 50, Scale bar: 200 nm. D) UV-Vis spectra of **SQ** and co-assembled 10mol% of **SQ-RGD** and/or **SQ-10AB** (c = 30 µM) in PBS (pH7.4).

hiPSCs 3D encapsulation and release from squaramide-based supramolecular hydrogels. To apply the integrin-targeting squaramide hydrogel for 3D hiPSCs culture, we first evaluated the effect of encapsulation and release from the materials on cell viability due to the sensitivity of the hiPSCs. As illustrated in Figure S8, hiPSCs were first dissociated into small clumps by EDTA (0.5 mM). By gentle pipetting, dissociated hiPSCs were mixed and seeded within SQ-10RGD (3.1 mM, PBS). The cell-gel mixture was left at 37˚C for 15 min to gelate using the self-recovery property of the hydrogel. The cell-

gel construct was cultured at 37˚C for 2 h with medium added on top. After that, the cell-gel construct was disrupted gently by pipetting and dilution with excess PBS (~100 times) to release the cells as aggregates. The released cell aggregates were stained with LIVE/DEAD and showed high cell viability (Figure S3.8), indicating that these sensitive cells can be maintained viable during the encapsulation, release and centrifugation process.

Impact of the integrin-targeting peptides RGD and AB on the growth of encapsulated hiPSCs. The growth of hiPSCs in synthetic materials in 3D can be affected by multiple factors, such as use of RhoA GTPas signaling effector Rho kinase (ROCK) inhibitors in the culture, whether the cells are dissociated into clumps or singlets prior to seeding, as well as starting cell seeding density in the materials. In this study, a control hiPSC line L44 was first seeded as small clumps and cultured in SQ. The two common reagents to reduce dissociation-induced cell death are ROCK inhibitor Y-27632 (R) and RevitaCell™ (C), we thus compared the effect of the R and C on the 3D culture of hiPSCs in the SQ. As shown in Figure S9, hiPSCs treated with R or C in a 5-day culture period did not show a significant difference in morphology and/or size distribution; consequently, the more specific inhibitor C was used for subsequent experiments. Notably, cells treated with R or C for 4 days displayed a more narrow size distribution to those treated for 1 day, therefore further experiments were performed with 4-day treatment. To screen the optimal concentration of peptides, cell metabolic activity test were performed for cells encapsulated in hydrogel with various mol% of **SQ-RGD** and **SQ-AB**. It turned out that cell metabolic activity peaked at 10 mol% of **SQ-RGD** and 5 mol% of **SQ-AB** in the tested range (Figure S3.10). Compared with SQ, cells in SQ-10RGD and SQ-5AB showed 1.3 and 3.3 times enhancement in cell metabolic activity, respectively, which strongly suggests that peptide modification, especially the use of the AB peptide, supports increased metabolic activity of cells. Moreover, cells expanded in SQ, SQ-10RGD and SQ-5AB showed high cell viability as evidenced by

LIVE/DEAD staining of spheroids in 3D. The released hiPSCs, when stained with 5-ethynyl-2'-deoxyuridine (EdU), showed a significant number of proliferative cells (Figure S3.11 and S3.12). Thereafter, the integrin-targeting squaramide hydrogels were prepared in a molar ratio **SQ-RGD**:**SQ-AB** of 3:7. At the end of the culture period, large numbers of cells were observed to be viable and proliferating from LIVE/DEAD and EdU staining (Figure S3.13). Importantly, increased cell expansion can be reached within the integrin-targeting squaramide hydrogels after a 3-day culture, with an increase of 5.0, 7.9 and 3.7-fold relative to the initial cell number in SQ-5COM, SQ-10COM and SQ-15COM, respectively. After a 5-day culture, an increase in expansion was obtained in these hydrogels that was 6.9, 6.3 and 6.3-fold relative to the cell number, respectively (Figure S3.13). Expansion of cells in SQ-10COM decreased slightly from 3-day culture to 5-day-culture, hinting that the cells may reach a maximum in their growth a couple days before passage when cultured in SQ-10COM for 5 days. In addition, hiPSCs released from the integrin-targeting squaramide hydrogel were further analyzed using fluorescence activated activated cell sorting (FACS) to assess the pluripotency maker expression. As shown in Figure S3.13D, over 75% and 96% cells were positive in expression of pluripotency markers TRA-1-60 and SSEA4 pointing to a retention of pluripotency after release.

Overall, hiPSCs seeded as clumps in SQ-10COM using 4-day RevitaCell™ supplyment treatment resulted in 6.3-fold expansion after 5 days of culture. High cell viability of hiPSCs, active proliferation throughout the spheroids and expression of pluripotency markers were confirmed in this supramolecular hydrogel through the use of various fluorescent techniques after the 3D culture.

To explore the application potential of this matrix, the hiPSC line L20 that is fully characterized for its cardiac differentiation potential was seeded as both small clumps (clumps seeding, CS) and single cells (single cell seeding, SS) in SQ-10COM. First, the effect of using the RevitaCell™ treatment on the culture was evaluated after

incubation on 0(C0), 1(C1) and 4(C4)-days. Brightfield microscopy images over 4 days of culture showed the formation of compact hiPSCs spheroids and their increase in size over time in SQ-10COM. The average diameter of the hiPSC spheroids measured on D1 and D4 were 111 ± 36 µm and 158 ± 48 µm, respectively, based on a population of 250 spheroids (Figure 3.2B). Among them, 55% of counted spheroids showed diameters over 100 µm on D1, which turned into 90% on D4. Notably, treatment of the hiPSCs with the RevitaCell™ supplement for 0, 1 and 4 days resulted in comparable expansion folds, which were 5.7 (C0), 5.1 (C1) and 5.8 (C4)-fold, respectively, indicating that the integrin-targeting squaramide hydrogel can support hiPSC growth with the use of less ROCK inhibitor. After optimization of RevitaCell™ treatment, cell expansion within hydrogels presenting different peptide were assessed. In case of cell expansion, presentation of either the RGD and AB peptide resulted in an improved expansion fold of 2.2 and 3.8-fold, respectively. Notably, by introducing RGD and AB peptides, SQ-10COM supported hiPSCs expansion to a greater extent with a higher fold of 5.8 indicating a combinational effect between these two peptides with respect to supporting hiPSCs growth (Figure 3.2D). One major goal for using rock inhibitor for hiPSCs culture is to reduce cell death during the dissociation. Therefore, hiPSCs were dissociated by Accutase to obtain singlets and encapsulated within SQ-10COM. As seen in the brightfield microscopy images in Figure S3.14A, compact hiPSCs spheroids were formed and increased in size over the 4-day culture. The average diameter of hiPSC spheroids measured on D1, D2 and D4 were 57 ± 13 µm, 75 ± 19 µm and 91 ± 25 µm, respectively, based on a population of 300 spheroids (Figure S3.14B). Among them, 15% of counted spheroids showed diameters over 70 µm on D1, which turned into 55% on D2 and 84% on D4, respectively. In the case of SQ, there were far fewer spheroids formed after 4 days of culture. Importantly, expansion of the hiPSCs in SQ-10COM significantly increased in comparison to the SQ, with values of 5.8 and 1.2-fold, respectively (Figure S3.14C). In addition, hiPSCs after culture in the SQ-10COM showed over 77% and 97% expression of pluripotency markers TRA-1-60 and SSEA4,

respectively (Figure S3.14D). In all, the combination of the RGD and AB peptides in the supramolecular hydrogels enable rock inhibitor-independent growth of L20 hiPSCs from their seeding as clumps, proving as an effective matrix for the 3D culture of hiPSCs.

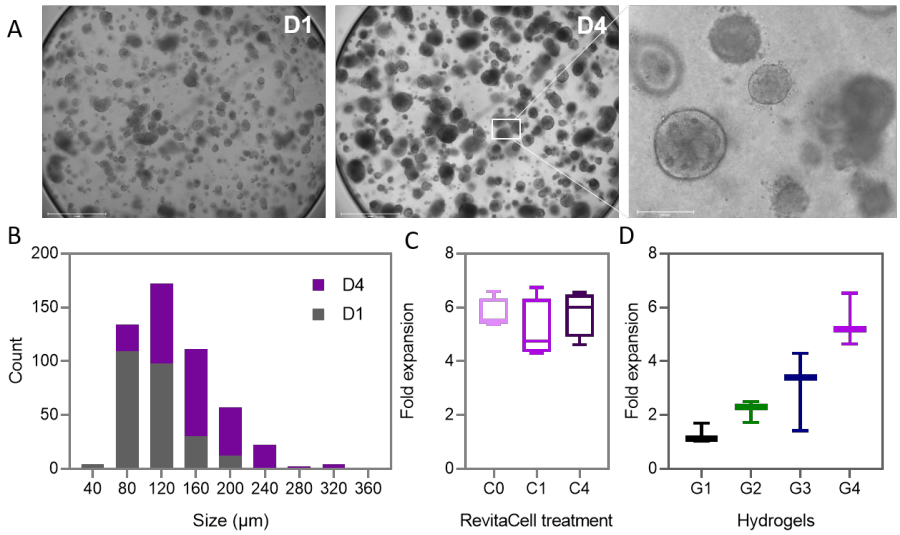

Figure 3.2. A) Bright field microscopy images of spheroids cultured in SQ-10COM with 1(C1)-day treatment of RevitaCell™ supplement, scale bar: 750 µm (left), 750 µm (middle) and 200 µm (right). B) Size distribution of hiPSCs during 4-day culture in SQ-10COM (C1), 250 spheroids were counted. C) Expansion fold of hiPSCs during 4-day culture with 0(C0), 1(C1) and 4(C4)-days incubation of RevitaCell™ Supplement. D) Expansion fold of hiPSCs during 4-day culture in SQ (G1), SQ-10RGD (G2), SQ-10AB (G3), and SQ-10COM (G4).

Viability, proliferation, pluripotency marker expression and differentiation of hiPSCs after expansion in integrin-targeting squaramide hydrogel. Similar to L44 hiPSCs, cell viability, proliferation and pluripotency of L20 hiPSCs after culture in the SQ-10COM was assessed on D4 (Figure 3.3). LIVE/DEAD staining was performed in 3D, generally showing a large population of live cells in tightly compacted colonies. To assess hiPSC proliferation, the colonies were first gently released from the hydrogel by dilution with

PBS prior to use of the EdU staining kit (Figure 3.3B). Notably, the cells were confirmed to be proliferating through the spheroid on staining with EdU, consistent with the observed increase in cell number. Subsequently, pluripotency of the hiPSCs was further assessed with fluorescently-labelled antibodies, TRA-1-60 and SSEA-4, by FACS. HiPSCs were released as single cells after a 4-day culture in SQ-10COM. As plotted in Figure 4C, hiPSCs expanded in SQ-10COM showed a SSEA4 positive population (94%) that was similar to 2D cultured cells. On the other hand, hiPSCs cultured in 2D and 3D showed different percentages in TRA-1-60 expression. In comparison to 2D (~74%), cells expanded in SQ-10COM showed a slight increase in expression of TRA-1-60, with percentages of 83.9 ± 2.0%, 79.1 ± 2.0% and 76.7 ± 3.0% in C0, C1 and C4 culture. Importantly, removal of RevitaCell™ supplement did not alter pluripotency marker expression. Overall, LIVE/DEAD and EdU staining showed high cell viability and average proliferation through the hiPSC spheroids and a high maintenance of pluripotency markers after 3D expansion in the integrin-targeting squaramide hydrogel.

To assess the differentiation potential of hiPSCs after expansion in SQ-10COM, we released hiPSCs as clumps and used the STEMdiff™ Cardiomyocyte Differentiation Kit to prepare cardiomyocytes. The released hiPSCs grew as a monolayer and started to polarize and elongate on day 4. Clear network formation and gaps between cells can be identified on day 6. The elongated cells formed thicker networks that were distinguished clearly from the background from day 10 to day 16. In the meantime, increased and stronger spontaneous beating was observed on day 8 and day 16 (Supplementary Video S3.1, S3.2 and S3.3). The cardiomyocytes differentiation of hiPSCs released from the integrin-targeting squaramide hydrogel support the maintenance of pluripotency in culture and their further downstream application.

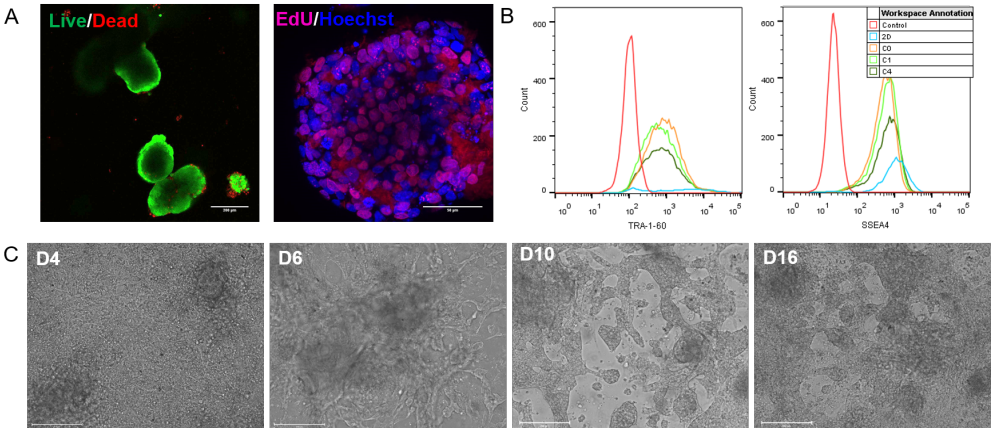

Figure 3.3. Characterization of L20 hiPSCs after 4-day culture in SQ-10COM. A) LIVE/DEAD staining of hiPSCs with calcein AM (viable cells, *green*) and propidium iodide (PI) (dead cells, *red*). Scale bar: 200 µm. Representative images of EdU staining in hiPSCs. Proliferating cells were labelled with EdU-Alexa fluor 594 (*red*) and cell nuclei were stained with Hoechst 33342 (*blue*). Scale bar: 50 µm. B) FACS analysis of pluripotency markers in hiPSCs expanded in SQ-10COM and that maintained on 2D. C) Bright field images of hiPSCs that were expanded and released from SQ-10COM and further processed for cardiomyocyte differentiation. Scale bar: 200 µm.

hiPSC release, re-seeding and expansion in integrin-targeting squaramide hydrogels. Several strategies have been used to release cells embeded in hydrogels including introducing enzymatic degradation, thermo or photo-responsiveness of the materials. These strategies usually require an initial investment into their synthetic design and end with limited modularity. Because squaramide-based supramolecular hydrogels can be easily broken down by dilution using excess PBS or medium based on their soft and non-covalent nature, cell release can be achieved by easily using gentle dilution. As illustrated in Figure 3.4A, expanded hiPSC spheroids were first gently released by dilution, dissociated and re-seeded into integrin-targeting squaramide hydrogel. From bright field microscopy images, hiPSCs were re-seeded as small clumps (D0) and grew into spheroids with larger size (D4). Even though dead cells can be identified both

around and within the aggregates, these passaged and re-grown hiPSCs aggregates displayed high cell viability observed from the fluorescent images by LIVE/DEAD staining (Figure 3.4B and 3.4C).

One concern in the long-term culture of hiPSCs is the retention of their genetic status. To further assess whether these hiPSCs retain their genetic stability, i.e. that no abnormalities have arisen during culture, we performed Global Screening Array of genome DNA samples that were collected from hiPSCs cultured in integrin-targeting hydrogel in 3D and on 2D substrates. We quantified the relative signal intensities of each single nucleotide polymorphism (SNP) and detected no copy number abnormalities (resolution: ~50kb) (Figure 3.4D). Comparing 700 k SNPs of hiPSC lines under different culture conditions, we found no significant difference between cells cultured within 3D hydrogels and those maintained on 2D. This result confirms that hiPSCs maintained their genetic characteristics after culture in the integrin-targeting squaramide hydrogels.

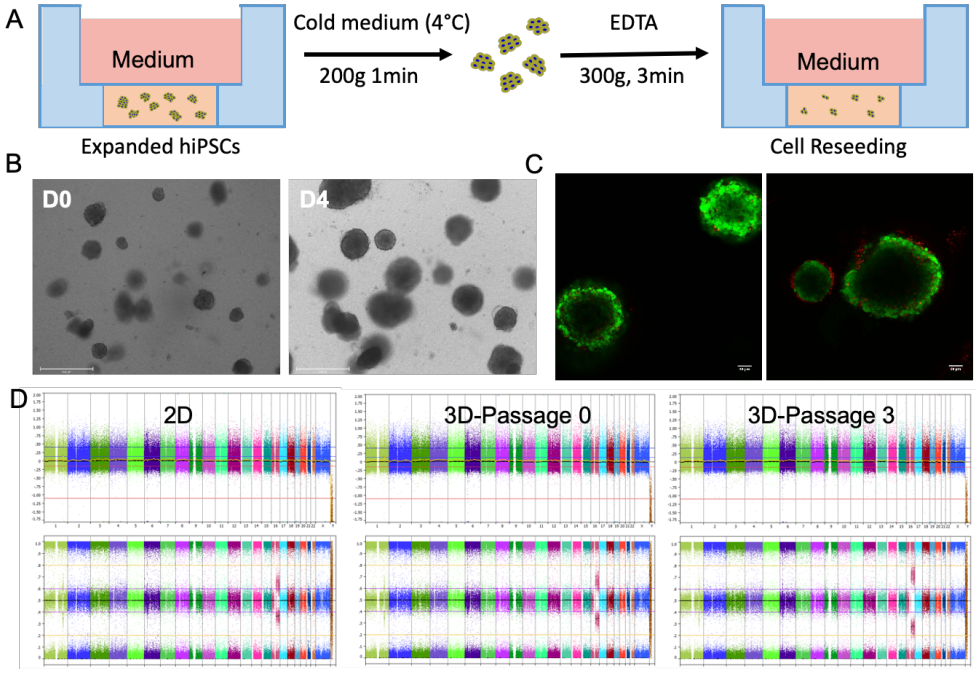

Figure 3.4. A) Cell release and re-seeding protocol in SQ-10COM. B) Bright field microscopy images of hiPSCs after re-seeding in SQ-10COM. Scale bar: 500 µm. C) LIVE/DEAD staining confirms viability of hiPSCs after re-seeding. Scale bar: 100 µm. D) Global Screening Array analysis of 700k single nucleotide polymorphisms (SNP). Genomic DNA were collected from the 2D culture condition on vitronectin and in SQ-C10COM in 3D after one round and three rounds, respectively.

3.4 Conclusions

A multicomponent supramolecular self-assembly system with integrin-targeting peptides was successfully designed, synthesized and characterized. The native **SQ** and integrin-targeting monomers **SQ-RGD** and **SQ-AB** co-assemble into filamentous supramolecular polymers and entangle together to form a hydrogel which maintains the optical clarity, soft texture and self-healable properties. The integrin-targeting squaramide hydrogel boosts hiPSC growth with cell seeding either as single cells or clumps showing high cell viability, active proliferation and expansion fold during a 4-

day culture. Moreover, comparable cell expansion was achieved in the absence of ROCK inhibitor by introducing these two integrin-targeting peptides. In addition, the easy cell release by dilution and pipetting, together with retention of pluripotent markers, confirm this hydrogel to be a potent bio matrix for hiPSCs culture. Furthermore, the hiPSCs are genetically stable after three rounds of passage within this integrin-targeting squaramide hydrogel, demonstrating their great potential in hiPSCs expansion.

3.5 References

[1] B. A. Baghbaderani, X. Tian, B. H. Neo, A. Burkall, T. Dimezzo, G. Sierra, X. Zeng, K. Warren, D. P. Kovarcik, T. Fellner, M. S. Rao, *Stem Cell Reports* **2015**, *5*, 647.

[2] R. Madonna, *Mol. Biotechnol.* **2012**, *52*, 193.

[3] V. K. Singh, M. Kalsan, N. Kumar, A. Saini, R. Chandra, *Front. Cell Dev. Biol.* **2015**, *3*, 1.

[4] Y. Shi, H. Inoue, J. C. Wu, S. Yamanaka, *Nat. Rev. Drug Discov.* **2017**, *16*, 115.

[5] O. Lindvall, Z. Kokaia, A. Martinez-Serrano, *Nat. Med.* **2004**, *10*, 42.

[6] D. Jing, A. Parikh, J. M. Canty, E. S. Tzanakakis, *Tissue Eng. Part B Rev.* **2008**, *14*, 393.

[7] M. Serra, C. Brito, C. Correia, P. M. Alves, *Trends Biotechnol.* **2012**, *30*, 350.

[8] C. Kropp, D. Massai, R. Zweigerdt, *Process Biochem.* **2017**, *59*, 244.

[9] Y. Fan, M. Hsiung, C. Cheng, E. S. Tzanakakis, *Tissue Eng. - Part A* **2014**, *20*, 588.

[10] S. M. Badenes, T. G. Fernandes, C. S. M. Cordeiro, S. Boucher, D. Kuninger, M. C. Vemuri, M. M. Diogo, J. M. S. Cabral, *PLoS One* **2016**, *11*, 1.

[11] Z. Tong, A. Solanki, A. Hamilos, O. Levy, K. Wen, X. Yin, J. M. Karp, *EMBO J.* **2015**, *34*, 987.

[12] Y. Ma, M. Lin, G. Huang, Y. Li, S. Wang, G. Bai, T. J. Lu, F. Xu, *Adv. Mater.* **2018**, *30*, 1.

[13] Z. Zhao, R. Fang, Q. Rong, M. Liu, *Adv. Mater.* **2017**, *29*, 1.

[14] Y. Lei, D. V. Schaffer, *Proc. Natl. Acad. Sci. U. S. A.* **2013**, *110*, 1.

[15] Y. Lei, D. Jeong, J. Xiao, D. V. Schaffer, *Cell. Mol. Bioeng.* **2014**, *7*, 172.

[16] B. L. Ekerdt, C. M. Fuentes, Y. Lei, M. M. Adil, A. Ramasubramanian, R. A. Segalman, D. V. Schaffer, *Adv. Healthc. Mater.* **2018**, *7*, 1.

[17] C. M. Madl, S. C. Heilshorn, *Annu. Rev. Biomed. Eng.* **2018**, *20*, 21.

[18] J. Zhou, J. Li, X. Du, B. Xu, *Biomaterials* **2017**, *129*, 1.

[19] M. J. Webber, E. A. Appel, E. W. Meijer, R. Langer, *Nat. Mater.* **2015**, *15*, 13.

[20] E. Prince, E. Kumacheva, *Nat. Rev. Mater.* **2019**, *4*, 99.

[21] T. H. Barker, *Biomaterials* **2011**, *32*, 4211.

[22] C. Frantz, K. M. Stewart, V. M. Weaver, *J. Cell Sci.* **2010**, *123*, 4195.

[23] R. Mobasseri, L. Tian, M. Soleimani, S. Ramakrishna, H. Naderi-Manesh, *Mater. Sci. Eng. C* **2018**, *84*, 80.

[24] D. Dong, T. Hao, C. Wang, Y. Zhang, Z. Qin, B. Yang, W. Fang, L. Ye, F. Yao, J. Li, *Biomaterials* **2018**, *157*, 149.

[25] B. E. Vogel, S. J. Lee, A. Hildebrand, W. Craig, M. D. Pierschbacher, F. Wong-Staal, E. Ruoslahti, *J. Cell Biol.* **1993**, *121*, 461.

[26] L. Jolla, *Cell* **1991**, *113*, 919.

[27] J. R. Klim, L. Li, P. J. Wrighton, M. S. Piekarczyk, L. L. Kiessling, *Nat. Methods* **2010**, *7*, 989.

[28] S. Musah, S. A. Morin, P. J. Wrighton, D. B. Zwick, S. Jin, L. L. Kiessling, *ACS Nano* **2012**, *6*, 10168.

[29] L. Li, S. A. L. Bennett, L. Wang, *Cell Adh. Migr.* **2012**, *6*, 59.

[30] T. J. Rowland, L. M. Miller, A. J. Blaschke, E. L. Doss, A. J. Bonham, S. T. Hikita, L. V. Johnson, D. O. Clegg, *Stem Cells Dev.* **2010**, *19*, 1231.

[31] S. R. Braam, L. Zeinstra, S. Litjens, D. Ward-van Oostwaard, S. van den Brink, L. van Laake, F. Lebrin, P. Kats, R. Hochstenbach, R. Passier, A. Sonnenberg, C. L. Mummery, *Stem Cells* **2008**, *26*, 2257.

[32] E. M. Ovadia, D. W. Colby, A. M. Kloxin, *Biomater. Sci.* **2018**, *6*, 1358.

[33] S. Hendrikse, M. Baker, N. Sachs, R. Gosens, M. Bastings, P. Dankers, B. Meijer,

Front. Bioeng. Biotechnol. **2016**, DOI 10.3389/conf.FBIOE.2016.01.01494.

[34] R. Prohens, A. Portell, M. Font-Bardia, A. Bauzá, A. Frontera, *Cryst. Growth Des.* **2014**, *14*, 2578.

[35] V. Saez Talens, P. Englebienne, T. T. Trinh, W. E. M. Noteborn, I. K. Voets, R. E. Kieltyka, *Angew. Chemie* **2015**, *127*, 10648.

[36] L. A. Marchetti, L. K. Kumawat, N. Mao, J. C. Stephens, R. B. P. Elmes, *Chem* **2019**, *5*, 1398.

[37] C. Tong, T. Liu, V. Saez Talens, W. E. M. Noteborn, T. H. Sharp, M. M. R. M. Hendrix, I. K. Voets, C. L. Mummery, V. V. Orlova, R. E. Kieltyka, *Biomacromolecules* **2018**, *19*, 1091.

3.6 Supporting Information

3.6.1 Materials

All chemicals for the synthesis **SQ** and **SQ-N_3** were obtained from commercial suppliers and used without further purification. Vitronectin XF™, CryoStor CS10 and ROCK inhibitor Y-27632 were obtained from Stem Cell Technologies. Essential™ 8 medium was received from Thermo Fisher Scientific. Ethylenediaminetetraacetic acid disodium salt (EDTA), Dulbecco's Phosphate Buffered Saline (DPBS), calcein AM (AM = acetoxymethyl) and propidium iodide (PI) were obtained from Sigma-Aldrich. The Click-iT EdU Imaging kit and RevitaCell™ supplement were obtained from Invitrogen. Anti-TRA-1-60-PE and anti-SSEA4-FITC monoclonal antibodies were from Miltenyi Biotec. ReliaPrep™ gDNA Tissue Miniprep System was purchased from Promega.

3.6.2 Instruments

HPLC purification of the monomers was executed on setup equipped with C18 column. A gradient from 10%-90% CH_3CN (0.1% TFA) in H_2O (0.1% TFA) over 15 min at a flow rate of 12 mL/min was used. LC-MS analysis was performed on a TSQ Quantum Access MAX system equipped with a Gemini 3 µm C18 110 Å 50×4.60 mm column (UV detection at 214 nm and 254 nm). The mobile phase was a gradient of 10-90% of H_2O-CH_3CN with 0.1% trifluoroacetic acid over 13.5 minutes. High resolution mass spectra (HR-MS) were collected on a Thermo Finnigan LTQ Orbitrap mass spectrometer that equipped with an electrospray ion source in positive mode (resolution R=60000). The spectra were collected by direct injection of samples (2 µM in H_2O-CH_3CN 50/50 v/v) and recorded with a mass range of 150-2000 using dioctylphthalate (m/z = 391.28428) as a "lock mass". Oscillatory rheology experiments were executed on a Discovery HR-2 hybrid rheometer using a cone-plate geometry (40 mm, 1.995°) at 37 ± 0.2 °C with a Peltier-based temperature controller and solvent trap. Cryo-TEM images were acquired

on a Tecnai F12 (FEI) equipped with a field emission gun operating at 120 keV using a Gatan UltraScan charge-couple device (CCD) camera (Gatan) with a defocus between −6 and −9 µm. UV absorption spectra were recorded on a Cary 300 Bio UV-vis spectrometer, scanning from 200 nm to 400 nm with 1 nm intervals with a scan rate of 120 nm/min. Bright field images were taken on an EVOS FL AUTO2 equipped with temperature and a CO_2 gas controller. Confocal fluorescent images were acquired on Leica SP8 confocal laser scanning microscope equipped with 10× air objective, 40× oil objective and 63x oil objective. Images were processed in the Fiji Image J software.

3.6.3 Synthetic procedures

Synthesis of SQ and SQ-N_3. Native (**SQ**) and azide -functionalized (**SQ-N_3**) squaramide-based monomer synthesis are described in Chapter 2.

Peptide synthesis. Detailed synthetic procedures for RGD peptides, and the conjugation between RGD peptides and **SQ-N_3** are described in Chapter 2. αvβ5-binding peptides (KKQRFRHRNRKG) (**AB**) was synthesized on an automatic CEM peptide synthesizer on a 100 µmol scale. Fmoc-Rink amide AM resin with a loading of 0.39 mmol/g was used for AB peptides. Amino acid coupling was performed with 4 eq. of the amino acid, 4 eq. of the activator HCTU and 8 eq. of DIPEA. Fmoc deprotection was executed with pyridine: DMF (2:8 v/v). 4-Pentynoic acid was coupled to the N-terminus of the peptide using 5 eq. of HCTU and 10 eq. of DIPEA in DMF at room temperature for 1 h. The alkyne functionalized peptides were cleaved from the resin by a TFA solution (2.5% H_2O and 2.5% TIPS) for 4h, precipitated in cold diethyl ether, dissolved in water, and lyophilized to obtain the white solid. The alkyne functionalized AB peptides are labeled as **AB_A**. The sequence was confirmed by mass collected from LC-MS. **AB**: LC-MS: t =1.47 min, m/z: 1609.68; **AB_A**: LC-MS: t =0.81 min, m/z: 1689.51.

Synthesis of SQ-AB. Sodium L-ascorbate (36.5 mg, 184.3 µmol) and Copper(II) sulfate pentahydrate (6.1 mg, 24.4 µmol) were first dissolved in water (100 µL) separately and

mixed by vortex for 30 s to obtain bright yellow solution. Afterwards, tris(3-hydroxypropyltriazolylmethyl) amine (THPTA, 5.3 mg, 12.2 µmol) dissolved in ethanol (200 µL) and SQ-C10-Azide (47 mg, 29.2 µmol) dissolved in DMF (1.2 mL) were added to the mixture. Lastly, **AB_A** (125.4 mg, 74.2 µmol) dissolved in DMF: H_2O (400 µL, v/v 1:1) was added and the reaction mixture was stirred at room temperature for 2h. The crude was first dialysed against water (Mw 500-1000 Da) for 48 h and purified by HPLC. The product was concentrated by evaporation and lyophilized overnight to obtain a white solid. Yield: 17%, 16.5 mg. LC-MS: t = 5.51 min, m/z: 1099.51, 1650.42. HR-MS: $[M+4H]^{4+}$: calcd: 826.2516, found: 826.2514; $[M+5H]^{5+}$: calcd: 661.2027, found: 661.2022.

3.6.4 Hydrogel preparation protocol.

SQ was prepared as previously published.[1] The multicomponent hydrogels with short peptides were prepared as described in Chapter 2. Briefly, DMSO stock solutions of **SQ** (25 mM), **SQ-RGD** (5 mM) and **SQ-AB** (5 mM) were made separately, and then pipetted in the appropriate ratios into a new vial and vortexed to obtain a transparent mixture. The mixed solutions were left under nitrogen flow overnight to remove DMSO. The obtained films were suspended in PBS (pH 7.4) under sterilized flow cabinet resulting in a final monomer concentration of 3.1 mM, followed by 30 s vortex and sonication in ice-water bath until transparent solutions were obtained (~30 min). Lastly, the transparent solutions were incubated at 37°C for 30 min and left on the bench overnight at room temperature prior to further testing.

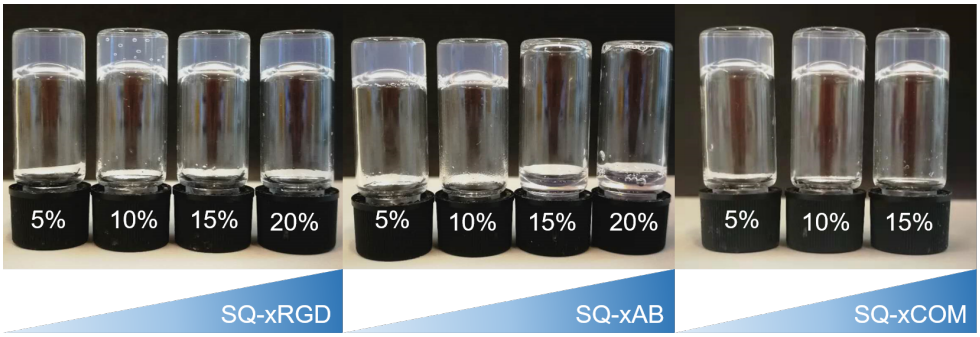

Figure S3.1. Gel inversion test of hydrogels based on **monomer SQ** and increasing mol% of monomer **SQ-RGD** (left), **SQ-AB** (middle) or both monomers with molar ratio of 7:3 (right). All monomers concentration were kept at 3.1 mM in PBS (pH7.4).

3.6.6 UV–Vis Spectroscopy

UV-Vis spectra were recorded on a Cary 300 UV-Vis spectrophotometer using a quartz cuvette with a path length of 1 cm. Stock solutions of monomers **SQ**, **SQ-RGD** and **SQ-AB** in DMSO were first made separately, and mixed in various ratios in a separate vial and vortexed. The mixed monomers were left overnight under nitrogen flow to remove the DMSO. Then, the obtained films were suspended in PBS (pH7.4) with a final monomer concentration at 1.0 mM, followed by vortexing for 30 s and sonication in ice-water bath to obtain transparent solutions. The solutions were left on the bench overnight and diluted prior to the measurement.

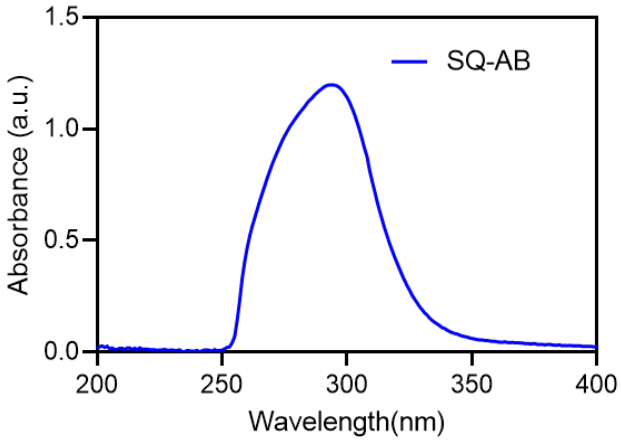

Figure S3.2. UV-Vis spectra of **SQ-AB** in DMSO with monomer concentration of 15µM.

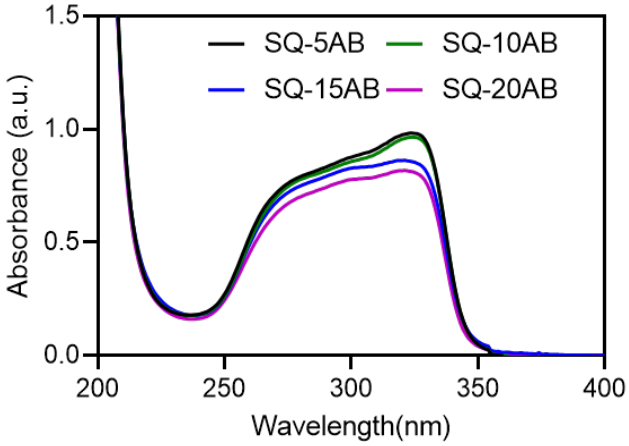

Figure S3.3. UV-Vis of **SQ** with increasing mol% of **SQ-AB**. All monomers concentration were kept at 30 µM in PBS (pH7.4).

3.6.5 Oscillatory Rheology

Oscillatory rheology experiments were carried out on a Discovery HR-2 hybrid rheometer using cone-plate geometry (40 mm, 1.995°) at 37 ± 0.2 °C with a Peltier-based temperature controller and a solvent trap. The SQ, SQ-10RGD, SQ-10AB and SQ-10COM were prepared according to the protocol above in a final monomer

concentration of 3.1 mM. The hydrogels (600 µL), after being left to equilibrate overnight, were pipetted onto the bottom plate and the geometry was lowered to a gap distance of 54 µm. Time sweep measurements were executed at a frequency of 1.0 Hz and strain of 0.05%, and frequency sweeps were conducted from 0.01−2 Hz with 0.05% strain. Subsequently, a step-strain measurement was performed after a plateau was reached in the storage modulus in the time sweep. Then, 100% strain was applied on the hydrogels for 120 s. The hydrogels were left to recover for 20 min while measuring at 0.05% strain (f = 1.0 Hz) and continued with a frequency sweep (from 0.01 to 2 Hz, γ = 0.05%), during which the storage modulus returned to the original plateau. This measurement was repeated for two cycles.

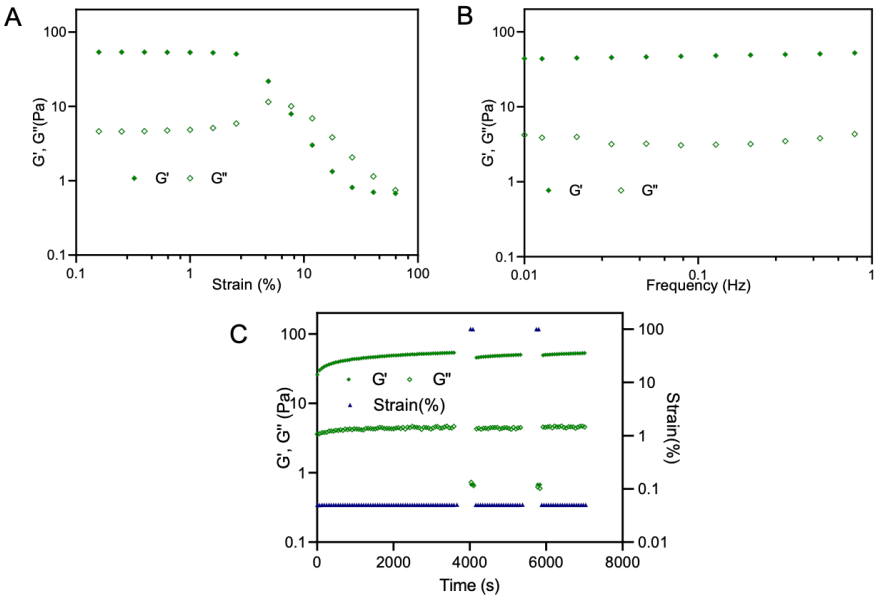

Figure S3.4. Oscillatory rheology measurements of SQ-10RGD (3.1 mM) in PBS at 37 °C: A) Amplitude sweep with a frequency of 1 Hz and strain from 0.1% to 100% (1 Hz). B) Frequency sweep in a range of 0.01 Hz to 2 Hz with strain of 0.05% (N = 3). C) Step-strain measurements with a frequency of 1 Hz.

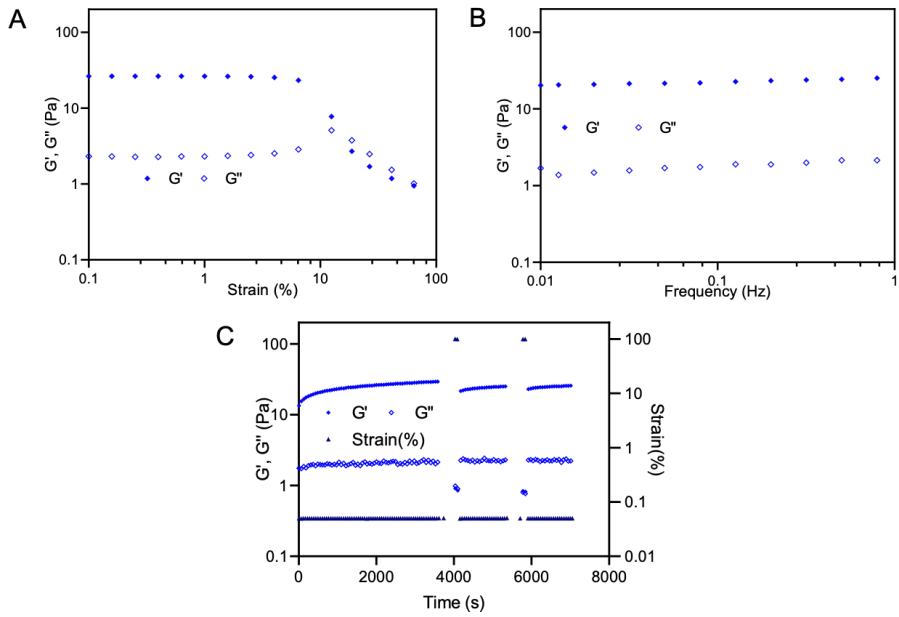

Figure S3.5. Oscillatory rheology measurements of SQ-10AB (3.1 mM) in PBS at 37 °C: A) Amplitude sweep with a frequency of 1 Hz and strain from 0.1% to 100% (1 Hz). B) Frequency sweep in a range of 0.01 Hz to 2 Hz with strain of 0.05% (N = 3). C) Step-strain measurements with a frequency of 1 Hz.

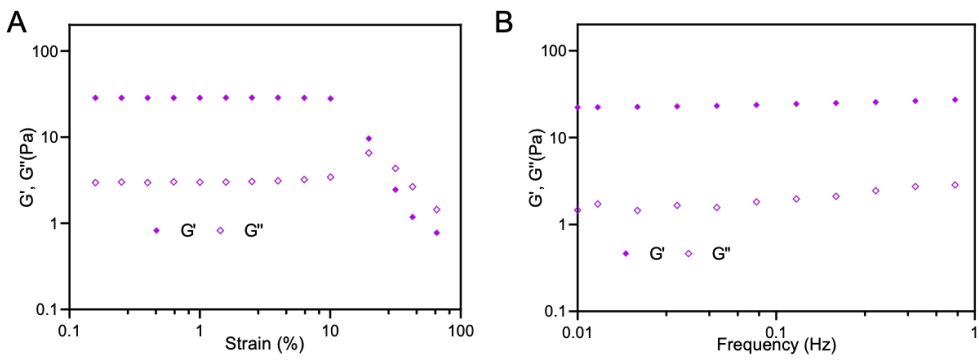

Figure S3.6. Oscillatory rheology measurements of SQ-10COM (3.1 mM) in PBS at 37 °C: A) Amplitude sweep with a frequency of 1 Hz and strain from 0.1% to 100% (1 Hz). B) Frequency sweep in a range of 0.01 Hz to 2 Hz with strain of 0.05% (N = 3).

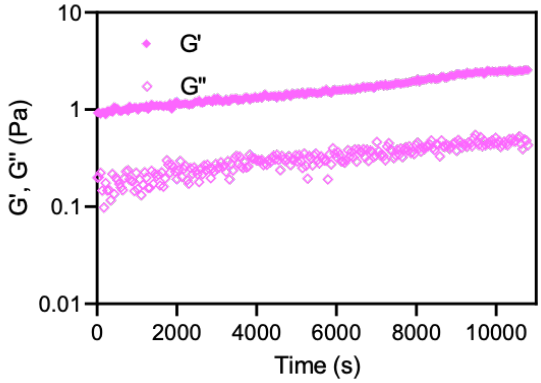

Figure S3.7. Time sweep measurement of SQ-20AB at 37 °C with strain at 0.05% and frequency of 1 Hz.

3.6.5 Cryo-TEM

Cryo-TEM images of vitrified samples were acquired on a Tecnai F20 (FEI Company, The Netherlands) equipped with a field emission gun operating at 200 keV using a Gatan UltraScan charge-couple device (CCD) camera (Gatan company, Germany) with a defocus between −6 and −9 µm. Cryo-TEM samples were prepared by applying 3 µL of SQ-10COM (3.1 mM) without further dilution to a freshly glow-discharged 300 mesh copper grid with a lacey-carbon support film (Supplier-Electron Microscopy Sciences, Pennsylvania, USA). Excess liquid was blotted away for 2 s (95% humidity, 21 °C, Whatman filter paper) and plunge-frozen in liquid ethane at −183 °C using a Leica EM GP (Leica Microsystems, Wetzlar, Germany) before imaging.

3.6.7 Cell Culture on 2D

Human induced pluripotent stem cell line (hiPSCs) LUMC0044iCTRL44.9 (L44) was obtained from Leiden University Medical Center (LUMC). hiPSCs were cultured on six-well plates coated with vitronectin in E8 medium (Stem Cell Technologies). Cells were

passaged every 6 days with 0.5 mM EDTA (Sigma-Aldrich) with split ratio of 1:20. Specifically, on the passage day, cells were first washed with PBS and incubated with EDTA (0.5 mM) for 5 min at 37°C followed by 1 min at room temperature. After aspirating the EDTA solution, E8 medium (2 mL) was added to each well. A 2 mL pipet was used to vigorously wash cells with the E8 medium to dissociate them (6-8 times). The replated cells were first treated with E8 medium supplied with Revita- Cell™ (1:200) for 24 h and then refreshed with E8 medium free of RevitaCell™ every day prior to passage. Another hiPSCs LUMC0020iCTRL-6.9 (L20) were maintained by passaging twice per week with the same protocol with a split ratio of 1:10.

3.6.8 hiPSCs encapsulation, release and passage in 3D

For encapsulation, hiPSCs were first dissociated from the vitronectin-coated plates by EDTA (0.5 mM) described above. A small amount (100 µL) of dissociated cells suspension were collected and treated with Trypsin/EDTA (0.05%) at 37°C for 5 min, followed by counting with a hemocytometer to determine the cell number. hiPSCs were pelleted and re-suspended in E8 medium containing RevitaCell™ (1:200) to reach 2.5×10^7 cells/mL, respectively. The prepared cell suspension (20 µL) was mixed with SQ (180 µL) by gently pipetting before being transferred to a µ-Slide well plate (12 µL/well). After gelation at 37 °C for 15 min, the hydrogels were mounted with an additional amount of E8 medium (48 µL) containing RevitaCell™ (1:200) or ROCK inhibitor (10 µM) for culture. The medium was refreshed every 8h for all cultures. For single cell seeding, hiPSCs were dissociated by incubation with Accutase™ (1 mL/well) for 5 min at 37˚C, following with counting, pelleting by centrifuge and re-suspending in E8 medium containing RevitaCell™ (1:200) and seeding into hydrogel as described above.

To release the cells as spheroids, the cell-gel mixtures were gently pipetted, diluted by PBS (pH 7.4) (5 mL) and collected by centrifuge at 100 g for 3 min. The

released cell aggregates were further stained by EdU. To release hiPSCs as single cells, the cell-gel mixtures were gently pipetted and diluted by trypsin/EDTA (0.05%) (125 µL), following with incubation at 37˚C for 5 min. The dissociation was stopped by adding E8 medium containing RevitaCell™ (1:200) (500 µL) and pelleted by centrifuge at 300 g for 5 min. The cell pellet was ready to use for following analysis.

To passage the hiPSCs in squaramide hydrogels, the cell-gel mixtures were gently transferred from 15-well slide into a 15-mL tube that contains 5 mL cold E8 medium. After gently pipetting with a 2-mL serological pipette three times, cells were released and collected by centrifuge (200 g, 1 min). The obtained cell pellets were incubated with EDTA solution (0.5 mM) for 4 min at room temperature. The dissociation was stopped by removing EDTA solution and adding E8 medium containing RevitaCell™ (1:200) (500 µL) and pelleted by centrifuge at 300 g for 5 min. Finally, the cells were encapsulated in the SQ-10COM gel for further culture as described above.

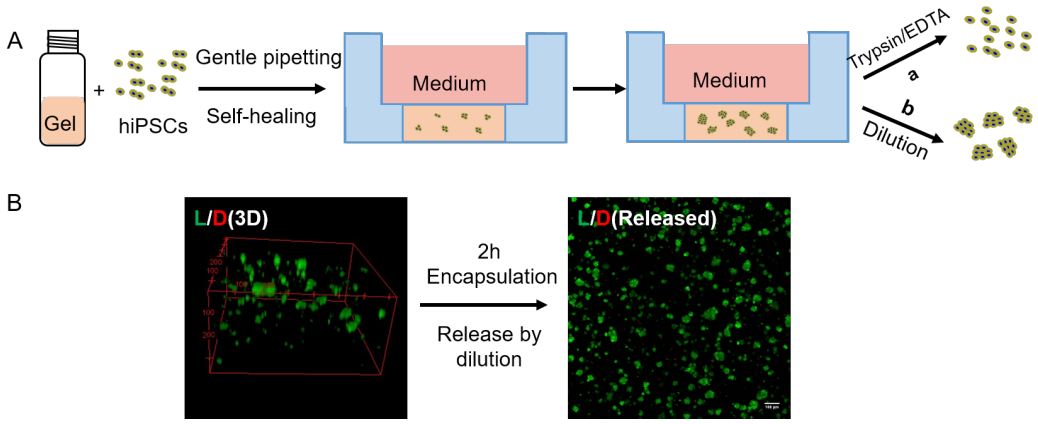

Figure S3.8. A) Encapsulation and release of hiPSCs from SQ-10RGD: Encapsulation was achieved using the self-healing property of the supramolecular materials on gently pipetting with hiPSCs, and gel dissociation was performed by dilution and gentle pipetting with PBS (pH 7.4) which resulted in the release of hiPSC as clumps, or with Trypsin/EDTA (0.05%) which released hiPSCs as single cells for counting and FACS

measurement. B) Clumps released from hydrogels showed high cell viability with LIVE/DEAD staining. Scale bar 100: µm.

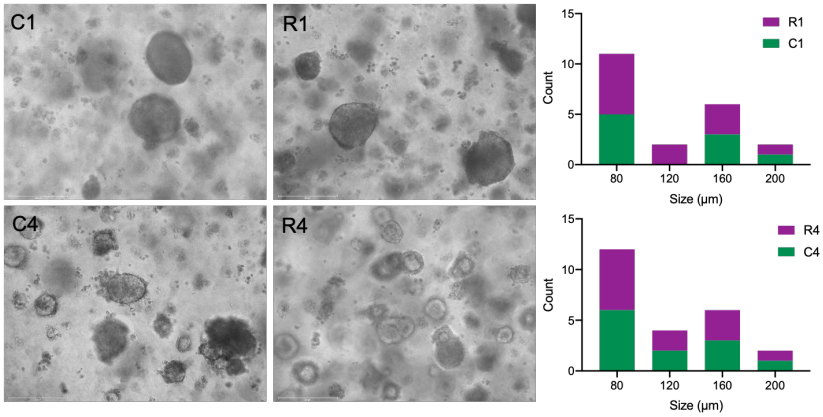

Figure S3.9. Morphology and size distribution of hiPSCs spheroids after 5-day culture in SQ hydrogels. hiPSCs were treated with Rock Inhibitor Y-27632 for 1(R1) and 4(R4) days or RevitaCell™ Supplement for 1 (C1) and 4 (C4) days. Scale bar: 200 µm.

3.6.9 Determination of spheroids diameter and expansion fold.

At pre-determined time points, hiPSCs spheroids were imaged using the EVOS FL AUTO2 equipped with a temperature and CO_2 gas controller. Z-stack images were acquired under a 10× objective. The spheroid diameter was measured in Fiji by drawing a straight line horizontally (angle < 3°) with the corresponding scale. During the imaging, the EVOS incubator was turned on to maintain an environment of 37°C and 5% CO_2 for the hiPSCs. To calculate the expansion fold, hiPSCs were released from hydrogel as single cells by the method described above. The released cells were counted using a hemocytometer and divided by the number of cells initially seeded within the gels to determine the expansion fold.

3.6.10 Metabolic activity of hiPSCs

The Resazurin metabolism assay was performed to examine metabolic activity of hiPSCs in the supramolecular hydrogels on day 1 and 3. hiPSCs were encapsulated in hydrogels as described above and cultured at 37°C. At pre-determined time points, medium (40 µL) was removed from each well. The cell-gel mixture (20 µL) was pipetted into a black 96-well plate, and fresh medium (70 µL) and resazurin stock solution (10 µL, 5.4 mM) were added to each well. The plate was incubated at 37°C for 2h and protected from light. Medium without cells was used as a negative control. The fluorescence intensity was recorded on the TECAN plate reader with an excitation wavelength of 540 nm and an emission wavelength of 590 nm.

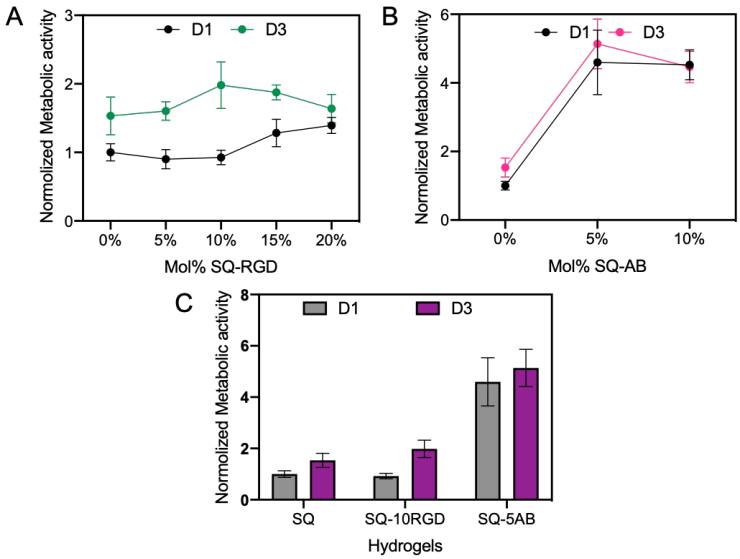

Figure S3.10. A) hiPSCs cultured in the RGD-containing squaramide hydrogel show concentration-dependent metabolic activity in the range of 5 – 20 mol%, with the optimal amount of **SQ-RGD** being 10mol %; B) hiPSCs cultured in AB-containing squaramide hydrogels showed a maximum in metabolic activity using 5 mol% of **SQ-AB**. C) Metabolic activity of hiPSCs cultured in SQ-10RGD and SQ-5AB hydrogels normalized against the SQ hydrogel.

3.6.10 LIVE/DEAD staining

LIVE/DEAD staining of released hiPSCs. The viability of released hiPSCs from hydrogels was assessed using a LIVE/DEAD staining test with calcein AM and propidium iodide. Briefly, released hiPSCs aggregates were first pelleted by centrifuging at 100 g for 3 min and then treated with PBS (200 µL) containing calcein AM (2 µM) and propidium iodide (1.5 µM) at room temperature for 10 min. After staining, the cells were washed with PBS (200 µL) and resuspended in PBS (50 µL) before imaging. The cell suspension was transferred to a chamber slide and imaged on a Leica SP8 confocal laser scanning microscope equipped using a 10× objective. Fluorescent images were acquired at a resolution of 1024 × 1024 pixels using an excitation wavelength of 488 nm and an emission filter of 500−545 nm for calcein AM and an excitation wavelength of 532 nm and an emission filter of 594−686 nm for propidium iodide.

LIVE/DEAD staining of hiPSCs in 3D. The viability of expanded hiPSCs in the hydrogels in 3D were assessed using the same LIVE/DEAD staining reagents above. At pre-determined time points, the medium was removed from top of the hydrogel by pipetting, rinsed with PBS two times (pH 7.4, 45 µL) and incubated with the staining solution (calcein AM (2 µM) and propidium iodide (1.5 µM)) at 37 °C for 30 min. Afterwards, the staining solution was removed and the hydrogel was rinsed again with PBS two times before imaging. The stained cell-laden hydrogel was imaged with Leica SP8 confocal laser scanning microscope equipped under 10× and 40x objectives.

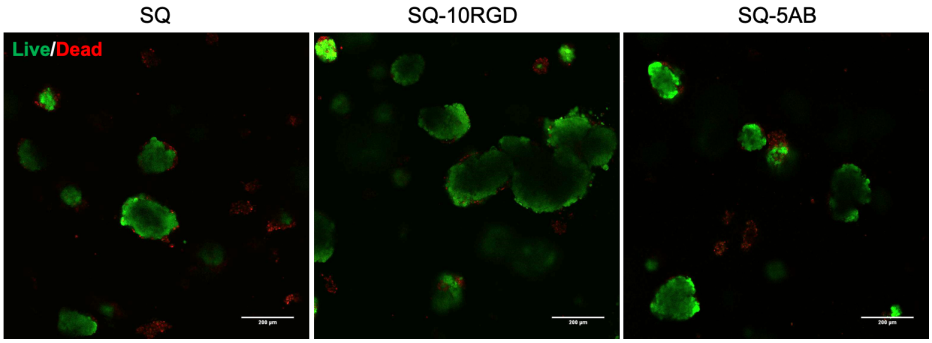

Figure S3.11. Cell viability assay of hiPSCs after 5 days of culture in SQ, SQ-10RGD and SQ-5AB, respectively. LIVE/DEAD staining with calcein AM (viable cells, *green*) and propidium iodide (PI) (dead cells, *red*). Scale bar: 200 µm.

3.6.12 EdU staining

Before EdU staining, hiPSCs spheroids were released from hydrogel by the method described above. The labelling of proliferating cells was executed according to Click-iT EdU Alexa Fluor 594 Imaging Kit (Invitrogen). Briefly, the released hiPSC spheroids were first incubated with EdU solution (10 µM) at 37 °C for 4h. After labelling, hiPSCs spheroids were fixed with 5% (w/v) paraformaldehyde solution at room temperature for 15 min and then incubated with PBS containing 0.5% Triton X-100 at room temperature for 20 min. After washing, the Click-iT® reaction cocktail was first added and incubated for 30 min, followed by a second wash and Hoechst 33342 (5 µg/mL) incubation for another 30 min to stain nuclei. The stained hiPSCs spheroids were transferred into a chamber slide after washing with PBS and imaged with Leica SP8 confocal laser scanning microscope equipped with a 63× oil objective. Fluorescent Z-stack images were acquired at a resolution of 1024 × 1024 pixels with a step size at 1 µm. The Z-stack images from 3D hiPSCs spheroids were projected into 2D by the Fiji software.

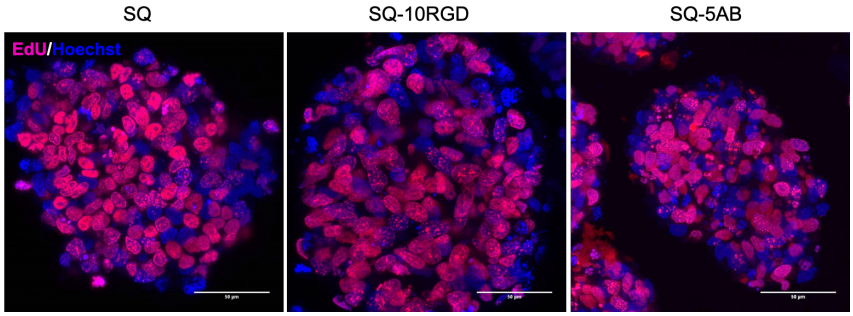

Figure S3.12. Representative images of EdU staining in hiPSCs spheroids released from SQ, SQ-10RGD and SQ-5AB hydrogels, respectively. Proliferating cells were labelled with EdU-Alexa fluor 594 (*red*) and cell nuclei were stained with Hoechst 33342 (*blue*). Scale bar: 50 µm.

3.6.13 Flow cytometry measurement

HiPSCs were released from the supramolecular hydrogels as single cells with trypsin/EDTA (0.05%) to assess the pluripotency marker expression of cells expanded in 3D hydrogels. The single cell suspension was incubated with TRA-1-60-PE and SSEA-4-FITC fluorescently labeled antibodies (1: 10 dilution in FACS buffer) at 4 °C for 30 min. After washing with PBS, hiPSCs were suspended in FACS buffer and recorded on a Guava® easyCyte Flow Cytometer.

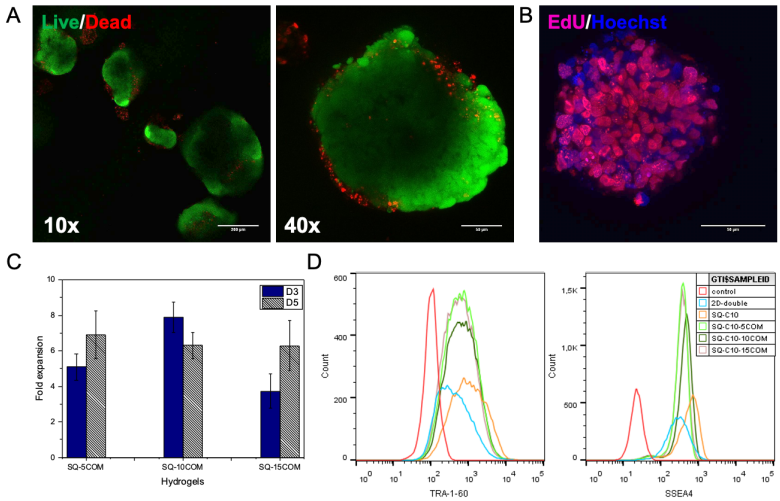

Figure S3.13. A 5-day culture of hiPSCs seeded as clumps in integrin-targeting squaramide hydrogels. A) LIVE/DEAD cell staining of hiPSCs after 5 days of culture in SQ-10COM. Scale bar: 200 µm (10x) and 50 µm (40x). B) Representative images of EdU staining from hiPSCs spheroids that were released from SQ-10COM. Scale bar: 50 µm. C) Expansion fold of hiPSCs in integrin-targeting squaramide hydrogels that were quantified on day 3 and 5. D) FACS measurement of pluripotency marker expression of TRA-1-60 and SSEA4 from hiPSCs after 5 days of culture.

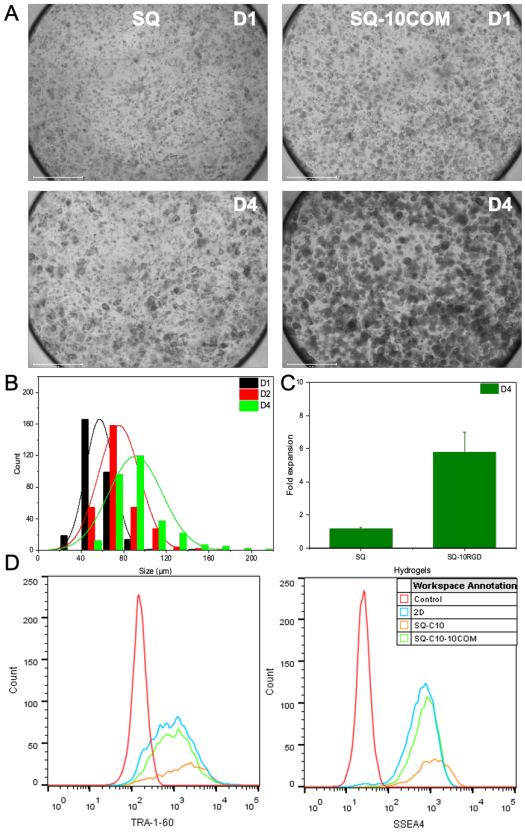

Figure S3.14. A 4-day culture of hiPSCs seeded as single cell in SQ-10COM. A) Brightfield microscopy images of hiPSCs spheroids. Scale bar: 750 µm. B) Size distribution of hiPSC spheroids expanded in SQ-10COM, 300 spheroids were counted. C) Expansion fold of hiPSCs in SQ and SQ-10COM hydrogels quantified after 4 days of culture. D) FACS measurement of pluripotency marker expression of TRA-1-60 and SSEA4 from hiPSCs after 4 days of culture.

3.6.14 Cardiomyocytes differentiation

HiPSCs were released as clumps from a Matrigel coated plate according the protocol described in Figure S3.8 (path b). The differentiation of hiPSCs were performed using the STEMdiff™ Cardiomyocyte Differentiation Kit from StemCell Technologies. At pre-determined time points, hiPSCs were imaged using the EVOS FL AUTO2 equipped with

a temperature controller and CO_2 gas. The video of beating hiPSCs-derived cardiomyocytes were recorded on the EVOS FL AUTO2.

Video S3.1. Spontaneously beating cardiomyocytes cells differentiated from hiPSCs (Day 8) (https://surfdrive.surf.nl/files/index.php/s/HiVGGR1yG2MneDg)

Video S3.2. Spontaneously beating cardiomyocytes cells differentiated from hiPSCs (Day 10) (https://surfdrive.surf.nl/files/index.php/s/g9jFZlHaMHfPBxg)

Video S3.3. Spontaneously beating cardiomyocytes cells differentiated from hiPSCs (Day 16) (https://surfdrive.surf.nl/files/index.php/s/lJWA8LmopH5Xvd8)

3.6.15 Global screening array

The Global Screening Array (GSA) (Illumina) was used according to standard procedures, followed by an analysis in GenomeStudio software (Illumina) using the GSA manifest files. GenomeStudio final reports were used to analyze and visualize in Nexus Discovery (BioDiscovery El Segundo). A report resolution of ~50 kb was used to analyze the data for chromosomal aberrations.

3.6.16 Reference

[1] C. Tong, T. Liu, V. Saez Talens, W. E. M. Noteborn, T. H. Sharp, M. M. R. M. Hendrix, I. K. Voets, C. L. Mummery, V. V. Orlova, R. E. Kieltyka, *Biomacromolecules* **2018**, *19*, 1091.

CHAPTER 4

Dynamic, cyclic thiosulfinate-crosslinked hydrogels enable cardiomyocyte natural behaviour in 3D

This chapter is prepared as an original research paper: Tingxian Liu, Merel Janssen, Maaike Bril, Roxanne E. Kieltyka*

4.1 Abstract

Dynamic materials have emerged as valuable substrates for a broad range of applications in 3D cell culture because of their viscoelastic properties that closely mimic the *in vivo* cell microenvironment. Disulfide-based crosslinks in covalent polymer materials have shown dynamic character through thiol-disulfide exchange. However, control over their formation in these materials remaining challenging. Herein, we report a strategy for generating disulfide crosslinks in polymer materials in a controlled manner cyclic thiosulfinate-functionalized monomers. Mono-S-oxo-1,2-dithiolane (**ODT**) was reacted with 4-arm polyethylene glycol (PEG) to obtain the hydrogel macromer, **PEG-4ODT**, and subsequently with thiol PEGs to rapidly form hydrogels with dynamic and self-recovering properties. To increase the stability of the formed networks, static thiol/vinyl sulfone crosslinks were introduced into the same hydrogel, while retaining their self-healing character and improving their stablility for long term cell culture (14 days). Additionally, this viscoelastic hydrogel supported the culture of hESC-derived cardiomyocytes in 3D, showing cells with elongated morphologies, spontaneous beating and cell alignment while none of them was observed in static hydrogels. The **ODT** unit was proven to be efficient in rapid hydrogel formation while maintaining the viscoelastic character of the materials. Together with thiol/vinyl sulfone crosslinks, the dynamic hydrogel was validated as an efficient matrix for the long term 3D culture of cardiomyocytes that facilitates their native behavior (*e.g.* alignment, beating) and further underlines the importance of the use of dynamic materials for 3D cell culture applications.

4.2 Introduction

The progress of 3D cell culture models is rapidly advancing research in areas of drug discovery, disease modeling, regenerative medicine and tissue engineering due to their indispensable roles in narrowing the gap between *in vitro* culture and *in vivo* conditions.[1–3] The abundant choice in cell source offers the possibility to develop a wide range of models that can mimic healthy and diseased states of tissues. Induced pluripotent stem cells stand out in this regard because of their capacity to differentiate into virtually any cell type of the human body while retaining genetic features of the patient they are obtained from, providing a personalized view in the above areas. In the field of drug discovery there is an interest to develop improved cellular models to better predict toxicity of therapeutic candidates. However, cardiomyocytes derived from induced pluripotent stem cells show distinct morphological, electrical and functional properties in comparison to their adult counterparts because of their fetal-like character.[4–6] These immature features limit their ability to accurately predict patient responses, but further underscore the need to better understand the conditions necessary to promote their maturity.

Natural materials, such as Matrigel, gelatin and collagen, have been widely explored to support the growth cells and tissues. Although they provide numerous biological cues, these matrices are chemically undefined and lack the potential to tune their mechanical properties to match a variety of tissues.[7–10] In contrast, synthetic polymer hydrogels provide an alternative water-rich platform that is chemically defined, with tunable mechanics that can approximate the stiffnesses of a range of tissues.[11–13] In these materials static crosslinks efficiently maintain the gel state during culture, however the materials lack the ability to recapitulate viscoelasticity of native tissues affecting parameters such as cell migration that is critical for morphogenesis.[14] Thus,

synthetic polymer materials that can achieve the stiffness of adult tissues, but contain viscoelastic properties are necessary to support cell behavior in complex processes such as those that are found in development to further refine the available cell culture models.

Dynamic covalent bonds that combine strength of static covalent bonds and reversibility of non-covalent interactions have been broadly applied in the field of polymer chemistry to engineer the viscoelasticity of covalent polymer materials.[15–18] Boronates,[19] disulfides,[20] Diels–Alder adducts,[21,22] thioesters,[16,23] Schiff bases,[24] aldehydes and hydrazides have been frequently reported in this line.[25,26] However, the use of these bonds as crosslinks on their on can be insufficient with respect to machanics and stability in applications such as 3D cell culture. Thus, their combination with static covalent bonds has been examined as a strategy to further control these features for applications in tissue culture. The obtained network benefits from the synergy in properties between both crosslinks, *e.g.* physical and reversible crosslinks that are dynamic and self-healable, and static covalent crosslinks that provide mechanical stiffness and stability.[27–31] For example, Anseth and co-workers employed the boronate chemistry to fabricate an adaptable PEG hydrogel, in which the cis-1,2-diols are crosslinked with boronic acids resulting in a dynamic hydrogel displaying a fast stress relaxation profile. A secondary static crosslink is required support a stable 3D cell culture platform in presence of serum containing media.[19]

Among the dynamic covalent bonds, disulfide chemistry is attractive for biomaterials applications because of its biological relevance and reversibility under mild conditions with respect to various stimuli (*e.g.* redox, light, heat). However, the introduction of crosslinks based on disulfides can sometimes prove challenging due to premature cross-linking of the polymers prior to their application. Hence, latent or protecting group strategies have been used to facilitate their introduction into polymer materials. Latent strategies using cyclic 1,2-dichalcogenides, such as 1,2-dithiolanes,

are attractive because of their capacity to form poly(disulfides) on ring opening polymerization through the addition of nucleophiles or light in water. Moreover, thiol/cyclic 1,2-dithiolane exchange reactions were faster than that of thiol and linear disulfide,[32,33] and these reactions are reversible and tunable, depending on the substituent pattern on the cyclic dithiolane ring.[34] Waymouth and co-workers designed novel water-soluble triblock (ABA) copolymers with pendant 1,2-dithiolanes that form hydrogels based on thiol-initiated ring opening polymerization of pendant 1,2-dithiolanes with shear-thinning and dynamic flow behaviors as a result of the formed disulfide polymers.[20,35] Recently, we reported use of cyclic 1,2-dithiolanes to crosslink with norbornene on linear PEG polymers through UV irradiation obtaining hydrogel materials with branched macromolecular architectures and self-recovering properties.[36] However, due to the use of small molecules or light to facilitate their crosslinking, their application can be challenging when more sensitive cell types are involved and thus, latent strategies that enable gel formation in a controlled and rapid manner with high cytocompatibility remain necessary.

Thiosulfinates are intermediates obtained in the oxidation of thiols to sulfonic acids. While efficient in making disulfide-containing compounds, in most cases, the linear thiolsulfinates easily decompose upon heating. Recently, Donnelly *et al.* reported several chemically stable cyclic thiosulfinates that were easily synthesized by oxidication of cyclic disulfide. The use of cyclic thiosulfinates for protein crosslinking was validated, reacting rapidly (~10 min, >95% conversion) in comparison to days in the case of 1,2-dithiane.[37] Because of the rapid protein cross-linking kinetics, we became interested in the capacity of this latent thiol strategy to crosslink polymer materials for 3D cell culture applications. We introduced 1,2-dithiolane-1-oxide (**ODT**) on a 4-arm PEG macromer (**PEG-4ODT**) and evaluated its triggering by thiol-functionalized PEG (**PEG-4SH**) to form polymer materials with disulfide crosslinks. We further examined the use of this cross-linking chemistry to prepare scaffolds with modular stiffness for

the 3D culture of embryonic pluripotent stem cell derived cardiomyocytes focusing on understanding the consequence of their dynamic character driving native cell behaviours.

4.3 Results and Discussion

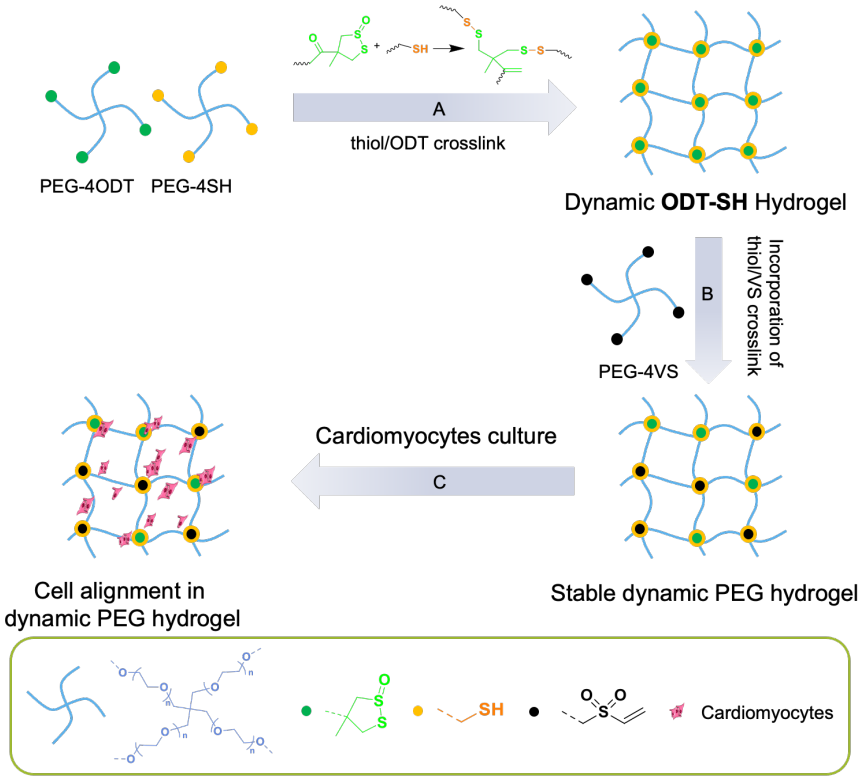

Scheme 4.1. A) Preparation of dynamic ODT-SH hydrogels: mixing of PEG macromers **PEG-4ODT** and **PEG-4SH** yields dynamic disulfide crosslinked hydrogels with tunable stiffnesses. B) After incorporation of thiol/VS crosslinks by mixing of **PEG-4VS** macromers, a stable and dynamic PEG hydrogel was obtained. C) Cardiomyocytes that were 3D cultured in this dynamic PEG hydrogel displayed natural cell behavior: cell alignment.

ODT-crosslinked hydrogel preparation and characterization. Two PEG macromers, end-functionalized with a cyclic disulfide (dithiolane, **DT**), and a cyclic thiosulfinate

(**ODT**) were first synthesized (Scheme S4.1). **DT** and **ODT** with carboxylic acid handles were synthesized according to previous reports,[38] prior to coupling coupled onto hydroxy PEG macromers through Steglich esterification in presence of N,N'-dicyclohexylcarbodiimide (DCC) and 4-dimethylaminopyridine (DMAP). The **DT** (**PEG-4DT**) and **ODT**-functionalized 4-arm PEG macromers (**PEG-4ODT**) were obtained by precipitation in cold diethyl ether and dialyzed against water with a high degree of end-functionalization (**PEG-4DT** ca. 86%, Figure A4.5; **PEG-4ODT** ca. 90%, Figure A4.6). Following a similar protocol, the **ODT**-functionalized linear PEG macromer (**PEGdiODT**) was prepared with a high degree of functionalization of 86%. Detailed synthetic information can be found in the Supporting Information.

To prepare the hydrogels, stock solutions of PEG macromers **PEG-4DT** and **PEG-4ODT** were first dissolved in PBS (pH 7.4) and mixed in particular ratios to result in their gelation. Gel inversion tests were first performed on hydrogels consisting of **PEG-4ODT** and **PEG-4SH** (**ODT-SH** hydrogels) at a fixed thiol/ODT molar ratio to gain insight into the concentrations where gels are formed and gelation time. Transparent hydrogels were formed when the total PEG macromer concentrations were higher than 4 mM with thiol/ODT molar ratios at 1:1 and 2:1 (Figure S4.1 and S4.2), while no hydrogels were formed using the same conditions for **PEG-4DT** and **PEG-4SH**. This result points to the decreased reactivity of thiol/DT pair in comparison thiol/ODT pair, and is consistent with an earlier report of Agar and co-workers.[37] Notably, **ODT-SH** hydrogels formed within 5 min when the PEG macromer concentration was higher than 6 mM, showcasing the rapid kinetics of the thiol/ODT reaction and suitability for 3D cell culture applications. Moreover, the gelation kinetics were faster than the thiol/VS bioconjugation reaction where 10 mins were necessary to form hydrogels on a PEG macromer concentration of 12 mM (Figure S4.3). To better understand the thiol/ODT reaction on polymer materials, linear PEG macromers with **ODT** were also prepared. Hydrogels were formed at a total PEG macromer concentration of 10 mM suggesting

the reaction of one **ODT** moiety with more than one thiol group to form a crosslinked network between linear PEGs. This rapid crosslinking between thiol and **ODT** opens a new route to prepare hydrogels from both star and linear PEG macromers under cell culture conditions.

Oscillatory rheology measurements were performed to quantitatively assess the gelation time and mechanical properties of the disulfide networks. The **ODT-SH** hydrogels showed storage moduli (G') that were significantly greater than the loss moduli (G'') with tunable stiffness and gelation time based on macromer concentration. In contrast, the mixing of **PEG-4DT** and **PEG-4SH** resulted in a rheological profile consistent with the lack of gel formation (G''>G') (Figure 4.1A). The stiffness of **ODT-SH** hydrogels can be tuned from 200 Pa to 5 kPa by varying total PEG macromer concentration from 4.5 to 8 mM. Moreover, the gelation time also decreased from 10 to less than 1 min with increasing the total PEG macromer concentration (Figure 4.1B). For **ODT-SH** hydrogel consisting of 3.0 mM **PEG-4ODT** and 3.0 mM **PEG-4SH**, the linear viscoelastic (LVE) region showed a limit of applied strain of 322%. Frequency sweep measurements demonstrated that G' was greater than G'' by two orders of magnitude over the frequency range from 0.01 Hz to 10 Hz, confirming the formation of viscoelastic materials (Figure S4.6). To probe the contribution of the dynamic thiol/ODT crosslinks to the **ODT-SH** hydrogel mechanical properties, we tested their capacity to self-recover by performing a step-strain experiment. The storage modulus (G') recovered more than 90% of its original value after the application of large strain (700 %) within 2 min (Figure 4.1C). Alternating the strain from high (700%) to low (0.05%) in a cyclic manner further exposed the potential recovery property of the materials. Considering their subsequent application as 3D cell culture materials, the mechanical properties of the hydrogels were further tested at 37˚C. The data showed that G' measured at room temperature was 5.4, 3.5, 2.2 and 1.9 times higher than the samples measured at 37˚C when total PEG macromer concentrations were 4.5, 5, 6,

and 8 mM, respectively (Figure 4.1D). The decreased stiffness of the materials likely results from the increased rate of thiol/disulfide exchange at 37˚C,[39] further indicating the formation of disulfide crosslinks and the inherent dynamic character of the network. Importantly, the **ODT-SH** hydrogel retained its viscoelastic and self-healing properties at 37˚C, opening the door to its future use in 3D cell culture applications (Figure S4.7).

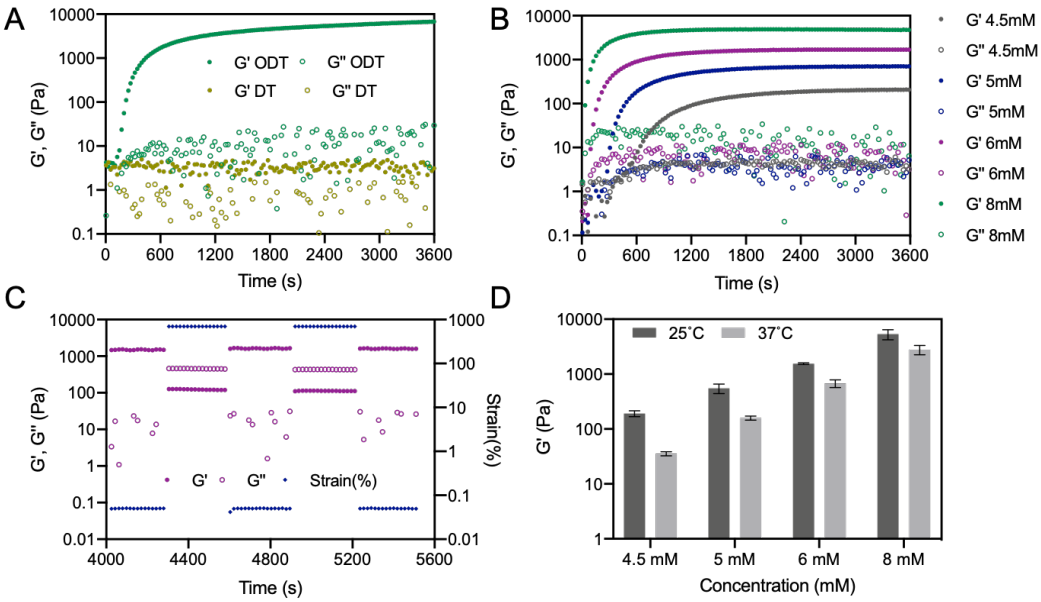

Figure 4.1. A) Storage (G') and loss moduli (G'') of **ODT-SH** hydrogels and **DT-SH** networks collected by a time sweep measurement at 25 ± 0.2˚C with a fixed frequency of 1 Hz and strain of 0.05%. B) Time sweep measurements of **ODT-SH** hydrogels with total PEG macromer concentrations of 4.5, 5, 6 and 8 mM. G' and G'' were collected at 25 ± 0.2˚C with a fixed frequency of 1 Hz and strain of 0.05% until a plateau in the moduli was obtained. C) Step-strain measurements of **ODT-SH** hydrogel (6 mM) at 25 ± 0.2˚C with a frequency of 1 Hz; Low (0.05%) and high strain (700%) were applied for 300s alternatively for two times. D) Averaged storage moduli (G') of **ODT-SH** hydrogels that measured under 25 ± 0.2˚C and 37 ± 0.2˚C with total PEG macromer concentrations at 4.5, 5, 6 and 8 mM, respectively. (N = 3)

To characterize crosslinking of thiol/ODT at molecular level, nuclear magnetic resonance (NMR) and liquid chromatography–mass spectrometry (LCMS) experiments were performed using model molecules. The reaction between **ODT** unit and glutathione (GSH) in deuterated water (D_2O) was monitored by NMR spectroscopy, and changes to **ODT** were followed tracking the chemical shift of the -CH_3 group. Unreacted **ODT** shows a chemical shift of 1.62 ppm for the -CH_3 group, whereas its reaction with GSH shows an upfield shift 1.48 ppm to 1.31 ppm. After 75 h incubation using a thiol/ODT molar ratio of 1:1, 51% ODT was consumed and this value increased to 100% when the thiol/ODT molar ratio was increased to 2:1, 4:1 and 8:1, implying that **ODT** reacts with GSH in a 1:2 molar ratio. Moreover, LCMS data supports the determined ratios from NMR, as **ODT** molecules were transferred into compound **M1** (t=2.55 min, m/z 777.25), as previously reported for the crosslinking of proteins with cyclic thiosulfinate. When **ODT** was treated with excess GSH (thiol/ODT molar ratio at 4:1 and 8:1), a major shift from 1.31 to 1.48 ppm was recorded and a new compound **M3** (t=3.17, m/z 942.67) was identified. These results indicate that the thiol/ODT crosslinking reaction involves two steps: one, the **ODT** reacts with GSH in a molar ratio of 1:2; two, **M1** undergoes further thiol/disulfide exchange in presence of thiols to form product **M3** (Figure S4.5).

To investigate the applicability of the thiol/ODT chemistry for 3D cell culture, NIH 3T3 cells were encapsulated within the **ODT-SH** hydrogels. PEG macromer concentrations were kept at 6 mM and thiol/ODT molar ratios were varied from 1:1, 2:1 and 4:1 (Figure S4.10). From LIVE/DEAD staining results, over 95% cells remained viable after 2 h culture and were homogeneously distributed throughout the gel. After 48 h cell culture, while the cells maintained high viability (> 80%) they settled down to the bottom due to the dissolution of hydrogel over the culture period. This result is likely due to the dynamic character of the polymer materials due to the disulfide

crosslinks, as similar behavior has been reported for other dynamic hydrogels.[19,40] Thus, to overcome the rapid gel erosion encountered in the **ODT-SH** hydrogels under the cell culture conditions, static thiol/VS crosslinks based on permanent covalent bonds were introduced into the polymer networks at the expense of the thiol/ODT crosslinks.

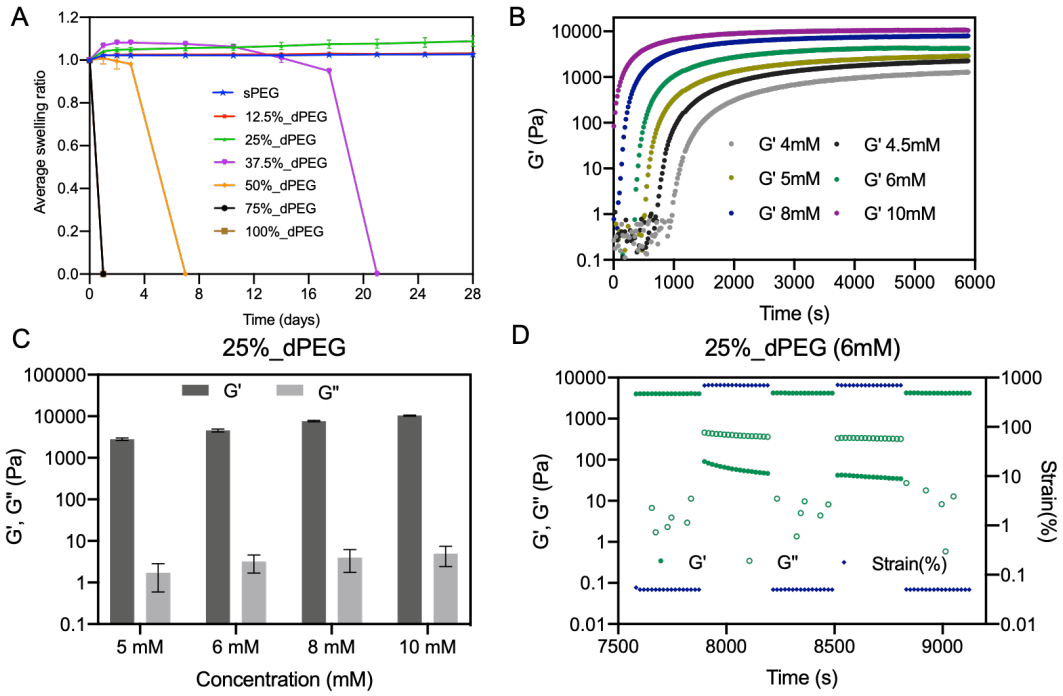

Figure 4.2. Characterization of dynamic PEG hydrogels that consist of both dynamic and static crosslinks. A) Swelling measurements of PEG hydrogels: swelling ratios were examined as a function of the percentage of dynamic disulfide crosslinks on a total PEG macromer concentration of 6 mM. B) Oscillatory rheology time sweep measurements of **25%_dPEG** hydrogels at total PEG macromer concentrations of 4, 4.5, 5, 6, 8 and 10 mM. Storage (G') and loss moduli (G'') were collected at 37 ± 0.2˚C with a fixed frequency of 1 Hz and strain of 0.05% until a plateau in the moduli was reached. C) Averaged (N = 3) plateau moduli, G' and G'', of **25%_dPEG** hydrogels at total PEG macromer concentrations of 5, 6, 8 and 10 mM from frequency sweep measurements.

D) Step-strain measurements of **25%_dPEG** (6 mM) at 37 ± 0.2˚C at a frequency of 1 Hz; low (0.05%) and high strain (700%) were applied in alternation for 300s over two cycles.

Dynamic PEG hydrogel preparation and characterization. Hydrogels prepared from exclusively thiol/VS crosslinks are known to be stable and support cell culture in presence of medium containing serum.[41] Therefore, swelling experiments were performed on gels with both static and dynamic covalent crosslinks to determine the ratio of dynamic and static bonds necessary to prepare gels stable for cell culture experiments. Hydrogels with 12.5%-100% thiol/ODT crosslinks were prepared keeping the total PEG macromer concentration at 6 mM, and then incubated with cell culture medium at 37˚C. As observed in earlier viability experiments, **ODT-SH** hydrogels that consist of exclusively thiol/ODT crosslinks were completely dissolved within 24 h. In contrast, hydrogels formed from 100% thiol/VS crosslinks (**sPEG**) remain stable over the entire duration of the experiment (28 days) (Figure 4.2A). However, hydrogels containing 25% or less thiol/ODT crosslinks showed comparable stability to the **sPEG** hydrogel over a 28-day period. Based on their stability under cell culture conditions, the **25%_dPEG** network was selected for further culture experiments.

The consequence of including permanent cross-links on the mechanical properties of the **25%_dPEG** network was further examined using oscillatory rheology. Similar trends were observed to the **ODT-SH** hydrogels in the various experiments. The stiffness of **25%_dPEG** hydrogels displayed a concentration-dependent trend, in which G’ varied from 1.3 kPa to 10.4 kPa with varying the total PEG macromer concentrations from 4 to 10 mM. The gelation time decreased with increasing PEG macromer concentration from 16 min to less than 1 min (Figure 4.2B and 4.2C). The LVE region was determined by performing an amplitude sweep experiment in a range of strain from 0.1% to 1000% and a fixed frequency of 1 Hz. In the case of **25%_dPEG** hydrogels (5 mM and 6 mM), G’ and G’’ remained constant until 56% strain, whereas for

25%_dPEG hydrogels (8 mM and 10 mM) a shift from the linear regime was observed at a strain of 99%. During frequency sweep measurements ranging from 0.01 Hz to 10 Hz, in all test concentrations, G' was greater than G'' by two orders of magnitude confirming the formation of viscoelastic materials from hybrid crosslinks (Figure S4.8). Most importantly, a high self-recovery capacity (~90%) was observed in all **25%_dPEG** hydrogels after applying high strain (700%) and low strain (0.05%) alternatively for two cycles (Figure 4.2D and S4.9). Overall, the combination of the long-term stability and high self-recovery capacity of the covalent networks with 25% dynamic thiol/ODT crosslinks can be useful for healthcare applications.

As a first approach to cell culture within **25%_dPEG** hydrogel**,** cell encapsulation and viability experiments were performed. NIH 3T3 cells were encapsulated in 3D within **25%_dPEG** hydrogels using total PEG macromer concentrations of 4.5, 6 and 10 mM and cultured for 4 days. LIVE/DEAD staining of the hydrogels after this time period showed that the cells were mainly green-stained for all tested conditions indicating that the **25%_dPEG** hydrogel is cytocompatible (Figure 4.3). It should be noted that a lot of cells settled down in case of 6 mM hydrogels after 4 days of culture. Since the swelling ratio of **25%_dPEG** hydrogel at this concentration stays stable at 1.06, we infer that there is an interaction between dynamic hydrogels and cellular thiols or disulfides that results in the dissolution of network leading to cell sedimentation. Even though cell sedimentation occurred gradually after 4 days of culture, the **25%_dPEG** hydrogel still supported cells within the well. When a higher concentration of PEG macromers of **25%_dPEG** hydrogel was used (10 mM), cells were supported in 3D with a reasonable cell viability (>60%) during the 4 days of culture, after which cell-laden hydrogel can be easily taken up by a spatula. Taken together, **25%_dPEG** hydrogel was proven to be cell compatible at both low (4.5 mM) and high (10 mM) PEG macromer concentrations and long-term culture can be realized by introducing the second thiol/VS crosslink into 100% thiol/ODT hydrogels.

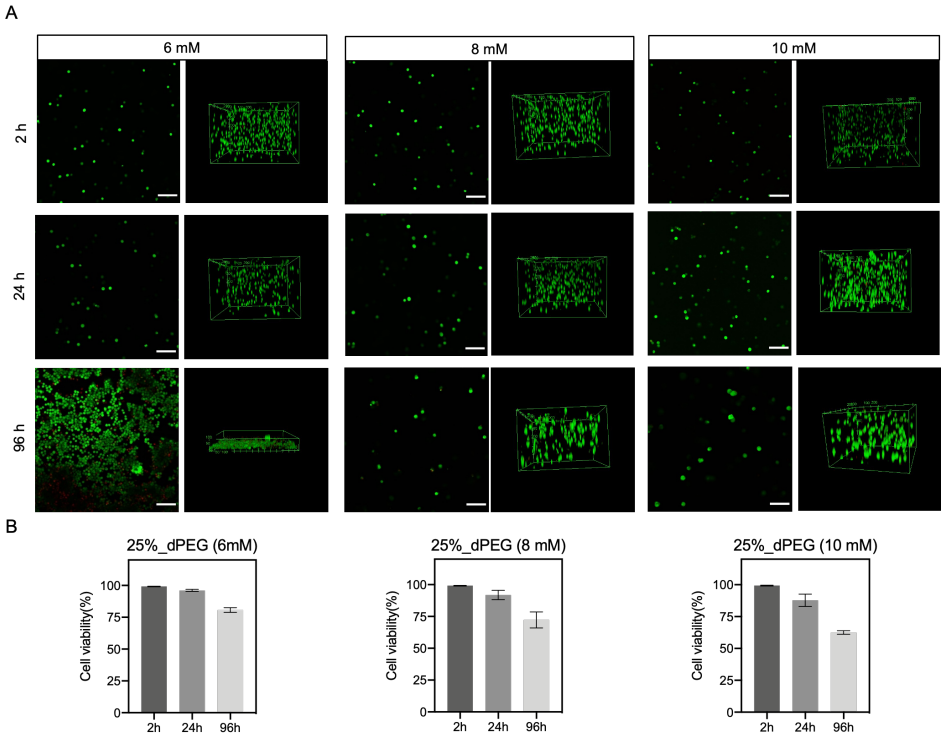

Figure 4.3. 3D cell culture in **25%_dPEG** hydrogels with total PEG macromer concentrations of 6, 8 and 10 mM. A) Representative 2D images and z-stack 3D overview of cells in **25%_dPEG** hydrogel (6 mM) after 2, 24 and 96h culture. Cells were stained with calcein AM (viable cells, *green*) and propidium iodide (PI) (dead cells, *red*). Scale bar = 100 µm. B) Cell viability percentages were calculated by cell counting in Fiji after LIVE/DEAD staining. The means and standard deviations are marked inside the graphs, N=3.

Maturation of hESC-derived CMs within 25%_dPEG hydrogel. The matrix microenvironment plays an important role in guiding cell behavior, for example, the morphology, spontaneous contraction and eventually, maturation of CMs. Few examples have been reported in fabricating dynamic materials while decoupling the biological cues to understand their effect on cell fate. In this work, a genetically modified hESC cell line was used that shows fluorescence through GFP for the cardiac transcription marker Nkx2.5 and mRuby for α-actinin. First, the hESC-derived CMs were

prepared by seeding hESCs on Matrigel coated plates and differentiated as a monolayer using the STEMdiff™ Cardiomyocyte Differentiation Kit. Bright field and fluorescence microscopy images of their differentiation in 2D were taken over a 28-day period as a control. As shown in Figure S4.11, the hESCs started to express the cardiac transcription factor Nkx2.5 (GFP fluorescence) on day 7, and the expression became more uniform across the cells during their further differentiation. Conversely, expression of α-actinin as observed from the fluorescence of mRuby is hardly visible until day 9, increasing in intensity after day 14 and maintained a uniform expression until day 28. Notably, sarcomeres were visualized through the mRuby labeled α-actinin showing mainly disordered structure that does not resemble the organization of sarcomeric α- actinin in native human myocardium.[42] RT-PCR experiments were subsequently performed to obatin a quantitative insight into cardiac and pluripotent gene expression. As seen in Figure S4.12, expression of pluripotent genes Oct4, Sox2 and Nanog was significantly decreased over the differentiation period ($P<0.0001$). Meanwhile, increased expression of cardiac structural genes cTnT, MYH6 and MYH7 were measured that is in line with the experimental observation of spontaneously beating cardiomyocytes in the culture. Cx43 protein that codes for gap junctions that are critical for synchronous contraction of CMs, showed significantly decreased expression after 8 days of differentiation ($P<0.01$) and remained low during the whole differentiation process supporting the inhomogeneous beating of cardiomyocytes. Taken together, the increased expression of cardiac makers and genes together with significantly decreased pluripotency gene expression demonstrated the successful differentiation of the hESC reporter line to cardiomyocytes in 2D.

The hESC-CMs were collected after being prepared as a monolayer and reseeded in 3D in the **25%_dPEG** and **sPEG** hydrogels to study their cell behavior in 3D with respect to various stiffnesses. From the confocal microscopy images, hESC-CMs cultured within all tested hydrogels maintained the expression of Nkx2.5_GFP and the

α-actinin_mRuby (Figure 4.4). Spontaneous beating was not immediately observed after seeding in 3D, but after 3 days of culture, hESC-CMs encapsulated in **25%_dPEG** (6 mM, 4.5 kPa) hydrogel started beating, becoming more robust with further culture. The loss and recovery of spontaneous beating of CMs is on par with literature reports that show 2-3 days are necessary to regain this behavior.[43,44] In case of **sPEG** hydrogel, hESC-CMs did not spontaneously beat after reseeding, and even after further culture pointing out the importance of a dynamic environment to promote native hESC-CM behavior. Recovery of the beating of hESC-CMs was observed on day 14 for **25%_dPEG** hydrogels with higher concentration and stiffness (8 mM, 8 kPa), whereas further increasing the stiffness did not yield any cell beating in **25%_dPEG** hydrogels (10 mM, 10.5 kPa). This observation can be rationalized by the inverse correlation between substrate stiffness and CM contraction,[45] that is, increased stiffness is expected to delay the recovery of hESC-CM contraction.

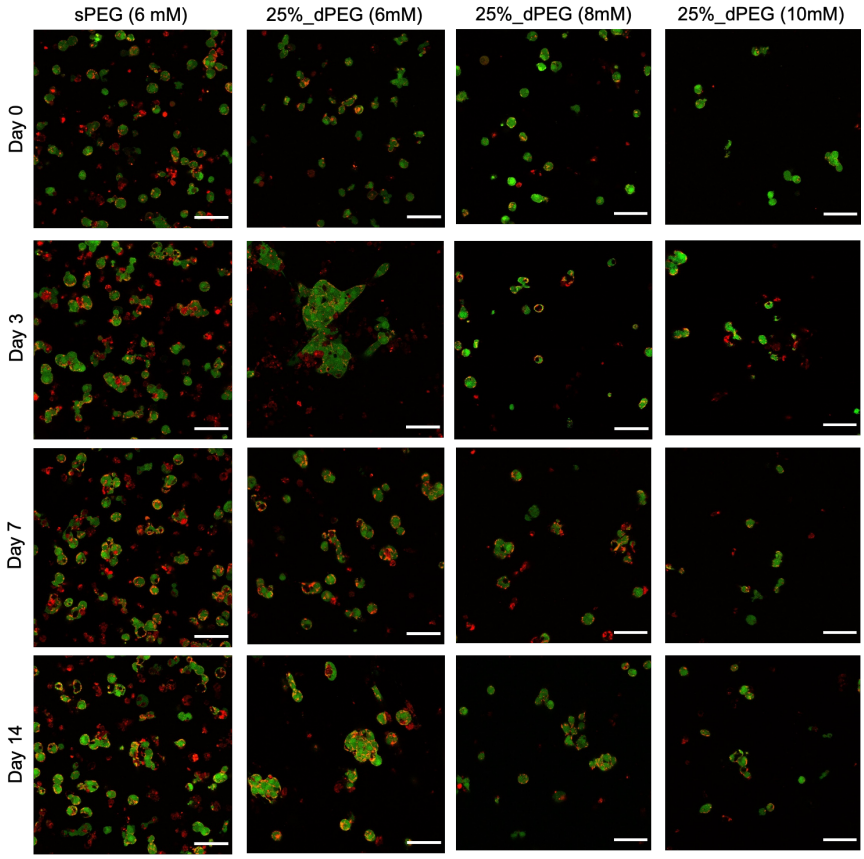

Figure 4.4. Representative confocal microscopy images of hESC-CMs reseeded and cultured within **25%_dPEG** and **sPEG** hydrogels for 14 days after differentiation on Matrigel. Merged flurescent images of cardiac transcription factor Nkx2.5_GFP (Green) and the sarcomeric protein α-actinin_mRuby (Red) of the hESC-CMs after 0, 3, 7 and 14 days of reseeding, respectively. Scale bar: 50 µm.

Morphology of hESC-CMs within the **25%dPEG** and **sPEG** hydrogel were captured by brightfield microscopy using a 10x objective (Figure 4.5). In comparison to the round morphology of hESC-CMs in **sPEG** hydrogel, hESC-CMs cultured in **25%_dPEG** (6 mM) hydrogel displayed an elongated shape. More interestingly, after one day of culture, hESC-CMs started to spontaneously align in this soft and dynamic hydrogel (G' 4.5 kPa), behaving similarly to the alignment of CMs in native tissues. Also, hESC-CMs started to show a similar alignment in the **25%_dPEG** hydrogel (8 mM) on day 14. In case of stiff

25%_dPEG hydrogel (10 mM), cells displayed a round morphology and no alignment were observed over the culture period. This trend in cell behavior in **25%_dPEG** hydrogel with respect to the beating of hESC-CMs, therefore, it is likely the dynamic nature of the hydrogel plays critical role in supporting their native behaviors.

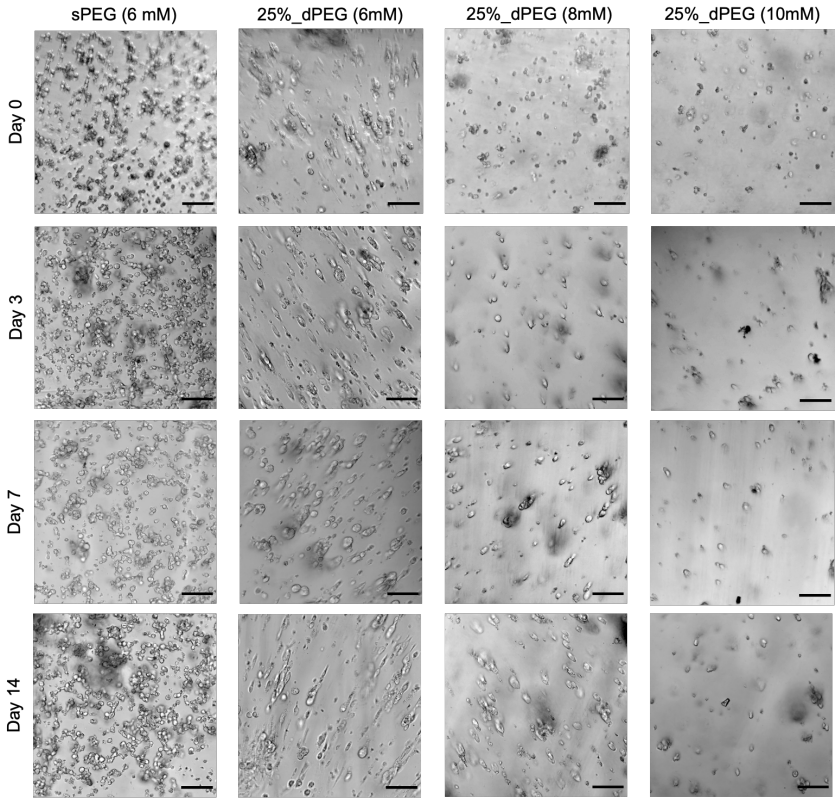

Figure 4.5. Bright field microscopy images of hESC-CMs that differentiated in 2D for 14 days and then cultured in **25%_dPEG** (6, 8, 10 mM) and **sPEG** (6 mM) hydorgels for 3, 7 and 14 days, respectively. Scale bar: 100 µm.

To gain more quantitative information about cardiomyocyte maturation in the dynamic hydrogels in 3D, RT-PCR experiments were performed at two different time points. Gene expression analysis revealed that the relative expression levels of Cx43 and MYH7 were comparable in 2D and 3D hydrogel-based cultures (Figure 4.6). The hESC-CMs that were cultured in **25%_dPEG** hydrogels (6 mM) displayed a significantly higher cardiac troponin T, cTnT, expression than in 2D ($p < 0.05$) (Figure 4.6B). This

increase was not observed for hESC-CMs cultured in **sPEG** hydrogels (6 mM). This result could explain the differenence in spontaneous beating that was observed in **sPEG** and **25%_dPEG** (6 mM) hydrogels as the cTnT protein controls the interaction between actin and myosin that work together in cardiomyocyte contraction. Moreover, a significant increase in MYH6 expression was observed for cells in **sPEG** and **25%_dPEG** hydrogels (6 mM), in comparison to those maintained in 2D ($P<0.05$ and $P<0.01$, respectively) (Figure 4.6C). Also, a significant difference in expression of MYH7 was measured in 2D with a 17-fold increase in expression at day 28 in 2D, while in 3D in **25%_dPEG** hydrogels, a 1.5, 6 and 2-fold increase in 6 mM, 8 mM and 10 mM hydrogels, respectively, was obtained. The observation of an increase expression of MYH7 expression in 2D culture but a more subtle change in the 3D culture samples is most likely due to the variable cell density of the CMs within the hydrogels. Therefore, seeding a higher cell density within the gels or prolonging the culture time of hESC-CMs in the hydrogels in 3D is recommended to enhance the isoform transition from MYH6 to MYH7. Taken together, 14-day culture of hESC-CMs in a soft and dynamic hydrogels, **25%_dPEG** (6 mM), facilitated spontaneous beating and alignment, significantly increased expression of cTnT and MYH6 accompanied by an elongated morphology. Hence, these experiments set the stage for the further examination of our hydrogels to mature hESC-CMs.

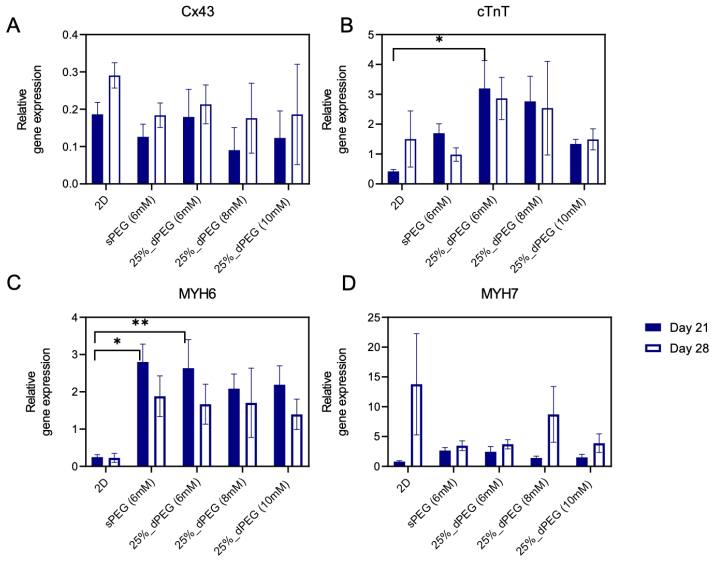

Figure 4.6. Relative gene expression profiles of hESC-CMs cultured on Matrigel in 2D for 21 and 28 days, or differentiated in 2D for 14 days and then encapsulated within 3D PEG hydrogels for another 7 days and 14 days culture. A: Cx43. B: cTnT. C: MYH6. D: MYH7. The means and standard deviations are marked inside the graphs, N = 6, *P < 0.05, ** P< 0.01.

4.4 Conclusions

A novel strategy to engineer disulfide-based hydrogel matetials using latent cyclic thiosulfinate is disclosed. Quick gelation, on the order of minutes, self-recovery and cytocompatible cell encapsulation was achieved. During 3D culture, dissolution of the hydrogel was observed when exclusively disulfide crosslinks are used. To obatin stable long-term cell culture, hydrogels with formulation of 25% dynamic crosslinks (thiol/ODT) and 75% static crosslinks (thiol/VS), or **25%_dPEG** hydrogels, needed to be employed. This ratio showed self-recovery properties, and simultaneous increase in stability over 4 weeks as shown by swelling measurements. The **25%_dPEG** hydrogels supported the culture of hESC-CMs with elongated morphologies, rapid recovery of cell spontaneous beating and cell alignment, demonstrating the crucial role of dynamic

matrix in supporting their natural behavior. Together with the significant increased expression of cardiac genes cTnT and MYH6, it is established that these materials show tremendous potential for cardiomyocytes maturation studies in the future.

4.5 References

[1] S. A. Langhans, *Front. Pharmacol.* **2018**, *9*, 1.

[2] M. Caiazzo, Y. Okawa, A. Ranga, A. Piersigilli, Y. Tabata, M. P. Lutolf, *Nat. Mater.* **2016**, *15*, 344.

[3] R. Y. Tam, L. J. Smith, M. S. Shoichet, *Acc. Chem. Res.* **2017**, *50*, 703.

[4] R. E. Michler, *Methodist Debakey Cardiovasc. J.* **2013**, *9*, 187.

[5] D. Zhang, I. Y. Shadrin, J. Lam, H. Q. Xian, H. R. Snodgrass, N. Bursac, *Biomaterials*. **2013**, *34*, 5813.

[6] S. S. Nunes, J. W. Miklas, J. Liu, R. Aschar-Sobbi, Y. Xiao, B. Zhang, J. Jiang, S. Massé, M. Gagliardi, A. Hsieh, N. Thavandiran, M. A. Laflamme, K. Nanthakumar, G. J. Gross, P. H. Backx, G. Keller, M. Radisic, *Nat. Methods.* **2013**, *10*, 781.

[7] L. Jin, T. Feng, H. Ping, R. Zerda, A. Luo, J. Hsu, A. Mahdavi, M. Sander, **2013**, *110*, 3907.

[8] S. Kim, J. Turnbull, S. Guimond, *J Endocrinol.* **2011**, *209*, 139.

[9] J. Sapudom, T. Pompe, *Biomater. Sci.* **2018**, *6*, 2009.

[10] A. Higuchi, Q. Ling, S. Hsu, A. Umezawa, *Chem. Rev.* **2012**, *112*, 4507.

[11] M. P. Lutolf, J. A. Hubbell, *Nat. Biotechnol.* **2005**, *23*, 47.

[12] C. Xu, W. Lee, G. Dai, Y. Hong, *ACS Appl. Mater. Interfaces.* **2018**, *10*, 9969.

[13] S. Ligation, E. Cambria, K. Renggli, C. C. Ahrens, C. D. Cook, C. Kroll, A. T. Krueger, B. Imperiali, L. G. Gri, *Biomacromolecules.* **2015**, *16*, 2316.

[14] G. P. Raeber, M. P. Lutolf, J. A. Hubbell, *Biophys. J.* **2005**, *89*, 1374.

[15] M. W. Tibbitt, *Mater. Today Chem.* **2019**, *12*, 16.

[16] T. E. Brown, B. J. Carberry, B. T. Worrell, O. Y. Dudaryeva, M. K. McBride, C. N. Bowman, K. S. Anseth, *Biomaterials* **2018**, *178*, 496.

[17] Z. Wei, S. Gerecht, *Biomaterials* **2018**, *185*, 86.

[18] E. Hui, K. I. Gimeno, G. Guan, S. R. Caliari, *Biomacromolecules* **2019**, *20*, 4126.

[19] S. Tang, H. Ma, H. C. Tu, H. R. Wang, P. C. Lin, K. S. Anseth, *Adv. Sci.* **2018**, *5*, 1.

[20] G. A. Barcan, X. Zhang, R. M. Waymouth, *J. Am. Chem. Soc.* **2015**, *137*, 5650.

[21] C. M. Madl, S. C. Heilshorn, *Chem. Mater.* **2019**, *31*, 8035.

[22] S. Mukherjee, M. R. Hill, B. S. Sumerlin, *Soft Matter* **2015**, *11*, 6152.

[23] M. D. Konieczynska, J. C. Villa-Camacho, C. Ghobril, M. Perez-Viloria, K. M. Tevis, W. A. Blessing, A. Nazarian, E. K. Rodriguez, M. W. Grinstaff, *Angew. Chemie* **2016**, *128*, 10138.

[24] Z. Wei, D. M. Lewis, Y. Xu, S. Gerecht, *Adv. Healthc. Mater.* **2017**, *6*, 1.

[25] P. K. Sharma, S. Taneja, Y. Singh, *ACS Appl. Mater. Interfaces* **2018**, *10*, 30936.

[26] L. L. Wang, C. B. Highley, Y. C. Yeh, J. H. Galarraga, S. Uman, J. A. Burdick, *J. Biomed. Mater. Res. - Part A* **2018**, *106*, 865.

[27] L. Cai, R. E. Dewi, S. C. Heilshorn, *Adv. Funct. Mater.* **2015**, *25*, 1344.

[28] C. Han, H. Zhang, Y. Wu, X. He, X. Chen, *Sci. Rep.* **2020**, *10*, 14997.

[29] C. B. Rodell, J. W. M. Jr, S. M. Dorsey, R. J. Wade, L. L. Wang, Y. J. Woo, J. A. Burdick, *Adv. Funct. Mater.* **2015**, *25*, 636.

[30] L. Ouyang, C. B. Highley, C. B. Rodell, W. Sun, J. A. Burdick, *ACS Biomater. Sci. Eng.* **2016**, *2*, 1743.

[31] H. Clevers, P. Matthias, *Nat. Publ. Gr.* **2016**, *539*, 560.

[32] J. A. Bums, G. M. Whitesides, *J. Am. Chem. Soc.* **1990**, *112*, 6296.

[33] R. Singh, G. M. Whitesides, *J. Am. Chem. Soc.* **1990**, *112*, 6304.

[34] D. P. Donnelly, J. N. Agar, S. A. Lopez, *Chem. Sci.* **2019**, *10*, 5568.

[35] X. Zhang, R. M. Waymouth, *J. Am. Chem. Soc.* **2017**, *139*, 3822.

[36] C. Tong, J. A. J. Wondergem, D. Heinrich, R. E. Kieltyka, *ACS Macro Lett.* **2020**, 882.

[37] D. P. Donnelly, M. G. Dowgiallo, J. P. Salisbury, K. C. Aluri, S. Iyengar, M. Chaudhari, M. Mathew, I. Miele, J. R. Auclair, S. A. Lopez, R. Manetsch, J. N. Agar, *J. Am. Chem. Soc.* **2018**, *140*, 7377.

[38] X. Marat, K. Lucet-Levannier, L. Marrot, **2013**, U.S. Patent No. US8530511B2.

[39] P. Nagy, *Antioxidants Redox Signal.* **2013**, *18*, 1623.

[40] M. D. Konieczynska, M. W. Grinstaff, *Acc. Chem. Res.* **2017**, *50*, 151.

[41] S. A. Stewart, M. B. Coulson, C. Zhou, N. A. D. Burke, H. D. H. Stöver, *Soft Matter* **2018**, *14*, 8317.

[42] K. Ronaldson-bouchard, P. Stephen, K. Yeager, T. Chen, L. Song, D. Sirabella, K. Morikawa, D. Teles, M. Yazawa, G. Vunjak-Novakovic, *Nature*. **2018**, *556*, 239.

[43] C. Xu, Y. Li, Y. Chen, C. Priest, M. A. Laflamme, W. Zhu, B. Van Biber, L. Hegerova, K. Delavan-, J. Lebkowski, J. D. Gold, *Regenerative Medicine*. **2011**, *6*, 53.

[44] L. Van Den Brink, K. O. Brandão, L. Yiangou, M. P. H. Mol, C. Grandela, C. L. Mummery, A. O. Verkerk, R. P. Davis, *Stem Cell Res.* **2020**, *43*, 101698.

[45] K. Shapira-schweitzer, D. Seliktar, *Acta Biomater*. **2007**, *3*, 33.

4.6 Supporting information

4.6.1 Materials

Tetra-arm hydroxy-terminated PEG (Mw 10 kDa) and thiol-terminated PEG (Mw 10 kDa) were obtained from Creative PEGWorks and Jenkem Technology, respectively. Poly(ethylene glycol) (Mw 6 kDa) and α,Ω-Bis-mercapto poly(ethylene glycol) (Mw 6 kDa) were purchased from Fluka and Iris Biotech GMBH. Deuterated dimethyl sulfoxide (DMSO-d_6) and chloroform ($CDCl_3$) were purchased from Eurisotop. All other chemicals and reagents for synthesis were purchased from Sigma Aldrich and used without further purification. Dulbecco's modified Eagle medium (DMEM) was from Gibco, Life Technologies. Vitronectin XF^{TM}, Essential 8^{TM} medium and Ethylenediaminetetraacetic acid disodium salt (EDTA) were purchased from ThermoFisher Scientific. Dulbecco's Phosphate Buffered Saline (DPBS), calcein AM (AM = acetoxymethyl) and propidium iodide (PI) were obtained from Sigma-Aldrich.

4.6.2 Instruments

^{1}H NMR and ^{13}C NMR spectra were acquired on a Bruker DMX-400 and Bruker DPX-300 MHz at 298K. LC-MS analysis was performed on a TSQ Quantum Access MAX system equipped with a Gemini 3 µm C18 110 Å 50×4.60 mm column (UV detection at 214 nm and 254 nm, mass detection range: 160 to 3000 (Da)). The mobile phase consisted of a gradient of 10-90% of H_2O-ACN with 0.1% trifluoroacetic acid (TFA) over 13.5 minutes. HPLC purification of the monomers was executed on setup equipped with C18 column. A gradient from 10%-90% ACN (0.1% TFA) in H_2O (0.1% TFA) over 15 min at a flow rate of 12 mL/min was used. Oscillatory rheology experiments were executed on a Discovery HR-2 hybrid rheometer using a cone-plate geometry (40 mm, 1.995°) at 37 ± 0.2 °C with a peltier-based temperature controller and solvent trap. High resolution mass spectra (HR-MS) were collected on a Thermo Fisher LTQ Orbitrap mass

spectrometer equipped with an electrospray ion source in positive mode (resolution R = 60000). The spectra were collected by direct injection of samples (2 µM in H_2O-ACN 50/50 v/v) and recorded with a mass range of 150-2000 and dioctylpthalate (m/z = 391.28428) as a "lock mass". Confocal fluorescent images were acquired on Leica TCS SP8 and SPE confocal laser scanning microscopes equipped with a 10× air objective and a 40× oil immersion objective. Images were processed using the Fiji Image J software. Real-time polymerase chain reaction (RT-PCR) measurements were performed on an ABI PRISM 7700 machine (Applied Biosystems®) using SYBR Green technology.

4.6.2 Synthetic procedures

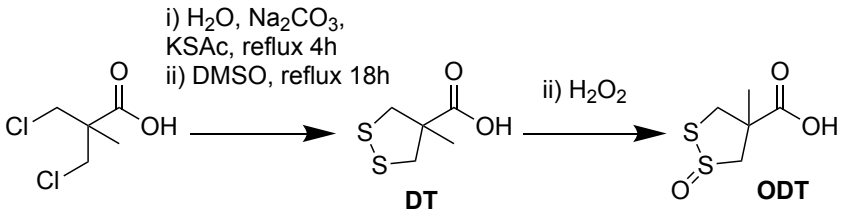

Scheme S4.1. Synthesis route of cyclic 1,2-dithiolane (**DT**) and cyclic 1,2-thiosulfinates (**ODT**)

Synthesis of DT. The synthesis of **DT** was performed as previously reported.[1] Briefly, 3,3-dichloropivalic acid (4.00 g, 23.39 mmol) was suspended in water (40 mL) within a 3-neck round bottom flask. Sodium carbonate (2.38 g, 22.46 mmol) was slowly added, followed by potassium thioacetate (5.38 g, 47.11 mmol). The resulting clear solution was heated to 100 °C, followed by the addition of sodium carbonate (7.8 g, 73.59 mmol). After refluxing overnight, DMSO (4 mL) was added and left to stir for another 12 h at 100 °C. The reaction mixture (pH ~ 9) was allowed to cool to room temperature and was acidified with hydrochloric acid (pH ~ 1). The yellow precipitate was filtered off and washed with ice-cold water and dried overnight in an vacuum oven to obtain as **DT** a yellow solid. Yield: 62.5%, 2.4 g. ^{1}H-NMR (DMSO-d_6, 400 MHz): 3.57-3.54 (d, 2H),

2.99-2.97 (d, 2H), 1.38 (s, 3H). ^{13}C-NMR (DMSO-d_6, 100 MHz): 175.42, 56.95, 46.97, 23.19.

Synthesis of ODT. Synthesis of **ODT** was performed according to a previously published protocol.[1][2] Compound **A** (3.0 g, 18.3 mmol) was dissolved in acetone (30 mL). Hydrogen peroxide aqueous solution (50%, 1.3 mL, 22.9 mmol) was added into the solution. The reaction mixture was stirred at room temperature for 24h, followed by a concentrate by N_2 flow. Afterwards, the crude was purified by flash column chromatography on silica gel with 20% EtOAc in PE. The purified fractions were collected, evaporated and dried in vacuum oven overnight to obtain **ODT** as a white solid. Yield: 47.1%, 1,55 g. ^{1}H-NMR (DMSO-d_6, 400 MHz): major isomer 4.40-4.36 (d, 1H), 3.82-3.74 (q, 2H), 3.11-3.08 (d, 1H), 1.57 (s, 3H); minor isomer 4.22-4.19 (d, 1H), 3.97-3.94 (q, 1H), 3.43-3.40 (d, 1H), 3.32-3.29 (d, 1H), 1.50 (s, 3H). ^{13}C-NMR (DMSO-d_6, 100 MHz): major isomer 174.65, 71.59, 58.66, 46.17, 23.43; minor isomer 174.32, 70.44, 56.39, 44.67, 21.59 HR-MS: $[M+H]^+$: calcd: 180.9988, found: 180.9986.

Synthesis of PEG-4DT. DT (0.20 g, 1.21 mmol) and N,N'-dicyclohexylcarbodiimide (0.25 g, 1.21 mmol) were dissolved in dry $CHCl_3$ (5 mL) and stirred at room temperature for 30 min as solution one. In a separate flask, tetra-arm hydroxyl-terminated PEG (Mw 10k) (0.30 g, 0.03 mmol) and 4-dimethylaminopyridine (15 mg, 0.12 mmol) were dissolved in dry $CHCl_3$ (5 mL). Subsequently, the PEG solution was added dropwise into the **DT** containing solution one and the reaction mixture were left stirring at room temperature for 24 h. The crude reaction mixture was first filtered prior to precipitation in cold diethyl ether, washed, re-dissolved in DCM, and re-precipitated from cold diethyl ether. The obtained products after three rounds of precipitation were re-dissolved in water, dialyzed against water for 48 h and lyophilized to obtain **PEG-4DT** as a light yellow solid. Yield: 83.3%, 0.25 g. ^{1}H-NMR ($CDCl_3$, 400 MHz): 4.29-4.27 (m, 2H), 3.80-3.44 (m, 224H), 2.93-2.90 (m, 2H), 1.47 (s, 3H).

Synthesis of PEG-4ODT. ODT (0.48 g, 2.69 mmol) and N,N'-dicyclohexylcarbodiimide (0.632 g, 3.06 mmol) were dissolved in dry DMF (10 mL) and stirred at room temperature for 30 min. In a separate flask, tetra-arm hydroxyl-terminated PEG (Mw 10k) (1.15 g, 0.11 mmol) and 4-dimethylaminopyridine (60 mg, 0.50 mmol) were dissolved in dry DMF/DCM (10 mL, 1:1, v/v). Subsequently, the PEG solution was added dropwise into the **ODT** solution and the reaction mixture was left stirring at room temperature for 24 h. The reaction crude was first filtered and the filtrate was precipitated in cold diethyl ether, washed, re-dissolved in DCM, and precipitated from cold diethyl ether. The obtained products after three rounds precipitation were re-dissolved in water, dialyzed against water for 48 h and lyophilized to obtain **PEG-4ODT** as a white solid. Yield: 82.6%, 0.95 g. ^{1}H-NMR ($CDCl_3$, 400 MHz): 4.53-4.49 (m, 1H), 4.29-4.27 (m, 2H), 3.90 (d, 1H), 3.81-3.44 (m, 224H), 3.04-3.00 (d, 1H), 2.95-2.87 (d, 1H), 1.68 (s, 3H).

Synthesis of PEGdiODT. ODT (0.32 g, 1.76 mmol) and N,N'-dicyclohexylcarbodiimide (0.40 g, 1.94 mmol) were dissolved in dry DMF (10 mL) and stirred at room temperature for 30 min. In a separate flask, linear hydroxyl-terminated PEG (Mw 6k) (1.18 g, 0.20 mmol) and 4-dimethylaminopyridine (121 mg, 0.99 mmol) were dissolved in dry DMF/DCM (10 mL, 1:1, v/v). Subsequently, the PEG solution was added dropwise into the **ODT** solution and the reaction mixture was left stirring at room temperature for 24 h. The reaction crude was first filtered and the filtrate was precipitated from cold diethyl ether, washed, dissolved in DCM, and re-precipitated from cold diethyl ether. The obtained products after three rounds precipitation were re-dissolved in water, dialyzed against water for 48 h and lyophilized to obtain **PEGdiODT** as a white solid. Yield: 75.4%, 0.89 g. ^{1}H-NMR ($CDCl_3$, 400 MHz): 4.53-4.49 (m, 2H), 4.32-4.27 (m, 4H), 3.93-3.90 (d, 2H), 3.82-3.44 (m, 540H), 3.04-3.01 (m, 2H), 1.69 (s, 3H).

Peptide synthesis. RGD peptides (CGGGRGDS) (cRGD) were synthesized on an automatic CEM peptide synthesizer on a 100 µmol scale. Fmoc-Rink amide AM resin

with a loading of 0.74 mmol/g was used. Fmoc-Rink amide AM resin with a loading capacity of 0.74 mmol/g was used. Amino acid coupling was performed with 4 eq. of the amino acid, 4 eq. of the activator HCTU and 8 eq. of DIPEA. Fmoc-deprotection was executed using a solution of pyridine and dimethylformamide (DMF) (2:8 v/v). The peptides were cleaved from the resin using a TFA solution containing 2.5% H_2O, 2.5% 1,2-ethanedithiol and 2.5% triisopropylsilane (TIPS) for 3h, precipitated in cold diethyl ether, dried, dissolved in water and purified by HPLC using a gradient 1-10% ACN/H_2O over 15 min. The product was concentrated by evaporation and lyophilized overnight to obtain a white solid. LC-MS: t =0.65 min, m/z calcd: 604.26, found: 603.07.

4.6.3 Hydrogel preparation

Hydrogels were prepared by separately dissolving PEG macromers in PBS (pH 7.4) and mixing them in the desired molar ratio. Specifically, to prepare the thiol/ODT crosslinked hydrogel, stock solution of **PEG-4ODT** (100 µL) was mixed with a freshly prepared solution of **PEG-4SH** (100 µL), and pipetted to obtain a homogeneous solution with a final PEG macromer concentrations in the range of 1-12 mM. The precursor solution was left at room temperature to gelate. Hydrogels with static crosslinks (**PEG-4VS** and **PEG-4SH**) and with linear PEG macromers (**PEGdiODT** and **PEGdiSH**) were prepared in the same way. To prepare the hybrid hydrogels, stock solutions of **PEG-4ODT** (60 µL) and **PEG-4VS** (60 µL) were mixed with freshly prepared solutions of **PEG-4SH** (60 µL), and pipetted to obtain a homogeneous solution with final PEG macromer concentrations between 4.5-10 mM. The precursor solution was left at room temperature for gelation. Gelation time was determined until the gel did not flow on vial inversion.

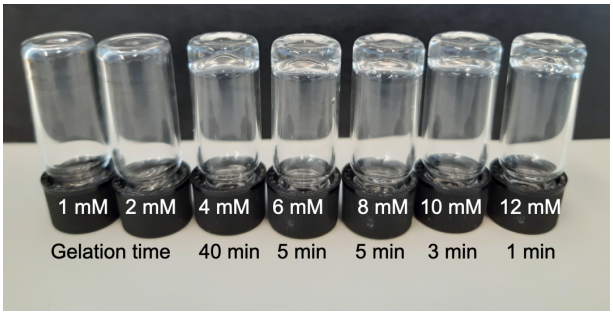

Figure S4.1. Gel inversion test of **ODT-SH** hydrogels prepared from macromers **PEG-4ODT** and **PEG-4SH** with thiol/ODT molar ratio at 1:1.

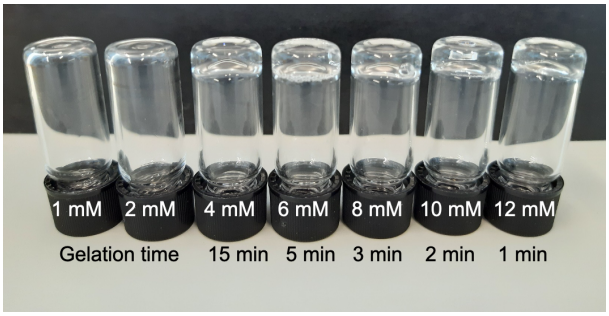

Figure S4.2. Gel inversion test of **ODT-SH** hydrogels prepared from macromers **PEG-4ODT** and **PEG-4SH** with thiol/ODT molar ratio at 2:1.

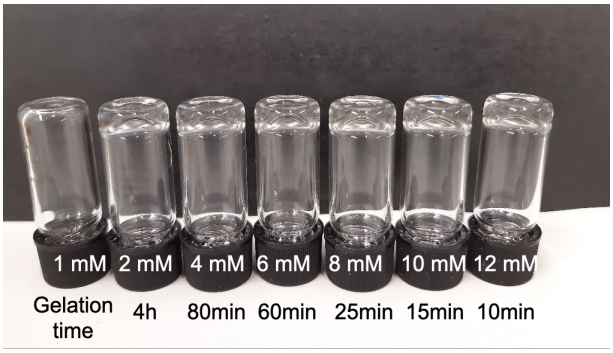

Figure S4.3. Gel inversion test of **VS-SH** hydrogels prepared from macromers **PEG-4VS** and **PEG-4SH** with thiol/VS molar ratio at 1:1.

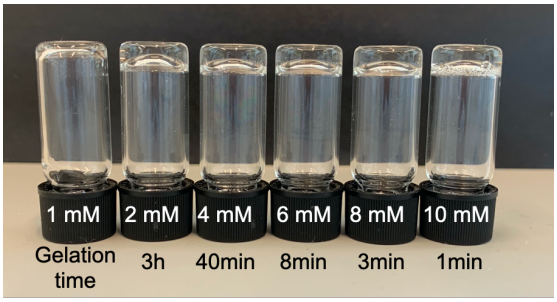

Figure S4.4. Gel inversion test of **25%_dPEG** hydrogels prepared from macromers **PEG-4ODT**, **PEG-4VS** and **PEG-4SH** with thiol/ODT molar ratio at 1:1 and thiol/VS molar ratio at 1:3.

4.6.4 NMR analysis

ODT was weighed in a 2.0 mL glass vial and dissolved in deuterated water with a final concentration at 20 mM. In a separate vial, glutathione (GSH) was freshly weighed and dissolved in deuterated water with final concentrations at 20 mM, 40 mM, 60 mM and 80 mM, respectively. The **ODT** solution (300 µL) was mixed with freshly prepared GSH solution (300 µL) by vortex for 10 s prior to its transfer into a NMR tube. The samples were incubated at 37 ˚C until desired time points and NMR spectra were collected on a Bruker DMX-400 at 298K.

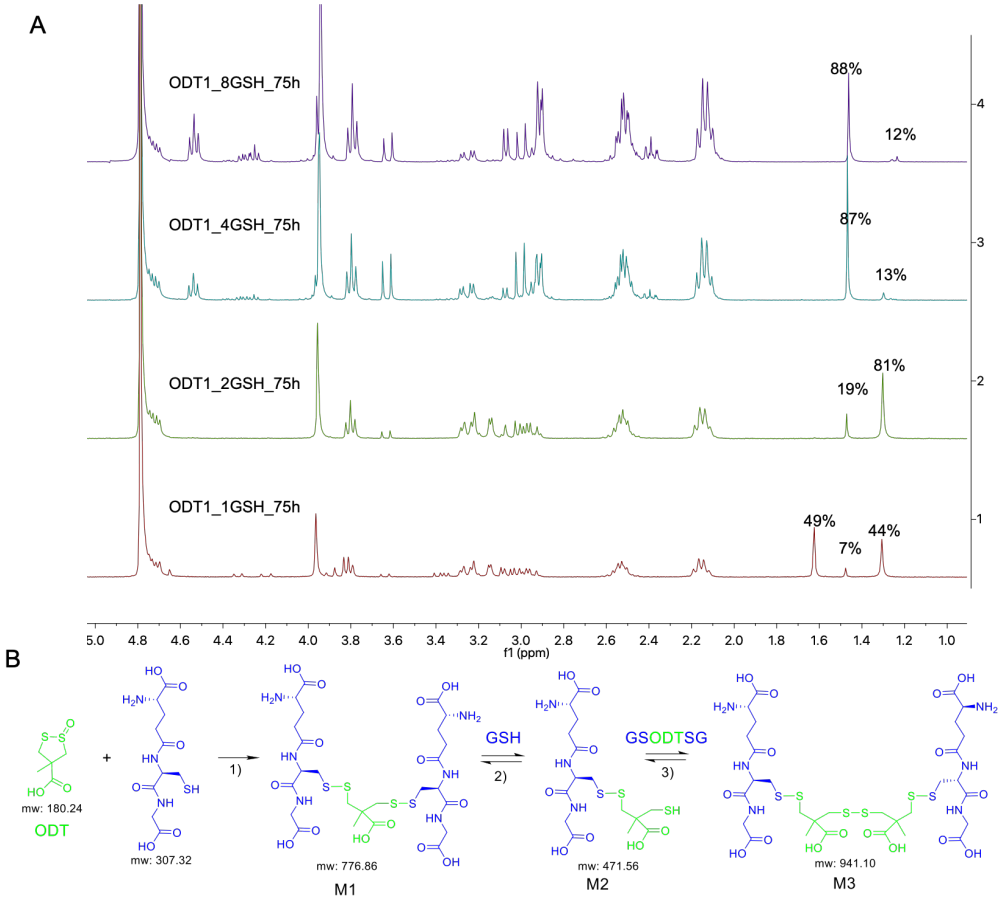

Figure S4.5. A) ^{1}H-NMR spectra of **ODT** and GSH mixture after 75-h incubation at 37˚C. B) Proposed mechanism of thiol (blue) and cyclic thiosulfinates (green) crosslinking. 1) **ODT** was reacted with GSH with in a molar ratio of 1:2 in the same mechanism reported from Agar and co-workers; [2] 2) thiol/disulfide exchange between GSH and **M1** to result in a new free thiol, **M2**; 3) further thiol/disulfide exchange to give a new disulfide product **M3**.

4.6.5 Oscillatory Rheology

Oscillatory rheology experiments were carried out on a Discovery HR-2 hybrid rheometer using parallel plate geometry (20 mm diameter) at 37 ± 0.2 °C with a peltier-based temperature controller and a solvent trap. The prepared hydrogel (100 µL) was

pipetted onto the bottom plate and the geometry was lowered to a gap distance of 300 µm. Time sweep measurements were executed at a frequency of 1.0 Hz and strain of 0.05% and frequency sweeps were conducted from 0.01−10 Hz with 0.05% strain. Subsequently, a step-strain measurement was performed after a plateau was reached in the storage modulus during the time sweep. Then, 700% strain was applied on the hydrogels for 300 s. The hydrogels were left to recover for 300 s while measuring at 0.05% strain (f = 1.0 Hz) and continued with a frequency sweep (from 0.01 to 10 Hz, γ = 0.05%), during which the storage modulus returned to the original plateau. This measurement was repeated for three cycles.

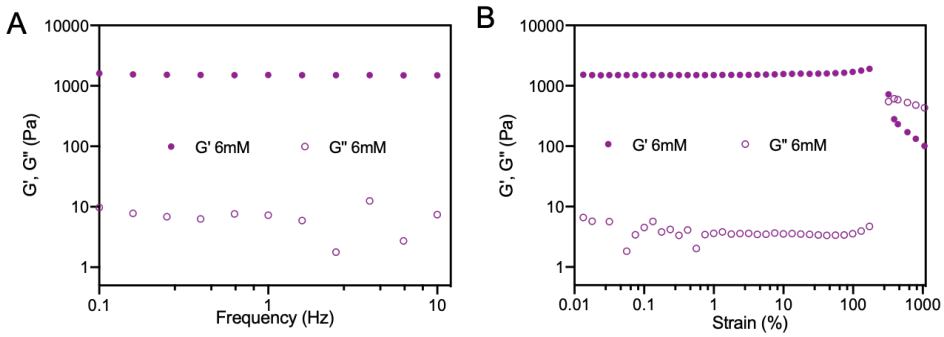

Figure S4.6. A) Frequency sweep measurements of **ODT-SH** hydrogels in PBS (pH 7.4) at 25 ± 0.2 °C. Frequency sweep data was collected in a range of 0.01 Hz to 10 Hz with strain of 0.05%. B) Amplitude sweep measurements of **ODT-SH** hydrogels (6 mM) in PBS (pH 7.4) at 25 ± 0.2 °C with frequency of 1 Hz and strain from 0.1% to 1000%.

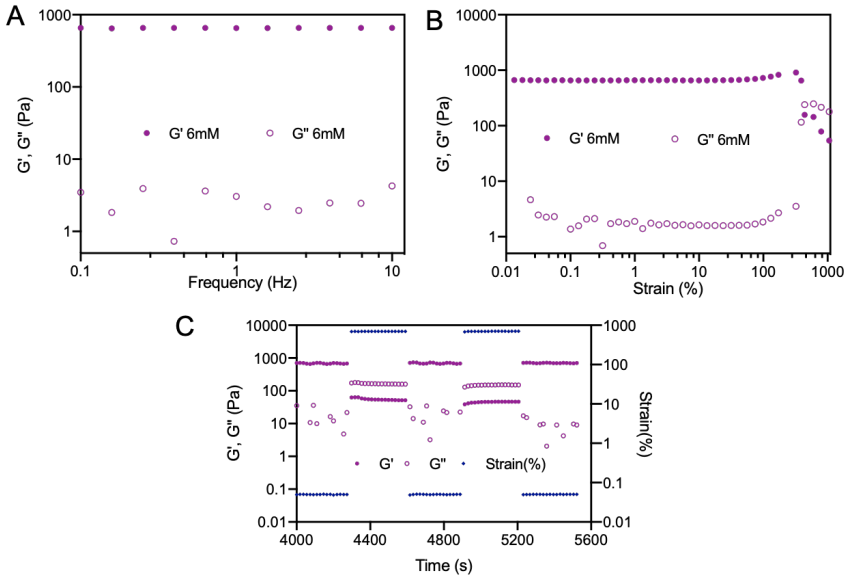

Figure S4.7. A) Frequency sweep measurement of **ODT-SH** hydrogels (6 mM) in PBS (pH 7.4) at 37 ± 0.2 °C. Frequency sweep data was collected in a range of 0.01 Hz to 10 Hz with strain of 0.05%. B) Amplitude sweep measurements of **ODT-SH** hydrogels (6 mM) in PBS (pH 7.4) at 37 ± 0.2 °C with frequency of 1 Hz and strain from 0.1% to 1000%. C) Step-strain measurements of **ODT-SH** hydrogels (6 mM) at 37 ± 0.2˚C with a frequency of 1 Hz; Low (0.05%) and high strain (700%) were applied alternatively for two cycles.

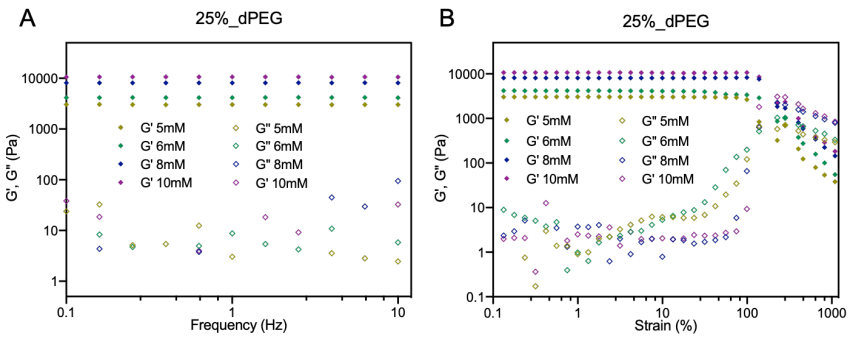

Figure S4.8. A) Frequency sweep measurements of **25%_dPEG** hydrogels in PBS (pH 7.4) at 37 ± 0.2 °C. Frequency sweep data were collected in a range of 0.1 Hz to 10 Hz with strain of 0.05%. B) Amplitude sweep measurements of **25%_dPEG** hydrogels at 37 ± 0.2 °C with frequency of 1 Hz and strain from 0.1% to 1000%.

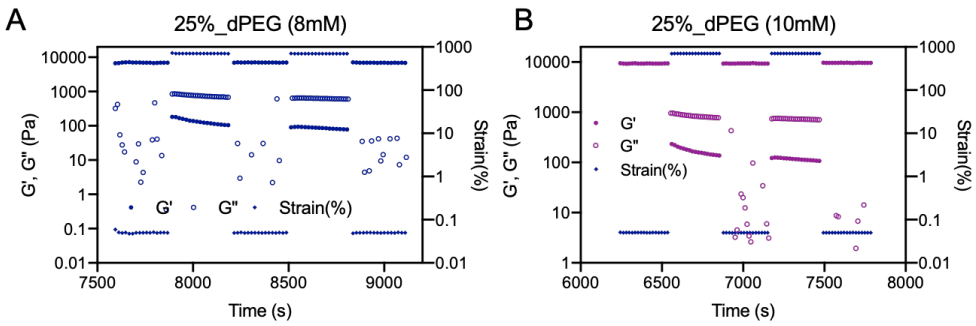

Figure S4.9. Step-strain measurement of **25%_dPEG** hydrogels in PBS (pH 7.4) at 37 ± 0.2 °C. Low strain (0.05%) and high strain (700%) were alternated twice in a sequence for 300 s applied twice for 120s. The data was collected at a frequency of 1 Hz.

4.5.6 Swelling measurements

Hydrogels (200 µL) were prepared according to gelation protocol descripted above and were allowed to stand for 2h. The wet weight of hydrogels were measured as W_0. Afterwards, DMEM medium (200 µL) was added on top of hydrogel and incubated at 37˚C. At desired time points, the supernatant solution was carefully removed and the wet weight of the hydrogels were measured as Wt. The percentage of hydrogel degradation or swelling ratios was calculated by the following equation: weight change (%) = W_t/W_0 x 100%.

4.5.7 LIVE/DEAD staining

NIH 3T3 cells were cultured in high glucose DMEM supplemented with 10% Fetal Calf Serum, 1% Glutamax, and 0.2% penicillin-streptomycin in a 37 °C incubator with 5% CO2. Prior to encapsulation, cells were dissociated by trypsin, collected by centrifuge and re-suspended in PBS with a final cell centration at 2 x 10^7 cells/mL. To prepare the **ODT-SH** hydrogel, **PEG-4ODT** stock solution (80 µL) was first mixed with freshly prepared cRGD (PBS, 10 µL) by pipetting. After 5 min incubation, a cell suspension (20 µL) was added and mixed, followed by the addition of a freshly prepared **PEG-4SH**

solution (90 μL). The precursor solution was mixed and pipetted into μ-Slide angiogenesis slide by 12μL/well. After incubated at 37˚C for 15 min, fresh culture medium (48 μL) was added on top and cells were cultured at 37 °C. At pre-determined time points, the medium on top of the hydrogel was removed by pipetting, rinsed twice with PBS (pH 7.4, 45 μL) and incubated with a prepared staining solution (45 μL) (calcein AM (2 μM) and propidium iodide (1.5 μM)) at 37 °C for 20 min. The staining solution was removed and the hydrogel was rinsed again with PBS two times (45μL). The stained cell-laden hydrogel was imaged through z-stack on Leica TCS SP8 confocal laser scanning microscope equipped with a 10× air objective. Fluorescent images were acquired at a resolution of 1024 × 1024 pixels using an excitation wavelength of 488 nm and an emission filter of 500−545 nm for calcein AM and an excitation wavelength of 532 nm and an emission filter of 594−686 nm for propidium iodide. Cell viability was determined by counting the calcein AM-stained green cells (viable) and PI-stained red cells (dead) in ImageJ. For each hydrogel sample at each time point, three Z-stack images were counted (~2000 cells). To prepare **25%_dPEG** hydrogel, **PEG-4ODT** stock solution (50 μL) was first mixed with freshly prepared cRGD (PBS, 10 μL) by pipetting. After 5 min incubation, **PEG-4VS** solution (50 μL) and cell suspension (20 μL) was added and mixed, following with addition of freshly prepared **PEG-4SH** solution (70 μL). The precursor solution was mixed and pipetted into μ-Slide angiogenesis slide by 12μL/well. After incubated at 37˚C for 15 min, fresh culture medium (48 μL) was added on top and cells were cultured at 37 °C. Cytocompatibility test of **25%_dPEG** hydrogels was performed in the same protocol described above.

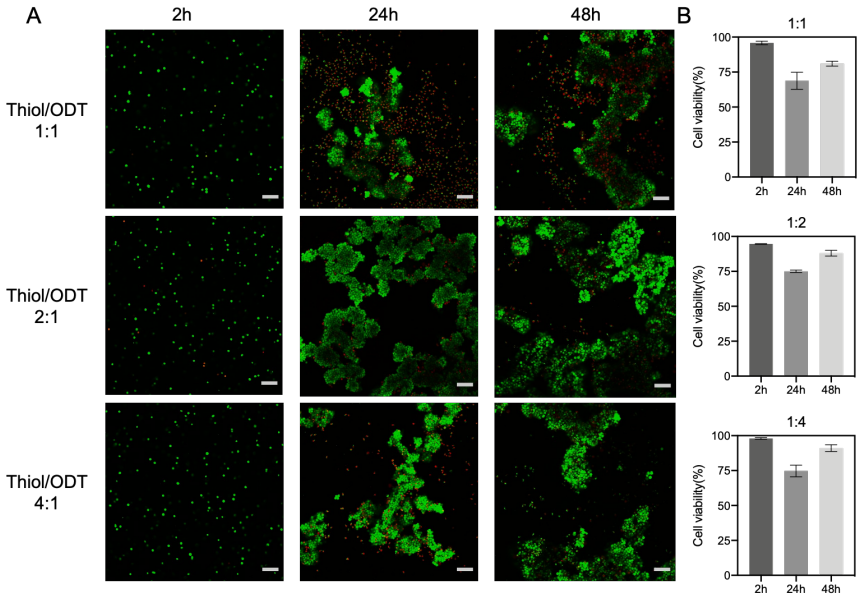

Figure S4.10. Cytocompatibility of **ODT-SH** hydrogels (6 mM) with thiol/ODT molar ratios at 1:1, 2:1 and 4:1. A) Representative z-stack images of cells in hydrogels after 2h, 24h and 48h culture. Cells were stained with calcein AM (viable cells, *green*) and propidium iodide (PI) (dead cells, *red*). Scale bar: 100 µm. B) Quantification of cell viability. Error bars represent standard deviations of means.

4.6.8 hESC culture and differentiation

Human embryonic stem cell line (hESCs) was obtained from Prof. Dr. Robert Passier in University of Twente (The Netherlands). hESCs were cultured on six-well plates coated with vitronectin. Cells were passaged by use of EDTA solution (0.5 mM) with replating densities at 180K cells/well and 100K cells/well on Mondays and Thursdays, respectively. In detail, on the passage day, cells were first washed with PBS and incubated with EDTA solution for 5 min at 37°C. After aspirating the EDTA solution, Essential 8^{TM} medium (RevitaCell 1:200, 2 mL) was added. A P1000 micropipette was used to suspend and dissociate cells (6-8 times). Cells were first collected by a 5-min centrifuge at 300g and then replated into new plates. The replated cells were treated

with medium supplied with Revita Cell (1:200) for 24h and refreshed with E8 medium and cultured until next passage.

Prior to the start of cardiomyocyte differentiation, Matrigel coated plates were prepared according to a reported protocol.[3] On the passage day, hESCs were seeded on the Matrigel coated plates and differentiated to cardiomyocytes using the STEMdiff™ Cardiomyocyte Differentiation Kit (Stem Cell Technologies). Fluorescent images of hESC-derived cardiomyocytes (hESC-CMs) were acquired on a Leica SP8 confocal microscope at predetermined time points using an excitation wavelength of 488 nm and an emission filter of 500-545 nm for GFP and an excitation wavelength of 532 nm and an emission filter of 600-680 nm for mRuby.

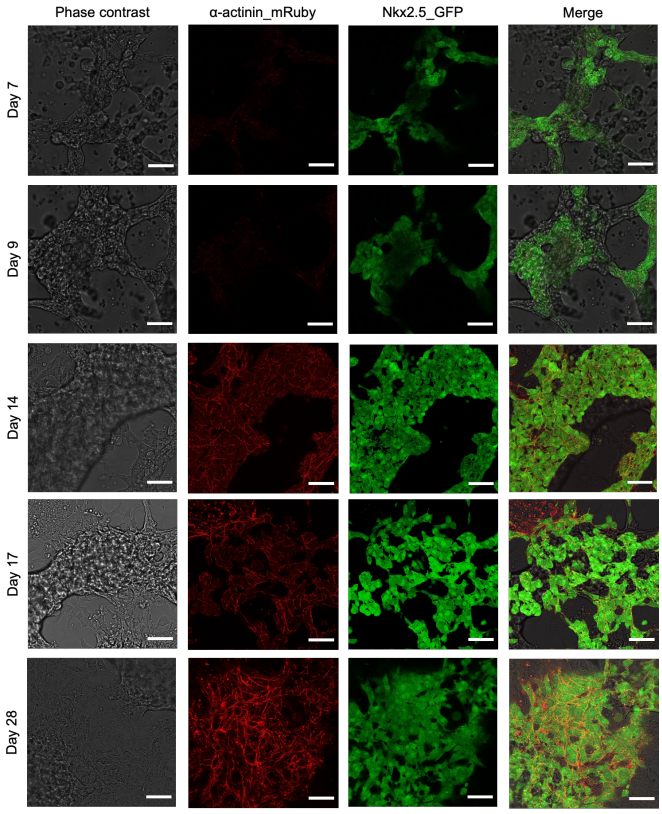

Figure S4.11. Representative images of hESC-CM differentiation on Matrigel in 2D over 28 days . Fluorescent images of cardiac transcription factor Nkx2.5_GFP (green) and the sarcomeric protein, α-actinin_mRuby (red). Brightfield microscopy images were

captured after 7, 9, 14, 17 and 28 days differentiation, respectively. Merged images were prepared in Fiji. Scale bar: 50 µm.

4.6.9 hESC-CMs encapsulation and culture in 3D

After 14-days differentiation, hESC-CMs were first washed with DPBS and then dissociated by incubation with a TrypLE Select (1x) solution for 5 min at 37 °C. The TrypLE Select solution was removed and cells were suspended in Cardiomyocyte Maintenance medium by a P1000 micropipette. (8-10 times) Then, hESC-CMs were collected, spun down and resuspended in Cardiomyocyte Maintenance medium with a cell density at 5 x 10^7 cells/mL. Afterwards, hESC-CMs were encapsulated within **25%_dPEG** hydrogels and **sPEG** hydrogel in the same way as NIH 3T3 cells. Complete cardiomyocyte maintenance medium (48 µL) was added on top of the gel and was refreshed every other day. At desired timepoints, bright field images were acquired on SP8 confocal microscope using 10x and 20x objectives. Fluorescent images were acquired at a resolution of 1024 x 1024 pixels and a z-step size of 2.00 µm, using an excitation wavelength of 488 nm and an emission filter of 500-545 nm for GFP and an excitation wavelength of 532 nm and an emission filter of 600-680 nm for mRuby.

4.6.10 RT-PCR

At pre-determined time points, cells were lysed with GTC lysis buffer (500 µL) at room temperature for 1 min and stored at -20 °C until RNA isolation was initiated. For cells released from the hydrogels, GTC (500 µL) was added and incubated at room temperature for 6 min. After that, the gels were spun down (5 min, 500g) and the supernatant was collected in a new Eppendorf tube.

Total RNA was collected using the standard phenol/chloroform extraction method and 500 ng RNA was reverse transcribed using RevertAid Reverse Transcriptase. For RT-PCR, cDNA (4 µL) was mixed with primers mix (Table S4.1) and

SensiMix SYBR low-ROX mix and analysis was performed on a 7500 Fast Real-time PCR system (Applied Biosystems). Gene expression was normalized to the averaged gene expression of two housekeeping genes, the tyrosine 3-monooxygenase/tryptophan 5-monooxygenase activation protein zeta coding gene YWHAZ and the 60S ribosomal protein L37 coding gene RPL37. Outlier tests were performed on dCt values and relative expression values (ROUT method, Q=1%). One-way ANOVA tests were used to determine significant changes in gene expression (95% confidence interval), followed by a Tukey test to determine significant changes between groups.

Table S4.1. Primer sequences used for RT-PCR

Gene	Forward 5’- 3’	Reverse 5’ -3’
Sox2	TGGTTACCTCTTCCTCCCACTCCAG	TAGTGCTGGGACATGTGAAGTCTGC
Nanog	TCCAGCAGATGCAAGAACTCTCCAAC	CACCATTGCTATTCTTCGGCCAGTTG
Oct4	GCTTGGAGACCTCTCAGCCTGAG	TTTIGCTCCAGCTTCTCCTTCTCCAG
cTnT	AGTTCGACCTGCAGGAGAAGTTCAAG	TATTTCCAGCGCCCGGTGACTTTAG
Cx43	GTCTGAGTGCCTGAACTTGCCTTTTC	TCCAGCAGTTGAGTAGGCTTGAACC
MYH6	TTCGAGC CAAGAGC CGTGACATTG	TTACAGGTTGGCAAGAGTGAGGTTCC
MYH7	GTCAACAAGCTGCGGGCCAAG	CTGAGCAGATCAAGATGTGGCAAAGC
YWHAZ	TGAAGAGTCATACAAAGACAGCACGCT	TTGGAAGGCCGGTTAATTTTCCCCT
RPL37	TGGAGTGCCAAGGCTAAAAGACGAA	GGGTTTAGGTGTTGTTCCTTCACGGA

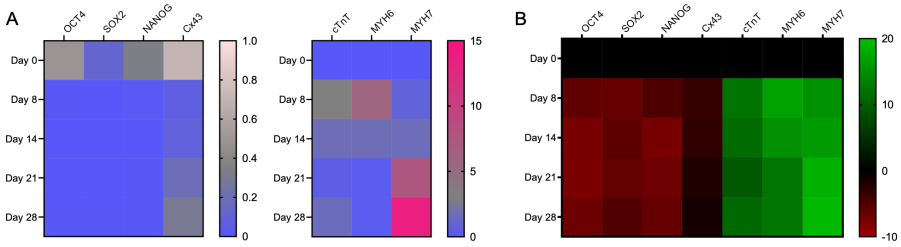

Figure S4.12 Gene expression profiles of hESC-CMs differentiation on Matrigel in 2D over 28-days. A) Relative gene expression of the pluripotency genes OCT4, SOX2 and NANOG (scale: 0-1.0) and the cardiac gene Cx43 (scale: 0-1.0), cTnT, MYH6 and MYH7 (scale: 0-15). B) C: Fold change (log2) for all genes in comparison to expression on day 0. N = 6

4.6.11 Appendix: NMR spectra

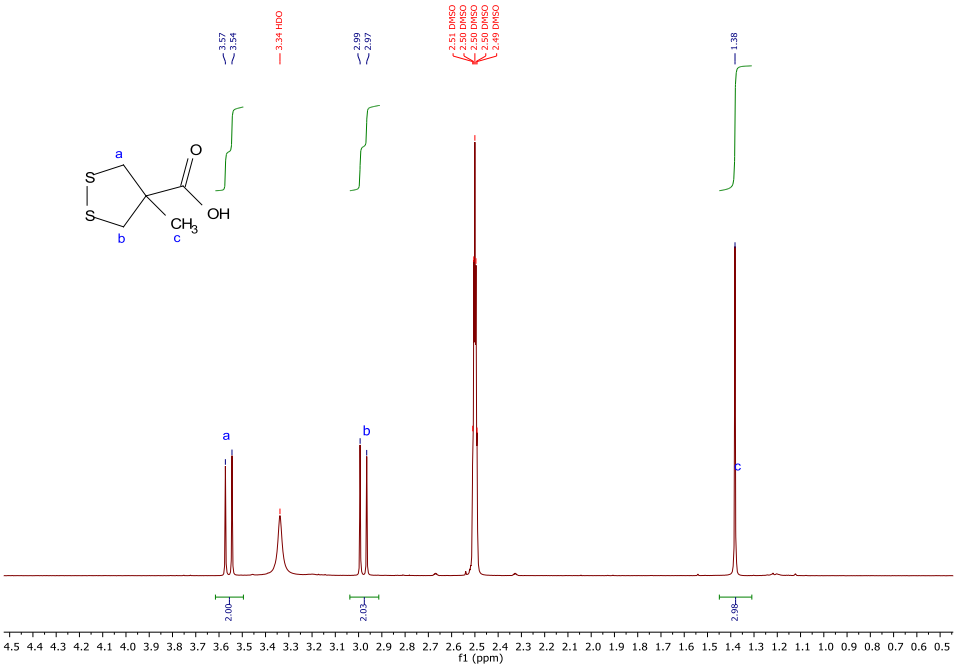

Figure A4.1. ^{1}H-NMR (400 MHz, 298K, DMSO-d_6) spectrum of **DT**

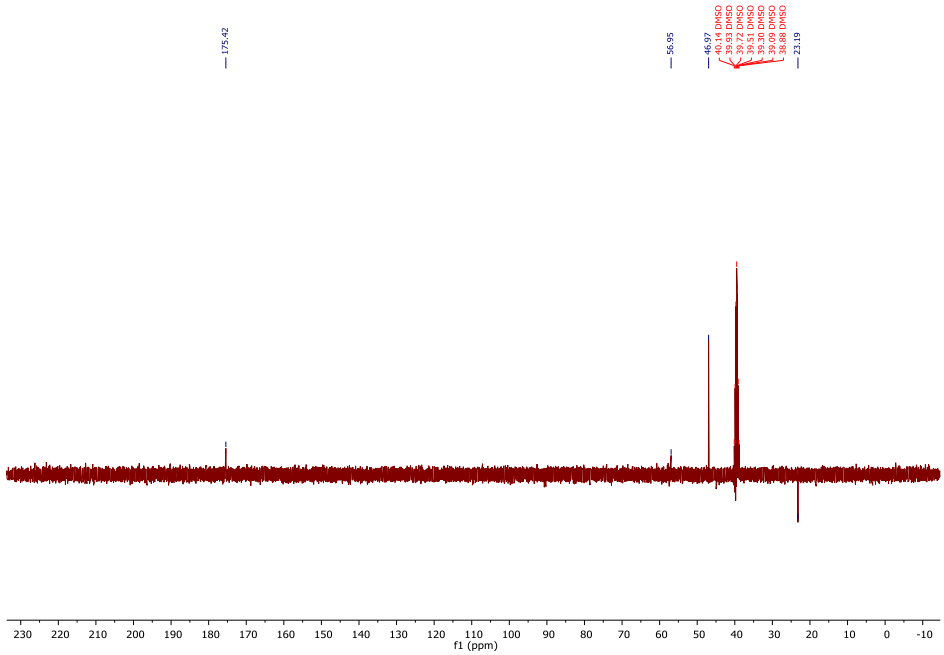

Figure A4.2. ^{13}C-NMR (400 MHz, 298K, DMSO-d$_6$) spectrum of **DT**

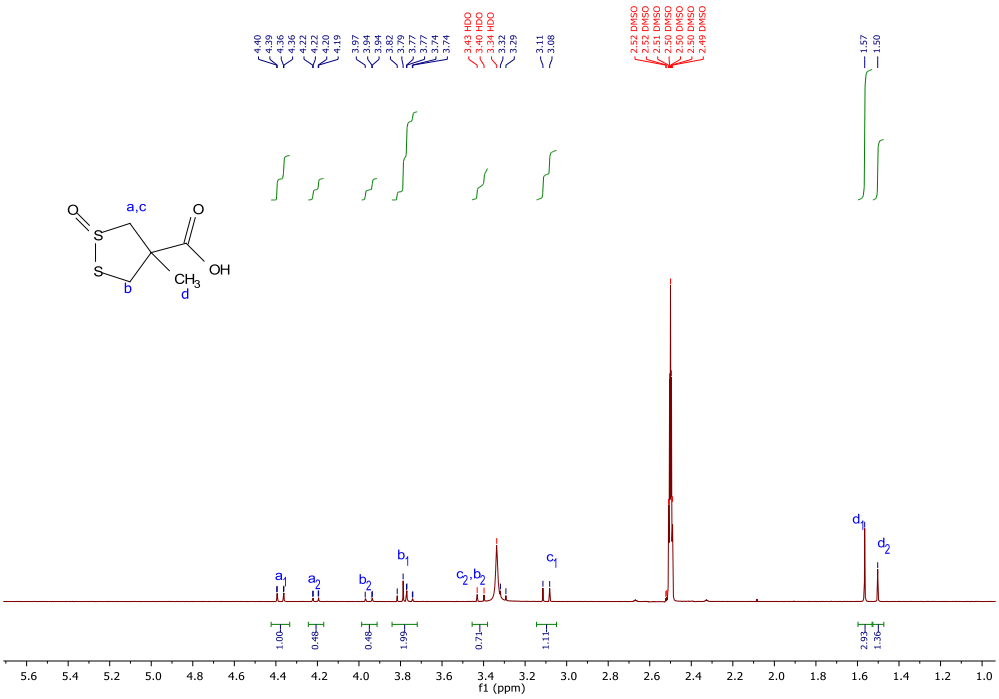

Figure A4.3. ^{1}H-NMR (400 MHz, 298K, DMSO-d$_6$) spectrum of **ODT**

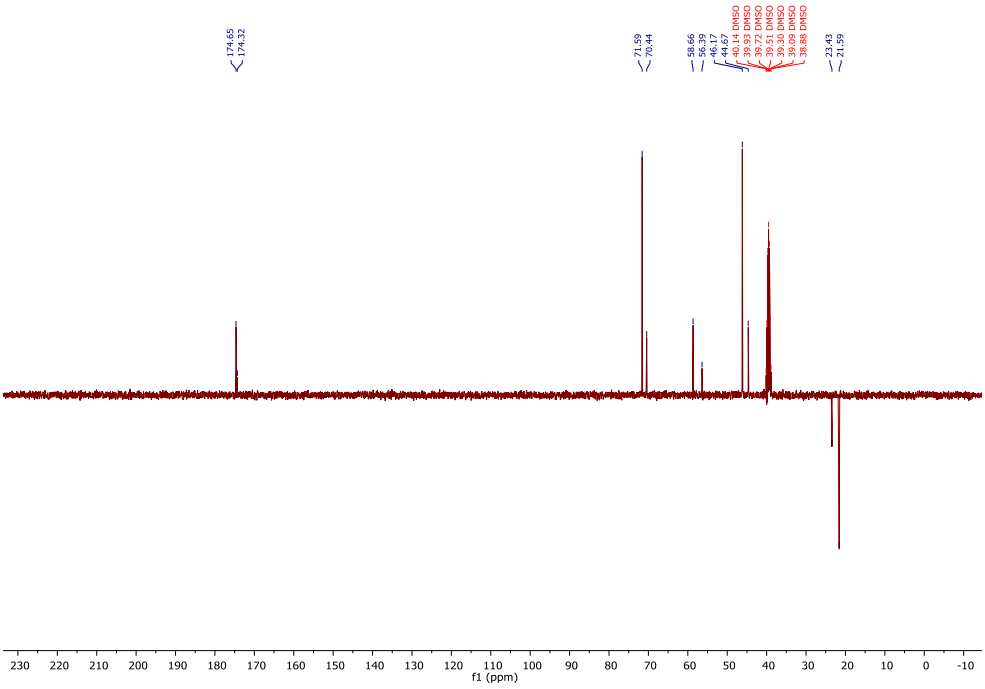

Figure A4.4. ^{13}C-NMR (400 MHz, 298K, DMSO-d_6) spectrum of **ODT**

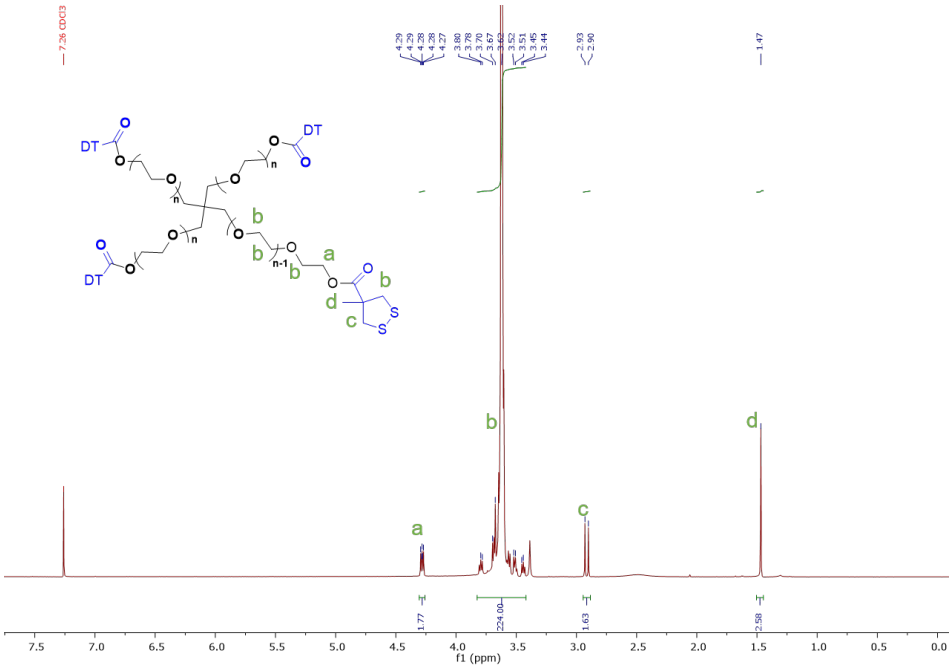

Figure A4.5. ^{1}H-NMR (400 MHz, 298K, $CDCl_3$) spectrum of **PEG-4DT**. The degree of functionalization was 86%.

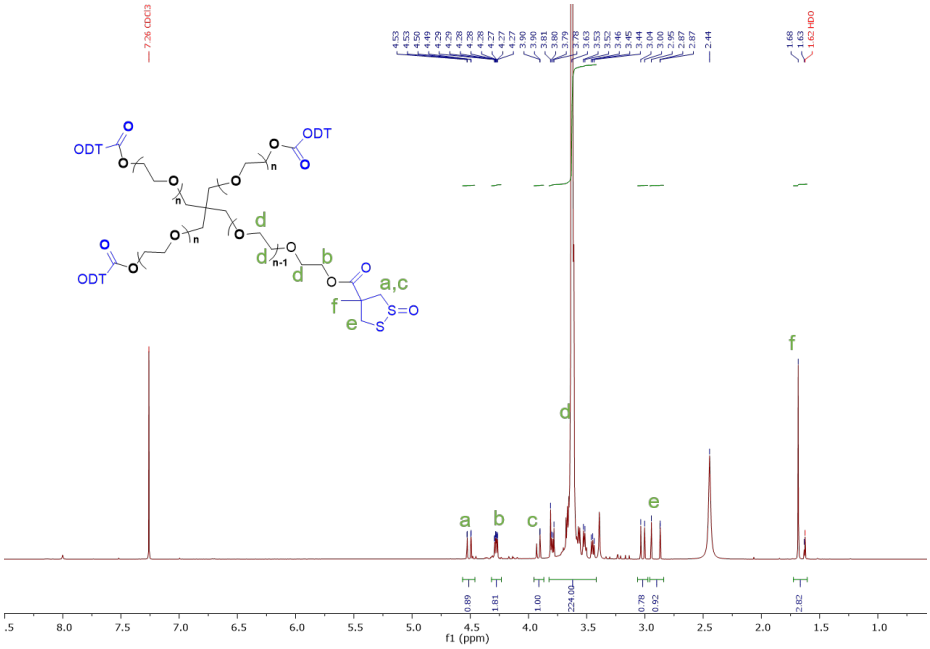

Figure A4.6. ^{1}H-NMR (400 MHz, 298K, $CDCl_3$) spectrum of **PEG4-ODT**. The degree of functionalization was 90%.

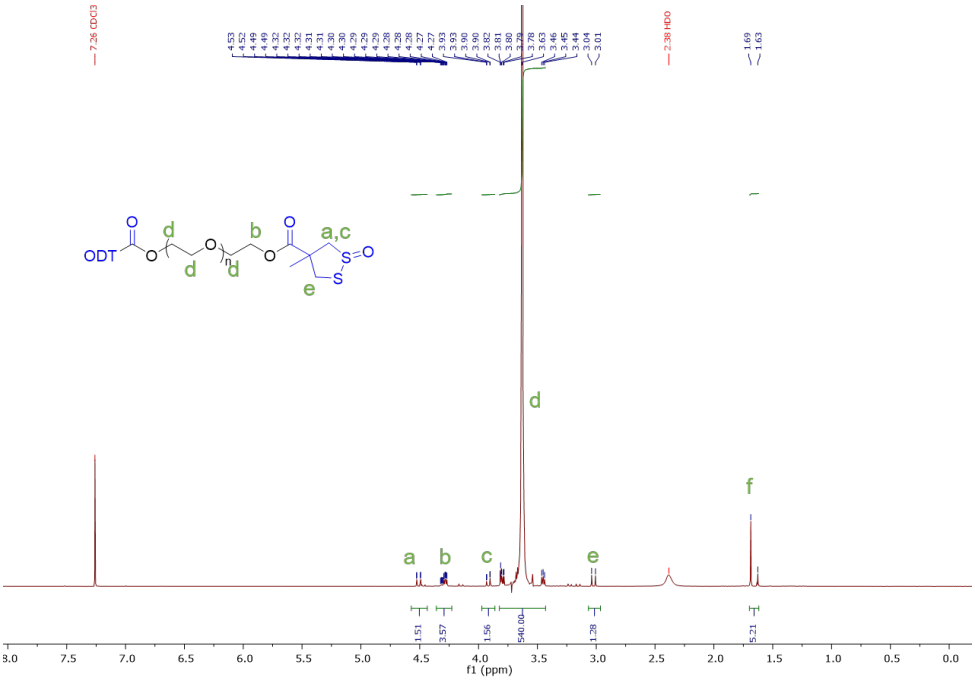

Figure A4.7. ^{1}H-NMR (400 MHz, 298K, $CDCl_3$) spectrum of **PEGdiODT**. The degree of functionalization was 86%.

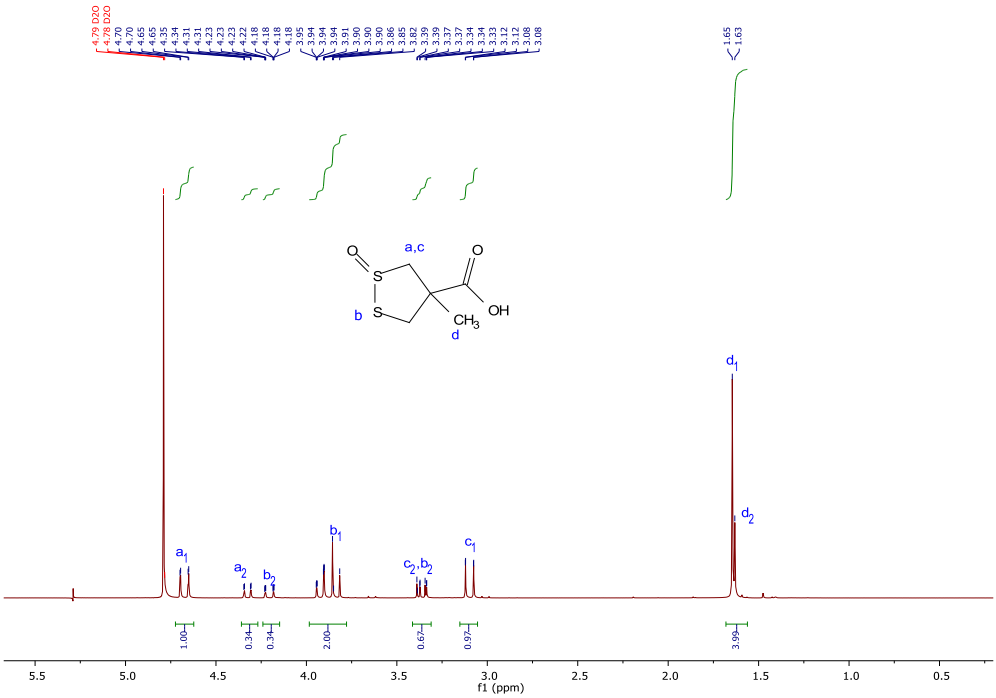

Figure A4.8. ^{1}H-NMR (400 MHz, 298K, D_2O) spectrum of **ODT**.

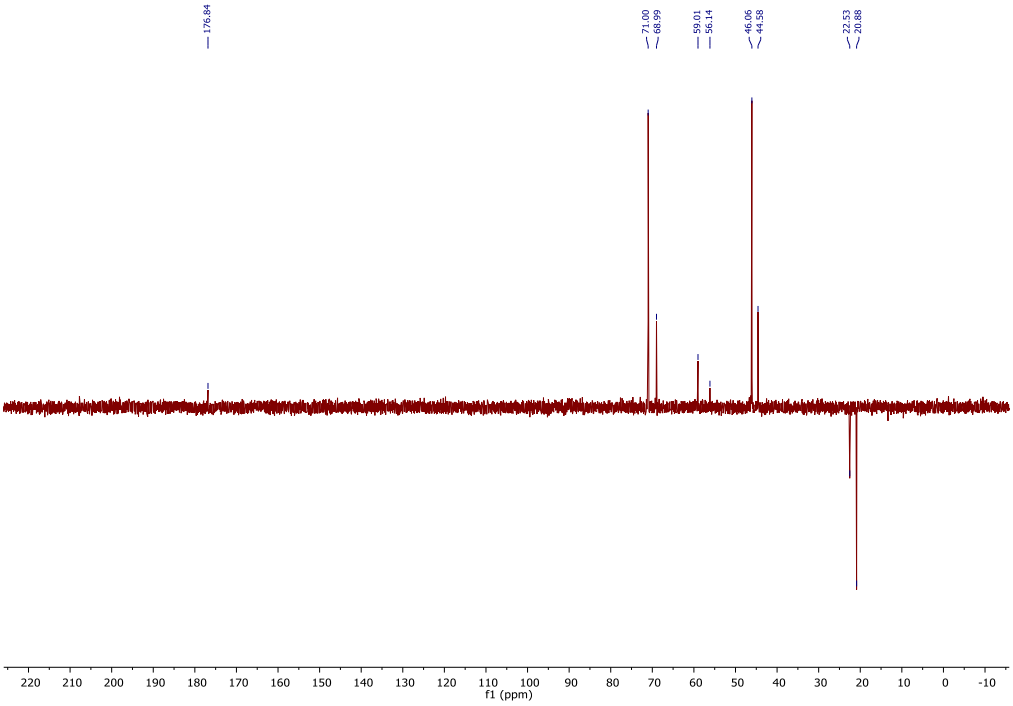

Figure A4.9. ^{13}C-NMR (100 MHz, 298K, D_2O) spectrum of **ODT**

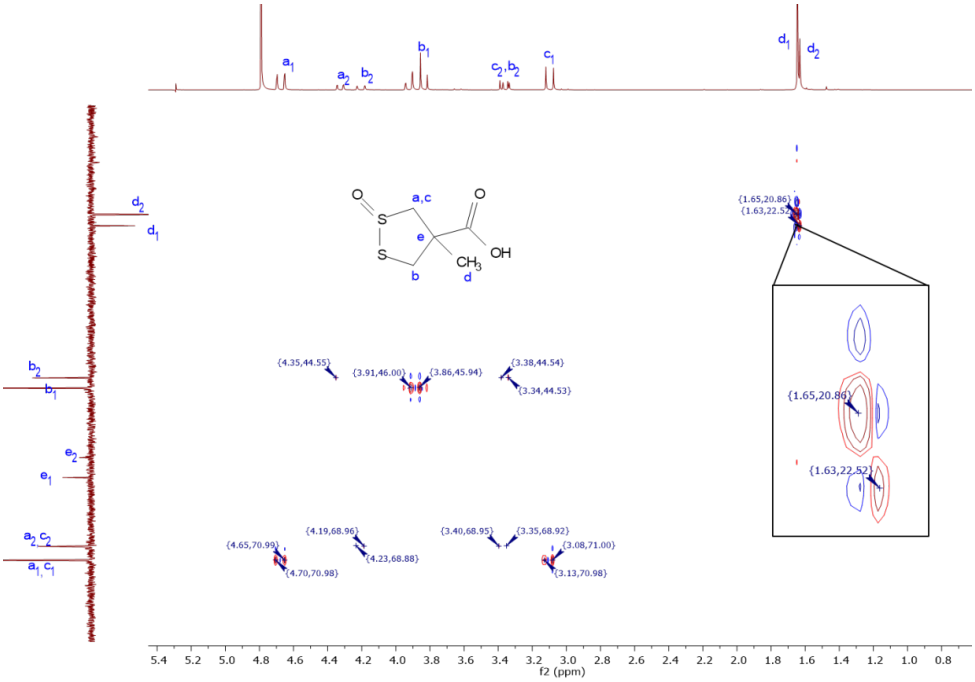

Figure A4.10. HSQC (400 MHz, 298K, D_2O) spectrum of **ODT**

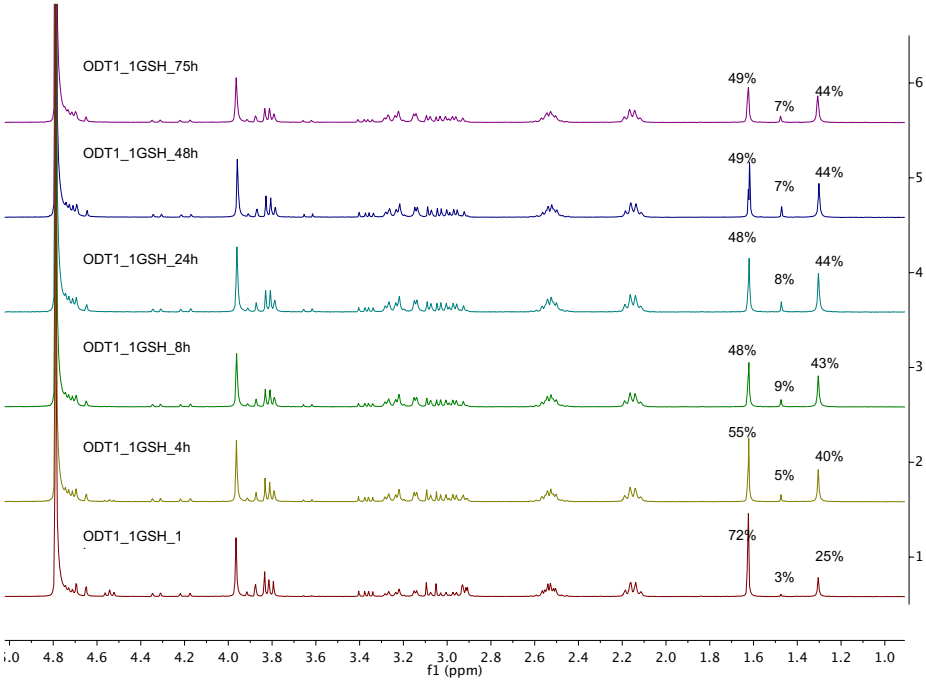

Figure A4.11. ^{1}H-NMR (400 MHz, 298K, D_2O) spectrum of the **ODT** and **GSH** mixture at specific time points with a molar ratio of thiol/ODT at 1:1

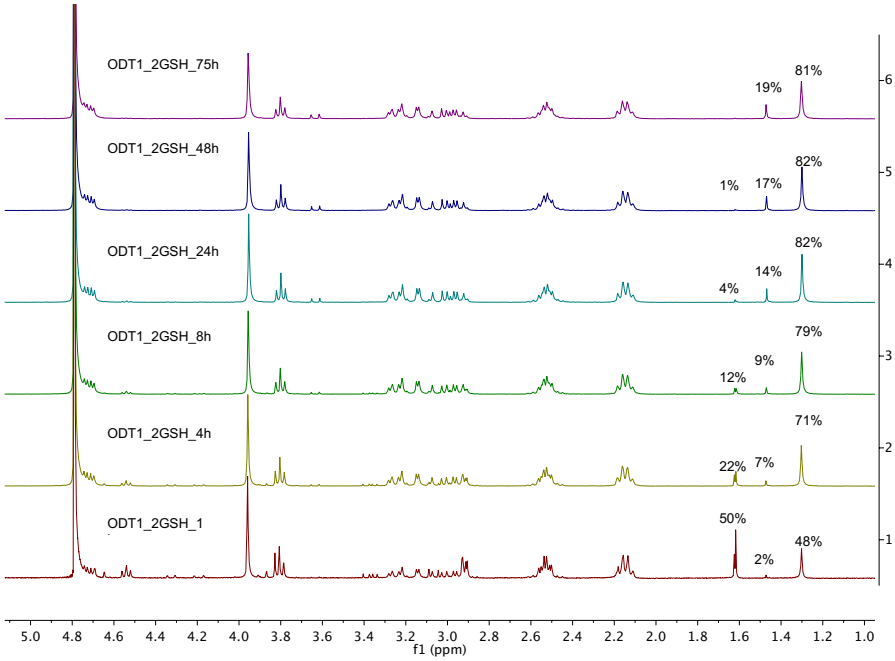

Figure A4.12. ^{1}H-NMR (400 MHz, 298K, D_2O) spectrum of the **ODT** and **GSH** mixture at specific time points with a molar ratio of thiol/ODT at 2:1

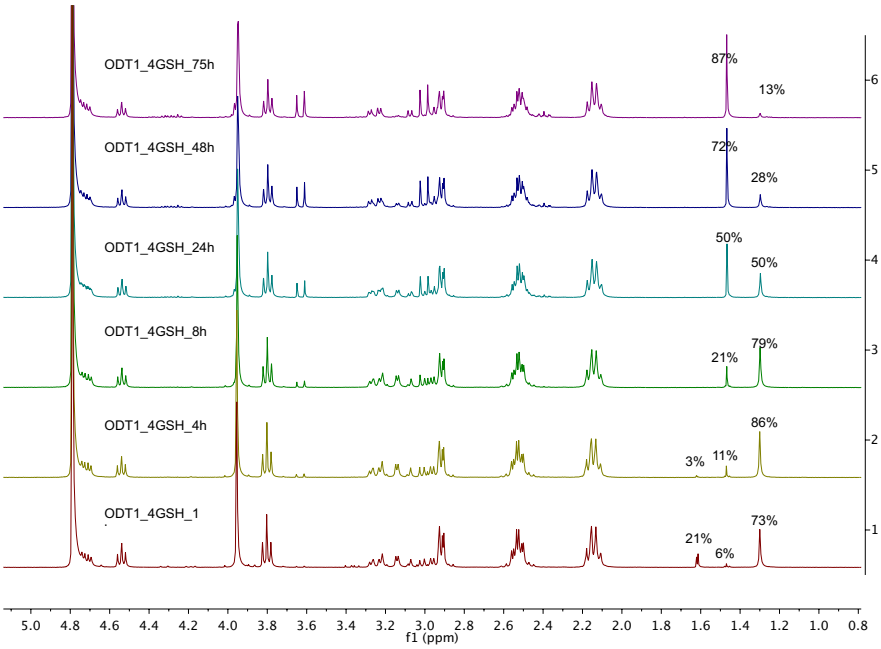

Figure A4.13. ^{1}H-NMR (400 MHz, 298K, D_2O) spectrum of the **ODT** and **GSH** mixture at specific time points with a molar ratio of thiol/ODT at 4:1

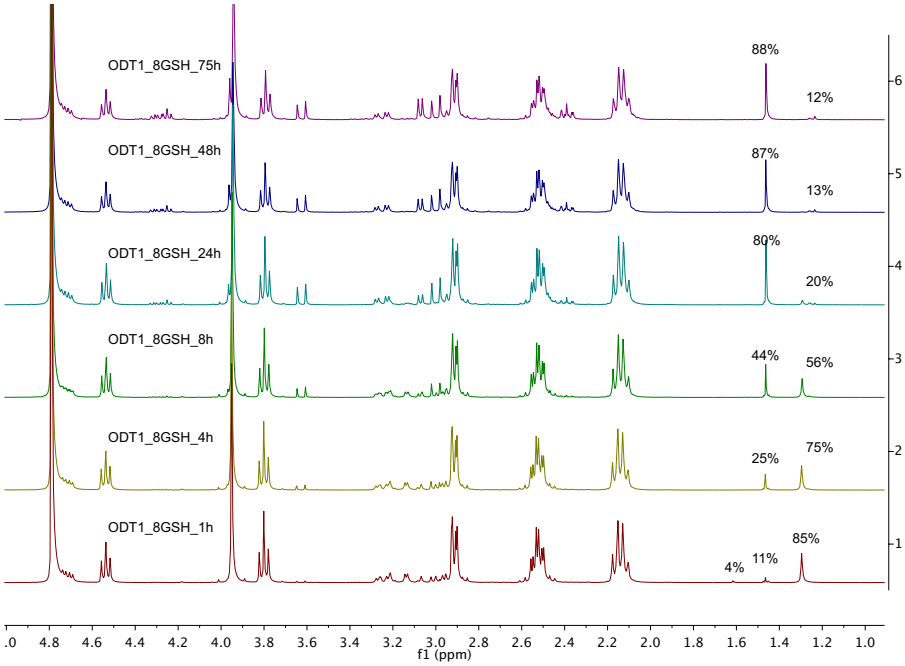

Figure A4.14. ^{1}H-NMR (400 MHz, 298K, D_2O) spectrum of the **ODT** and **GSH** mixture at specific time points with a molar ratio of thiol/ODT at 8:1

4.6.12 References

[1] X. Marat, K. Lucet-Levannier, L. Marrot, **2013**, U.S. Patent No. US8530511B2.

[2] D. P. Donnelly, M. G. Dowgiallo, J. P. Salisbury, K. C. Aluri, S. Iyengar, M. Chaudhari, M. Mathew, I. Miele, J. R. Auclair, S. A. Lopez, R. Manetsch, J. N. Agar, *J. Am. Chem. Soc.* **2018**, *140*, 7377.

[3] E. Giacomelli, M. Bellin, V. V. Orlova, C. L. Mummery, *Curr. Protoc. Hum. Genet.* **2017**, *95*, 21.9.1.

CHAPTER 5

Engineering macroporous hydrogels using the tetrazine-norbornene click reaction

This chapter is prepared as an original research paper: Tingxian Liu, Wei Tang, Roxanne E. Kieltyka*

5.1 Abstract

Macropores play critical role in transport and exchange of nutrition, oxygen and waste for cells, influencing parameters such as cell morphology, growth, migration and differentiation. However, approaches to engineer the user-defined macropores in a controlled manner in synthetic hydrogel materials remains to be explored. In this study, the inverse electron demand Diels–Alder (IEDDA) reaction that is known as an efficient chemical reaction for bioconjugation and crosslinking due to its fast kinetics, orthogonality and biocompatibility, is employed to engineer macroporous hydrogel structures from nitrogen gas that is formed in the IEDDA reaction in the hydrogelation process. To tune the pore size, I synthesized tetrazine derivatives with substituents that vary in electron donating character on a poly(ethylene glycol) PEG macromonomer and examined their reaction with a second PEG macromonomer containing norbornene groups (Tz-Nb reaction) to generate hydrogel materials of varied stiffness and stable macropores arising from the simultaneous gas formation in the cross-linking reaction. Hydrogen-substituted tetrazines (TZ3) displayed faster reaction kinetics and hydrogelation over those bearing methyl or methylene substituents on the tetrazine ring as demonstrated by oscillatory rheology. The faster gelation of the Tz3-Nb-based PEG hydrogel minimized coalescence of the bubbles during their formation, resulting in hydrogels with significantly smaller pores with an average diameter of 268 ± 94 µm in comparison to the slower reacting Tz2-Nb-based PEG hydrogels (382 ± 99 µm). Moreover, the faster gelation process of Tz3-Nb crosslinks prevented cell sedimentation, providing a three-dimensional distribution of cells throughout the hydrogel. Additionally, the Tz-Nb-based PEG hydrogels supported the culture of primary chondrocytes with high cell viability and secretion of glycosaminoglycans demonstrating their potential for chondrocyte culture. Overall, we disclose a chemical method to control hydrogel macropore size by tuning the rate of Tz-Nb reaction, and

examine their potential for supporting cartilage matrix production during 3D cell culture.

5.2 Introduction

The development of biocompatible synthetic polymer materials has promoted the progress of biomedical fields that involve engineering of the cell microenvironment *in vitro* such as 3D cell culture, drug discovery, cancer therapy and tissue regeneration.[1–4] Synthetic polymer scaffolds or hydrogels that imbibe large quantities of water have been widely studied in this area because of their capacity to mimic the water-rich character of native tissues. To closely engineer the native microenvironment, hydrogels are designed with both biochemical and biophysical cues for in vitro cell culture relying on cell-binding peptides for cell adhesion and proliferation, dynamic or degradable crosslinks to support matrix remodeling, and mechanical stiffness to guide cell morphological changes, migration, and even stem cell differentiation.[5–7] Among all hydrogel parameters, the pore size is an essential one that can dramatically influence cell behaviour through providing sufficient nutrition and oxygen transport, exchange of waste compounds and space for growth of extracellular matrix components. Biomedical applications involving vascularization, wound healing, bone tissue regeneration, stem cell differentiation or maturation have demonstrated the need for pore sizes in the micron range, for example, pores with 100 µm diameter fully support mesenchymal stem cell adhesion while larger pores (325 µm) facilitate cell migration.[8–13]

Beside the pore size that guides cell behaviour via the interface between cells and pores, their distribution within the materials or their porosity, the pore volume over the total hydrogel volume, can also be envisaged to influence cell behaviour. Even by increasing the pore size and pore densities, hydrogel porosity can be increased, their homogeneity and structural information will also be critical to engineering porous

materials for biological applications.[14] In order to better understand the potential to tune these parameters in synthetic materials, several approaches to generate pores with diameters from several to several hundred micrometers have been reported.[15,16] Salt particles (sodium chloride) or porogens (*e.g.* sodium hydrogen carbonate, silica and agarose beads) in the polymer solutions for hydrogelation have been applied in combination with particulate leaching or dissolution to modulate pore size.[17] Freeze drying is another technique that has been examined for pore formation that makes use of ice crystal formation that occurs with rapid cooling. Additionally, gas forming reactions have emerged as an inexpensive and efficient way to intentionally introduce macropores into hydrogels by using blowing agents such as sodium and ammoniun bicarbonate.[18] While macropores can be generated, these approaches are challenged for use in cell culture where 3D encapsulation is involved. In contrast, the unintentional formation of pores has been observed in 3D bioprinting with VA-086, a photoinitiator that generates nitrogen gas on decomposition with light.[19] Although the photointiator is efficient in improving the cell viability during the bioprinting, the formed hydrogels are turbid due to the trapped gas bubbles. Though the amount of gas formed can be tuned by varing the initiator concentration, the simultaneous generation of radicals to crosslink the polymers can limit its applicability. Therefore, a biocompatible strategy that would provide a handle for controlled bubble formation is very attractive to engineer macroscale pores in hydrogels in a user-defined manner.

The Inverse electron demand Diels–Alder (IEDDA) reaction stands out for the construction of hydrogel materials because of its capacity to form covalent bonds with high selectivity and robust kinetics under physiological conditions.[20–22] The IEDDA reaction proceed with significantly improved secondary reaction constants ranging from hundreds to thousands and in comparison to conventional click reactions, does not require the use of metals as catalysts.[23,24] As a bioconjugation strategy, the IEDDA reaction has also been used to introduce of bioactive peptide or protein cues for

binding to cells, fluorescent labels for live cell imaging, and to engineer degradable or dynamic building blocks in biomaterials.[25–27] Moreover, bioorthogonal hydrogels that based on IEDDA-crosslinkable polymers including polyethylene glycol (PEG), alginates, hyaluronic acid and poly(styrene-alt-maleic anhydride) have been shown to be efficient for drug delivery, cell encapsulation and 3D cell culture.[28–32] The IEDDA reaction mechanism consists of the [4+2] cycloaddition of 1,2,4,5-tetrazines and various dienophiles generating dihydropyridazines as an intermediate product that transform into pyridazines with oxidation and the formation of N_2 gas. When combined with hydrogelating polymers macro-sized pores have been observed from IEDDA reactions according to cryo-scanning electron microscopic images, but the use of this reaction to tune the pores within the hydrogels has not been examined thus far.[29] Due to the large number of IEDDA reaction pairs available that possess different reactivity, reaction kinetics and stability, the door is open to control the formation of macropores within these materials for a range of 3D cell culture applications.

We therefore became interested to understand the potential for tuning macropore size and distribution within the hydrogel materials by tuning the reaction rate between norbornene and tetrazine deratives. Three tetrazine building blocks were synthesized with substituents with decreased electron donating character, including 3-methyl and 6-phenyl (TZ1), 3-methylidene and 6-phenyl (TZ2) and 3-hydrogen and 6-phenyl (TZ3).[33] The norbornene and various tetrazines derivatives were then functionalized on 4-arm PEG star polymers to obtain hydrogels with macroporous structures of various size and porosity, mechanical properties and gelation kinetics. To examine the use of the IEDDA reaction pairs of various rates and their formed microporous structures in 3D cell culture, human primary chondrocytes that deposit large quantities of extracellular matrix were used reading out cell viability and glycosaminoglycan (GAGs) production.

5.3 Results and Discussion

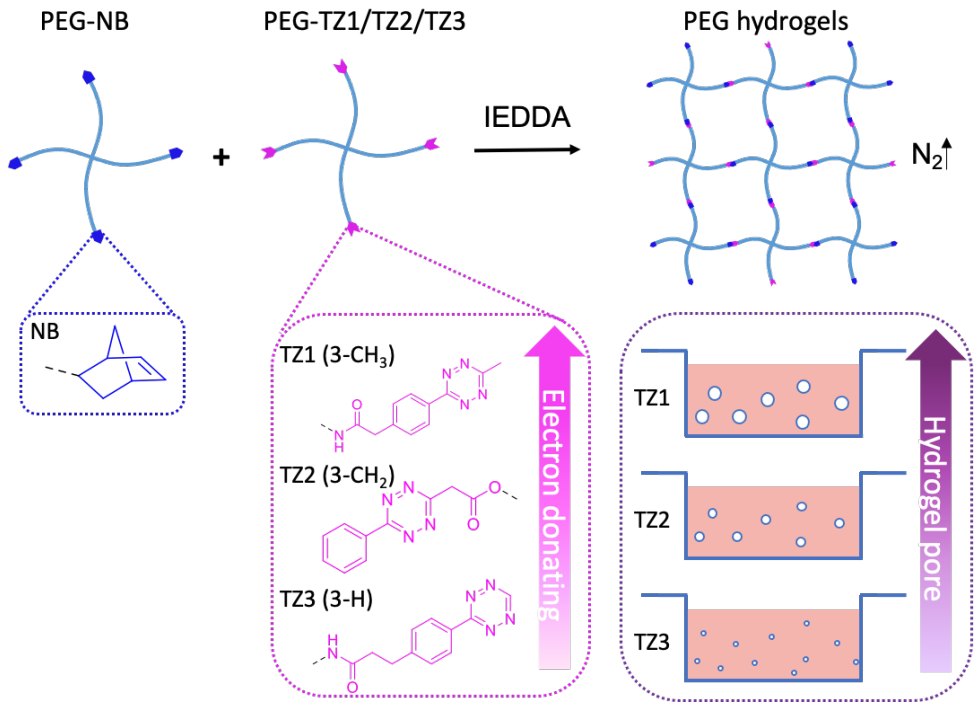

Scheme 5.1. Scheme of the IEDDA-bioconjugation reaction on PEG macromonomers and macropore formation in Tz-Nb-based PEG hydrogels with tetrazines bearing substituents of varying electron donating character. Mixing of PEG macromolecules **PEG-NB** and **PEG-TZ1/TZ2/TZ3** yields PEG hydrogels through cross-linking of the reactive groups and nitrogen gas is produced and captured in the hydrogels during the gelation process providing macropores of different size.

PEG macromonomer synthesis. A library of tetrazines with varied electron donating substituents were synthesized to screen their reactivity with norbornene by the IEDDA reaction on PEG macromonomers.[33–35] However, due to the limited design space for tetrazines that can react quickly with *trans*-cyclooctene, norbornene was selected as the dienophile, due to its availability and moderate reactivity in comparison to the highly reactive *trans*-cyclooctene.[24] The conventional synthesis of tetrazines starts by reacting aromatic or aliphatic nitriles with hydrazine to obtain the dihydrotetrazine as

an intermediate product, followed by an oxidation process to arrive to the final product. To improve the yield, catalysts such as sulphur, *N*-acetylcysteine, nickel and zinc triflates are used and more recently, a one-pot synthesis of tetrazines was also reported.[36,37] Based on the one-pot synthesis method, we successfully synthesized three tetrazines derivatives that have different electron donating and electron withdrawing substituents on positions 3 and 6 of the tetrazine ring (**TZ1**, **TZ2**, **TZ3**), with comparable yields that range from 27% to 45%. The generated carboxylic acid groups on the tetrazine and norbornene rings were used for further coupling onto hydroxy terminated PEG macromonomers through Steglich esterification or on amine-terminated PEG macromonomers by amide bond formation, resulting in yields of 70-80%. Tetrazine- (**PEG-TZ1**/**TZ2**/**TZ3**) and norbornene-functionalized 4-arm PEG macromonomers (**PEG-NB**) were obtained by precipitation in cold diethyl ether and dialyzed against water with a high degree of end-functionalization (**PEG-NB** ca. 90%; **PEG-TZ1** ca. 75%; **PEG-TZ2** ca. 90%; **PEG-TZ3** ca. 90%). Detailed synthetic procedures can be found in the Supporting Information.

PEG hydrogel preparation and characterization. Hydrogel formation based on the Tz-Nb crosslinks and their gelation time and stiffness were first examined by gel inversion and rheological measurements. PEG macromonomers **PEG-TZ** and **PEG-NB** were first dissolved in PBS (pH 7.4) or DMEM independently preparing stock solutions at various concentrations prior to mixing of the macromonomers in an equimolar ratio. Free standing and transparent hydrogels with gas bubbles of different sizes were observed by eye through a gel inversion test providing evidence for occurrence of the IEDDA reaction between the Tz and Nb groups (Figure S5.1). Oscillatory rheology was used to further quantify the mechanical properties and kinetics of gelation using equimolar precursor solutions prepared with final PEG macromonomer concentrations at 4 and 8 mM, respectively. Time sweep measurements provided insight into the gelation time through assessing the critical gelation point where G’ > G’’. Whereas Tz1-Nb-based PEG

hydrogels with a total PEG macromonomer concentration of 4 mM required ~ 4 h to reach the critical gelation point, Tz2-Nb and Tz3-Nb reaction pairs achieved gelation on the order of minutes, namely, 38 and 6 min, respectively (Figure 5.1). As expected, a longer gelation time for Tz1-Nb-based PEG hydrogels was demonstrated due to the increased electron donating effect of the substituents on the 3-position from TZ3 to TZ1 that decrease reactivity. Further increasing the total PEG macromonomer concentration to 8 mM, all hydrogels gelated within a shorter time, that is 40 min, 12 min and less than 1 min for Tz1-Nb, Tz2-Nb and Tz3-Nb-based PEG hydrogels, respectively. Similarly, Tz3-Nb-based hydrogels showed a 17-fold and 58-fold decreased critical gelation time in comparison to Tz1-Nb and Tz2-Nb-based hydrogels, respectively, demonstrating faster reaction kinetics of TZ3 with nobornene over TZ1 and TZ2. Through substitution of the tetrazine ring, control over the rate of hydrogel formation through Tz-Nb crosslinking was achieved. Because the gelation kinetics play an important role in cell encapsulation with fast gelation enabling a homogeneous cell distribution while slow gelation results in cell sedimentation, gelation times were further examined in the context of cell encapsulation in 3D. As an example, it was earlier demonstrated that reaction of unfunctionalized 4-arm PEG tetrazines and dinorbornene peptides (within minutes) resulted in hydrogels suitable for 3D cell encapsulation[28], whereas the slow reaction (over 5h) of furan and methylfuran gels resulted in high cell sedimentation.[38] Therefore, hydrogels based on TZ2 and TZ3 were further examined for their capacity to prepare gel phase materials for applications in 3D cell culture.

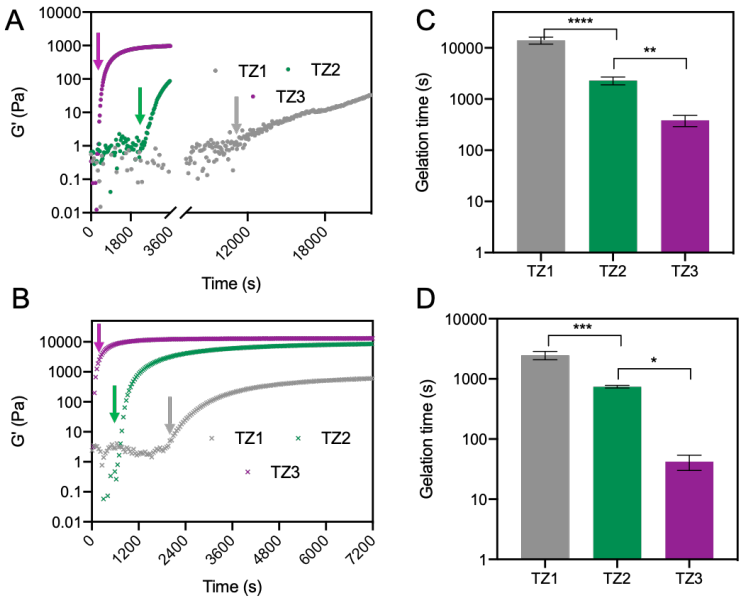

Figure 5.1. Tz-Nb-based PEG hydrogels that prepared with a norbornene/tetrazine molar ratios of 1:1. Time-sweep measurements of 4-arm PEG hydrogels with final PEG macromonomer concentrations of A) 4 mM and B) 8 mM. Arrows indicate the onset of gelation. Qualitative measurements of gelation time of hydrogels with PEG concentrations at C) 4 mM and D) 8 mM. The means and standard deviations are marked inside the graphs. (*P< 0.05, **P< 0.01, ***P< 0.001, ****P< 0.0001 one-way Anova)

From time sweep data, further mechanical information on the formed hydrogels was obtained from the measured plateau storage moduli (G'). The stiffness of Tz-Nb-based PEG hydrogels prepared from **PEG-TZ2** can be tuned from 1 Pa to 8.5 kPa by varying total PEG macromonomer concentrations from 2 mM to 8 mM, whereas for **PEG-TZ3** this range was higher in G' from 1 Pa to 12 kPa (Figure 5.2A). While, the case of Tz1-Nb-based PEG hydrogels displayed much lower storage moduli, showing a maxmium value at 1 kPa even with highest concentration of PEG macromonomer (16 mM), demonstrating the necessity of a faster reaction and gelation to engineer materials with higher mechanical properties (Figure S5.4). An amplitude sweep

experiment was performed from 0.1% to 1000% strain to determine linear viscoelastic (LVE) region of the materials. The end of the linear regime for the Tz2-Nb and Tz3-Nb-based hydrogels were at 300% and 127% with total PEG concentrations at 4 mM, and that were 99% and 123% with 8 mM PEG macromonomer concentration, respectively, after which permanent deformation occurred (Figure S5.4). Frequency sweep data shows that G' was significantly greater than G'' over an order of magnitude confirming the formation of elastic hydrogels (Figure S5.3).

To gain insight into the extent of crosslinking and stability of the hydrogel network, the equilibrium swelling ratio was determined for the Tz-Nb-based PEG hydrogels. The prepared hydrogels were incubated at 37˚C with PBS or DMEM medium and the weight of the hydrogels were measured at different time points. In the presence of PBS, whereas hydrogels based on TZ2 and TZ3 displayed stable weight ratios during the whole incubation, there was an 13% increase in the weight of the TZ1-based hydrogels after 15-day incubation with PBS (Figure 5.2B). This relatively higher swelling ratio (>1.14) of the Tz1-Nb-based hydrogel indicated a fraction of uncrosslinked polymer network that is consistent with a lower degree of functionalization of TZ1 on the PEG polymer in comparison to that of TZ2 and TZ3, that were 75% for TZ1 and over 90% for TZ2 and TZ3. In the case of DMEM, Tz2-Nb-based PEG hydrogels swelled slightly with a ratio of 4% during first two days and then showed clear decrease in swelling on day 3 and stabilized over the remainder of the experiment. Hydrogels based on TZ1 exhibited a decreased swelling ratios that end with 0.93 while TZ3-based hydrogel showed slightly incresed swelling behavior (1.07) (Figure S5.2). Still, neither hydrogels showed changes over the whole incubation period (15 days), demonstrating their stability during incubation with both PBS and DMEM, further supporting their use as scaffolds for 3D cell culture.

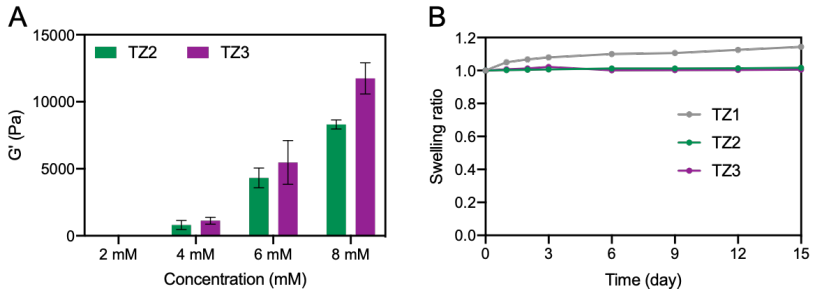

Figure 5.2 A) Averaged storage moduli (G') of Tz-Nb-based PEG hydrogels that were prepared in PBS and collected at 37 ± 0.2˚C by a time-sweep measurement with a fixed frequency of 1 Hz and strain of 0.05%. (N = 3) B) Swelling ratios of NB/TZ-based PEG hydrogels were measured over a period of 15-day incubation with PBS at 37˚C.

Macroscale pore measurement. During the IEDDA cycloaddition reaction between NB/TZ-based PEG macromonomers, nitrogen gas is released. According to the calculation, over 224 mg L^{-1} would be released when preparing Tz-Nb-based PEG hydrogels from 4 to 10 mM. This gas amount is far more than the solubility of nitrogen gas in water that is known as 15 mg L^{-1}. Therefore, the supersaturated nitrogen gas in the hydrogel results in the formation of bubbles. Owing to the different density between gas and liquid phase, bubbles usually move upwards and grow into larger new ones through coalescence. As this process can be influenced by the viscosity of the liquids they are prepared in by modulating bubble coalescence,[39,40] the use of hydrogelating materials based starting from synthetic polymer solutions can steer this process. Therefore, in the following experiment, we aimed to quantitatively assess the formed the macropore diameters to understand the connection between gelation rate and pore formation. Fluorescent RGD peptide sequences (NB-GGKGGGRGDS) containing a norbornene on the N-terminus and FITC label on the lysine side-chain were designed and coupled to Tz-Nb PEG hydrogels to visualize their formation. Because the fluorescent moiety is coupled to the forming polymer network, the resulting macropores were anticipated to appear as regions lacking fluorescence by confocal microscopy.

To probe the effect of the IEDDA gelation rate on macropore size, both slow and fast gelating hydorgels consisting of Tz2 and Tz3-based PEG macromonomers were prepared. Soft (1 kPa) and stiff (12 kPa) hydrogels by varying total polymer concentration with 4 and 8/10 mM for each Tz-Nb-based PEG hydrogel were obtained. The fluorescent hydrogels were imaged through taking z-stacks by confocal microscopy and the gas bubbles as indicated by the black spaces were measured in Fiji, as seen from Figure 5.3A and Figure S5.5. Pores were clearly formed and were distributed separately within the fluorescent hydrogels, confirming that the gelation process stopped the bubbles from coalescing. Size distributions of pore diameters were relatively broad ranging from 100 µm to 700 µm. A clear fraction of smaller size bubbles (< 300 µm) was observed in the most rapid hydrogel Tz3-Nb pointing to the importance of reaction rate on bubble formation (Figure 5.3B). Moreover, smaller pore diameters in Tz3-Nb PEG hydrogels having a total PEG concentration at 8 mM (268 $\pm$ 94 µm) were obtained over that of Tz2-Nb PEG hydrogels (382 $\pm$ 99 µm). Similarly, with a lower overall polymer concentration, hydrogels formed from TZ3 displayed significantly smaller bubbles (339 $\pm$ 135 µm) than gels consisting of TZ2 (417 $\pm$ 86 µm) (Figure 5.3C), demonstrating that faster gelation process resulted in hydrogels with smaller macropores and slower gelation resulted in larger macropores. Taken together, a control over hydrogel pore size can be achieved by tuning the rate of reaction through substitution of the tetrazine rings with electron donating substituents on the positions 3 or 6 with unsubstituted tetrazines reacting with norbornenes more rapidly than those substituted with methylenes on the 3-position to form smaller pores. With this tunable handle to control the pore size, the hydrogel porosity can also been tuned. And other parameters in terms of pore densities and their effect on cell behaviour can be explored in further study.

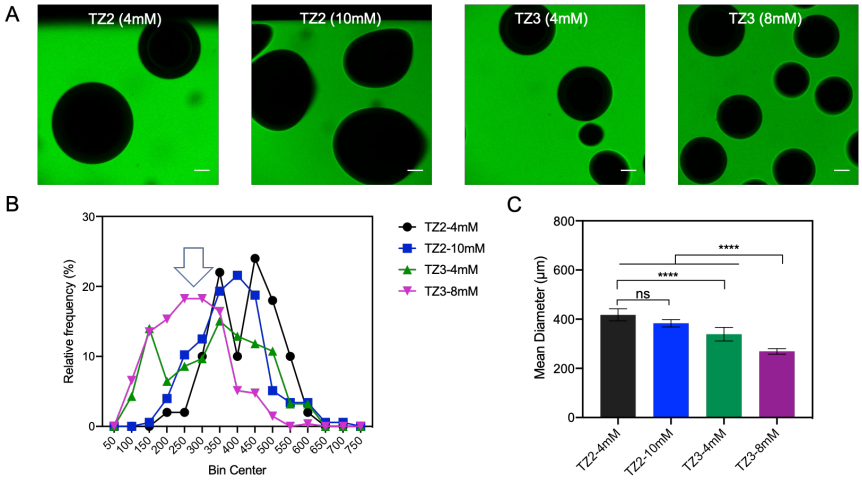

Figure 5.3. A) Representative images of FITC-labelled Tz-Nb-based PEG hydrogels prepared from **PEG-NB** and **PEG-TZ2/TZ3** polymers (hydrogels, *green;* pores*, black spaces*). Scale bar 100 µm. B) Size distribution and C) Mean diameter ± 95% confidence intervals from quantitative analysis of macropore diameters that formed in FITC-labelled PEG hydrogels. (****P< 0.0001 one-way Anova)

Primary chondrocytes culture within PEG hydrogel. In previous reports, it was demonstrated that the crosslinking between dinorbornene peptides and a Tz-functionalized PEG polymer can be used for 3D cell culture.[28,29] These results motivated us to explore potential of the Tz-Nb PEG hydrogels of various reactivities in the current work for 3D cell culture applications. We are particularly interested in the culture of primary chondrocytes because they play in important role in cartilage homeostasis, with their imbalance resulting in degenerative disease. Earlier reports have demonstrated that porous hydrogels with pore sizes between 250 to 500 µm have been demonstrated to be beneficial for chondrocyte growth and matrix production of collagen and proteoglycans through providing extra space for the newly formed biopolymers.[41,42] We thus became interested in evaluating the rate of the Tz-Nb reaction on 3D cell seeding and the effect of the formed pore sizes prepared by the in situ forming gas reaction on primary chondrocyte matrix production.

Primary chondrocytes were cultured for two passages after isolation from healthy cartilage and seeded into PEG hydrogels with a cell density of 2 x 10^6 cells/mL and cultured overnight followed by a 4-day differentiation process. LIVE/DEAD staining of chondrocytes were performed on day 2 and 5 of the culture to gain information on cell viability in the synthetic polymer matrices. From the z-stack images, Tz2-Nb-based PEG hydrogels showed cell sedimentation owing to the slower gelation process compared with those containing Tz3-Nb crosslinks. Still, the cells were largely viable in the matrices as shown by their green-staining for all tested conditions, with cell viabilities ranging from 80-97% that were calculated by counting live and dead cell populations after the LIVE/DEAD staining (Figure 5.4). Moreover, after 5 days of cell culture, the macropores stayed visible in the hydrogels demonstrating the stability of macropores after bubble formation and facilitating nutrition exchange.

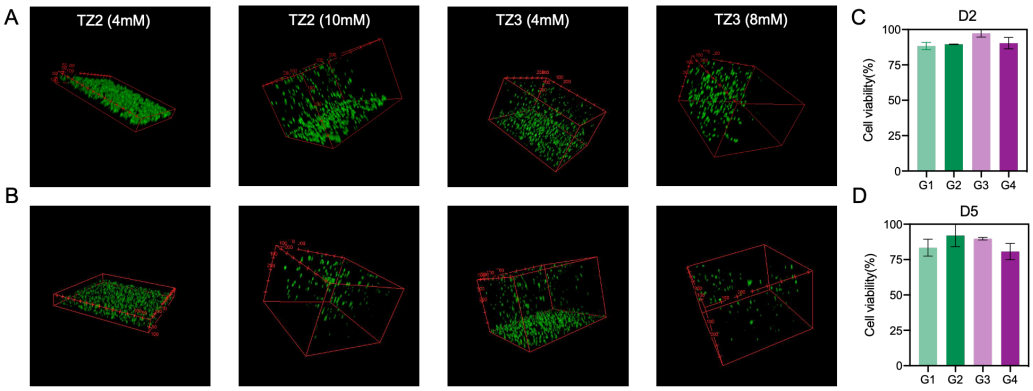

Figure 5.4. Cytocompatibility of Tz-Nb-based PEG hydrogels (NB:TZ molar ratio 1:1). Representative z-stack images of cells cultured in the hydrogels at A) day 2 and B) day 5. Cells were stained with calcein AM (viable cells, *green*) and propidium iodide (PI) (dead cells, *red*). Scale bar = 100 µm. Quantification of cell viability by cell counting in ImageJ after culture C) day 2 and D) day 5. Error bars represent standard deviations of the data.

Chondrocytes actively secrete extracellular matrix consisting of collagen (mainly type II) proteins, proteoglycans and hyaluronan. To detect matrix secretion, the histochemical stain Alcian blue was used to detect and quantify glycosaminoglycans

(GAGs) colourimetrically through their dark blue colour.[43,44] When the chondrocytes are assembled as pellets, extracellular matrix production is observed 2-3 days after differentiation. In this study, chondrocytes were encapsulated within hydrogels and fixed after differentiation on day 4 and stained with Alcian blue. Cells cultured in soft hydrogels (G' = 1 kPa) showed a dark, dense blue "membrane" around the cells on staining (indicated by the white arrows in Figure 5.5). In contrast, in stiff Tz-Nb-based PEG hydrogels (G' = 12 kPa), blue stained cells were hardly found suggesting that primary chondrocytes prefer a softer environment to facilitate GAGs secretion.

Matrix cues such as those of a biochemical and biophysical nature have been reported to affect ECM production and redifferentiation of chondrocytes.[45,46] In 3D culture systems in a stiff microenvironment, primary chondrocytes usually show a spherical morphology and display increased matrix production, for example, in fibrin and GelMA hydrogels with Young's moduli around 30 kPa.[43,47] In the current study, the chondrocytes showed matrix production in relatively softer hydrogels and in areas where cells tended to aggregate. The observed result could be due to the close cell-cell contacts that are made.[48] While the correlation between hydrogel pore size and chondrocyte matrix production needs to be explored more thoroughly, these preliminary results suggest that primary chondrocytes survive and secrete GAGs in Tz-Nb-based PEG hydrogels and further demonstrate their potential for further use in biomedical applications.

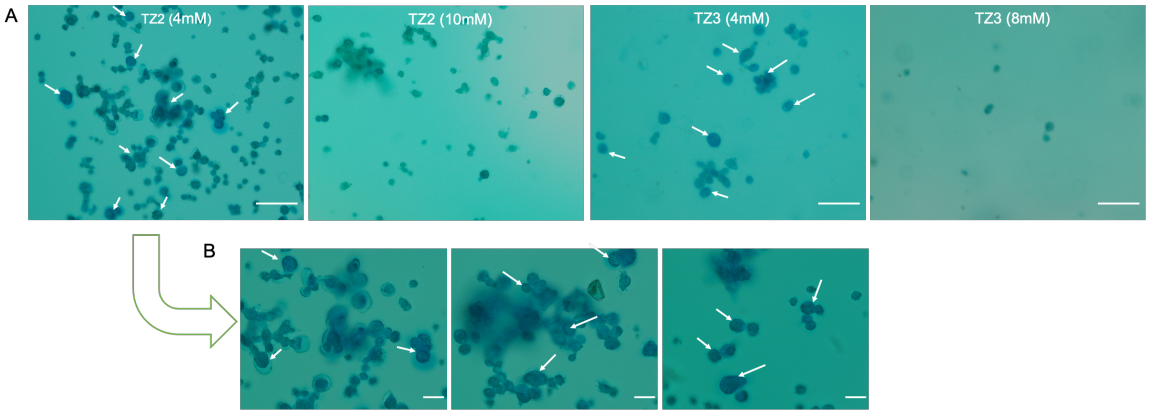

Figure 5.5. A) Images of Alcian blue stained primary chondrocytes in Tz-Nb-based PEG hydrogels under a 20x objective on an Olympus microscope. B) Representative images of Alcian blue stained primary chondrocytes in Tz2-Nb-based PEG hydrogels with a total polymer concentration of 4 mM. Imaged were collected under a 40x objective. Arrows highlight dark blue-stained extracellular matrix of chondrocytes in hydrogels that are mechanically soft (G' 1 kPa). Scale bar: 100 µm.

5.4 Conclusions

In summary, we hereby show a control over the pores size of a PEG-based hydrogels through controlling the rate of the tetrazine-norbornene reaction. Three tetrazines that have varied electron donating substituents were successfully synthesized and coupled onto multi-arm PEG polymers, respectively. The PEG-TZ macromonomers were further crosslinked with Nb-functionalized multi-arm PEG polymers through the IEDDA reaction, forming elastic hydrogels of varying stiffness. The nitrogen gas produced during the IEDDA reaction on the polymers enable microporous hydrogel formation. The gelation kinetics and pore sizes and porosity were observed to depend highly on the IEDDA reaction rates and PEG macromonomer concentrations, with higher reaction rates and polymer concentrations yielding faster gelation. The fastest gelation behaviour was observed in TZ3 that lacks electron donating substitution and is

consistent with its rapid crosslinking kinetics. Rheological experiments demonstrated that these Tz-Nb-based PEG hydrogels can be prepared with storage moduli ranging from 0.7 kPa to 12 kPa through increasing concentration and the reaction rate of the components by tetrazine selection. The faster gelation of the Tz3-Nb PEG hydrogel minimized the bubble coalescence during bubble formation, resulting in the formation of hydrogels with a significantly smaller pores with an average diameter of 268 ± 94 µm was obtained in comparison to Tz2-Nb-based PEG hydrogels (382 ± 99 µm). All the Tz-Nb-based PEG hydrogels were demonstrated to be stable in presence of PBS and DMEM medium as shown in swelling tests, despite a fraction of uncrosslinked PEG macromonomer in the Tz1-Nb-based PEG hydrogel. The high stability of the hydrogels further allowed them to be used as a synthetic matrix for 3D cell culture. 3D encapsulated primary chondrocytes in soft Tz-Nb-based PEG hydrogels displayed high viability and notable changes in cartilage matrix secretion, demonstrating their potential application in cartilage tissue engineering, though further quantitative analysis is necessary to gain conclusion about effect of hydrogel pore size on matrix production. In conclusion, we showed a control over hydrogel pore size and porosity can be achieved by tuning the reaction rate of the IEDDA components by substituting tetrazine rings to control over physicochemical aspects matrix properties for *in vitro* cell culture applications in 3D.

5.5 References

[1] F. Edalat, I. Sheu, S. Manoucheri, A. Khademhosseini, *Curr. Opin. Biotechnol.* **2012**, *23*, 820.

[2] C. Bonnans, J. Chou, Z. Werb, *Nat. Rev. Mol. Cell Biol.* **2014**, *15*, 786.

[3] G. Huang, F. Li, X. Zhao, Y. Ma, Y. Li, M. Lin, G. Jin, T. J. Lu, G. M. Genin, F. Xu, *Chem. Rev.* **2017**, *117*, 12764.

[4] J. Nicolas, S. Magli, L. Rabbachin, S. Sampaolesi, F. Nicotra, L. Russo, *Biomacromolecules* **2020**, *21*, 1968.

[5] K. M. Schultz, K. A. Kyburz, K. S. Anseth, *Proc. Natl. Acad. Sci. U. S. A.* **2015**, *112*, E3757.

[6] X. Li, Y. Chen, N. Kawazoe, G. Chen, *J. Mater. Chem. B* **2017**, *5*, 5753.

[7] N. Huebsch, E. Lippens, K. Lee, M. Mehta, S. T. Koshy, M. C. Darnell, R. M. Desai, C. M. Madl, M. Xu, X. Zhao, O. Chaudhuri, C. Verbeke, W. S. Kim, K. Alim, A. Mammoto, D. E. Ingber, G. N. Duda, D. J. Mooney, *Nat. Mater.* **2015**, *14*, 1269.

[8] X. Xie, X. Li, J. Lei, X. Zhao, Y. Lyu, C. Mu, D. Li, L. Ge, Y. Xu, *Mater. Sci. Eng. C* **2020**, *116*, 111165.

[9] T. Tokatlian, C. Cam, T. Segura, *Adv. Healthc. Mater.* **2015**, *4*, 1084.

[10] V. Zubillaga, A. Alonso-varona, S. C. M. Fernandes, A. M. Salaberria, T. Palomares, *Int. J. Mol. Sci.* **2020**, *21*, 1.

[11] B. Conrad, L. H. Han, F. Yang, *Tissue Eng. - Part A* **2018**, *24*, 1631.

[12] S. S. Ng, K. Saeb-Parsy, S. J. I. Blackford, J. M. Segal, M. P. Serra, M. Horcas-Lopez, D. Y. No, S. Mastoridis, W. Jassem, C. W. Frank, N. J. Cho, H. Nakauchi, J. S. Glenn, S. T. Rashid, *Biomaterials* **2018**, *182*, 299.

[13] I. Bružauskaitė, D. Bironaitė, E. Bagdonas, E. Bernotienė, *Cytotechnology* **2016**, *68*, 355.

[14] B. Podhorská, M. Vetrík, E. Chylíková-Krumbholcová, L. Kománková, N. R. Banafshehvaragh, M. Šlouf, M. Dušková-Smrčková, O. Janoušková, *Appl. Sci.* **2020**, *10*, 5.

[15] B. R. Thompson, T. S. Horozov, S. D. Stoyanov, V. N. Paunov, *J. Mater. Chem. A* **2019**, *7*, 8030.

[16] K. J. De France, F. Xu, T. Hoare, *Adv. Healthc. Mater.* **2018**, *7*, 1.

[17] O. D. Velev, E. W. Kaler, *Adv. Mater.* **2000**, *12*, 531.

[18] N. Adnan, S. Ghazali, S. S. Jamari, *Mater. Today Proc.* **2019**, *17*, 995.

[19] W. T. Han, T. Jang, S. Chen, L. S. H. Chong, H. Do Jung, J. Song, *Biomater. Sci.* **2020**, *8*, 450.

[20] W. Hu, Z. Wang, Y. Xiao, S. Zhang, J. Wang, *Biomater. Sci.* **2019**, *7*, 843.

[21] N. K. Devaraj, *ACS Cent. Sci.* **2018**, *4*, 952.

[22] Y. Liu, M. Liu, Y. Zhang, Y. Cao, R. Pei, *New J. Chem.* **2020**, *44*, 11420.

[23] A. C. Knall, C. Slugovc, *Chem. Soc. Rev.* **2013**, *42*, 5131.

[24] B. L. Oliveira, Z. Guo, G. J. L. Bernardes, *Chem. Soc. Rev.* **2017**, *46*, 4895.

[25] L. Bian, M. Guvendiren, R. L. Mauck, J. A. Burdick, *Proc. Natl. Acad. Sci. U. S. A.* **2013**, *110*, 10117.

[26] B. Yang, S. Tang, C. Ma, S. T. Li, G. C. Shao, B. Dang, W. F. DeGrado, M. Q. Dong, P. G. Wang, S. Ding, L. Wang, *Nat. Commun.* **2017**, *8*, 1.

[27] N. Gjorevski, N. Sachs, A. Manfrin, S. Giger, M. E. Bragina, P. Ordóñez-Morán, H. Clevers, M. P. Lutolf, *Nature* **2016**, *539*, 560.

[28] D. L. Alge, M. A. Azagarsamy, D. F. Donohue, K. S. Anseth, *Biomacromolecules* **2013**, *14*, 949.

[29] V. X. Truong, M. P. Ablett, S. M. Richardson, J. A. Hoyland, A. P. Dove, *J. Am. Chem. Soc.* **2015**, *137*, 1618.

[30] R. M. Desai, S. T. Koshy, S. A. Hilderbrand, D. J. Mooney, N. S. Joshi, *Biomaterials* **2015**, *50*, 30.

[31] V. Delplace, P. E. B. Nickerson, A. Ortin-Martinez, A. E. G. Baker, V. A. Wallace, M. S. Shoichet, *Adv. Funct. Mater.* **2020**, *30*, 1.

[32] D. S. B. Anugrah, M. P. Patil, X. Li, C. M. Q. Le, K. Ramesh, G. D. Kim, K. Hyun, K. T. Lim, *Express Polym. Lett.* **2020**, *14*, 248.

[33] M. R. Karver, R. Weissleder, S. A. Hilderbrand, *Bioconjug. Chem.* **2011**, *22*, 2263.

[34] J. Schoch, M. Wiessler, A. Jäschke, *J. Am. Chem. Soc.* **2010**, *132*, 8846.

[35] K. Lang, L. Davis, J. Torres-Kolbus, C. Chou, A. Deiters, J. W. Chin, *Nat. Chem.* **2012**, *4*, 298.

[36] W. Mao, W. Shi, J. Li, D. Su, X. Wang, L. Zhang, L. Pan, X. Wu, H. Wu, *Angew. Chemie - Int. Ed.* **2019**, *58*, 1106.

[37] J. Yang, M. R. Karver, W. Li, S. Sahu, N. K. Devaraj, *Angew. Chemie - Int. Ed.* **2012**, *51*, 5222.

[38] C. M. Madl, S. C. Heilshorn, *Chem. Mater.* **2019**, *31*, 8035.

[39] K. Yamada, H. Emori, K. Nakazawa, *Earth, Planets Sp.* **2008**, *60*, 661.

[40] A. Barbetta, A. Gumiero, R. Pecci, R. Bedini, M. Dentini, *Biomacromolecules* **2009**, *10*, 3188.

[41] H. Akkiraju, A. Nohe, *J. Dev. Biol.* **2015**, *3*, 177.

[42] S. M. Lien, L. Y. Ko, T. J. Huang, *Acta Biomater.* **2009**, *5*, 670.

[43] B. Bachmann, S. Spitz, B. Schädl, A. H. Teuschl, H. Redl, S. Nürnberger, P. Ertl, *Front. Bioeng. Biotechnol.* **2020**, *8*, 1.

[44] L. A. Smith Callahan, A. M. Ganios, E. P. Childers, S. D. Weiner, M. L. Becker, *Acta Biomater.* **2013**, *9*, 6095.

[45] W. Wei, Y. Ma, X. Yao, W. Zhou, X. Wang, C. Li, J. Lin, Q. He, S. Leptihn, H. Ouyang, *Bioact. Mater.* **2021**, *6*, 998.

[46] H. J. Lee, Y. Seo, H. S. Kim, J. W. Lee, K. Y. Lee, *ACS Omega* **2020**, *5*, 15567.

[47] X. Li, S. Chen, J. Li, X. Wang, J. Zhang, N. Kawazoe, G. Chen, *Polymers (Basel).* **2016**, *8*, 269.

[48] TS. de Windt, DB. Saris, IC. Slaper-Cortenbach, MH. van Rijen, D. Gawlitta, LB. Creemers, RA. de Weger, WJ. Dhert, LA.R. Vonk. J. Siman. *Tissue Eng Part A.* **2015**, *21*, 2536.

5.6 Supporting information

5.6.1 Materials

Tetra-arm hydroxy-terminated PEG (Mw 10kDa) was purchased from Creative PEGWorks and tetra-arm amine-terminated PEG (Mw 10kDa) was from Jenkem Technology. Deuterated dimethyl sulfoxide (DMSO-d_6) and chloroform ($CDCl_3$) were purchased from Eurisotop. All other chemicals and reagents for synthesis were purchased from Sigma Aldrich and used without further purification. Dulbecco's Modified Eagles Medium (DMEM) and fetal bovine serum (FBS), penicillin, streptomycin and trypsin-EDTA were from Gibco. Human basic fibroblast growth factor (hFGF) and human transforming growth factor β1 (hTGF-β1) were purchased from PeproTech. Dulbecco's Phosphate Buffered Saline (DPBS), calcein AM (AM = acetoxymethyl), propidium iodide (PI) and alcian-blue staining solution were obtained from Sigma-Aldrich.

5.6.2 Instruments

^{1}H-NMR and ^{13}C-NMR spectra were acquired on a Bruker DMX-400 and Bruker DPX-300 MHz at 298K. LC-MS analysis was performed on a TSQ Quantum Access MAX system equipped with a Gemini 3 µm C18 110 Å 50×4.60 mm column (UV detection at 214 nm and 254 nm, mass detection range: 160 to 2000 (Da)). The mobile phase consisted of a gradient of 10-90% of H_2O-ACN with 0.1% trifluoroacetic acid (TFA) over 13.5 minutes. HPLC purification of peptides was executed on a C18 column with a gradient of 1-10% ACN/H_2O over 15 min at a flow rate of 12 mL/min. High resolution mass spectra (HR-MS) were collected on a Thermo Fisher LTQ Orbitrap mass spectrometer equipped with an electrospray ion source in positive mode. Samples were prepared in a mixture solvent (DMSO-H_2O-ACN, 1 mg/mL) and injected directly. Oscillatory rheology experiments were performed on a Discovery HR-2 hybrid rheometer using a cone-plate

geometry (20 mm, 1.995°) at 37 ± 0.2 °C with a peltier-based temperature controller and solvent trap. Confocal fluorescent images were acquired on Leica TCS SP8 confocal laser scanning microscope equipped with a 10× air objective. Images were processed using the Fiji Image J software. Alcian-blue staining images were collected on an Olympus microscopy equipped with 20× and 40x air objectives.

5.6.3 Synthesis and experimental details

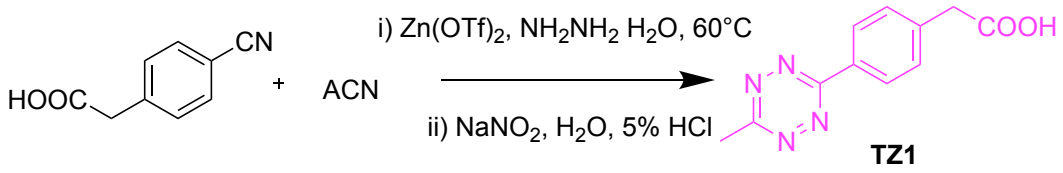

Scheme S5.1. Synthesis route of **TZ1**[1]

Synthesis of TZ1. 4-Cyanophenylacetic acid (1.15 g, 7.13 mmol), $Zn(OTf)_2$ (1.30 g, 3.57 mmol) and acetonitrile (3.60 mL, 68.93 mmol) were mixed under N_2 (50 mL). A solution of hydrazine hydrate (16.80 mL, 346.33 mmol) was added dropwise. The reaction mixture was stirred overnight at 60˚C. After that, the obtained orange-yellow solution was cooled to room temperature, followed by the addition of $NaNO_2$ (9.60 g, 139.15 mmol) in H_2O (50 mL). Next, the reaction mixture was acidified to pH=1 by the dropwise addition of HCl (4M), and extracted with EtOAc (100 mL x 3). The combined organic layers were washed with brine (100 mL x 3), dried over anhydrous Na_2SO_4 and concentrated in vacuum overnight to obtain the product as a pink solid. Yield: 45.0%, 0.74 g. ^{1}H-NMR (DMSO-d_6, 400 MHz): 8.43-8.41 (d, 2H), 7.56-7.54 (d, 2H), 3.73 (s, 2H), 2.99 (s, 3H). ^{13}C-NMR (DMSO-d_6, 100 MHz): 172.29, 167.12, 163.22, 139.80, 130.58, 130.30, 127.35, 40.55, 20.85. HR-MS: $[M+H]^+$: calcd: 233.1033 (protonated), found: 233.1033.

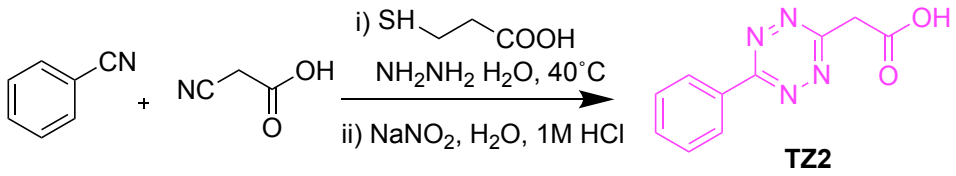

Scheme S5.2. Synthesis route of **TZ2**[2]

Synthesis of TZ2. Benzonitrile (510 µL, 4.95 mmol), 2-cyanoacetic acid (3.40 g, 39.97 mmol) and 3-mercaptopropionic acid (87 µL,0.99 mmol) were cooled to 0°C and mixed under N_2. To this mixture, hydrazine monohydrate (3.8 mL, 78.33 mmol) was added slowly and the resulting mixture was stirred at 40°C for 20 h. After that, cold aqueous solution of sodium nitrite (5.23 g, 75.80 mmol) was added and left to stir at room temperature for 30 min. The crude reaction mixture was adjusted to pH ~3 with the slow addition of ice-cold 1M HCl. (Caution: the addition of HCl resulted in formation of toxic nitrogen oxide gas) After stirring for 30 min, the crude was extracted with DCM (100 mL x 5). The organic layers were combined, dried over Na_2SO_4, and concentrated by rotary evaporation. Lastly, the crude was purified by flash column chromatography on silica gel with 10% EtOAC in DCM. The purified fractions were collected, evaporated and dried in vacuum oven overnight to obtain **TZ2** as a pink solid.

Yield: 27.1%, 0.29 g. ^{1}H-NMR (DMSO-d_6, 400 MHz): 8.52-8.46 (m, 2H), 7.75-7.65 (m, 3H), 4.41, 3.00 (s, 2H). ^{13}C-NMR (DMSO-d_6, 100 MHz): 169.94, 165.11, 163.63, 132.84, 131.55, 129.56, 127.73, 40.72. HR-MS: $[M+H]^+$: calcd: 217.0720, found: 217.0720.

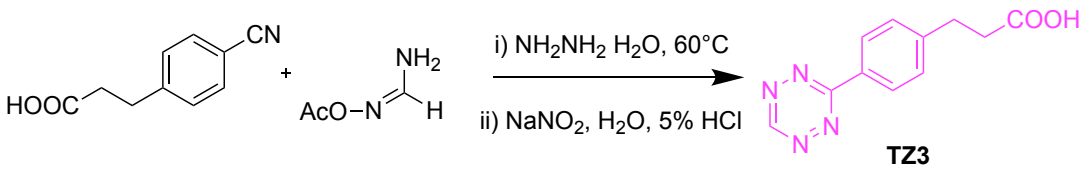

Scheme S5.3. Synthesis route of **TZ3**[3,4]

Synthesis of TZ3. A mixture of 3-(4-Cyanophenyl)propionic acid (1.10 g, 6.28 mmol) and formamidine acetate salt (4.12 g, 39.57 mmol) was cooled to 0°C under N_2.

Hydrazine monohydrate (8.0 mL, 164.92 mmol) was added slowly and the resulting mixture was warmed to 60°C and stirred for 3h. Once cooled, the reaction mixture was further stirred overnight and then neutralized to pH 7 with 5% aqueous HCl. Afterwards, a cold aqueous solution of sodium nitrite (2.76 g, 40.01 mmol) was added and stirred for another 30 min. Then, an ice-cold 5% aqueous HCl solution was added slowly until the solution reached pH ~3. (Caution: the addition of HCl resulted in formation of toxic nitrogen oxide gas) After leaving the reaction mixture to stir for another 30 min, the pink precipitate was collected by filtration, washed with 0.1% aqueous HCl and dried in vacuum to obtain **TZ3** a pink solid without further purification.

Yield: 33.8%, 0.49 g. ^{1}H-NMR (DMSO-d_6, 400 MHz): 10.55 (s, 1H), 8.42-8.39 (d, 2H), 7.54-7.52 (d, 2H), 2.96-2.93 (t, 2H), 2.64-2.60 (t, 2H). ^{13}C-NMR (DMSO-d_6, 100 MHz): 173.77, 165.61, 158.18, 146.54, 129.81, 129.61, 127.95, 34.82, 30.41. HR-MS: $[M+H]^+$: calcd: 233.1033 (protonated), found: 233.1033.

Synthesis of PEG-NB.[5] 5-norbornene-2-carboxcylic acid (600 µL, 4.43 mmol) and N,N'-dicyclohexylcarbodiimide (0.53 g, 4.64 mmol) were dissolved in dry DCM and reacted at room temperature for 30 min. In a separate reaction vessel, tetra-arm hydroxyl-terminated PEG (Mw 10 kDa) (2.00 g, 0.20 mmol) together with 4-(dimethylamino)pyridine (DMAP) (0.05 g, 0.44 mmol) and pyridine (0.33 mL, 4.10 mmol) were dissolved in dry DCM. Subsequently, the PEG solution was added dropwise into the activated norbornene solution and the reaction mixture was left to stir at room temperature for 24 h. The reaction crude was first filtered and the filtrate was precipitated from cold diethyl ether, washed, dissolved in DCM, and re-precipitated from cold diethyl ether. The obtained products after three rounds of precipitation were re-dissolved in water and lyophilized to obtain **PEG-NB** as a white solid. Yield:1.59 g, 79.5%. ^{1}H-NMR (400 MHz, 298K, $CDCl_3$): 6.20-5.92 (m, 2H), 4.25-4.15 (m, 2H), 3.81-3.40 (m, 224H). The degree of functionalization of the **NB** group was calculated to be 90% based on ^{1}H-NMR.

Synthesis of PEG-TZ1.[1] **TZ1** (0.19 g, 0.80 mmol), BOP (0.35 g, 0.80 mmol) and tetra-arm amine-terminated PEG (0.50 g, 0.05 mmol) were dissolved in a dry and N_2-purged flask with dry DMF. N,N-diisopropylethylamine (DIPEA) (0.56 mL, 3.21 mmol) was added and the reaction mixture were left stirring at room temperature over the weekend. After that, the DMF was removed by rotary evaporation and the obtained residue was dissolved in DCM (50 mL), and subsequently washed with NaH_2PO_4 (1M, 50 mL x 2) and brine (50 mL x 2). The organic layer was dried, concentrated and precipitated from cold diethyl ether. The obtained red solid was dissolved in DCM and precipitated from cold diethyl ether for another two rounds, after which the red solid was dissolved in water, dialyzed against water for 48 h and lyophilized to obtain **PEG-TZ1** as a pink solid. Yield: 0.38 g, 76.2%. ^{1}H-NMR (400 MHz, 298K, $CDCl_3$): 8.41-8.39 (m, 2H), 7.55-7.53 (m, 2H), 3.69-3.50 (m, 224H), 2.99 (s, 3H). The degree of functionalization of the **TZ1** group was calculated to be 75% based on ^{1}H-NMR.

Synthesis of PEG-TZ2. TZ2 (0.33 g, 1.54 mmol), N-(3-dimethylaminopropyl)-N'-ethylcarbodiimide hydrochloride (0.36 g, 1.87 mmol) and 4-(dimethylamino)pyridine (0.20 g, 1.61 mmol) were dissolved in a dry and N_2-purged flask with dry DCM and reacted for 10 min as solution one. In a separate reaction vessel, tetra-arm hydroxyl-terminated PEG (0.60 g, 0.06 mmol) was dissolved in dry DCM and added dropwise into solution one. The reaction mixture was left stirring at room temperature over the weekend. Afterwards, the reaction crude was first precipitated from cold diethyl ether. The obtained red solid was dissolved in DCM and the precipitated salts were filtered off. The filtrate was precipitated in cold diethyl ether, dissolved in DCM and re-precipitated from cold diethyl ether. The obtained products after three rounds of precipitation were dissolved in water, dialyzed against water for 48 h and lyophilized to obtain **PEG-TZ2** as a pink solid. Yield: 0.44 g, 73.3%. ^{1}H-NMR (400 MHz, 298K, DMSO-d_6): 8.52-8.50 (m, 2H), 7.74-7.67 (m, 3H), 4.54 (s, 2H), 4.26-4.24 (m, 2H), 3.68-3.48 (m, 224H). The degree of functionalization of the **TZ2** group was calculated to be 90% based on ^{1}H-NMR.

Synthesis of PEG-TZ3. TZ3 (0.14 g, 0.61 mmol), BOP (0.26 g, 0.59 mmol) and tetra-arm amine-terminated PEG (0.40 g, 0.04 mmol) were dissolved in a dry and N_2-purged flask with dry DMF. DIPEA (0.80 mL, 4.59 mmol) was added and the reaction mixture was left to stir at room temperature over the weekend. After that, DMF was removed by rotary evaporation and the obtained residue was dissolved in DCM (50 mL), and subsequently washed with NaH_2PO_4 (1M, 50 mL x 2) and brine (50 mL x 2). The organic layer was dried, concentrated and precipitated from cold diethyl ether. The obtained red solid was dissolved in DCM and precipitated from cold diethyl ether for another two rounds, after which the red solid was re-dissolved in water, dialyzed against water for 48 h and lyophilized to obtain **PEG-TZ3** as a pink solid. Yield:0.28 g, 70.5%. ^{1}H-NMR (400 MHz, 298K, CDCl3): 10.57 (s, 1H), 8.43-8.40 (m, 2H), 7.56-7.54 (m, 2H), 4.14-4.09 (m, 2H), 3.68-3.31 (m, 224H), 3.01-2.97 (m, 2H), 2.76-2.72 (m, 2H). The degree of functionalization of the **TZ3** group was calculated to be 90% based on ^{1}H-NMR.

Peptide synthesis. The RGD peptide (GGGRGDS) was synthesized on an automatic CEM peptide synthesizer on a 100 µmol scale as described in Chapter 2. Norborne functionalization was manually performed by on the resin. Briefly, the obtained resins (100 µmol) from peptide synthesizer were suspended in DMF (2 mL) for 15 min. 5-Norbornene-2-carboxylic acid (53.3 mg, 0.54 mmol) was coupled to the N-terminus of the peptide by incubation with HCTU (g, 0.50 mmol) and DIPEA (175 µL, 1.00 mmol) in DMF (4 mL) at room temperature for 1h. Afterwards, the norbornene-functionalized peptides (RGD-NB) were cleaved in a TFA solution containing 2.5% H_2O and 2.5% triisopropylsilane (TIPS) for 3h, and then precipitated from cold diethyl ether, dried, dissolved in water and purified by HPLC using a gradient 1-10% ACN/H_2O over 15 min. The product was concentrated by evaporation and lyophilized overnight to obtain a light yellowish solid. LC-MS: t =0.69 min, m/z $[M+H]^+$: calcd: 724.31, found: 724.47.

Another RGD peptide (GGKGGGRGDS) was synthesized on an automatic CEM peptide synthesizer on a 100 µmol scale and norbornene-functionalization was performed in

the same method as above. Afterwards, the obtained resins were washed with a Mtt-deprotection solution (DCM:TFA:TIPS 94/1/5 v/v/v) until the filtrate becomes colorless. Then, the resins were washed with DCM (5 mL x3) before reacting with 5(6)-carboxyfluorescein (193 mg, 0.51 mmol) in combination with HBTU (201 mg, 0.53 mmol) and DIPEA (60 µL, 0.34 mmol) in DMF (5 mL) on a shaker for 3h. The coupling was performed twice. When finished, the resins were washed with DMF (5 mL x 3) and DCM (5 mL x 3) and the peptides were cleaved in a TFA solution (2.5% H_2O, 2.5% TIPS) for 3h. The peptides were then precipitated in cold diethyl ether, dried, dissolved in water and purified by HPLC using a gradient 1-10% ACN/H_2O over 15 min. The product was concentrated by evaporation and lyophilized overnight to obtain a yellow solid (FITC-RGD). LC-MS: t =4.71 min, m/z $[M+H]^+$: calcd: 1324.50, found: 1325.47.

5.6.3 Hydrogel preparation

Hydrogels were prepared by separately dissolving PEG macromonomers in PBS (pH 7.4) and mixing in a molar ratio of 1:1. More specfically, a freshly prepared solution of **PEG-NB** (100 µL) was mixed with that of **PEG-TZ1/TZ2/TZ3** (100 µL), and vortexed for 10s to obtain a homogeneous solution with a final PEG macromonomer concentration from 2-16 mM. For gelation, the precursor solutions were left at 37˚C. Images were taken after a free-standing hydrogel was obtained.

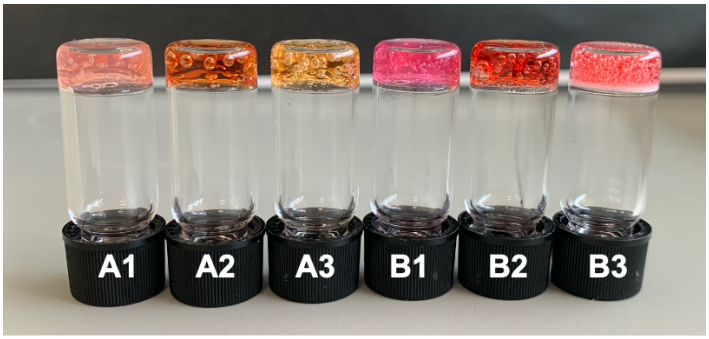

Figure S5.1. Gel inversion images of PEG hydrogels prepared from macromonomers **PEG-NB** and **PEG-TZ1/TZ2/TZ3** with a norbornene/tetrazine molar ratio of 1:1 in PBS (A,

pH 7.4) and DMEM medium (B), respectively. Numbers in the labels indicate the different tetrazine derivatives used for gel preparation.

5.6.4 Swelling measurements

Hydrogels (200 µL) were prepared according to gelation protocol described above and were allowed to stand at 37°C for 2h. After the gelation, the wet weight of these hydrogels was measured and denoted as W_0. Afterwards, PBS (pH7.4, 300 µL) or DMEM medium was added on top of hydrogel and incubated at 37˚C. At pre-determined time points, the supernatant solution was carefully removed and the wet weight of these hydrogels was measured and donoted as W_t. The swelling ratios over the time points were determined by the following equation: swelling ratio = W_t/W_0.

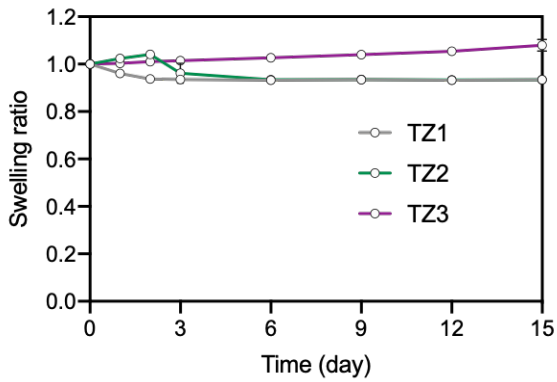

Figure S5.2. Swelling ratios of Tz-Nb-based PEG hydrogels in DMEM over a 15-day incubation period.

5.6.5 Oscillatory Rheology

Oscillatory rheology experiments were carried out on a Discovery HR-2 hybrid rheometer using parallel plate geometry (20 mm diameter) at 37 °C ± 0.2 °C with a Peltier-based temperature controller and a solvent trap. The prepared hydrogel (100 µL) was pipetted onto the bottom plate and the geometry was lowered to a gap distance

of 300 µm. Time sweep measurements were executed at a frequency of 1.0 Hz and strain of 0.05% and frequency sweeps were conducted from 0.01−10 Hz with 0.05% strain. Subsequently, amplitude sweeps were carried out with strains ranging from 0.1% to 2000% and a fixed frequency of 1.0 Hz.

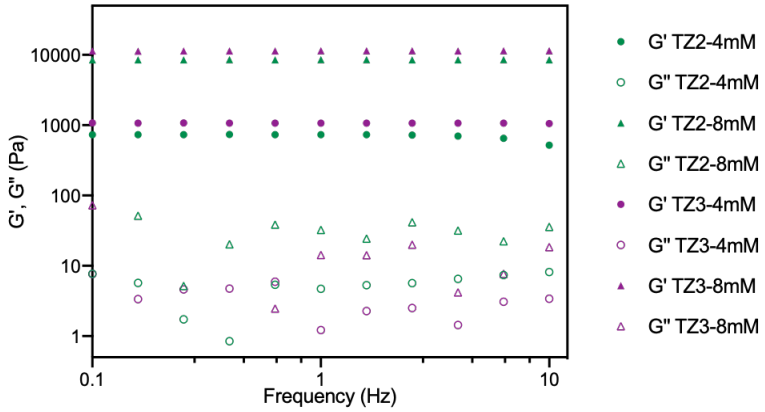

Figure S5.3. Frequency sweep measurements of Tz-Nb-based PEG hydrogels in PBS (pH 7.4) at 37 ± 0.2 °C. Norbornene/tetrazine molar ratios were kept at 1:1 and final PEG macromonomers concentrations were 4 mM and 8 mM, respectively. Frequency sweep data was collected in a range of 0.01 Hz to 10 Hz with strain of 0.05%.

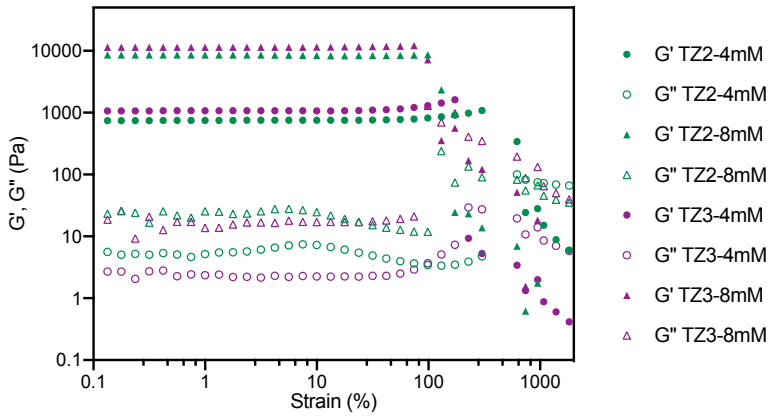

Figure S5.4. Amplitude sweep measurements of Tz-Nb-based PEG hydrogels at 37 ± 0.2˚C with a frequency of 1 Hz and strain from 0.1% to 2000%. Norbornene/tetrazine

molar ratios were kept at 1:1 and final PEG macromonomer concentrations were 4 mM and 8 mM, respectively.

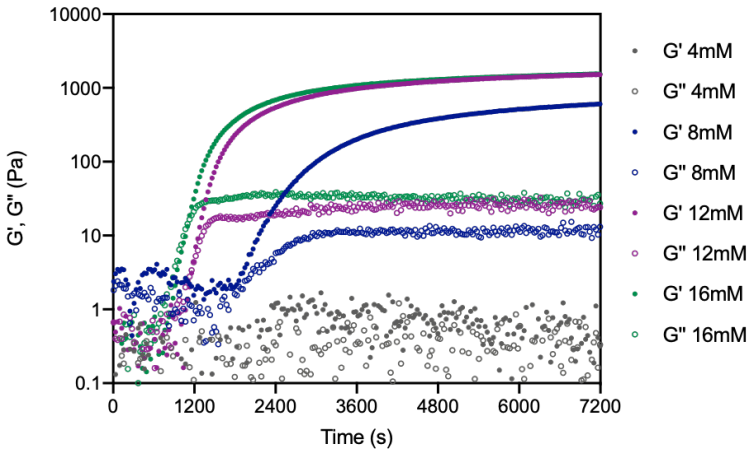

Figure S5.5. Time sweep measurements of Tz1-Nb-based PEG hydrogels at 37 ± 0.2˚C with a fixed frequency of 1 Hz and strain of 0.05%. Norbornene/tetrazine molar ratios were kept at 1:1 and final PEG macromonomer concentrations were 4, 8, 12 and 16 mM, respectively.

5.6.6 Pore size measurement

A fluorescent Tz-Nb-based PEG hydrogel was prepared similarly as described in **5.6.3**. Briefly, a freshly prepared solution of **PEG-NB** (60 µL) was mixed with solution of FITC-RGD (6 µL), vortexed for 10s, and incubated at room temperature for 30 min. Afterwards, a solution of **PEG-TZ1/TZ2/TZ3** (60 µL) was added and vortexed for 10s to obtain a homogeneous solution with final a PEG macromonomer concentration between 4-10 mM. The precursor solution was then transferred into µ-Slide VI 0.4 (ibidi) and incubated at 37˚C for 2h. Fluorescent images were acquired on Leica SP8 confocal microscope with a resolution of 512 × 512 pixels. An excitation wavelength of 488 nm and an emission filter of 500−545 nm for FITC was applied. The diameters of gas bubbles were measured in Fiji by drawing a straight line horizontally (angle < 3°) with the corresponding scale. Over 100 bubbles were measured for each condition.

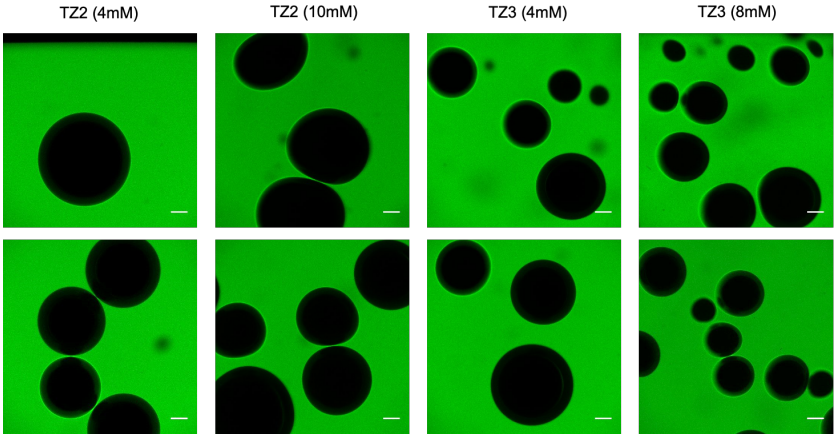

Figure S5.6. Representative images of bubbles formed in Tz-Nb-based PEG hydrogels. Scale bar: 100 µm.

5.6.7 Chondrocytes encapsulation and differentiation

Primary chondrocytes were cultured in DMEM supplemented with bFGF as a monolayer for two passages after isolation from healthy cartilage (Leiden University Medical Center). On the day of 3D cell encapsulation, the chondrocytes were dissociated by incubation with trypsin/EDTA for 5 min. Afterwards, DMEM supplemented with bFGF was added and cells were dissociated with a serological pipet by pipetting up and down. Cells were collected by centrifuge (300 g, 5 min) and resuspended to obtain a final cell concentration of 2 x 10^6 cells/mL. To prepare the hydrogel, a freshly prepared solution of **PEG-TZ1/TZ2 /TZ3** (75 µL) was first mixed with RGD-NB (40 mM, 7.5 µL) by pipetting. After 15 min incubation, a cell suspension (7.5 µL) was added and mixed, followed by the addition of a freshly prepared **PEG-NB** solution (60 µL). The mixture was pipetted into an angiogenesis slide with volume of 12 µL/well. After incubation at 37˚C for 20 min, a fresh DMEM solution containing bFGF (48 µL) was added on top and cells were cultured at 37 °C. After overnight incubation, the encapsulated chondrocytes were treated with freshly prepared chondrogenic differentiation medium (CDM).[6,7]

5.6.8 LIVE/DEAD staining

To evaluate cell viability, LIVE/DEAD staining of the encapsulated cells was performed at pre-determined time points as described in Chapter 4. In brief, cell-laden hydrogels were rinsed twice with PBS (pH 7.4, 45 µL) and incubated with a pre-prepared staining solution (45 µL) (calcein AM (2 µM) and propidium iodide (1.5 µM)) for 30 min to 1 h at 37 °C. After rinsing with PBS twice, the stained cell-laden hydrogel was imaged in a z-stack on Leica TCS SP8 confocal laser scanning microscope equipped with a 10× air objective. Fluorescent images were acquired at a resolution of 1024 × 1024 pixels. An excitation wavelength of 488 nm and an emission filter of 500−545 nm for calcein AM and an excitation wavelength of 532 nm and an emission filter of 594−686 nm for propidium iodide was set. Cell viability was determined by counting the calcein AM-stained green cells (viable) and PI-stained red cells (dead) in ImageJ.

5.6.9 Alcian blue staining

After a 4-day differentiation of the chondrocytes, the cell-laden hydrogels were rinsed with PBS (45 µL x 2) and incubated with 4% paraformaldehyde overnight prior to fixation. After that, the hydrogels were incubated with H_2O for 10 min (45 µL x 3) and afterwards with 3% acetic acid (pH 2.5). The alcian blue staining solution was added on top of the hydrogel and incubated for 3h at 37˚C. The stained hydrogels were washed by incubation with a 3% acetic acid solution for 2h (45 µL x 3) at 37˚C, followed by an overnight incubation with H_2O. Bright field microscopy images were collected on an Olympus microscope with 10x and 20x air objectives.

5.6.10 Appendix: NMR spectra

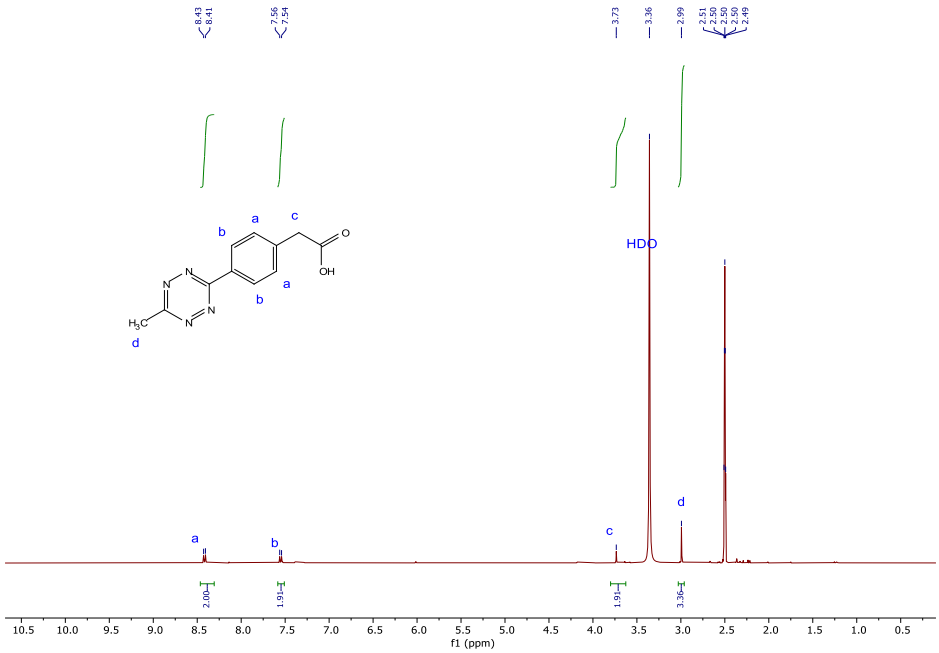

Figure A5.1. ^{1}H-NMR (400 MHz, 298K, DMSO-d_6) spectrum of **TZ1**

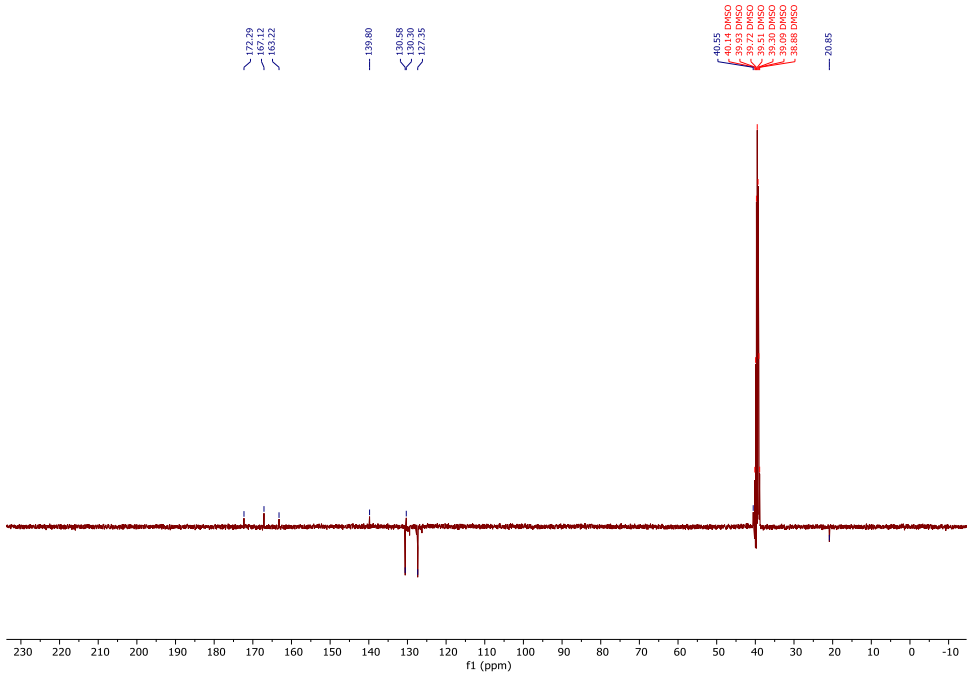

Figure A5.2. ^{13}C-NMR (400 MHz, 298K, DMSO-d_6) spectrum of **TZ1**

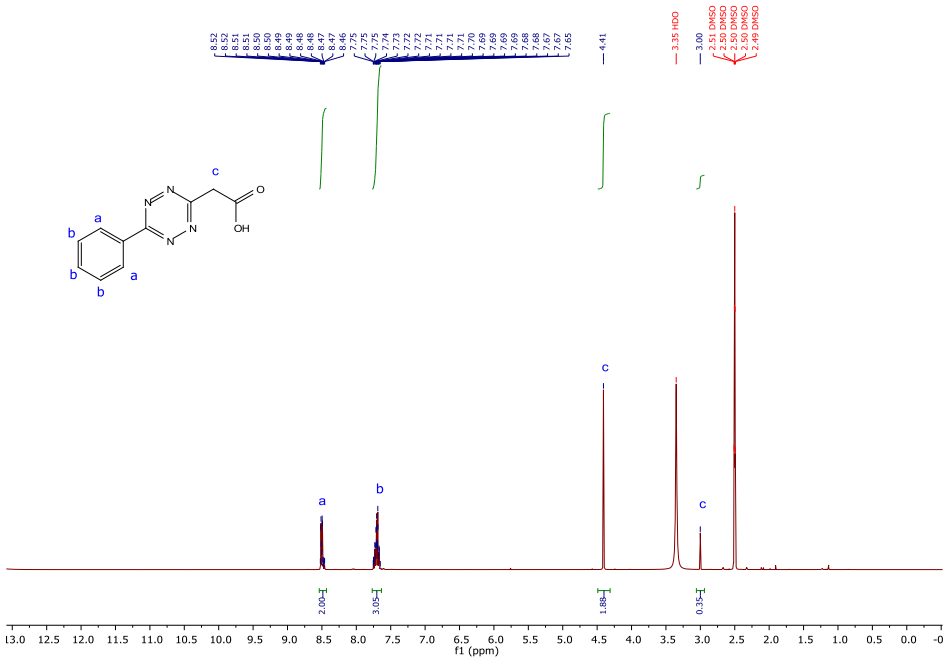

Figure A5.3. ^{1}H-NMR (400 MHz, 298K, DMSO-d$_6$) spectrum of **TZ2**

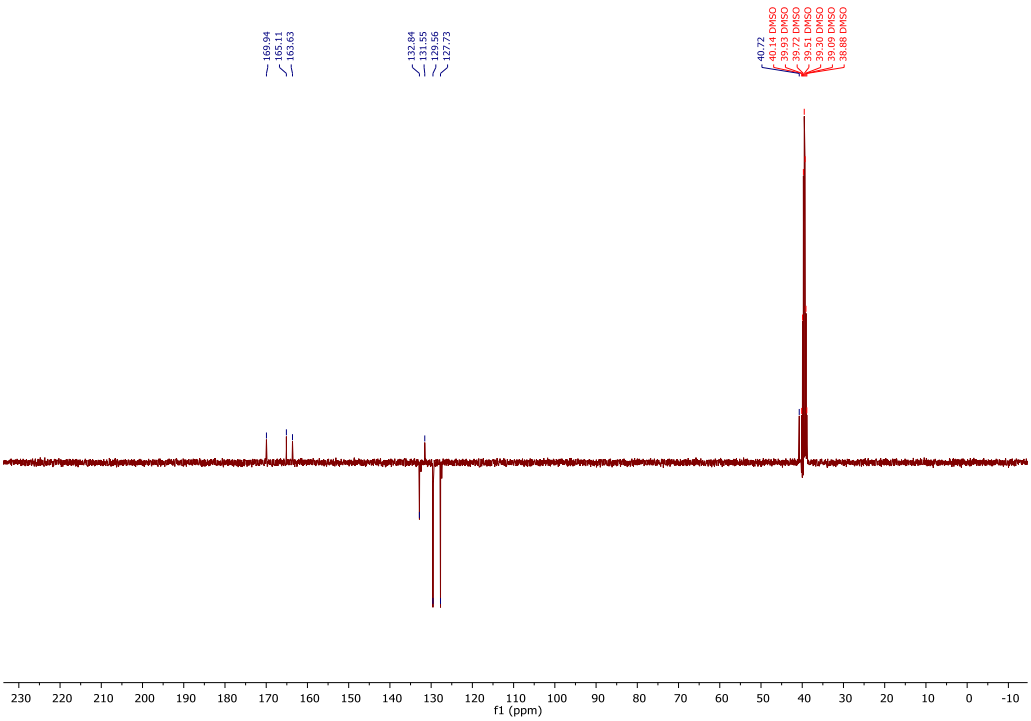

Figure A5.4. ^{13}C-NMR (400 MHz, 298K, DMSO-d$_6$) spectrum of **TZ2**

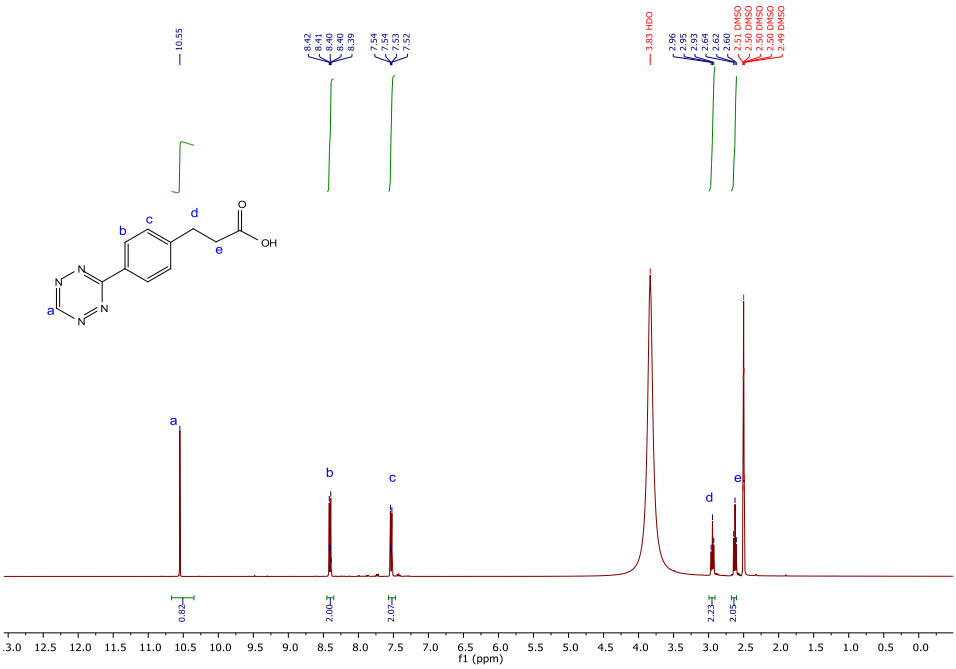

Figure A5.5. ^{1}H-NMR (400 MHz, 298K, DMSO-d_6) spectrum of **TZ3**

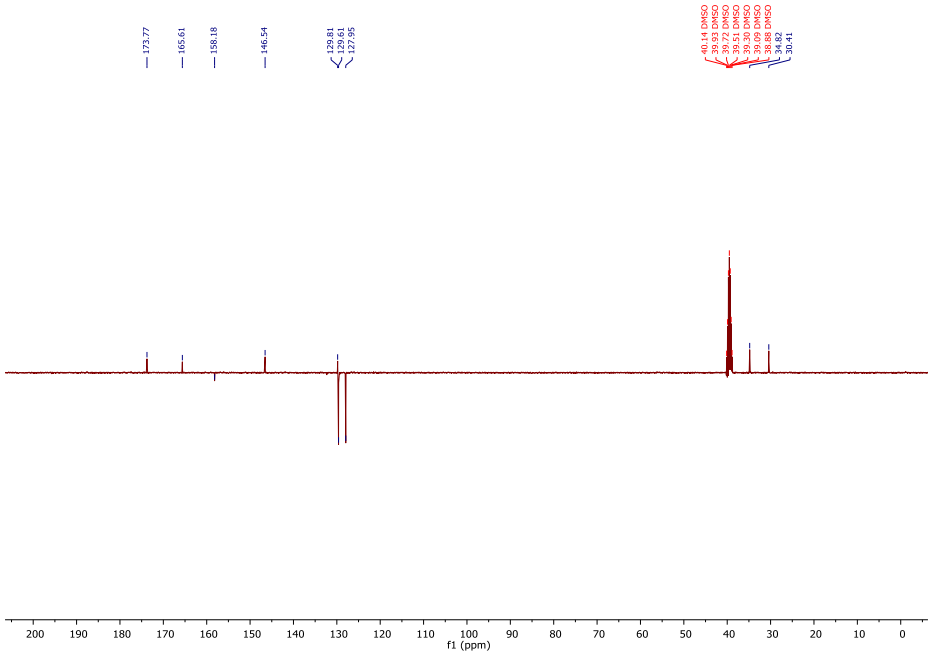

Figure A5.6. ^{13}C-NMR (100 MHz, 298K, DMSO-d_6) spectrum of **TZ3**

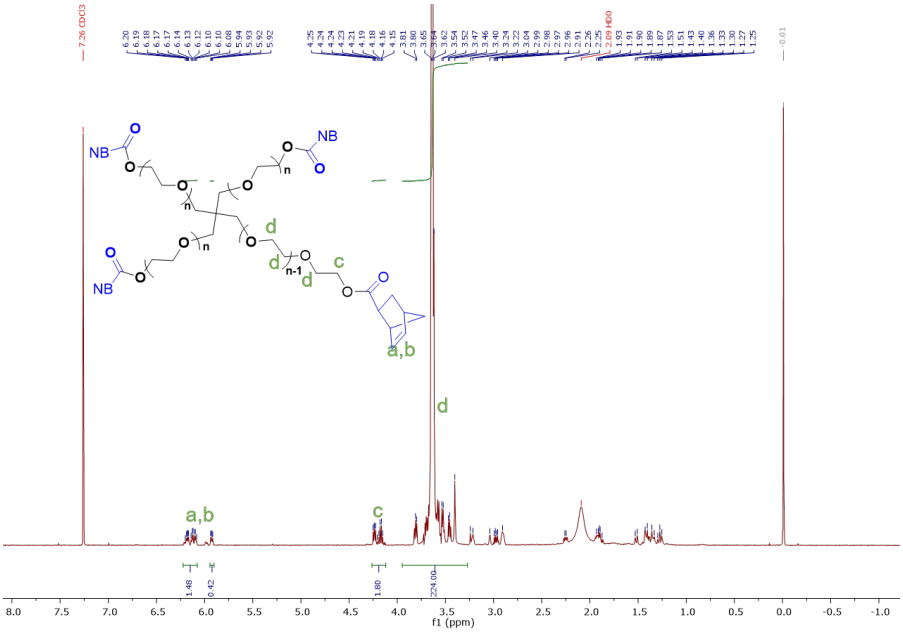

Figure A5.7. ^{1}H-NMR (400 MHz, 298K, $CDCl_3$) spectrum of **PEG-NB**. The degree of functionalization was 90%.

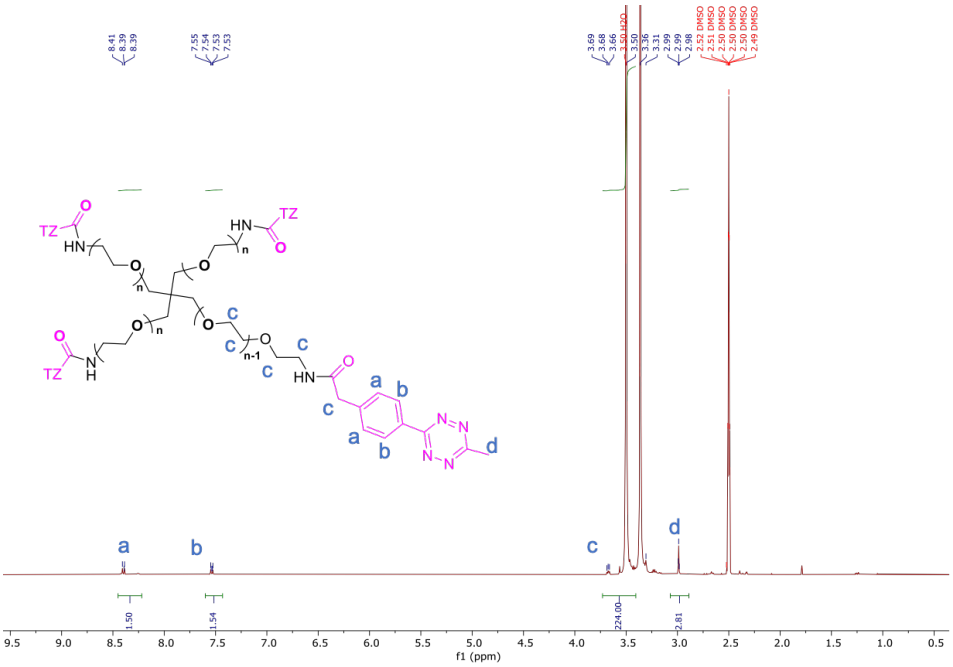

Figure A5.8. ^{1}H-NMR (400 MHz, 298K, $CDCl_3$) spectrum of **PEG-TZ1**. The degree of functionalization was 75%.

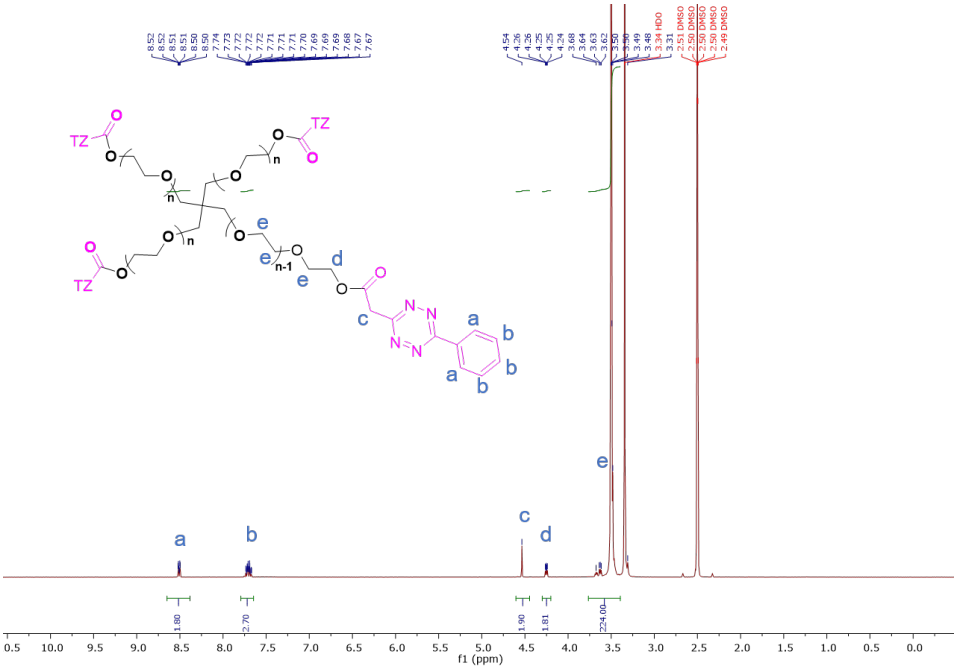

Figure A5.9. ^{1}H-NMR (400 MHz, 298K, DMSO-d6) spectrum of **PEG-TZ2**. The degree of functionalization was 90%.

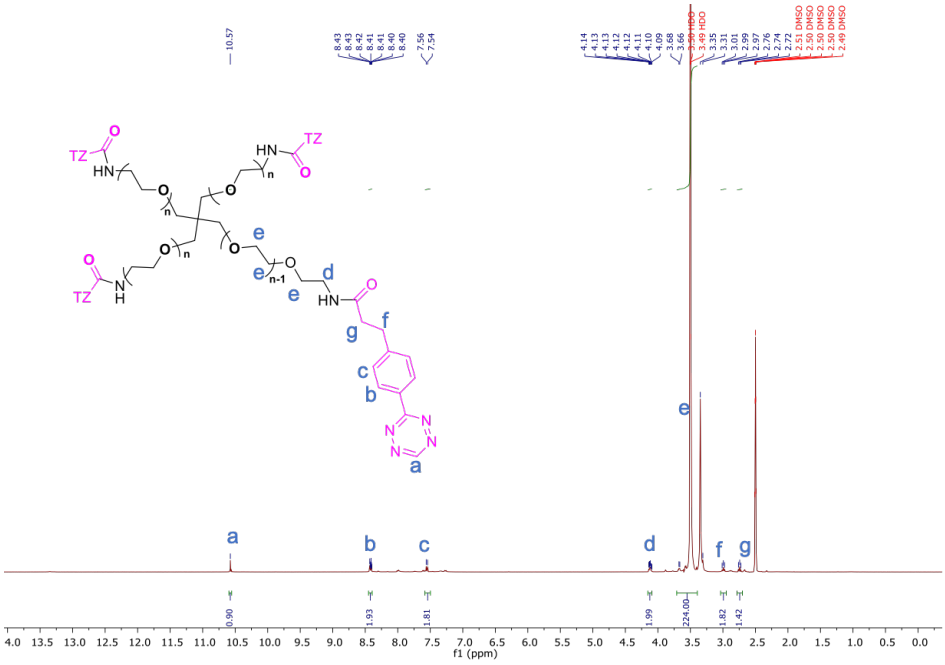

Figure A5.10. ^{1}H-NMR (400 MHz, 298K, DMSO-d6) spectrum of **PEG-TZ3**. The degree of functionalization was 90%.

5.6.11 References

[1] H. Zhan, H. De Jong, D. W. P. M. Löwik, *ACS Appl. Bio Mater.* **2019**, *2*, 2862.

[2] W. Mao, W. Shi, J. Li, D. Su, X. Wang, L. Zhang, L. Pan, X. Wu, H. Wu, *Angew. Chemie - Int. Ed.* **2019**, *58*, 1106.

[3] M. R. Karver, R. Weissleder, S. A. Hilderbrand, *Bioconjug. Chem.* **2011**, *22*, 2263.

[4] N. K. Devaraj, M. R. Karver, S. A. Hilderbrand, R. Weissleder, **2015** *US Patent No. US2015246893A1*.

[5] C. C. Lin, A. Raza, H. Shih, *Biomaterials* **2011**, *32*, 9685.

[6] K. Words, A. Green, **2002**, 338.

[7] C. Carapagnoli, N. M. Fisk, S. Kumar, L. Bellantuono, P. R. Bennett, I. A. G. Roberts, *Blood* **2000**, *96*, 2396.

CHAPTER 6

Summary and Perspectives

In vitro cell culture models have been essential tools to support biomedical research prior to *in vivo* studies, especially in the screening new drugs, testing of drug toxicity, exploring the mechanisms of disease and fabrication of microtissue or mini-organ models. A major challenge lies in how to offer cells with a microenvironment that more closely mimics the *in vivo* condition. Synthetic hydrogels that mimic the natural extracellular matrix in the biophysical and biochemical cues it provides to cells are in high demand, however the cell phenotypes as they are observed *in vivo* in numerous cases have yet to be attained. In this thesis, both chemically-defined supramolecular and covalent hydrogels are prepared that are encoded with bioactive peptides/ proteins, dynamics and porous structural features in order to explore how the modification of polymer materials with various biophysical cues affect cell behavior using various readouts. Through the design of a azide-alkyne clickable squaramide-based monomer, we have shown successful introduction of adhesive peptides that can be identified by cells, through an efficient supramolecular co-assembly approach to prepare the materials with the necessary peptide concentrations (**Chapter 2**). We further examine this flexible strategy for coupling of specific peptides to supramolecular monomers to provide matrix interactions for the culture of spheroids based on liver (HepG2) and induced pluripotent stem cells (**Chapter 2** and **Chapter 3**). Also, a dynamic covalent hydrogel system based on thiosulfinate-chemistry to form disulfide bonds was designed and validated to play an important role in supporting the differentiation of induced pluripotent stem cell derived cardiomyocytes. Cell alignment was only observed in dynamic covalent hydrogels within a particular stiffness range

and not on static hydrogels, further emphasizing the need for dynamics of the substrates in biomaterials design (**Chapter 4**). Lastly, gas-forming chemistries that enable control over porosity of the hydrogel materials at the macroscale were examined using the Inverse electron-demand Diels-Alder (IEDDA) reaction with reaction pairs that react with distinct kinetics (**Chapter 5**). Overall, we have engineered dynamic supramolecular and covalent biomaterials using different chemical tools to modulate their biophysical properties that the present to cells, providing guidelines for future biomaterials designs in the field of *in vitro* 3D cell culture.

In **Chapter 2**, a bioactive supramolecular hydrogel based on squaramide monomers is designed and shown to support HepG2 spheroid formation, proliferation and maturation as observed in the gene expression of liver-specific markers. The monomer consists of an azide-functionalized squaramide based scaffold that can be clicked to alkyne-modified RGD peptides through the CuAAC reaction, to provide the RGD-functionalized squaramide monomer. A supramolecular co-assembly approach with native squaramide monomer enabled the formation of bioactive hydrogels with a tunable control of the peptide concentration. Mechanically soft and self-recovering properties of this bioactive hydrogels have been shown in rheological measurements. NIH3T3 cells embedded within this hydrogel are capble of identifing RGD peptides showing cell spreading, branching and migration. In a further step, the bioactive hydrogels support functional maturation of HepG2 cells demonstrating higher gene expression of metabolic enzymes and hepatic markers in comparison to the commonly used Matrigel matrix, together with a compacted, viable and proliferative assembly. Collectively, this work demonstrates that a supramolecular co-assembly approach of squaramide-based monomers is an efficient method to engineer bioactive materials in a simple and controllable way that can be exploited for biomedical applications that require one or multiple bioactive cues.

In **Chapter 3**, a multicomponent supramolecular hydrogel based on squaramide monomers involving two integrin-targeting peptides is designed and applied for human induced pluripotent stem cell expansion in 3D is described. A similar supramolecular co-assembly approach is taken as described in chapter 2, with the exception that three monomers are co-assembled. The introduction of integrin targeting $\alpha v\beta 5$ and RGD into the supramolecular hydrogel materials results in mechanically weaker materials that maintain their self-recovering properties. The combination of peptides AB and RGD boost the growth of hiPSCs when the cells are seeded either as single cells or clumps, with high cell viability, proliferative activity and retention of pluripotency. Moreover, comparable cell expansion was achieved without a source of ROCK-inhibitor through the introduction of these two integrin-binding peptides in the materials. This chapter has demonstrated that successful multicomponent supramolecular co-assembly systems can be designed for different biological requirements in a flexible manner, broadening the application of these biomaterials. In addition, azide moiety on the squaramide monomers leaves the door open for further chemical crosslinking to mechanically manipulate this biomatrix to enable its use for 3D bioreactor culture of hiPSCs.

Chapter 4 describes the design and fabrication of a dynamic, viscoelastic hydrogel for the differentiation of hESC-derived cardiomyocytes. A new crosslinking moiety based on cyclic thiosulfinates used in proteins to form disulfide bonds, is introduced on covalent multi-arm PEG polymers (PEG-4ODT). Because of the lack of stability of the networks using only disulfide bonds, a mixed strategy invoving both dynamic and permanent bonds through the addition of PEG-4VS and PEG-4SH was taken to provide both disulfide and thiol-ene crosslinks within the materials. Rheological experiments verify the rapid gelation process, viscoelasticity and self-recovery properties of these hydrogels. Dynamic hydrogels (25%_dPEG) that consist of 25% dynamic crosslinks and 75% static crosslinks are demonstrated to show long-term stability in presence of PBS

and cell culture medium in swelling ratio measurements. The high stability of these materials under cell culture conditions enables the use of the 25%_dPEG hydrogels to be used as a synthetic matrices. Indeed, encapsulated hESC-CMs within these dynamic hydrogels show elongated morphologies, rapid recovery of cell spontaneous beating and alignment, demonstrating that cardiomyocytes prefer a soft and dynamic matrix for their culture. The significant increase in expression of cardiac genes, cTnT and MYH6, also verify the potential of applying this dynamic hydrogel for cardiomyocytes maturation in 3D. For further study, engineering more complex tissues can be explored within these dynamic materials, for example, co-assembly of cardiomyocytes with cardiac fibroblasts and endothelial cells to more closely mimic heart tissue *in vivo*.

Chapter 5 explores the use of the gas-forming IEDDA bioconjugation reaction on polymer materials to engineer porosity within them. The IEDDA reaction between tetrazine and norbornene on multi-arm PEG polymers was examined to yield elastic hydrogels and with the production of N_2 gas to form macro-sized bubbles in the hydrogel materials. Tetrazine and norbornene were used as reaction pairs because of their favourable reaction kinetics and further tuning of this parameter was achieved by synthesizing tetrazine derivatives containing electron-donating and electron-withdrawing substituents on ring positions 3 and 6. Higher reaction rate and higher PEG polymer concentrations resulted in faster gelation with smaller pore sizes (e.g. TZ3, pore size range = 170-360 µm). The IEDDA-based PEG hydrogels can be prepared with storage moduli ranging from 0.7 kPa to 12 kPa that are stable in the presence of PBS and cell culture medium. Additionally, primary chondrocytes encapsulated in soft IEDDA-based hydrogels displayed high viability and notable cartilage matrix secretion, demonstrating their potential application for cartilage tissue engineering applications. In the future, dynamic crosslinking strategies can be introduced into these modular porosity materials, through the use of interpenetrating or supramolecular polymer materials to prepare iPN or double network hydrogels to prepare a mechanically robust

and dynamic microenvironment for cells that better approximates the biophysical aspect of their microenvironment on several length scales.

Samenvatting

In vitro celkweek modellen zijn essentieel gebleken in het biomedische onderzoeksveld, als hulpmiddelen voorafgaand aan *in vivo* onderzoek, bijvoorbeeld in het screenen van nieuwe geneesmiddelen, het testen van toxiciteit, het onderzoeken van cellulaire mechanismen in ziektes en het vervaardigen van mini-orgaanmodellen. Een grote uitdaging in dit veld is het *in vitro* nabootsen van de micro-omgeving van de cellen *in vivo*. Voor deze toepassing zijn synthetische hydrogelen die fysische en biochemische signalen van de natuurlijke extracellulaire matrix (ECM) imiteren aantrekkelijk, echter is in veel gevallen het fenotype van de cellen *in vivo* nog niet bereikt in een synthetische matrix. In dit proefschrift is de ontwikkeling van gedefinieerde supramoleculaire en covalente hydrogelen en hun aanpassing met bioactieve peptide of eiwitten, dynamische of poreuze eigenschappen beschreven. Met deze materialen werd onderzocht hoe het aanpassen van een polymeer met verscheidene biofysische eigenschappen het celgedrag kan beïnvloeden. Door het ontwerpen van een azide-alkyn aanklikbare op squaramide-gebaseerde monomeer, zijn peptiden voor celadhesie op een efficiënte manier geïntroduceerd in een supramoleculair systeem, door het samenvoegen van verschillende monomeren om de materialen met de benodigde peptidenconcentraties te bereiden (**hoofdstuk 2**). Deze flexibele koppelingsstrategie is verder onderzocht om specifieke peptiden aan supramoleculaire monomeren te koppelen, om op lever (HepG2) en op pluripotente stamcel gebaseerde sferoïden van interacties met de omliggende matrix te voorzien (**hoofdstuk 2** en **3**). Ook is een dynamisch covalent hydrogel-systeem ontworpen, gebaseerd op thiosulfinaat disulfide bindingen, voor het ondersteunen van *in vitro* differentiatie van geïnduceerde pluripotente stamcellen tot cardiomyocyten. Parallelle oriëntatie van de cellen in de dynamisch covalente hydrogel was alleen te zien in gels met een bepaalde stijfheid en

werd niet geobserveerd in statische hydrogelen, wat het belang van dynamische eigenschappen in biomaterialen benadrukt (**hoofdstuk 4**). Tot slot werden gasvormende materialen op basis van Inverse Electron-demand Diels-Alder (IEDDA) reacties onderzocht, die het mogelijk maken porositeit in de hydrogelen te controleren (**hoofdstuk 5**). Samenvattend, dynamische supramoleculaire en covalente biomaterialen, gebaseerd op verschillende chemische strategieën, werden ontworpen om de biofysische eigenschappen van de materialen te controleren voor celkweek. Deze materialen kunnen als basis dienen voor het ontwerpen van toekomstige biomaterialen op het gebied van *in vitro* 3-dimensionale celkweek.

In hoofdstuk twee is een bioactieve supramoleculaire hydrogel ontworpen die de formatie, proliferatie en groei van HepG2 sferoïden ondersteunt. En lever specifieke markers werden gemeten. Het monomeer bestaat uit een azide gefunctionaliseerde squaramide die ge-'clicked' kan worden aan een alkyn gemodificeerd RGD peptide met behulp van een CuAAC gekatalyseerd reactie. Supramoleculaire co-assemblage van squaramide monomeren in hun native vorm resulteerde in een bioactieve hydrogel met controleerbare concentraties peptide. De hydrogel was mechanisch zacht en bezit zelfhelende eigenschappen zoals aangetoond mer rheologische metingen. Wanneer NIH3T3 cellen in de hydrogel geplaatst worden kunnen ze RGD peptiden herkennen en identificeren, wat leidt tot verspreiding, vertakking en migratie. Vervolgens is er – naast een compacte levensvatbare en proliferatieve assemblage – aan de hand van verhoogde genexpressie van metabolische enzymen en hepatische markers aangetoond dat de bioactieve hydrogels functionele groei van HepG2 cellen ondersteunen in vergelijking tot de gebruikelijke Matrigel matrix. Deze studie toont aan dat supramoleculaire co-assemblage van squaramide monomeren een efficiënte manier is om bioactieve hydrogels te ontwerpen. En om op een simpele en controleerbare manier gebruikt te worden voor biomedische applicaties waarin één of meerdere bioactieve signalen een vereist zijn.

In **Hoofdstuk** 3 werd een multicomponent supramoleculaire hydrogel beschreven die is opgebouwd uit squaramide monomeren met twee integrin-bindende peptiden. Deze hydrogel werd vervolgens gebruikt om humane geïnduceerde pluripotente stamcellen (hiPSC) te kweken in 3D. Een vergelijkbare supramoleculaire co-assemblage tactiek zoals beschreven in Hoofdstuk 2 werd toegepast, met de uitzondering dat in deze studie drie monomeren co-assembleren. De aanwezigheid van de integrin-bindende peptiden $\alpha v\beta 5$ en RGD in de supramoleculaire hydrogel resulteerde in een mechanisch zwakker materiaal met zelf-herstellende eigenschappen. De combinatie van de peptiden AB en RGD stimuleerden de groei van hiPSCs, en bovendien konden de cellen zowel als individuele cellen of als kleine cel clusters in de gel gezaaid worden waarbij een hoge cel vitaliteit, proliferatie en behoud van de pluripotente eigenschappen werd waargenomen. Tevens kon door de introductie van de twee integrin-bindende peptiden in het materiaal een vergelijkbare celexpansie bereikt worden zonder dat aanwezigheid van een ROCK remmer noodzakelijk was. Dit hoofdstuk toont aan dat multicomponent, supramoleculaire co-assemblage systemen succesvol ontworpen kunnen worden op een flexibele manier, afhankelijk van de vereiste biologische doelstellingen. Hierdoor kan de toepassing van deze biomaterialen verder worden uitgebreid. De introductie van een azide groep in de squaramide monomeren maakt verdere chemische crosslinking strategieën mogelijk om een matrix te ontwikkelen die gebruikt kan worden in een 3D bioreactor systeem voor het kweken van hiPSCs.

In **Hoofstuk** 4 werd het ontwerp en de fabricage van een dynamische, visco-elastische hydrogel voor de differentiatie van hESC-afgeleide cardiomyocyten beschreven. Hierbij werd een nieuwe crosslinking groep geïntroduceerd die is gebaseerd op cyclische thiosulfinaten. Deze cyclische thiosulfinaat groep werd geconjugeerd aan covalente, vierarmige PEG polymeren (PEG-4ODT). Echter, door een gebrek aan stabiliteit van de disulfide-gebonden netwerken moest een gecombineerde strategie toegepast worden waarbij zowel dynamische als permanente bindingen gevormd werden. Hiertoe

werden PEG-4VS en PEG-4SH polymeren aan het systeem toegevoegd omdat deze polymeren zowel disulfide als thioleen verbindingen kunnen vormen. Reologische metingen toonden de snelle vorming van een gel en de visco-elastische en zelf-herstellende eigenschappen van de gevormde hydrogel. Dynamische hydrogels (25%_dPEG), bestaande uit 25% dynamische crosslinks en 75% statische crosslinks, waren stabiel in de aanwezigheid van PBS en celkweek medium, zoals aangetoond met zwelling ratio experimenten. Deze hoge mate van stabiliteit onder celkweek condities maakt het mogelijk om 25%_dPEG hydrogel te gebruiken als een synthetische matrix voor celexperimenten. Zo vertoonden hESC-CMs die werden geëncapsuleerd in deze dynamische hydrogel een gestrekte celmorfologie, een snel herstel van celcontractie en cel uitlijning, waardoor duidelijk werd dat het kweken van cardiomyocyten de voorkeur heeft aan een zachte en dynamische matrix als cellulair microomgevins. Bovendien bewees de significante toename in expressie van de cardische genen cTnT en MYH6 de potentie van deze dynamische hydrogel als kweeksyteem voor cardiomyocyt maturatie in 3D. In vervolgonderzoek kunnen meer complexe weefsels nagebootst worden door het gebruik van deze dynamische hydrogel. Door bijvoorbeeld een co-cultuur te vormen van zowel cardiomyocyten als cardische fibroblasten en/of endotheel cellen in deze dynamische hydrogel, kan een betere nabootsing van in vivo hart weefsel bereikt worden.

Hoofdstuk 5 verkent de IEDDA bio-conjugatiereactie op polymeermateriaal, om zo porositeit in te bouwen in het materiaal. De IEDDA-reactie tussen tetrazine en norborneen op een multi-arm PEG-polymeer is onderzocht om elastische hydrogelen te maken. De vorming van stikstof gas in de polymer satie reactie creëert bubbels van macroformaat. Tetrazine en norborneen werden gebruikt voor deze reactie, vanwege hun gunstige reactiekinetiek. De reactiekinetiek waren verder geoptimaliseerd door elektrondonerende en elektronzuigende groepen op de 3- en 6-positie van tetrazine te iwtrvduceren. Een snelle reactiekinetiek en een hogere concentratie van PEG-polymeer

resulteerde in een snellere gelering en kleinere poriegrootte (Bijvoorbeeld TZ3, poriegrootte = 170-360 µm). De PEG hydrogelen gemaakt via de IEDDA-reactie kunnen worden bereid met opslagmodule van 0.7 kPa tot 12 kPa, en zijn stabiel in de aanwezigheid van PBS-buffer en celcultuurmedium. Bovendien vertonen primaire chondrocyten een hoge levensvatbaarheid wanneer ze zijn ingekapseld in een zachte IEDDA-gebaseerde hydrogel. Ook produceren deze cellen kraakbeenmatrix, waarmee de potentie voor kraakbeenweefselkweektoepassingen wordt aangetoond. In de toekomst kunnen dynamische crosslinkstrategieën worden geïntroduceerd in deze moduleerbare poreuze hydrogelen, vanwege het gebruik van interpenetrerende of supramoleculaire polymeermaterialen. Hierdoor kunnen iPN of dubbelnetwerkhydrogelen worden gemaakt. Met deze hydrogelen kan een mechanisch robuuste en dynamische micro-omgeving voor cellen worden gecreëerd die beter de biofysische aspecten nabootst op verschillende lengteschalen.

Curriculum Vitae

Tingxian Liu was born on November 15, 1990 in Xinyang, China. In 2008, She graduated from Shangcheng First Senior High School and was admitted as BSc student in Shandong University. After obtaining a BSc degree in Pharmacy, she started her MSc studies in Shandong University under the supervision of Prof. Na Zhang, where she became interested in the area of nanomedicine and life science, especially in gene therapy, drug delivery and biomaterials. Inspired from that, she applied for the PhD position in the group of Prof. dr. A. Kros after achieving the MSc degree in 2015.

She started her PhD study on“Dynamic polymer hydrogels as synthetic extracellular matrices for 3D cell culture”in September 2015, in the group of Supramolecular&Biomaterials Chemistry (SBC), Leiden Institute of Chemistry. The study was sponsored by Chinese Scholarship Council (CSC)-Leiden University joint scholarship and performed under the supervision of Dr. R. E. Roxanne and Prof. dr. A. Kros. Also, she collaborated with Dr. S.J. ter Braak (LACDR), Prof. B. van de Water (LACDR), Dr. Y.F.M. Ramos (LUMC), Prof. dr. D. Heinrich (Leiden University), and Prof. dr. P.C.J.J. Passier (LUMC) during the PhD study.

Now, she works as a senior researcher in the company (Yangshengtang Institute of Natural Medicine), focusing on neural differentiation of iPSCs and brain organoids for neurodegenerative disease modeling.

Academic presentations were listed as following:

1. Spacer length-dependent irreversible depolymerization of supramolecular polymers. 2020, Poster Presentation, CHAINS.
2. Squaramide based hydrogels support 3D culture of HepG2 spheroids with improved liver-specific function. 2019, Oral and Poster Presentation, CHAINS.

3. Expansion of human induced pluripotent stem cells in squaramide-based supramolecular hydrogels. 2019, Poster Presentation, Reedijk Symposium.
4. Co-assembly of integrin-targeting peptides on squaramide supramolecular materials facilitate 3D expansion of human induced pluripotent stem cells. 2019, Poster Presentation, Regeneration Day.
5. Morphological control over a squaramide-based supramolecular polymer in water. 2018, Poster Presentation, CHAINS.

List of publications

1. T. Liu[1], L. van den Berk[1], J.A.J. Wondergrem, C. Tong, M.C. Kwakernaak, B. ter Braak, D.M. Heinrich, B. van de Water, R.E. Kieltyka*, Squaramide-based supramolecular materials drive HepG2 spheroid differentiation. 2021, Adv. Healthcare Mater. 2021, 10, 2001903.

2. T. Liu, M. Janssen, M. Bril, R. E. Kieltyka*, Disulfide-based reversible covalent hydrogels starting from cyclic thiosulfinate macromers support cardiomyocytes contractility in 3D 2021, Submitted.

3. T. Liu, M. Janssen, L. Delfos, R. E. Kieltyka*, Co-assembly of integrin-targeting peptides on squaramide supramolecular materials facilitate 3D expansion of hiPSCs. 2021, In preparation.

4. T. Liu, Y.F.M. Ramos, R. E. Kieltyka*, Engineering macroporous hydrogels using the tetrazine-norbornene click reaction. 2021, In preparation.

5. V. Saez Talens, D.M.M. Makurat, T. Liu, W. Dai, C.L. Guibert, W.E.M. Noteborn, I.K. Voets, R.E. Kieltyka*, Shape modulation of squaramide-based supramolecular polymer nanoparticles, Polym. Chem., 2019, 10, 3146.

6. C. Tong, T. Liu, V. Saez Talens, W.E.M. Noteborn, T.H. Sharp, M.M.R.M. Hendrix, I.K. Voets, C.L. Mummery, V.V. Orlova, R.E. Kieltyka*, Squaramide-Based supramolecular materials for three-dimensional cell culture of human induced pluripotent stem cells and their derivatives. Biomacromolecules, 2018, 19, 1091.

7. C. Liu[1], T. Liu[1], Y. Liu, N. Zhang*, Evaluation of the potential of a simplified co-delivery system with oligodeoxynucleotides as a drug carrier for enhanced antitumor effect. Int J Nanomedicine, 2018, 13, 2435.

8. C. Liu, T. Liu, X. Yu, Y. Gu*, A preliminary study on the interaction between Asn-Gly-Arg (NGR)-modified multifunctional nanoparticles and vascular epithelial cells. Acta Pharmaceutica Sinica B, 2017, 7, 361.

9. T. Liu, M. Wang, T. Wang, Y. Yao, N. Zhang*, Co-delivery of doxorubicin and siRNA by a simplified platform with oligodeoxynucleotides as drug carrier. Colloids Surf B Biointerfaces, 2015, 126, 531.

10. L. Zhang[1], T. Liu[1], Y. Xiao, D. Yu, N. Zhang*, Hyaluronic Acid-Chitosan Nanoparticles to Deliver Gd-DTPA for MR Cancer Imaging, Nanomaterials, 2015, 5, 1379.

11. M. Wang, T. Liu, L. Han, W. Gao, S. Yang, F. Wang, N. Zhang*, Functionalized O-carboxymethyl-chitosan/polyethylenimine based novel dual pH-responsive nanocarriers for controlled co-delivery of DOX and gene, Polym. Chem., 2015, 6, 3324.

Acknowledgements

To look back, it has been over five years since I came to Netherlands for the PhD study, which will be one of the most wonderful and precious experience during my lifetime. Over the period, many people have offered valuable support and help for my PhD study as well as my daily life in Leiden. Herein, I would like to sincerely thank all of them.

First of all, I deeply appreciate the support from my supervisors Prof. dr. Alexander Kros and Dr. Roxanne E. Kieltyka, for the opportunity to join SBC group as a PhD student. Thank you both for the professional guide and advices in my thesis research. Specially, I want to express my profound gratitute to my daily supervisor Dr. Roxanne E. Kieltyka for her unconditional support, encouragement, and discussion, leading me to gain more in supramolecular chemistry, do better scientic research and be a scientist. I also want to thank the Chinese Scholarship Counxil (CSC) for their financial support while I stay in Netherlands. Thank Astrid for your kindly help during the PhD application.

Also, as a member of SBC group, I have got kindly support from my nice colleagues: Viorica, Victorio, Willem, Ciqing, Francesca, Mengjie, Ye, Merel, Mark.K, Lucie, Hugo, Mark.C, Maaike, Ying, Sandeepa, Joyal, Wei, Panagiota, Gabriela, Winant, Amiee, Elena, Niek, Roy, Dennis, Max, David, Jasper, Indigo, Jorn, Xue, Weizhe, Lin, Xuecheng, Dinghao, Xiaoyan, Wangyang and other SBC-ers. Thank you for your kindly help in the lab and academic discussions.

Besides, I would like to express my respect and gratitute to my collaborators: Dr. S.J. ter Braak (LACDR), Prof. B. van de Water (LACDR), Dr. Y.F.M. Ramos (LUMC), Prof. dr. D. Heinrich (Leiden University), and Prof. dr. P.C.J.J. Passier (LUMC). Thank you for your comments and suggestions that help me out during the reseach and make my work

more meaningful. Specially, I want to specially thank Joeri from LION for his help in 3D confocal imaging, Rolf from Univerisity of Twente for his help in sharing hESC cells and culturing advices, Dorien for her support in sharing iPSC and stem cell culture advices, and Ronald for his help in Global Screening Array analysis.

I also would like to thank a particular Chinese group in Leiden: Xue, Liming, Ming, Yongzhen, Andi, Liang, Qingju, Qing, Xiansha, Xu, Xiaoting, Wanbin, Xuequan, Sizhe, Heyang, Yurong, Chengyu and so on. Thank you all for your support. I would like to specially thank several close friends: Ciqing, Hui, Zhen, Junfei, Xiaobing, Ye, Mengjie, Jing, Yazhi, Ying and Wenlong, for your help in daily life, making nice memory while stay in Netherlands, and your accompany and encourangement while I am frustrating.

And I am grateful to Prof. Na Zhang from Shandong University for your help and support in applying the CSC Scholorship.

Lastly, I want to express gratitude to my parents and my brother for your uncontional love over the years. You always encourage me to make the choice on my own and chase the life I like while offerring support behind me. Also, I want to thank my boyfriend, Long, for staying with me and always sharing nice things when I am stressful from work. Thank you for your thoughful accompany!

Thank you to everyone during my PhD. It is my great pleasure to have met you and have a memorable experience for my life. Thank you!